Supplementary Information

Towards low-energy-light-driven bistable photoswitches: *ortho*-fluoroaminoazobenzenes

Kim Kuntze, Jani Viljakka, Evgenii Titov*, Zafar Ahmed, Elina Kalenius, Peter Saalfrank, and Arri Priimagi*

Thermally stable photoswitches that can be driven with low-energy light are rare, yet crucial for extending the applicability of photoresponsive molecules and materials towards, *e.g.*, living systems. Combined *ortho*-fluorination and -amination couples high visible-light absorptivity of *o*-aminoazobenzenes with the extraordinary bistability of *o*-fluoroazobenzenes. Herein, we report a library of easily accessible *o*-aminofluoroazobenzenes and establish structure–property relationships regarding spectral qualities, visible light isomerization efficiency and thermal stability of the *cis*-isomer with respect to the degree of *o*-substitution and choice of amino substituent. We rationalize the experimental results with Density Functional Theory calculations. The synthesized azobenzenes absorb at up to 600 nm and their thermal lifetimes range from milliseconds to months at 25°C. The most unique example can be driven efficiently from *trans* to *cis* with any wavelength from UV up to 595 nm, while still exhibiting thermal *cis*-lifetime of 81 days at room temperature.

DOI: xxx

Table of Contents

Supplementary Methods

General synthetic methods

Synthetic work was carried out in Tampere University. All reagents and solvents were commercial and purchased from Sigma Aldrich, TCI Europe, VWR or FluoroChem. When needed, dry solvents were acquired using an Inert PureSolv solvent purification system. Reactions were monitored with thin-layer chromatography (TLC) on commercial Merck Silica 60 F_{254} TLC plates, and the developed plates were visualized with UV irradiation (254 nm) or with potassium permanganate and cerium ammonium molybdate stains.

Accurate mass experiments were performed with Agilent 6560 Ion mobility Q-TOF mass spectrometer, which was equipped with dualAJS ESI ion source. The compounds were dissolved in DCM (1 mg/ml) and samples were prepared with 1 µM concentration in methanol. Samples were injected from syringe pump generally with 5 µl/min flowrate. ES tuning mix (Agilent technologies) was used for calibration. The exact mass values were calculated using Isotope Distribution Calculator (part of Agilent MassHunter Data Analysis Core) and the data was analyzed using MassHunter Workstation Software B08.00 from Agilent Technologies, USA. Characterization was done using accurate mass values (limit values < 3mDa or < 5 ppm) and fit of isotopic distributions. In case of overlapping distributions, the result was verified with measurement of ion mobility mass spectra (IM-MS).

Nuclear magnetic resonance spectra (NMR) were measured with a 500 MHz JEOL ECZR 500 (125 MHz for ^{13}C) at 25 °C and processed with the JEOL Delta NMR software version 5.3.1 (Windows). Chemical shifts are given in ppm and are referenced to solvent signals ($CHCl_3$: δ = 7.26 ppm (^1H), 77.16 ppm (^{13}C). Multiplicities are abbreviated as follows: singlet (s), doublet (d), triplet (t), quartet (q), pentet (p), and multiplet (m). Coupling constants (*J*) are given in Hz.

Because many of the products have long *cis*-lifetimes, some of the NMR spectra contain two peaks for each magnetically inequivalent nucleus, originating from the *trans* and *cis* isomers for which the amount of shielding is different. This results in each peak occurring twice, with the same intensity ratio. For example, in the ^1H spectrum of **4-F** there are two peaks for the four identical aromatic protons: a doublet at 6.57 ppm and a less intense doublet at 6.40 ppm, and similarly two singlets at 3.85 and 3.76 ppm with the same relative integral ratio. The reported peaks refer to those originating from the *trans* isomer unless otherwise stated.

The fluorine atoms split some of the carbon signals, resulting in more carbon peaks than expected. In some cases an effort was made to assign multiplicities to the carbon spectrum.

Because many of the syntheses were carried out in small scale (yields from 1 to 20 mg), the NMR spectra were also recorded from relatively dilute samples. Thus, the solvent (mainly chloroform, 7.26 ppm) and water (ca. 1.6–1.5 ppm) peaks appear relatively large and the latter may in some cases overlap with the aliphatic protons of the products. Also grease (around 1.2–0.9 ppm) is present in many samples, but none of the compounds gives signals in that region. The recurring water and grease signals are not labeled. Traces of solvent (ethyl acetate, dichloromethane) are labeled if present in significant amounts.

Compounds **1-F**, **2-F**, **1-pyr**, **1-pip**, **2-pyr$_1$**, **3-pyr$_1$**, **2-pyr$_2$** and **3-pyr$_2$** were already reported.[1]

Synthesis

4-F. 2,5-difluoro-4-methoxyaniline (1.0 g, 6.29 mmol), potassium permanganate (3.0 g, 19 mmol) and iron sulfate heptahydrate (3.0 g, 11 mmol) were refluxed in dichloromethane overnight, filtered through silica, dried with magnesium sulfate and concentrated under reduced pressure. The crude product was then purified with column chromatography (dichloromethane) to yield **4-F** as an orange-yellow crystalline product (246 mg, 25%). ^1H-NMR (500 MHz, $CDCl_3$) δ 6.57 (d, J = 10.9 Hz, 4H), 3.85 (s, 6H). ^{13}C-NMR (126 MHz, $CDCl_3$) δ 161.8 (t, J = 13.9 Hz), 157.3 (dd, J = 259.5, 7.2 Hz), 98.9 (d, J = 24.1 Hz), 56.2. ^{19}F-NMR (471 MHz, $CDCl_3$) δ -118.1 (d, J = 11.5 Hz). HRMS ((+)ESI-TOF): *m*/*z* calcd. for $C_{14}H_{10}F_4N_2O_2$+Na^+: 337.0571 $[M+Na]^+$; found: 337.0570.

1-dma. Monofluorinated precursor **1** (26.1 mg, 0.1 mmol) and dimethylamine (ethanol solution, 71 µl, 0.4 mmol) were stirred in acetonitrile (1 ml) at 50°C for 20 hours, after which more dimethylamine solution (500 µl, 2.8 mmol) was added and stirred at 50°C for another 24 hours. The reaction mixture was then concentrated and purified by column chromatography (20% ethyl acetate in hexane) to yield **1-dma** (3.1 mg, 11%) as an orange-yellow crystalline product. A large amount of **1-F** (not weighed) was also recovered. ^1H-NMR (500 MHz, $CDCl_3$) δ 7.85 (d, J = 8.6 Hz, 2H), 7.67 (d, J = 9.2 Hz, 1H), 6.97 (d, J = 8.6 Hz, 2H), 6.49 (s, 1H), 6.46 (dd, J = 9.0, 2.4 Hz, 1H), 3.87 (s, 3H), 3.85 (s, 3H), 3.05 (s, 6H). ^{13}C-NMR (126 MHz, $CDCl_3$) δ 162.4, 161.1, 152.4, 147.7, 138.4, 124.3, 118.4, 114.2, 105.6, 103.1, 55.6, 55.5, 45.2. HRMS ((+)ESI-TOF): *m*/*z* calcd. for $C_{16}H_{19}N_3O_2$+H^+: 286.1550 $[M+Na]^+$; found: 286.1564.

2-pip$_1$ and **2-pip$_2$**. Bis-*ortho*-fluorinated precursor **2-F** (150 mg, 0.539 mmol) and piperidine (530 µl, 5.39 mmol) were stirred in acetonitrile (7.5 ml) at room temperature for 2 hours. More piperidine (2.0 ml, 20.3 mmol) was added, and the reaction was continued for another 2 hours. The reaction mixture was then diluted with ethyl acetate, washed with water, dried with sodium sulfate, concentrated under reduced pressure and purified by column chromatography (5–10% ethyl acetate in hexane) to yield **2-pip$_1$** (74 mg, 40%) and **2-pip$_2$** (62 mg, 21%) as orange solids. **2-pip$_1$**: ^1H-NMR (500 MHz, $CDCl_3$) δ 7.90 (d, J = 9.2 Hz, 2H), 6.99 (d, J = 9.2 Hz, 2H), 6.37-6.37 (m, 1H), 6.31 (dd, J = 13.2, 2.3 Hz, 1H), 3.87 (s, 3H), 3.81 (s, 3H), 3.04 (t, J = 5.4 Hz, 4H), 1.74-1.69 (m, 4H), 1.59-1.55 (m, 2H, overlapping with water peak). ^{13}C-NMR (126 MHz, $CDCl_3$) δ 161.8, 160.9,

160.8, 155.0, 153.0, 152.4, 152.3, 148.1, 128.7, 128.6, 124.3, 114.2, 100.6, 95.1, 94.9, 55.7, 54.3, 26.3, 24.4. ^{19}F-NMR (471 MHz, $CDCl_3$) δ -122.1 (d, J = 13.2 Hz). HRMS ((+)ESI-TOF): *m/z* calcd. for $C_{19}H_{22}FN_3O_2$+Na^+: 366.1588 [M+Na]$^+$; found: 366.1597. **2-pip$_2$**: ^{1}H-NMR (500 MHz, $CDCl_3$) δ 7.92 (d, J = 9.2 Hz, 2H), 6.99 (d, J = 8.6 Hz, 2H), 6.29 (s, 2H), 3.87 (s, 3H), 3.82 (s, 3H), 2.95 (t, J = 5.2 Hz, 8H), 1.65-1.61 (m, 8H), 1.53-1.48 (m, 4H). ^{13}C-NMR (126 MHz, $CDCl_3$) δ 160.8, 160.6, 149.2, 148.6, 133.3, 123.8, 114.0, 98.3, 55.6, 55.3, 54.4, 26.4, 24.5. HRMS ((+)ESI-TOF): *m/z* calcd. for $C_{24}H_{32}N_4O_2$+H^+: 409.2598 [M+H]$^+$; found: 409.2590.

2-dma$_1$. Bis-*ortho*-fluorinated precursor **2-F** (50 mg, 0.18 mmol) and dimethylamine (ethanol solution, 127 µl, 0.72 mmol) were stirred in acetonitrile (2 ml) at 70°C temperature for 17 hours. The reaction mixture was then diluted with ethyl acetate, washed with water, dried with sodium sulfate, concentrated under reduced pressure and purified by column chromatography (5–10% ethyl acetate in hexane) to yield **2-dma$_1$** (13.5 mg, 25%) as well as **2-dma$_2$** (30 mg, 51%) as orange solids. **2-dma$_1$**: ^{1}H-NMR (500 MHz, $CDCl_3$) δ 7.87 (d, J = 8.6 Hz, 2H), 6.99 (d, J = 12.0 Hz, 2H), 6.30 (m, 1H), 6.25 (dd, J = 13.5, 2.6 Hz, 1H), 3.84 (d, J = 28.6 Hz, 6H), 2.90 (s, 6H). ^{13}C-NMR (126 MHz, $CDCl_3$) δ 161.7, 160.7 (d, J = 13 Hz), 155.0, 153.0, 151.9 (d, J = 6 Hz), 148.1, 128.0, 128.0, 124.2, 114.2, 99.4, 94.1, 93.9, 55.7, 44.9. ^{19}F-NMR (471 MHz, $CDCl_3$) δ -122.3 (d, J = 13.2 Hz). HRMS ((+)ESI-TOF): *m/z* calcd. for $C_{16}H_{18}FN_3O_2$+Na^+: 326.1275 [M+Na]$^+$; found: 326.1288. **2-dma$_2$**: ^{1}H-NMR (500 MHz, $CDCl_3$) δ 7.83 (d, J = 9.2 Hz, 2H), 6.97 (d, J = 9.2 Hz, 2H), 6.10 (s, 2H), 3.85 (d, J = 10.3 Hz, 6H), 2.87 (s, 12H). ^{13}C-NMR (126 MHz, $CDCl_3$) δ 161.5, 160.3, 150.6, 148.8, 129.4, 123.4, 114.1, 94.9, 55.6, 55.3, 44.8. HRMS ((+)ESI-TOF): *m/z* calcd. for $C_{18}H_{24}N_4O_2$+H^+: 329.1972 [M+H]$^+$; found: 329.1961.

2-prol$_1$. Bis-*ortho*-fluorinated precursor **2-F** (100 mg, 0.36 mmol) and L-prolinol (175 µl, 1.8 mmol) were stirred in acetonitrile (2 ml) at room temperature for 2 hours. The reaction mixture was then concentrated under reduced pressure and purified by column chromatography (50% ethyl acetate in hexane) to yield **2-prol$_1$** (78.4 mg, 61%) as an orange-brown crystalline product. ^{1}H-NMR (500 MHz, $CDCl_3$) δ 7.78 (d, J = 8.6 Hz, 2H), 6.98 (d, J = 9.2 Hz, 2H), 6.25 (s, 1H), 6.18 (dd, J = 13.2, 2.3 Hz, 1H), 4.05-4.05 (m, 1H), 3.86 (s, 3H), 3.79 (s, 3H), 3.72-3.72 (m, 1H), 3.52-3.52 (m, 2H), 3.15-3.15 (m, 1H), 2.45 (br, 1H), 2.01-2.01 (m, 2H), 1.89-1.89 (m, 1H), 1.80-1.80 (m, 1H). ^{13}C-NMR (126 MHz, $CDCl_3$) δ 161.7, 160.7 (d, J = 14 Hz), 156.5, 154.5, 147.8, 145.9, 127.3 (d, J = 7 Hz), 124.1, 114.4, 98.0, 92.7 (d, J = 24 Hz), 62.8, 60.8, 55.7, 55.6, 54.5, 28.4, 24.4. ^{19}F-NMR (471 MHz, $CDCl_3$) δ -122.2 (d, J = 12.4 Hz). HRMS ((+)ESI-TOF): *m/z* calcd. for $C_{19}H_{22}FN_3O_3$+Na^+: 382.1537 [M+Na]$^+$; found: 382.1537.

2-pres$_1$. Bis-*ortho*-fluorinated precursor **2-F** (200 mg, 0.72 mmol), L-proline methyl ester hydrochloride (478 mg, 2.9 mmol) and potassium carbonate (400 mg, 2.9 mmol) were stirred in acetonitrile (4 ml) at room temperature for 21 hours. The reaction mixture was then diluted with ethyl acetate, washed with water, dried with magnesium sulfate, concentrated under reduced pressure and purified by column chromatography (0–50% ethyl acetate in dichloromethane) to yield **2-pres$_1$** (97 mg, 35%) as an orange-brown crystalline product. ^{1}H-NMR (500 MHz, $CDCl_3$) δ 7.70 (d, J = 8.6 Hz, 2H), 6.97 (d, J = 9.2 Hz, 2H), 6.12 (s, 2H), 4.68-4.78 (m, 1H), 3.84 (s, 3H), 3.78 (s, 3H), 3.63-3.69 (m, 1H), 3.48-3.57 (m, 1H), 3.44 (s, 3H), 2.20-2.34 (m, 1H), 1.88-2.11 (m, 3H). ^{13}C-NMR (126 MHz, $CDCl_3$) δ 173.9, 161.4, 160.5 (d, J = 14 Hz), 155.0, 152.9, 147.9, 146.6, 146.6, 126.6 (d, J = 7 Hz), 124.3, 114.0, 96.6, 92.1 (d, J = 25 Hz), 63.8, 55.6, 55.5, 51.9, 51.8, 31.7, 23.3. ^{19}F-NMR (471 MHz, $CDCl_3$) δ -123.4 (d, J = 12.4 Hz). HRMS ((+)ESI-TOF): *m/z* calcd. for $C_{20}H_{22}FN_3O_4$+Na^+: 410.1487 [M+Na]$^+$; found: 410.1499.

2-pram$_1$. Bis-*ortho*-fluorinated precursor **2-F** (100 mg, 0.36 mmol) and L-prolinol (175 µl, 1.8 mmol) were stirred in acetonitrile (2 ml) at room temperature for 2 hours. The reaction mixture was then concentrated under reduced pressure and purified by column chromatography (50% ethyl acetate in hexane) to yield **2-pram$_1$** (78.4 mg, 59%) as an orange-brown crystalline product. ^{1}H-NMR (500 MHz, DMSO-D_6) δ 7.70 (d, J = 9.2 Hz, 2H), 7.29 (s, 1H), 7.03 (d, J = 8.6 Hz, 2H), 6.99 (s, 1H), 6.20 (dd, J = 14.3, 2.3 Hz, 1H), 6.05 (s, 1H), 4.24 (m, 1H), 3.80 (s, 3H), 3.73 (s, 3H), 3.64-3.71 (m, 1H), 3.37-3.47 (m, 1H), 2.09-2.21 (m, 1H), 1.71-1.93 (m, 3H). ^{13}C-NMR (126 MHz, DMSO-D_6) δ 175.1, 161.5, 160.5, 160.4, 155.1, 153.1, 147.7, 147.2, 125.8, 124.5, 114.9, 96.9, 92.0, 91.8, 64.9, 56.1, 56.0, 53.8, 31.6, 24.5. ^{19}F-NMR (471 MHz, DMSO-D_6) δ -122.6 (d, J = 13.2 Hz). HRMS ((+)ESI-TOF): *m/z* calcd. for $C_{19}H_{21}FN_4O_3$+Na^+: 395.1490 [M+Na]$^+$; found: 395.1506.

3-pip$_1$. Bis-*ortho*-fluorinated precursor **3-F** (16 mg, 0.057 mmol) and piperidine (110 µl, 1.1 mmol) were stirred in acetonitrile (1 ml) at room temperature for 20 hours, after which another 110 µl of piperidine was added and the reaction mixture stirred for another 2 hours. The crude mixture was concentrated under reduced pressure and purified by column chromatography (20% ethyl acetate in hexane) to yield **3-pip$_1$** (20.5 mg, quantitative) as a red solid. ^{1}H-NMR (500 MHz, $CDCl_3$) δ 7.77 (t, J = 9.2 Hz, 1H), 7.71 (d, J = 9.2 Hz, 1H), 6.69-6.79 (2H), 6.56 (d, J = 2.3 Hz, 1H), 6.51 (dd, J = 8.9, 2.6 Hz, 1H), 3.85 (s, 3H), 3.84 (s, 3H), 3.19 (t, J = 5.4 Hz, 4H), 1.82-1.78 (m, 4H), 1.64-1.59 (m, 2H). ^{13}C-NMR (126 MHz, $CDCl_3$) δ 162.9, 162.3, 162.3, 160.0, 153.4, 139.4, 135.6, 135.5, 118.8, 118.6, 110.8, 106.6, 104.3, 102.1, 101.9, 55.9, 55.5, 54.7, 26.4, 24.5. ^{19}F-NMR (471 MHz, $CDCl_3$) δ -122.1 (dd, J = 12.4, 7.9 Hz). HRMS ((+)ESI-TOF): *m/z* calcd. for $C_{19}H_{22}FN_3O_2$+H^+: 344.1769 [M+H]$^+$; found: 344.1756.

3-dma$_1$. Bis-*ortho*-fluorinated precursor **3-F** (30 mg, 0.11 mmol) and dimethylamine (ethanol solution, 76 µl, 0.43 mmol) were stirred in acetonitrile (1.5 ml) at 70°C for 24 hours. The reaction mixture was then concentrated under reduced pressure and purified by column chromatography (0–20% ethyl acetate in hexane) to yield **3-dma$_1$** (31 mg, 95%) as an orange solid. ^{1}H-NMR (500 MHz, $CDCl_3$) δ 7.65-7.79 (m, 2H), 6.67-6.80 (m, 2H), 6.40-6.54 (m, 2H), 3.84 (s, 6H), 3.06 (s. 6H). ^{13}C-NMR (126 MHz, $CDCl_3$) δ 162.8, 162.2, 162.1, 161.8, 159.8, 152.7, 138.6, 135.6, 135.6, 118.9, 118.6, 110.7, 105.8, 102.9, 102.0, 101.8, 55.9, 55.5, 45.2. ^{19}F-NMR (471 MHz, $CDCl_3$) δ -122.2 (dd, J = 11.9, 8.4 Hz). HRMS ((+)ESI-TOF): *m/z* calcd. for $C_{16}H_{18}FN_3O_2$+H^+: 304.1456 [M+H]$^+$; found: 304.1433.

3-prol$_1$. Bis-*ortho*-fluorinated precursor **3-F** (16 mg, 0.051 mmol) and L-prolinol (24.8 µl, 0.25 mmol) were stirred in acetonitrile (1 ml) at room temperature for 20 hours. The reaction mixture was then heated up to 45°C and stirred for another 22 hours. The crude mixture was concentrated under reduced pressure and purified by column chromatography (dichloromethane) to yield **3-prol$_1$** (9.0 mg, 49%) as an orange-brown crystalline product, as well as some unreacted **3-F**. ^{1}H-NMR (500 MHz, $CDCl_3$) δ 7.75 (d, J = 9.2 Hz, 1H), 7.57 (t, J = 8.6 Hz, 1H), 6.76-6.71 (m, 2H), 6.36 (s, 2H), 4.39 (s, 1H), 3.83 (d, J = 5.2 Hz, 6H), 3.69 (s, 2H), 3.49 (s, 1H), 1.75-2.15 (m, 5H). ^{13}C-NMR (126 MHz, $CDCl_3$) δ 162.9, 161.7, 147.9, 137.1, 135.8, 119.5, 118.9, 110.6, 104.5, 102.2, 102.1, 100.9, 63.3, 61.4, 55.9, 55.5, 54.0, 28.6, 23.8. ^{19}F-NMR (471 MHz, $CDCl_3$) δ -122.1 (dd, J = 11.9, 9.3 Hz). HRMS ((+)ESI-TOF): *m/z* calcd. for $C_{19}H_{22}FN_3O_3$+Na^+: 382.1537 [M+Na]$^+$; found: 382.1530.

3-pres$_1$. Bis-*ortho*-fluorinated precursor **3-F** (43.7 mg, 0.14 mmol), L-proline methyl ester hydrochloride (116 mg, 0.7 mmol) and potassium carbonate (110 mg, 0.8 mmol) were stirred in acetonitrile (1 ml) at room temperature for 20 hours. The reaction mixture was then heated up to 45°C

and stirred for another 22 hours. The crude mixture was concentrated under reduced pressure and purified by column chromatography (dichloromethane) to yield **3-pres$_1$** (6.5 mg, 12%) as an orange-brown crystalline product, as well as some unreacted **3-F**. ^{1}H-NMR (500 MHz, $CDCl_3$) δ 7.77 (d, J = 9.2 Hz, 1H), 7.50 (t, J = 9.2 Hz, 1H), 6.64-6.81 (2H), 6.20-6.40 (2H), 5.03 (q, J = 4.0 Hz, 1H), 3.84 (s, 3H), 3.84 (s, 3H), 3.73-3.80 (1H), 3.65 (dd, J = 16.6, 6.9 Hz, 1H), 3.45 (s, 3H), 2.28-2.41 (1H), 2.12-2.23 (1H), 1.97-2.08 (2H). ^{13}C-NMR (126 MHz, $CDCl_3$) δ 173.9, 163.1, 161.5 (d, J = 10.9 Hz), 159.3, 147.0, 136.4, 135.6 (d, J = 6.0 Hz), 119.2, 110.2, 104.5, 101.8 (d, J = 24.1 Hz), 100.1, 64.4, 55.9, 55.4, 51.8, 51.6, 31.8, 29.8, 23.2. ^{19}F-NMR (471 MHz, $CDCl_3$) δ -122.1 (dd, J = 11.5, 8.8 Hz). HRMS ((+)ESI-TOF): *m/z* calcd. for $C_{20}H_{22}FN_3O_4$+H^+: 388.1667 $[M+H]^+$; found: 388.1669.

3-pram$_1$. Bis-*ortho*-fluorinated precursor **3-F** (54.7 mg, 0.174 mmol) and L-prolinamide (99 mg, 0.87 mmol) were stirred in acetonitrile (1 ml) at room temperature for 24 hours. The reaction mixture was then heated up to 45°C and stirred for another 24 hours. The crude mixture was filtered, concentrated under reduced pressure and purified by column chromatography (1% methanol in ethyl acetate) to yield **3-pram$_1$** (4.6 mg, 7.1%) as an orange-brown crystalline product, as well as some unreacted **3-F**. ^{1}H-NMR (500 MHz, $CDCl_3$) δ 7.81 (d, J = 9.2 Hz, 1H), 7.61 (t, J = 8.9 Hz, 1H), 6.73 (t, J = 10.0 Hz, 2H), 6.42 (d, J = 10.3 Hz, 1H), 6.36-6.36 (m, 1H), 6.30 (s, 1H), 5.31 (s, 1H), 4.68-4.68 (m, 1H), 3.86-3.86 (m, 1H), 3.83 (d, J = 3.4 Hz, 6H), 3.56 (q, J = 8.4 Hz, 1H), 2.30-2.30 (m, 2H), 1.93-2.10 (m, 3H). ^{13}C-NMR (126 MHz, $CDCl_3$) δ 176.8, 162.9, 146.9, 136.9, 119.7, 119.2, 110.3, 105.4, 102.2, 102.0, 100.6, 66.5, 55.9, 55.5, 53.4, 32.0, 23.9. ^{19}F-NMR (471 MHz, $CDCl_3$) δ -122.1 (dd, J = 11.5, 8.8 Hz). HRMS ((+)ESI-TOF): *m/z* calcd. for $C_{19}H_{21}FN_4O_3$+Na^+: 395.1490 $[M+Na]^+$; found: 395.1485.

3-pip$_2$. Bis-*ortho*-fluorinated precursor **3-F** (40 mg, 0.144 mmol) and piperidine (2.0 ml, 2.2 mmol) were stirred at 60°C for 24 hours. The crude mixture was diluted with ethyl acetate, washed three times with water, dried with sodium sulfate, concentrated under reduced pressure and purified by column chromatography (10% ethyl acetate in hexane) to yield **3-pip$_2$** (23 mg, 39%) as a red crystalline product. ^{1}H-NMR (500 MHz, $CDCl_3$) δ 7.69 (d, J = 9.2 Hz, 2H), 6.57 (d, J = 2.3 Hz, 2H), 6.53 (dd, J = 8.9, 2.6 Hz, 2H), 3.84 (s, 6H), 3.17 (t, J = 5.2 Hz, 8H), 1.85-1.80 (m, 8H), 1.64-1.60 (m, 4H). ^{13}C-NMR (126 MHz, $CDCl_3$) δ 162.1, 153.1, 139.5, 118.2, 106.5, 104.4, 55.5, 54.7, 26.4, 24.5. HRMS ((+)ESI-TOF): *m/z* calcd. for $C_{24}H_{32}N_4O_2$+H^+: 409.2598 $[M+H]^+$; found: 409.2595.

4-pyr$_1$, **4-pyr$_{2\text{-sym}}$** and **4-pyr$_{2\text{-asym}}$**. Tetra-*ortho*-fluorinated precursor **4-F** (31.1 mg, 0.1 mmol) and pyrrolidine (16.5 µl, 0.2 mmol) were stirred in acetonitrile (1 ml) at room temperature for 2 hours. The reaction mixture was then concentrated under reduced pressure and purified by column chromatography (10–20% ethyl acetate in hexane) to yield **4-pyr$_1$** (19 mg, 52%) as an orange solid, **4-pyr$_{2\text{-sym}}$** (4.0 mg, 9.6%) as a red solid and **4-pyr$_{2\text{-asym}}$** (4.0 mg, 9.6%) as an orange-brown solid. Unreacted **4-F** (5 mg, 16%) was also recovered. **4-pyr$_1$**: ^{1}H-NMR (500 MHz, $CDCl_3$) δ 6.53 (d, J = 10.9 Hz, 2H), 6.07-6.03 (m, 2H), 3.81 (d, J = 8.0 Hz, 6H), 3.47 (t, J = 6.6 Hz, 4H), 1.92-1.90 (m, 4H). ^{13}C-NMR (126 MHz, $CDCl_3$) δ 161.7 (d, J = 14.5 Hz), 159.9 (t, J = 13.9 Hz), 157.9 (d, J = 7.2 Hz), 155.9 (d, J = 7.2 Hz), 155.7, 149.3 (d, J = 6.0 Hz), 126.5 (t, J = 10.3 Hz), 126.2 (d, J = 6.0 Hz), 98.8, 98.6, 91.7, 91.5, 56.0, 55.5, 52.5, 25.9. ^{19}F-NMR (471 MHz, $CDCl_3$) δ -119.7 (d, J = 11.5 Hz, 2F), -119.8 (d, J = 14.1 Hz, 1F). HRMS ((+)ESI-TOF): *m/z* calcd. for $C_{18}H_{18}F_3N_3O_2$+K^+: 404.0983 $[M+K]^+$; found: 404.0968. **4-pyr$_{2\text{-sym}}$**: ^{1}H-NMR (500 MHz, $CDCl_3$) δ 5.57-6.11 (m, 4H), 3.79 (s, 6H), 3.45 (t, J = 6.6 Hz, 8H), 1.83-1.95 (m, 8H). Integrated over both isomers for every peak. ^{13}C-NMR (126 MHz, $CDCl_3$) δ 160.2 (d, J = 14.5 Hz), 154.0 (d, J = 257.1 Hz), 148.6 (d, J = 7.2 Hz), 126.3 (d, J = 7.2 Hz), 95.5, 91.0 (d, J = 25.4 Hz), 55.5, 52.4, 25.9. ^{19}F-NMR (471 MHz, $CDCl_3$) δ -122.8 (d, J = 14.1 Hz, 4F). HRMS ((+)ESI-TOF): *m/z* calcd. for $C_{22}H_{26}F_2N_4O_2$+Na^+: 439.1916 $[M+Na]^+$; found: 439.1905. **4-pyr$_{2\text{-asym}}$**: ^{1}H-NMR (500 MHz, $CDCl_3$) δ 6.48 (d, J = 10.9 Hz, 2H), 5.70 (s, 2H), 3.81 (s, 3H), 3.78 (s, 3H), 3.38-3.38 (m, 8H), 1.90-1.90 (m, 8H). ^{13}C-NMR could not be acquired due to decomposition. ^{19}F-NMR (471 MHz, $CDCl_3$) δ -121.3 (d, J = 10.6 Hz). HRMS ((+)ESI-TOF): *m/z* calcd. for $C_{22}H_{26}F_2N_4O_2$+H^+: 417.2097 $[M+H]^+$; found: 417.2080.

4-pip$_1$, **4-pip$_{2\text{-sym}}$** and **4-pip$_{2\text{-asym}}$**. Tetra-*ortho*-fluorinated precursor **4-F** (31.1 mg, 0.1 mmol) and piperidine (39.4 µl, 0.4 mmol) were stirred in acetonitrile (1 ml) at 50°C for 2 hours. The reaction mixture was then concentrated under reduced pressure and purified by column chromatography (10–20% ethyl acetate in hexane) to yield **4-pip$_1$** (4.2 mg, 11%) as an orange solid, **4-pip$_{2\text{-sym}}$** (24 mg, 54%) as a red solid and **4-pip$_{2\text{-asym}}$** (4.8 mg, 11%) as an orange-brown solid. **4-pip$_3$** (3.4 mg, 6.7%) was also recovered. **4-pip$_1$**: ^{1}H-NMR (500 MHz, $CDCl_3$) δ 6.56 (d, J = 10.9 Hz, 2H), 6.37-6.37 (m, 1H), 6.30 (dd, J = 13.7, 2.9 Hz, 1H), 3.83 (d, J = 12.0 Hz, 6H), 3.07-3.07 (m, 4H), 1.72-1.72 (m, 4H), 1.52-1.60 (m, 2H under H_2O). ^{13}C-NMR (126 MHz, CDCl3) δ 161.8 (d, J = 13.3 Hz), 161.7, 161.0, 158.3 (d, J = 7.2), 158.2, 156.2, 156.2 (d, J = 8.5), 155.1, 153.3, 129.7, 100.7, 98.9, 98.7, 95.2, 95.0, 56.1, 55.7, 54.4, 26.1, 24.3. ^{19}F-NMR (471 MHz, CDCl3) δ -118.3 (d, J = 19.6 Hz, 2F), -120.7 (d, J = 14.1 Hz, 1F). HRMS ((+)ESI-TOF): *m/z* calcd. for $C_{19}H_{20}F_3N_3O_2$+Na^+: 402.1400 $[M+Na]^+$; found: 402.1376. **4-pip$_{2\text{-sym}}$**: ^{1}H-NMR (500 MHz, $CDCl_3$) δ 6.41 (s, 2H), 6.30 (d, J = 13.7 Hz, 2H), 3.81 (s, 6H), 3.05 (s, 8H), 1.73 (s, 8H). ^{13}C-NMR (126 MHz, $CDCl_3$) δ 160.9 (d, J = 15 Hz), 153.9, 153.3 (d, J = 268 Hz), 129.8, 100.9, 95.3, 95.1, 55.6, 54.7, 26.1, 24.3. ^{19}F-NMR (471 MHz, $CDCl_3$) δ -120.3 (d, J = 14.1 Hz). HRMS ((+)ESI-TOF): *m/z* calcd. for $C_{24}H_{30}F_2N_4O_2$+Na^+: 467.2229 $[M+Na]^+$; found: 467.2207. **4-pip$_{2\text{-asym}}$**: ^{1}H-NMR (500 MHz, $CDCl_3$) δ 6.52 (d, J = 10.3 Hz, 2H), 6.19 (s, 2H), 3.81 (two overlapping s, 6H), 3.02 (m, 8H), 1.67 (m, 8H), 1.53 (m, 4H). ^{13}C-NMR (126 MHz, $CDCl_3$) δ 162.2, 158.9, 157.4, 155.4, 150.5, 132.6, 98.6 (d, J = 27.7 Hz), 96.8, 56.0, 55.3, 54.5, 25.9, 24.5. ^{19}F-NMR (471 MHz, $CDCl_3$) δ -120.0 (d, J = 10.6 Hz). HRMS ((+)ESI-TOF): *m/z* calcd. for $C_{24}H_{30}F_2N_4O_2$+H^+: 445.2410 $[M+H]^+$; found: 445.2392.

4-dma$_1$, **4-dma$_{2\text{-sym}}$** and **4-dma$_{2\text{-asym}}$**. Tetra-*ortho*-fluorinated precursor **4-F** (31.1 mg, 0.1 mmol) and dimethylamine (5.6 M in ethanol, 37 µl, 0.2 mmol) were stirred in acetonitrile (1 ml) at room temperature for 2.5 hours. The reaction mixture was then concentrated under reduced pressure and purified by column chromatography (0–10% ethyl acetate in dichloromethane) to yield **4-dma$_1$** (8.4 mg, 25%) as an orange solid, **4-dma$_{2\text{-sym}}$** (6.8 mg, 19%) as an orange-red solid and **4-dma$_{2\text{-asym}}$** (1.0 mg, 2.7%) as a red-brown solid. Unreacted **4-F** (14.9 mg, 47%) was also recovered. **4-dma$_1$**: ^{1}H-NMR (500 MHz, $CDCl_3$) δ 6.55 (d, J = 10.3 Hz, 2H), 6.28-6.22 (m, 2H), 3.83 (s, 3H), 3.82 (s, 3H), 2.93 (s, 6H). ^{13}C-NMR (126 MHz, $CDCl_3$) δ 161.8, 161.7, 160.8, 158.1, 156.1, 155.5, 153.4, 152.9, 152.8, 147.2, 128.7, 99.2, 98.9, 98.7, 94.2, 94.0, 56.1, 55.7, 44.9. ^{19}F-NMR (471 MHz, $CDCl_3$) δ -118.8 (d, J = 11.5 Hz, 2F), -120.2 (d, J = 14.1 Hz, 1F). HRMS ((+)ESI-TOF): *m/z* calcd. for $C_{16}H_{16}F_3N_3O_2$+H^+: 340.1267 $[M+H]^+$; found: 340.1264. **4-dma$_{2\text{-sym}}$**: ^{1}H-NMR (500 MHz, $CDCl_3$) δ 6.31 (m, 2H), 6.24 (dd, J = 14.0, 2.6 Hz, 2H), 3.81 (s, 6H), 2.90 (s, 12H). ^{13}C-NMR (126 MHz, $CDCl_3$) δ 160.8 (d, J = 14.5 Hz), 154.7, 153.1 (d, J = 6.0 Hz), 129.1 (d, J = 6.0 Hz), 99.6, 94.3 (d, J = 26.6 Hz), 55.6, 45.1. ^{19}F-NMR (471 MHz, $CDCl_3$) δ -120.7 (d, J = 13.2 Hz). HRMS ((+)ESI-TOF): *m/z* calcd. for $C_{18}H_{22}F_2N_4O_2$+Na^+: 387.1603 $[M+Na]^+$; found: 387.1594. **4-dma$_{2\text{-asym}}$**: ^{1}H-NMR (500 MHz, $CDCl_3$) δ 6.50 (d, J = 10.9 Hz, 2H), 5.95 (s, 2H), 3.83 (s, 3H), 3.79 (s, 3H), 2.93 (s, 12H). ^{13}C-NMR (126 MHz, $CDCl_3$) δ 163.2, 152.0, 128.4, 98.7, 98.4, 93.0, 55.9, 44.5, 29.8. ^{19}F-NMR (471 MHz, $CDCl_3$) δ -120.2 (d, J = 10.6 Hz). HRMS ((+)ESI-TOF): *m/z* calcd. for $C_{18}H_{22}F_2N_4O_2$+H^+: 365.1784 $[M+H]^+$; found: 365.1762.

4-prol$_1$ and **4-prol$_{2\text{-sym}}$**. Tetra-*ortho*-fluorinated precursor **4-F** (31.1 mg, 0.1 mmol) and L-prolinol (39 µl, 0.4 mmol) were stirred in acetonitrile (1 ml) at room temperature for 15 hours. The reaction mixture was then concentrated under reduced pressure and purified by column chromatography (20% ethyl acetate in hexane) to yield **4-prol$_1$** (2.0 mg, 5.1%) as an orange solid and **4-prol$_{2\text{-sym}}$** (8.4 mg, 18%) as a red solid. Further substituted products decomposed during the reaction or purification and could not be isolated. **4-prol$_1$**: ^{1}H-NMR (500 MHz, $CDCl_3$) δ 6.55 (d, J = 10.3 Hz, 2H), 6.22 (s, 1H), 6.16 (dd, J = 13.7, 2.3 Hz, 1H), 4.10-4.20 (1H), 3.82 (s, 3H), 3.80 (s, 3H), 3.67-3.72 (1H, overlapping with the methoxy peak of the cis-isomer), 3.49-3.61 (2H), 3.13-3.22 (1H), 1.75-2.22 (5H). ^{13}C-NMR (126 MHz, $CDCl_3$) δ 161.7 (d, J = 15.7 Hz), 160.6 (t, J = 13.9 Hz), 157.9 (d, J = 7.2 Hz), 156.6 (s), 155.9 (d, J = 7.2 Hz), 154.6 (s), 146.9 (s), 127.9 (d, J = 6.0 Hz), 126.1 (t, J = 9.7 Hz), 98.9 (d, J = 27.8 Hz), 97.5 (s), 92.8 (d, J = 25.4 Hz), 62.9 (s), 60.7 (s), 56.1 (s), 55.6 (s), 54.2 (s), 28.3 (s), 24.2 (s). ^{19}F-NMR (471 MHz, $CDCl_3$) δ -119.6 (d, J = 11.5 Hz, 2F), -120.8 (d, J = 14.1 Hz, 1F). HRMS ((+)ESI-TOF): *m*/*z* calcd. for $C_{19}H_{20}F_3N_3O_3$+Na^+: 418.1349 [M+Na]$^+$; found: 418.1334. **4-prol$_{2\text{-sym}}$**: ^{1}H-NMR (500 MHz, $CDCl_3$) δ 5.85 (s, 2H), 5.78 (dd, J = 13.2, 2.3 Hz, 2H), 3.54 (m, 2H), 3.36 (s, 6H), 3.15 (m, 2H), 3.01 (m, 2H), 2.83-2.78 (m, 2H), 2.55 (m, 2H), 1.44-1.58 (m, 4H), 1.33-1.44 (m, 2H), 1.22-1.33 (m, 2H), 1.08-1.23 (s, 2H). ^{13}C-NMR (126 MHz, $CDCl_3$) δ 160.4 (d, J = 14.5 Hz), 156.3, 154.3, 145.2, 128.1 (d, J = 8.5 Hz, 98.0, 92.6 (d, J = 25.4 Hz), 62.0, 60.0, 55.2, 54.7, 27.1, 24.4. ^{19}F-NMR (471 MHz, $CDCl_3$) δ -123.4 (d, J = 13.2 Hz). HRMS ((+)ESI-TOF): *m*/*z* calcd. for $C_{24}H_{30}F_2N_4O_2$+Na^+: 499.2127 [M+Na]$^+$; found: 499.2109.

4-pres$_1$. Tetra-*ortho*-fluorinated precursor **4-F** (31.4 mg, 0.1 mmol) and L-proline methyl ester hydrochloride (66.4 mg, 0.4 mmol) were stirred in acetonitrile (1 ml) at 50°C for 11 hours and then at RT for another 16 hours. The reaction mixture was then diluted with ethyl acetate, washed with water, dried with magnesium sulfate, concentrated under reduced pressure and purified by column chromatography (0–5% methanol in dichloromethane) to yield **4-pres$_1$** (18.0 mg, 42%) as an orange solid as well as unreacted starting material (not weighed). ^{1}H-NMR (500 MHz, $CDCl_3$) δ 6.55 (d, J = 10.3 Hz, 2H), 6.12-6.08 (m, 2H), 4.72-4.87 (m, 1H), 3.83 (s, 3H), 3.82 (s, 3H), 3.63-3.70 (m, 1H), 3.57 (dd, J = 16.9, 7.2 Hz, 1H), 3.32 (s, 3H), 2.20-2.31 (m, 1H), 2.05-2.11 (m, 1H), 1.91-2.02 (m, 2H). ^{13}C-NMR (126 MHz, $CDCl_3$) δ 173.6,152.8, 161.5 (d, J = 14.5 Hz), 159.5 (t, J = 13.9 Hz), 157.0 (d, J = 7.2 Hz), 154.9 (d, J = 7.2 Hz), 147.5 (d, J = 6.0 Hz), 126.1 (t, J = 11.5 Hz), 125.7 (d, J = 6.0 Hz), 98.0 (d, J = 26.6 Hz), 95.7, 91.9 (d, J = 25.4 Hz), 63.6, 55.6, 55.2, 51.5, 51.2, 31.2, 22.6. ^{19}F-NMR (471 MHz, $CDCl_3$) δ -120.5 (d, J = 14.1 Hz, 1F), -121.1 (d, J = 10.6 Hz, 2F). HRMS ((+)ESI-TOF): *m*/*z* calcd. for $C_{20}H_{20}F_3N_3O_4$+K^+: 462.1037 [M+K]$^+$; found: 462.1026.

4-pres$_{2\text{-sym}}$. Tetra-*ortho*-fluorinated precursor **4-F** (31.4 mg, 0.1 mmol) and L-proline methyl ester hydrochloride (166 mg, 1.0 mmol) were stirred in acetonitrile (1 ml) at 60°C for 20 hours. The reaction mixture was then diluted with ethyl acetate, washed with water, dried with magnesium sulfate, concentrated under reduced pressure and purified by column chromatography (0–5% methanol in ethyl acetate) to yield **4-pres$_{2\text{-sym}}$** (6.0 mg, 13%) as an orange solid. ^{1}H-NMR (500 MHz, $CDCl_3$) δ 6.04-6.13 (m, 4H), 4.77 (dd, J = 8.6, 2.9 Hz, 2H), 3.80 (s, 6H), 3.73 (d, J = 2.3 Hz, 2H), 3.70 (d, J = 4.6 Hz, 2H, overlapping with cis-isomer of the para-methoxy peak), 3.59-3.67 (m, 2H), 3.47-3.55 (m, 2H), 3.30 (s, 6H), 2.17-2.25 (m, 2H), 2.00-2.08 (m, 2H), 1.91-2.00 (m, 4H). ^{13}C-NMR (126 MHz, $CDCl_3$) δ 173.7, 160.5 (d, J = 14.5 Hz), 154.9, 152.8, 148.6, 146.7 (d, J = 6.0 Hz), 126.0 (d, J = 7.2 Hz), 95.8, 91.2 (d, J = 26.6 Hz), 88.0, 64.0, 55.5, 51.7, 51.5, 31.8, 22.8. ^{19}F-NMR (471 MHz, $CDCl_3$) δ -123.4 (d, J = 13.2 Hz). HRMS ((+)ESI-TOF): *m*/*z* calcd. for $C_{26}H_{30}F_2N_4O_6$+Na^+: 555.2026 [M+Na]$^+$; found: 555.2011.

4-pram$_1$, **4-pram$_{2\text{-sym}}$** and **4-pram$_{2\text{-asym}}$**. Tetra-*ortho*-fluorinated precursor **4-F** (31.4 mg, 0.1 mmol) and L-prolinamide (45.6 mg, 0.4 mmol) were stirred in acetonitrile (1 ml) at 50°C for 22 hours. The reaction mixture was then concentrated under reduced pressure and purified by column chromatography (0–5% methanol in ethyl acetate) to yield **4-pram$_1$** (19.7 mg, 48%) as an orange solid, **4-pram$_{2\text{-sym}}$** (13.1 mg, 26%) as a red solid and **4-pram$_{2\text{-asym}}$** (2.9 mg, 5.8%) as an orange-brown solid. **4-pram$_1$**: ^{1}H-NMR (500 MHz, $CDCl_3$) δ 6.61 (s, 1H), 6.55 (d, J = 12.0 Hz, 2H), 6.25 (d, J = 12.6 Hz, 2H), 5.30-5.52 (1H), 4.41 (t, J = 6.6 Hz, 1H), 3.83 (s, 3H), 3.80 (s, 3H), 3.60-3.73 (1H), 3.13-3.29 (1H), 2.29-2.41 (1H), 2.06-2.16 (1H), 1.82-2.02 (2H). ^{13}C-NMR (126 MHz, $CDCl_3$) δ 176.1, 161.5 (d, J = 14.5 Hz), 160.5 (t, J = 13.3 Hz), 157.6 (d, J = 7.2 Hz), 156.2, 155.5 (d, J = 7.2 Hz), 154.1, 146.5, 127.6, 125.6, 98.4 (d, J = 26.6 Hz), 97.2, 94.0 (d, J = 24.1 Hz), 64.3, 55.7, 55.6, 54.2, 31.4, 24.4. ^{19}F-NMR (471 MHz, $CDCl_3$) δ -120.0 (d, J = 12.4 Hz, 2F), -120.7 (d, J = 14.1 Hz, 1F). HRMS ((+)ESI-TOF): *m*/*z* calcd. for $C_{19}H_{19}F_3N_4O_3$+Na^+: 431.1301 [M+Na]$^+$; found: 431.1299. **4-pram$_{2\text{-sym}}$**: ^{1}H-NMR (500 MHz, $CDCl_3$) δ 6.38 (s, 2H), 6.22 (s, 2H), 6.19 (d, J = 13.7 Hz, 2H), 5.44 (s, 2H), 4.47-4.44 (m, 2H), 3.79 (s, 6H), 3.63 (dd, J = 15.2, 6.6 Hz, 2H), 3.33 (q, J = 7.6 Hz, 2H), 2.24-2.36 (m, 2H), 2.05-2.14 (m, 2H), 1.88-2.04 (m, 4H). ^{13}C-NMR (126 MHz, $CDCl_3$) δ 176.2, 160.5 (d, J = 14.5 Hz), 153.8 (d, J = 257.1 Hz), 147.0, 126.9, 97.3, 93.2 (d, J = 25.4 H), 65.0, 55.2, 53.5, 31.6, 24.0. ^{19}F-NMR (471 MHz, $CDCl_3$) δ -123.4 (d, J = 14.1 Hz). HRMS ((+)ESI-TOF): *m*/*z* calcd. for $C_{24}H_{28}F_2N_6O_4$+Na^+: 525.2032 [M+Na]$^+$; found: 525.2013. **4-pram$_{2\text{-asym}}$**: ^{1}H-NMR (500 MHz, $CDCl_3$) δ 6.91 (s, 2H), 6.54 (d, J = 10.3 Hz, 2H), 6.00 (s, 2H), 4.96 (s, 2H), 4.50 (q, J = 4.4 Hz, 2H), 3.81 (d, J = 4.0 Hz, 6H), 3.47-3.53 (m, 2H), 3.09 (dd, J = 16.9, 7.2 Hz, 2H), 2.26-2.36 (m, 2H), 2.08-2.17 (m, 2H), 1.84-1.98 (m, 4H). ^{13}C-NMR (126 MHz, $CDCl_3$) δ 176.4, 163.5, 158.7, 156.7, 146.3, 128.0, 98.2, 97.9, 91.6, 64.4, 55.6, 55.0, 52.7, 31.3, 24.1. ^{19}F-NMR (471 MHz, $CDCl_3$) δ -123.4 (d, J = 10.6 Hz). HRMS ((+)ESI-TOF): *m*/*z* calcd. for $C_{24}H_{28}F_2N_6O_4$+K^+: 541.1772 [M+K]$^+$; found: 541.1765.

4-pip$_3$ and **4-pip$_4$**. Tetra-*ortho*-fluorinated precursor **4-F** (45 mg, 0.143 mmol) was stirred in piperidine at 50°C for 4 hours. The reaction mixture was concentrated under reduced pressure and purified by column chromatography (20% ethyl acetate in hexane) to yield **4-pip$_3$** (31 mg, 43%) and **4-pip$_4$** (27 mg, 33%) as brownish red products. **4-pip$_3$**: ^{1}H-NMR (500 MHz, $CDCl_3$) δ 6.35 (s, 1H), 6.31 (dd, J = 12.6, 2.3 Hz, 1H), 6.25 (s, 2H), 3.84 (s, 3H), 3.81 (s, 3H), 2.92-3.09 (12H), 1.40-1.65 (18H). ^{13}C-NMR (126 MHz, $CDCl_3$) δ 160.2, 158.8, 158.7, 154.5, 152.5, 150.4, 150.3, 148.8, 134.2, 130.7, 130.6, 100.0, 97.0, 94.2, 94.0, 55.1, 54.8, 54.1, 53.1, 25.6, 25.6, 24.1, 23.9. ^{19}F-NMR (471 MHz, $CDCl_3$) δ -124.9 (d, J = 12.4 Hz). HRMS ((+)ESI-TOF): *m*/*z* calcd. for $C_{29}H_{40}FN_5O_2$+H^+: 510.3239 [M+H]$^+$; found: 510.3219. **4-pip$_4$**: ^{1}H-NMR (500 MHz, $CDCl_3$) δ 6.28 (s, 4H), 3.84 (s, 6H), 2.86-3.06 (16H), 1.32-1.52 (24H). ^{13}C-NMR (126 MHz, $CDCl_3$) δ 159.0, 148.3, 135.1, 97.5, 54.8, 54.1, 25.7, 24.0. HRMS ((+)ESI-TOF): *m*/*z* calcd. for $C_{34}H_{50}N_6O_2$+H^+: 575.4068 [M+H]$^+$; found: 575.4050.

Nuclear Magnetic Resonance spectra

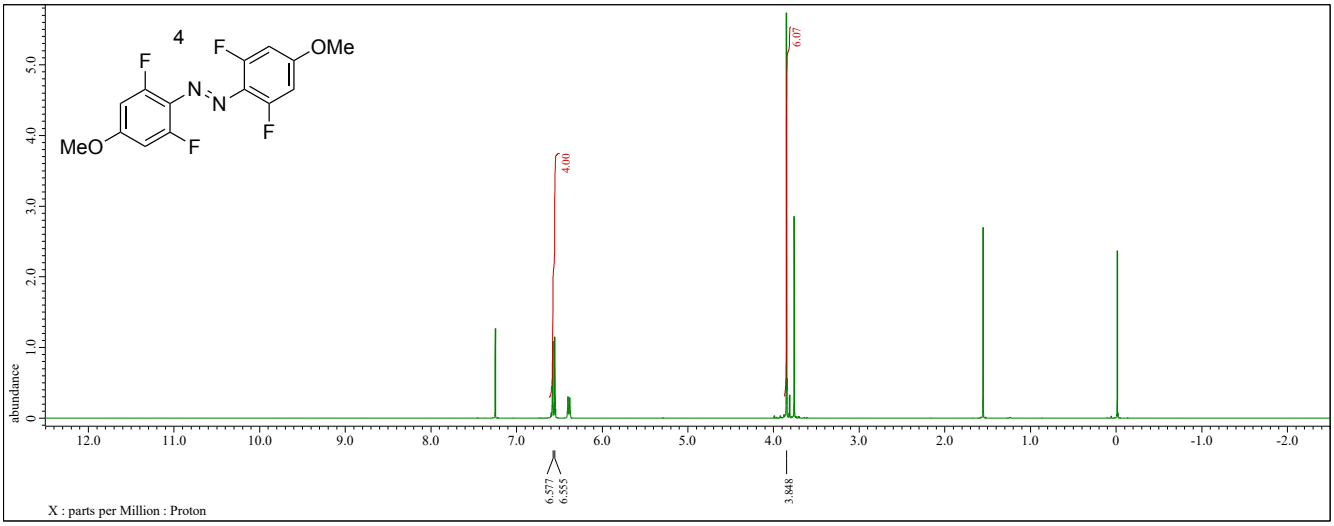

Figure S1. ^{1}H NMR spectrum of **4-F**.

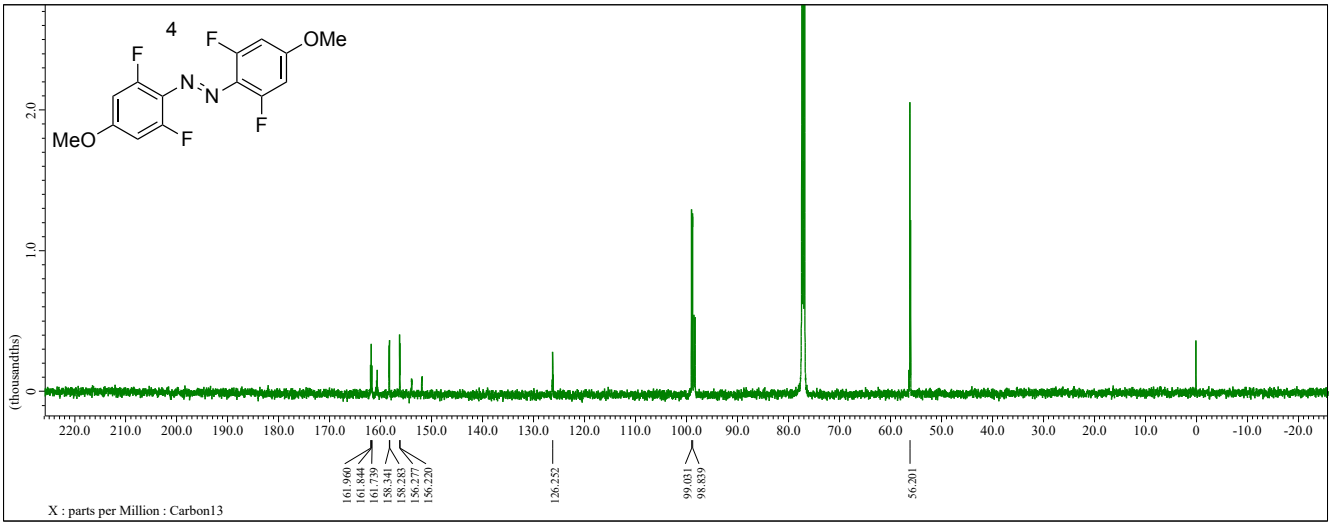

Figure S2. ^{13}C NMR spectrum of **4-F**.

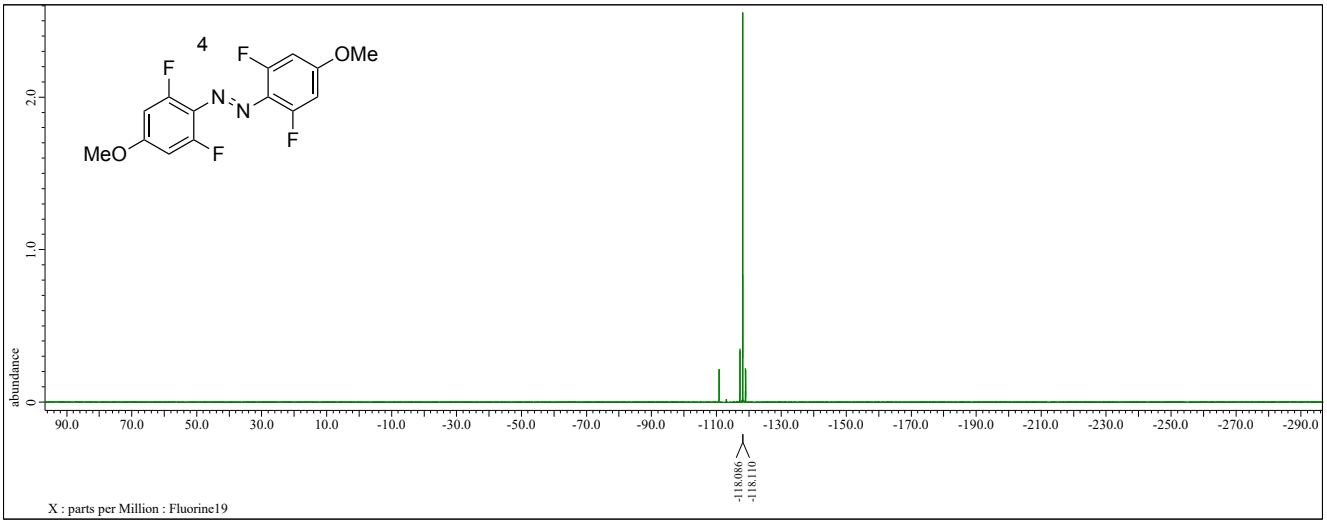

Figure S3. ^{19}F NMR spectrum of **4-F**.

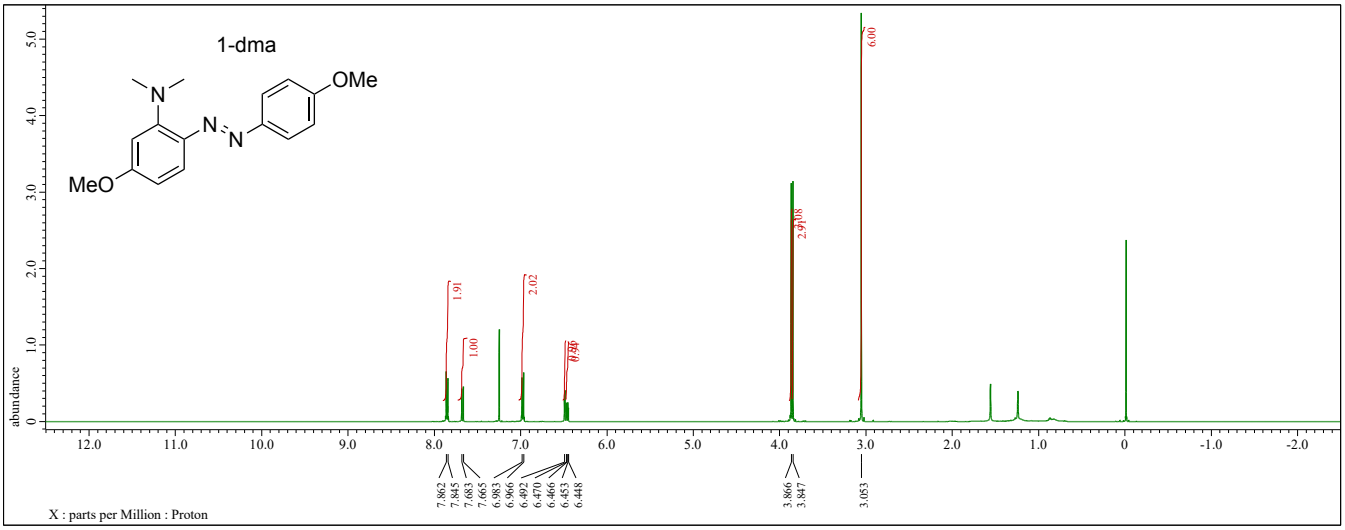

Figure S4. ^{1}H NMR spectrum of **1-dma**.

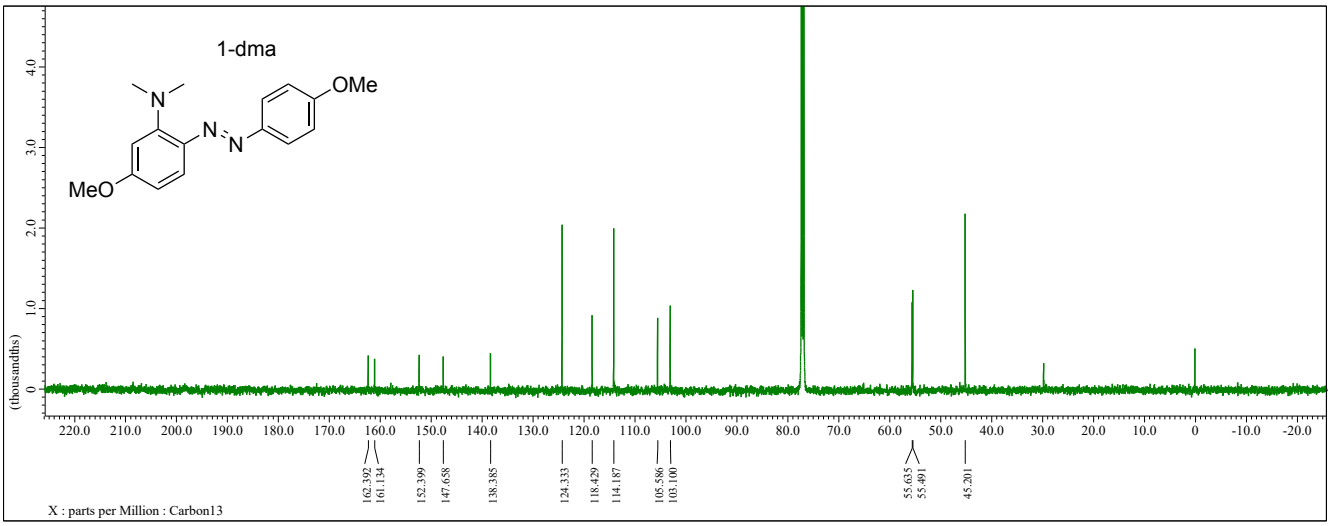

Figure S5. ^{13}C NMR spectrum of **1-dma**.

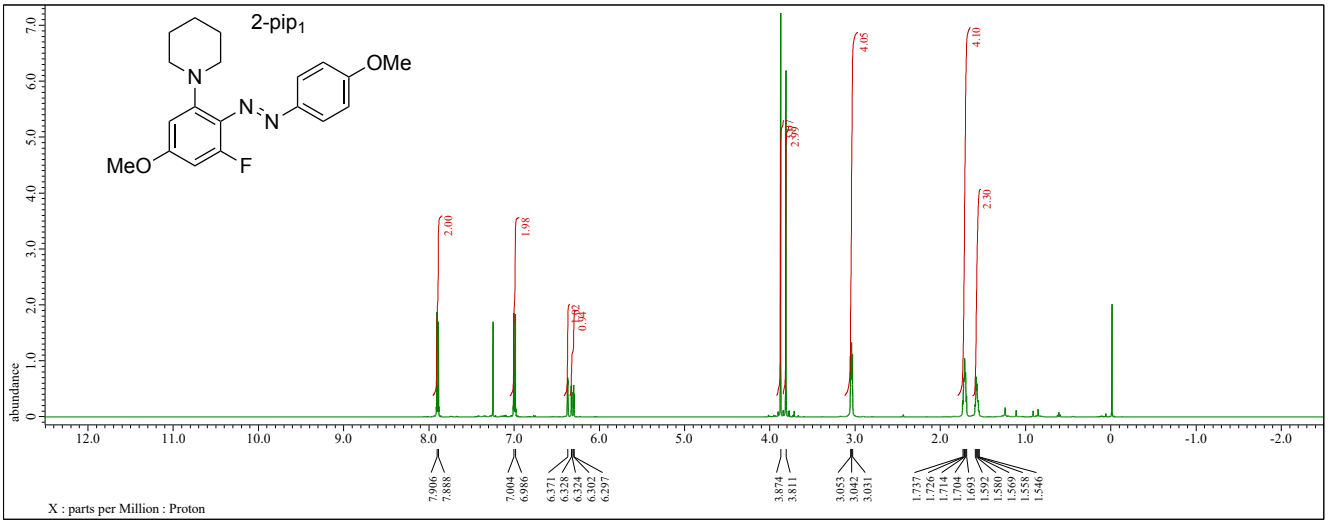

Figure S6. ^{1}H NMR spectrum of **2-pip$_1$**.

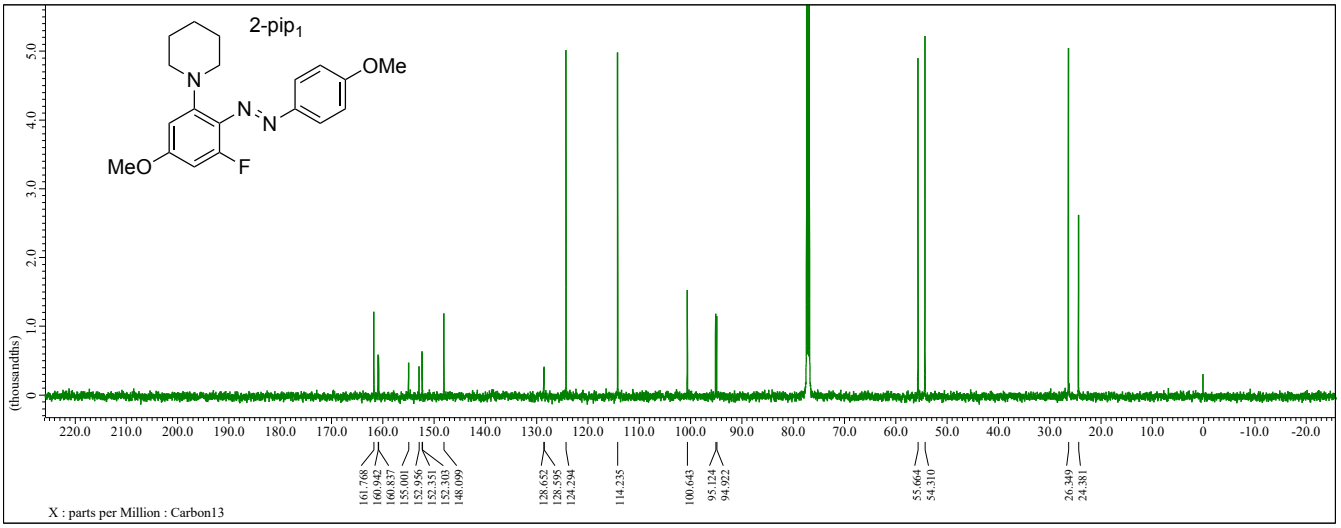

Figure S7. ^{13}C NMR spectrum of **2-pip$_1$**.

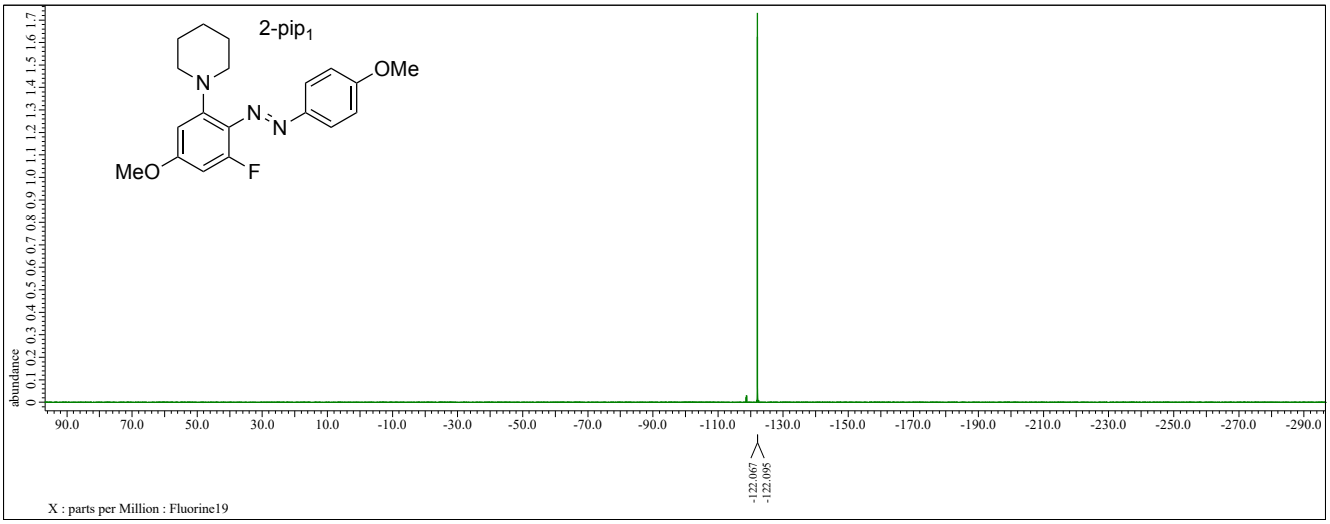

Figure S8. ^{19}F NMR spectrum of **2-pip$_1$**.

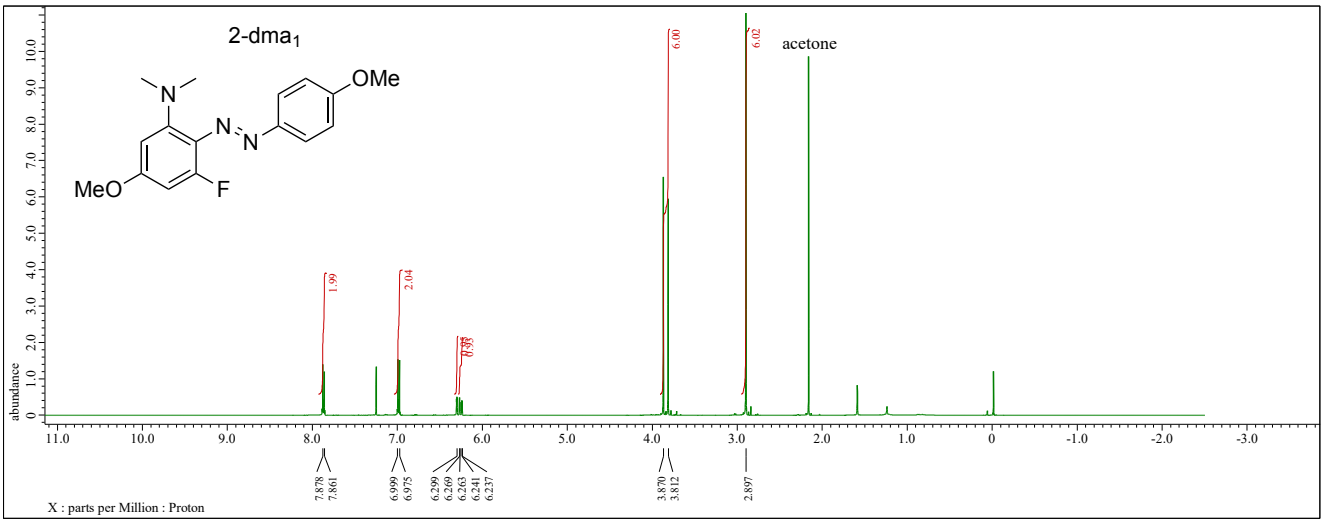

Figure S9. ^{1}H NMR spectrum of **2-dma$_1$**.

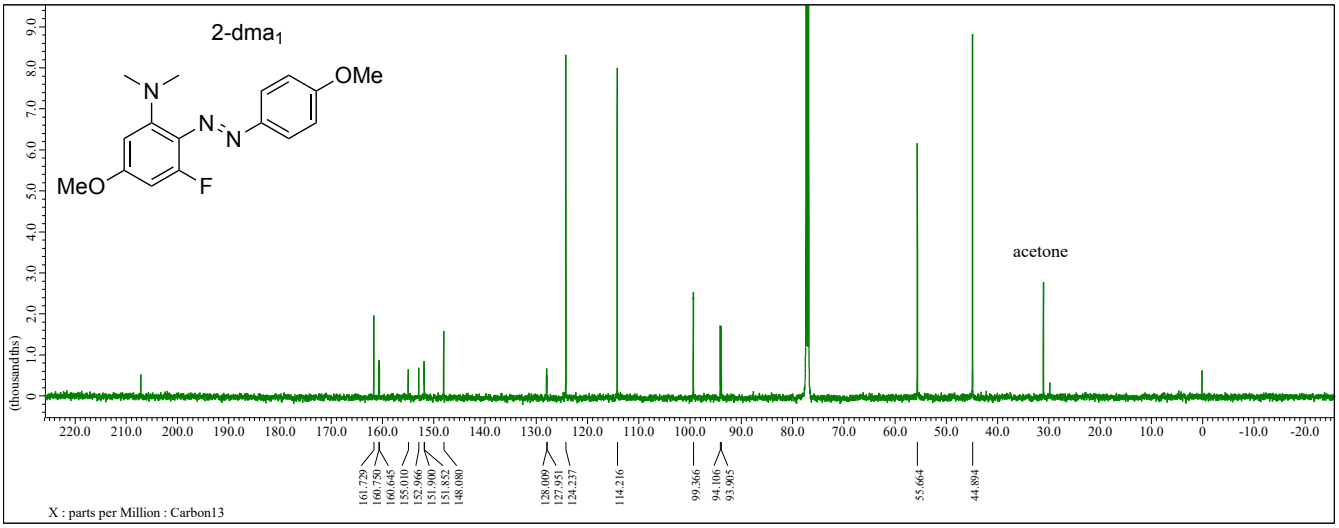

Figure S10. ^{13}C NMR spectrum of **2-dma$_1$**.

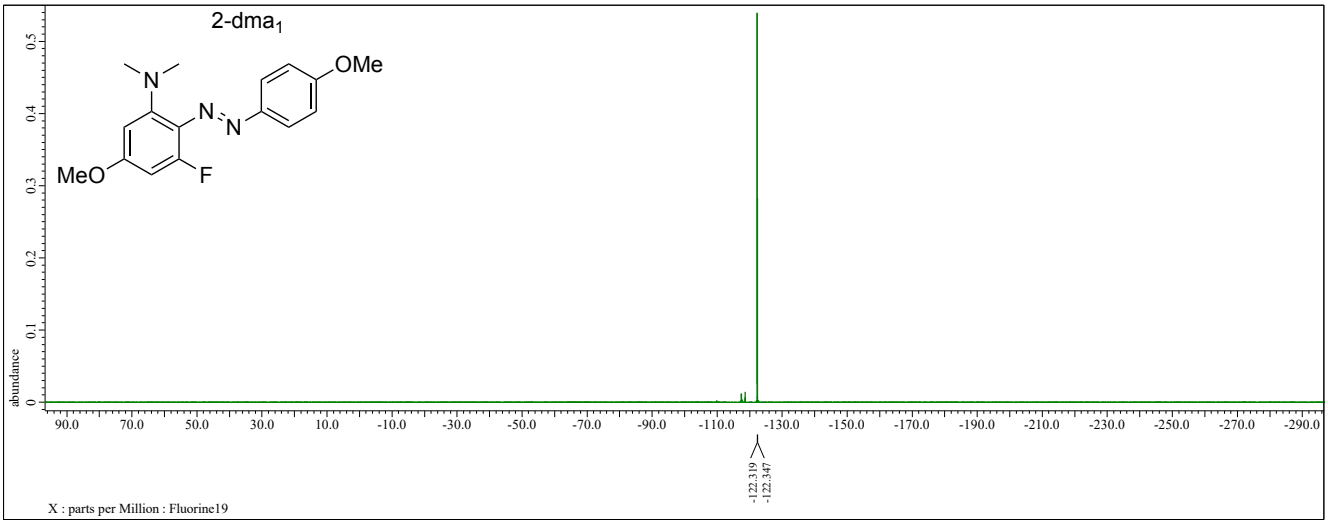

Figure S11. ^{19}F NMR spectrum of **2-dma$_1$**.

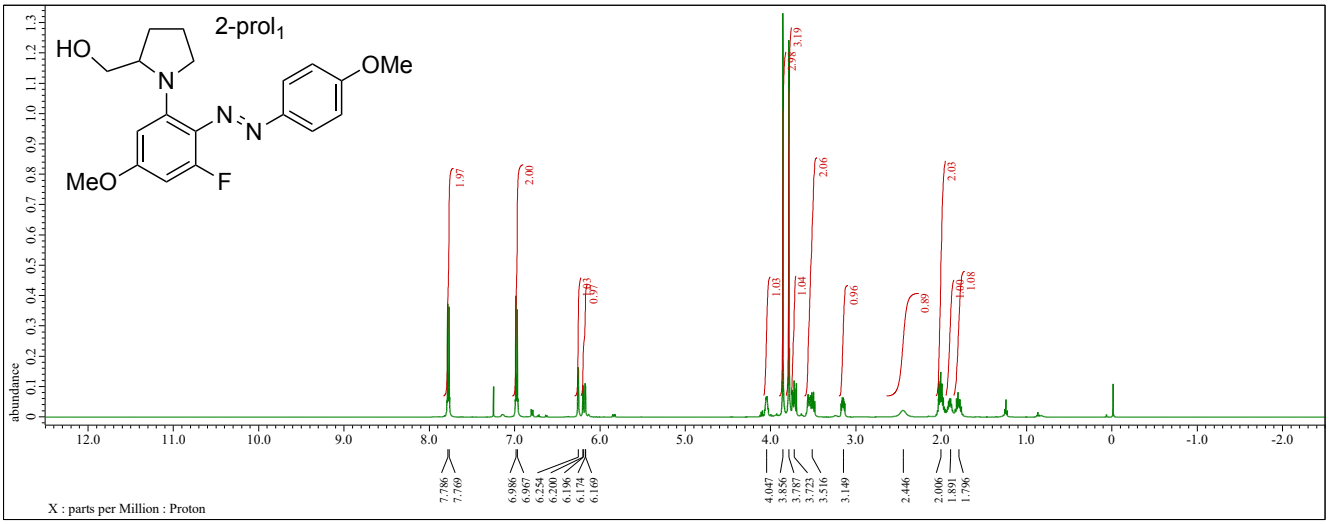

Figure S12. ^{1}H NMR spectrum of **2-prol$_1$**.

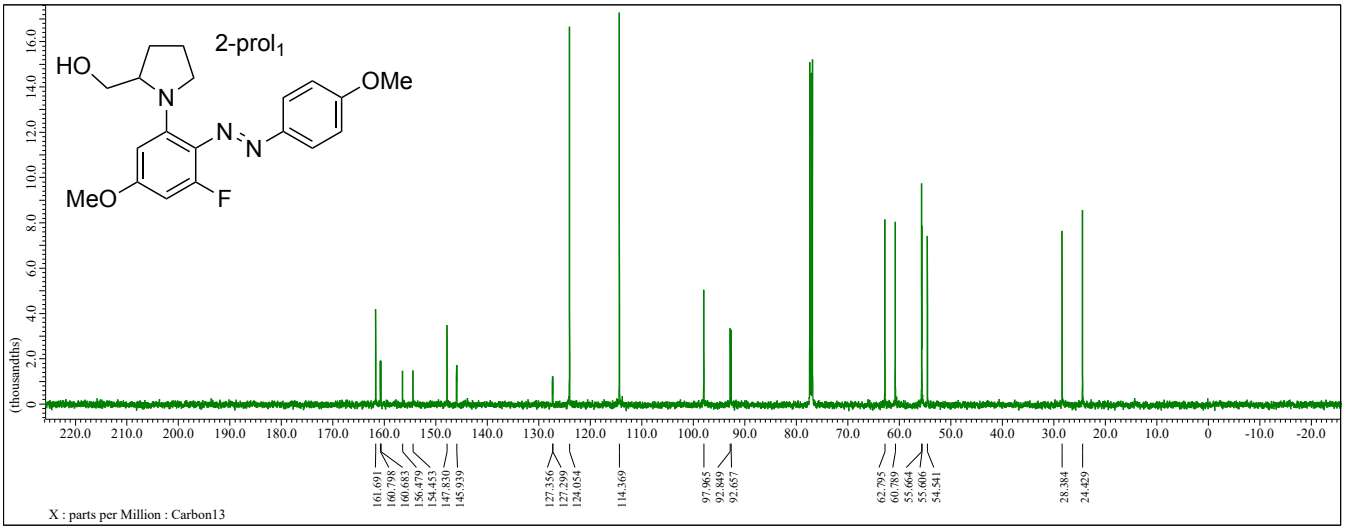

Figure S13. ^{13}C NMR spectrum of **2-prol$_1$**.

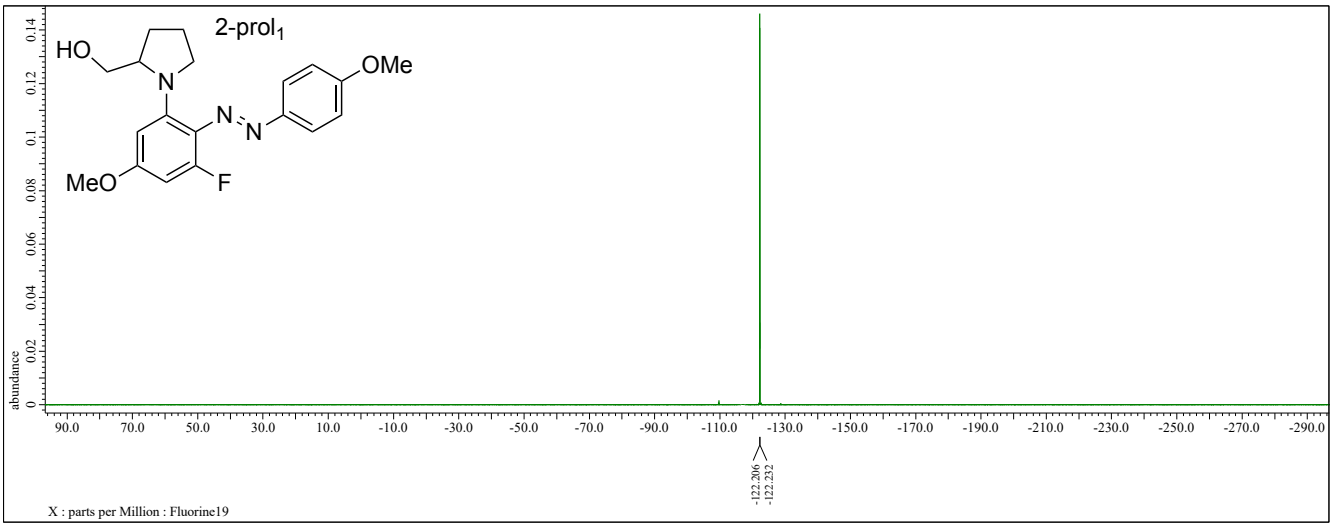

Figure S14. ^{19}F NMR spectrum of **2-prol$_1$**.

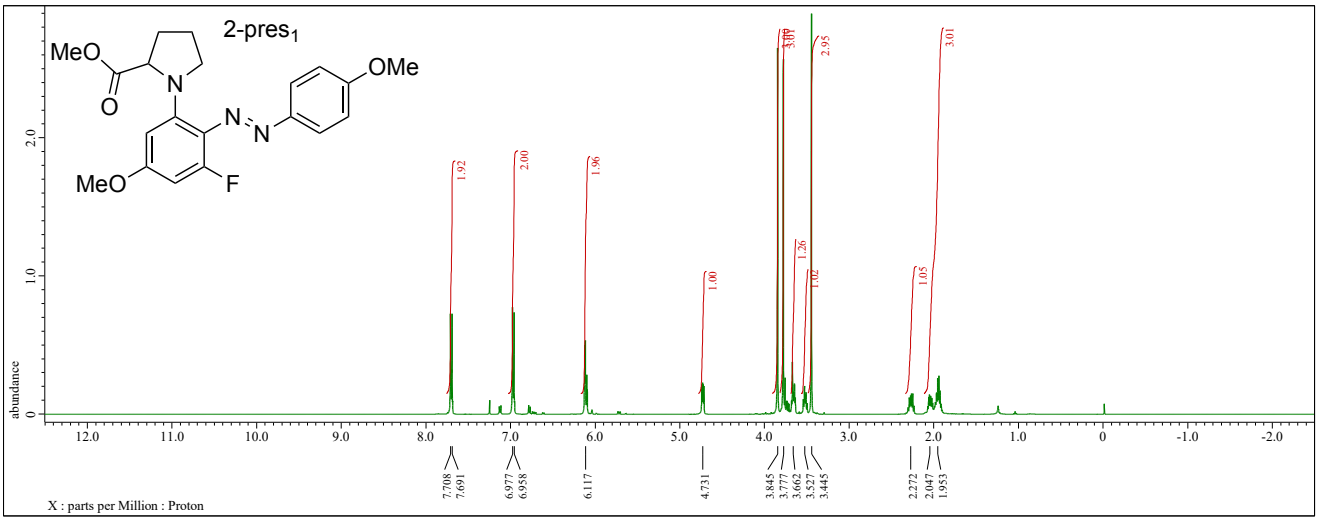

Figure S15. ^{1}H NMR spectrum of **2-pres$_1$**.

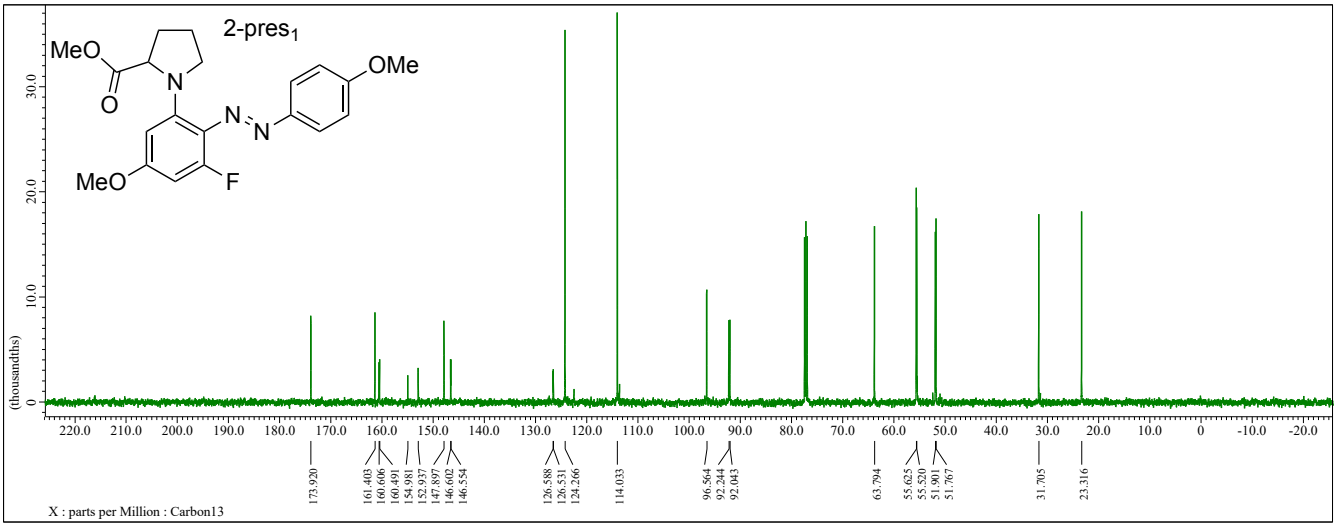

Figure S16. ^{13}C NMR spectrum of **2-pres$_1$**.

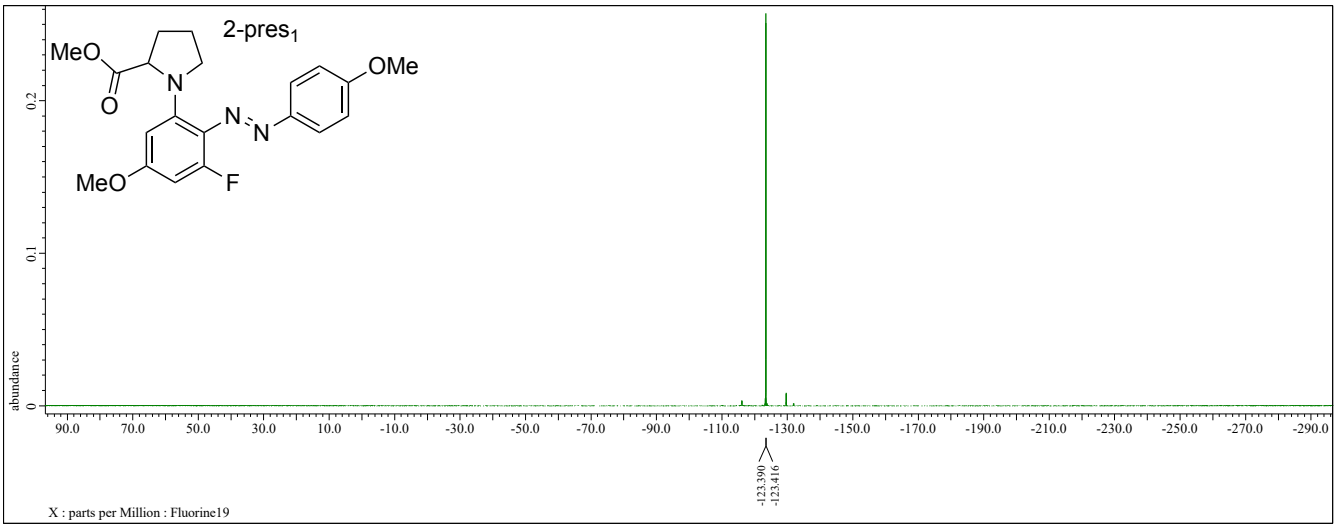

Figure S17. ^{19}F NMR spectrum of **2-pres$_1$**.

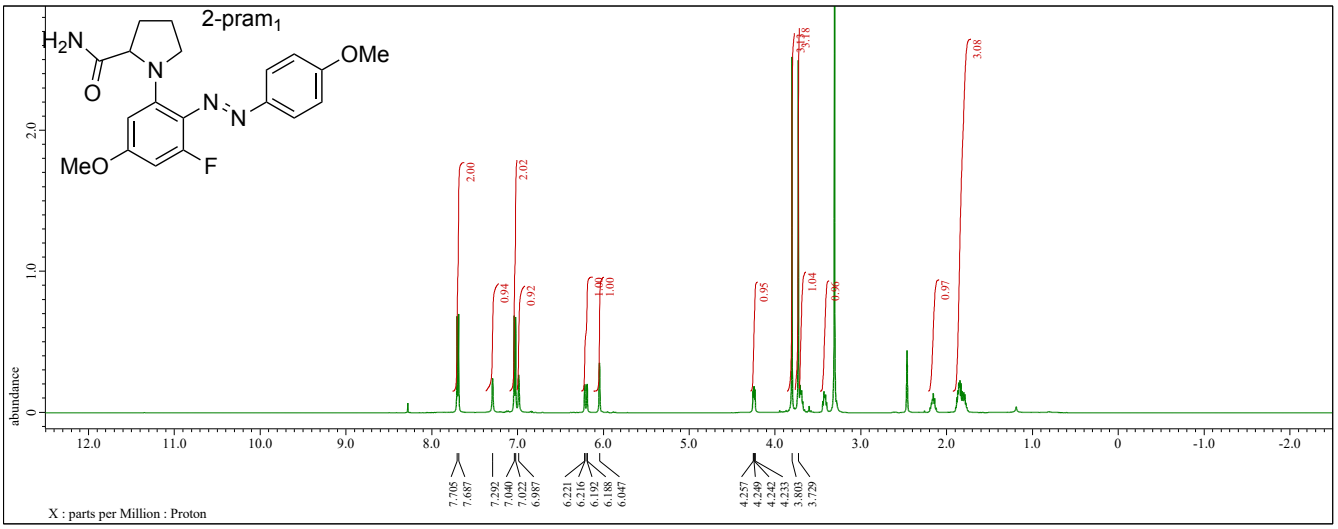

Figure S18. ^{1}H NMR spectrum of **2-pram$_1$**.

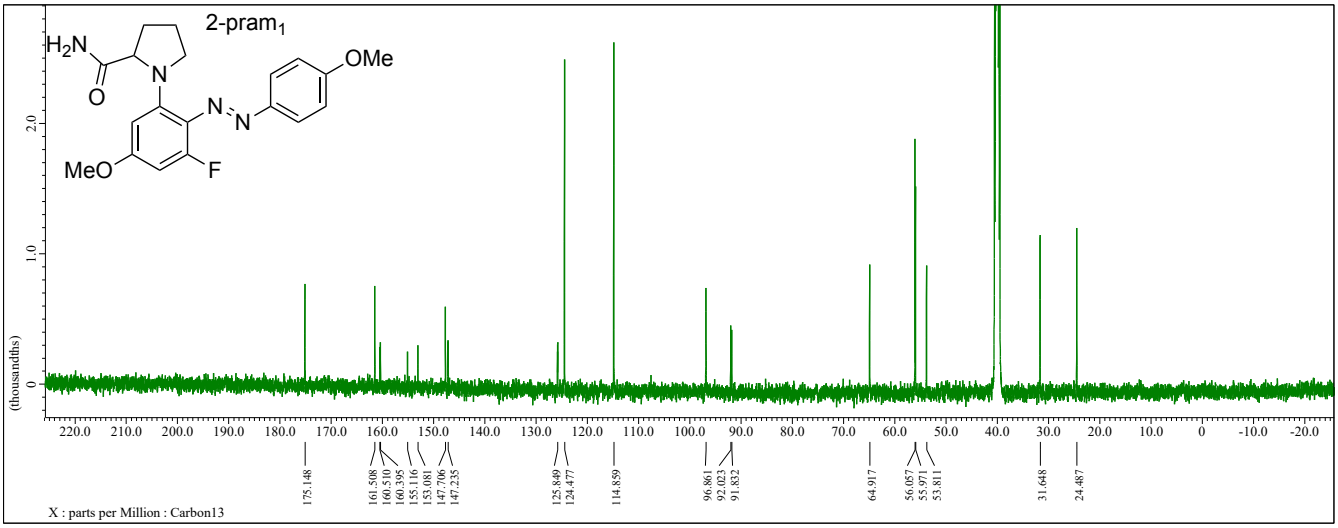

Figure S19. ^{13}C NMR spectrum of **2-pram$_1$**.

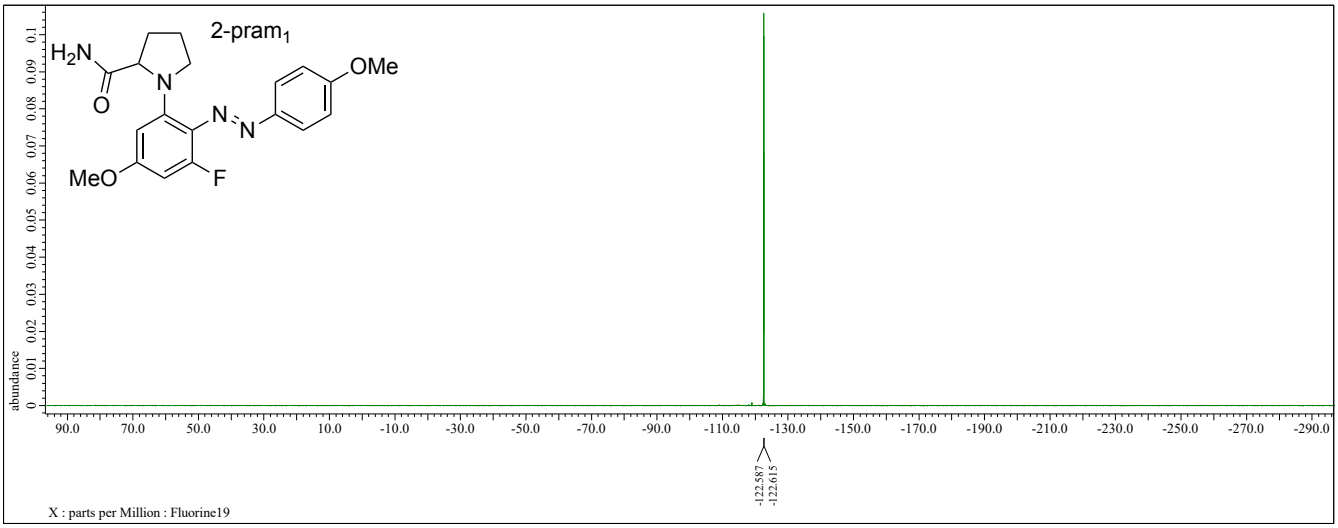

Figure S20. ^{19}F NMR spectrum of **2-pram$_1$**.

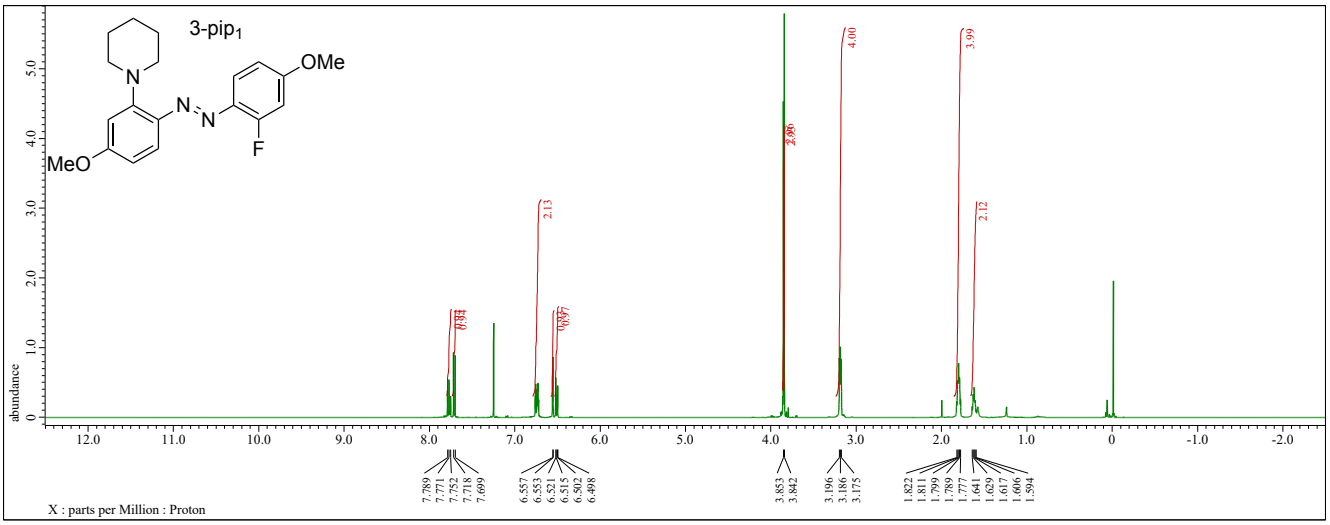

Figure S21. ^{1}H NMR spectrum of **3-pip$_1$**.

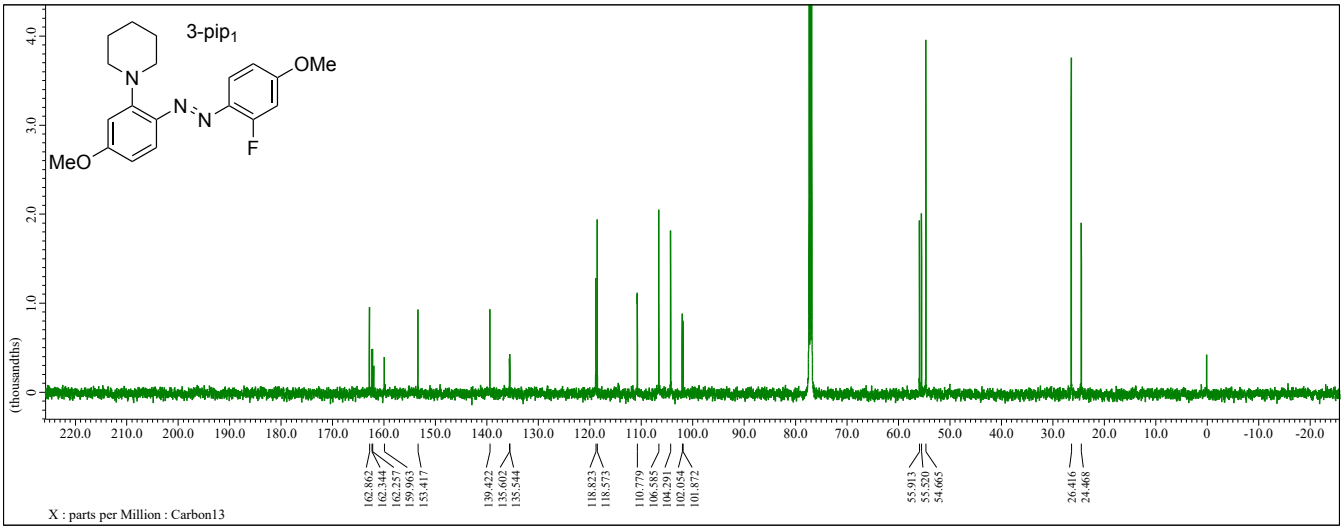

Figure S22. ^{13}C NMR spectrum of **3-pip$_1$**.

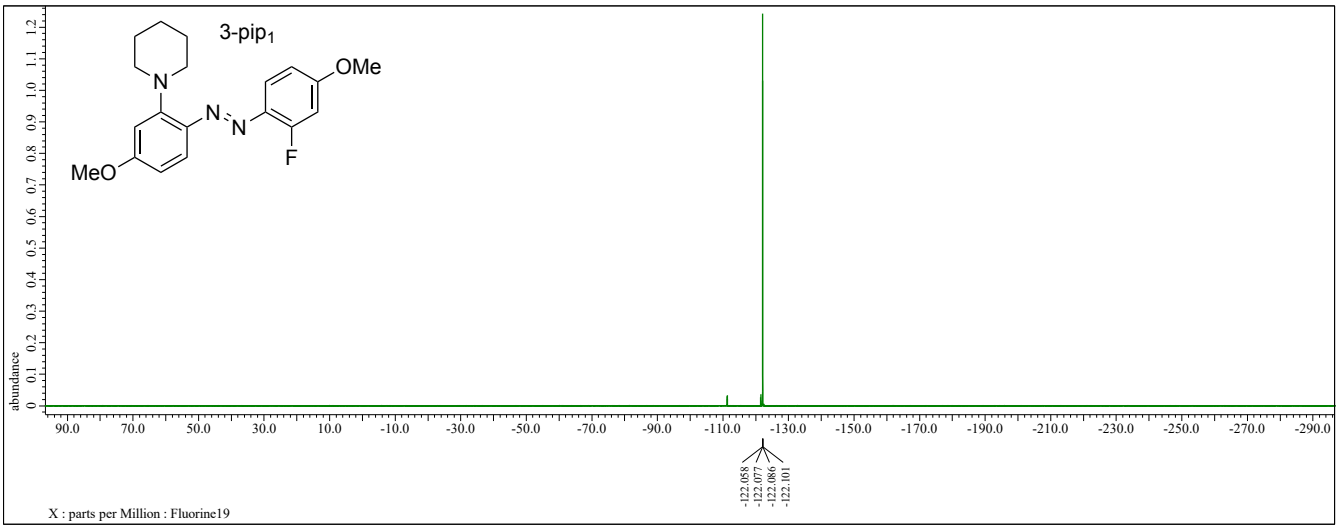

Figure S23. ^{19}F NMR spectrum of **3-pip$_1$**.

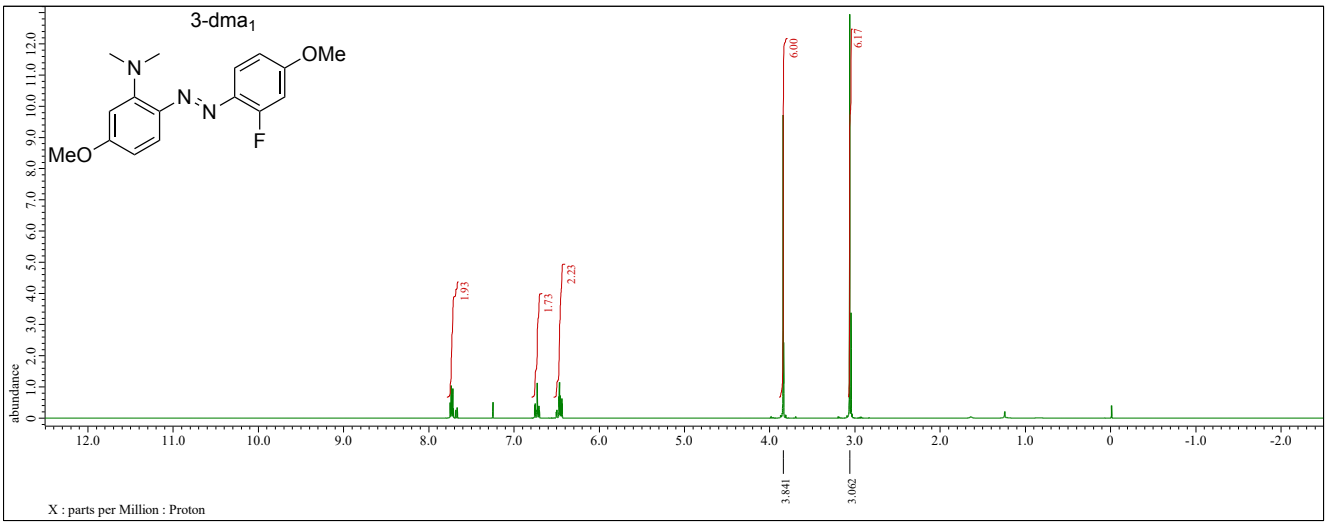

Figure S24. ^{1}H NMR spectrum of **3-dma$_1$**.

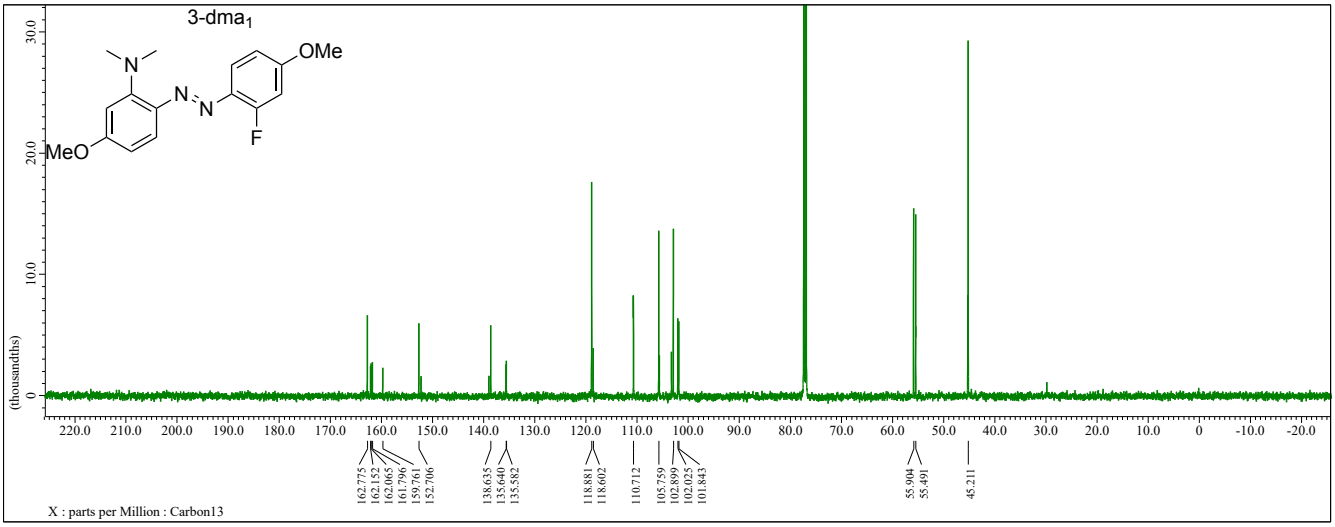

Figure S25. ^{13}C NMR spectrum of **3-dma$_1$**.

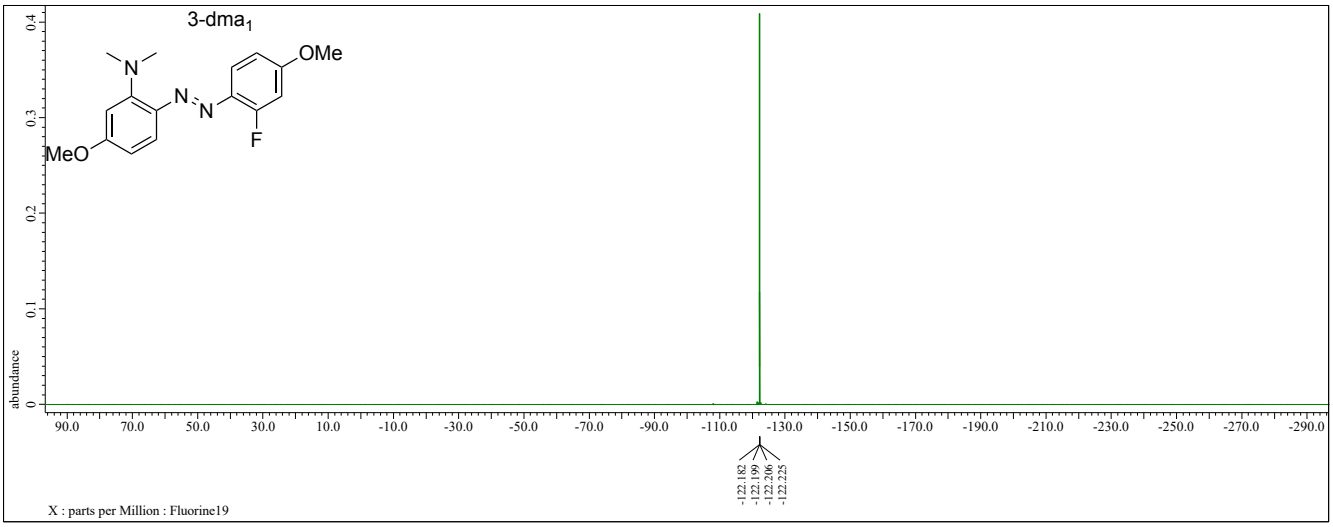

Figure S26. ^{19}F NMR spectrum of **3-dma$_1$**.

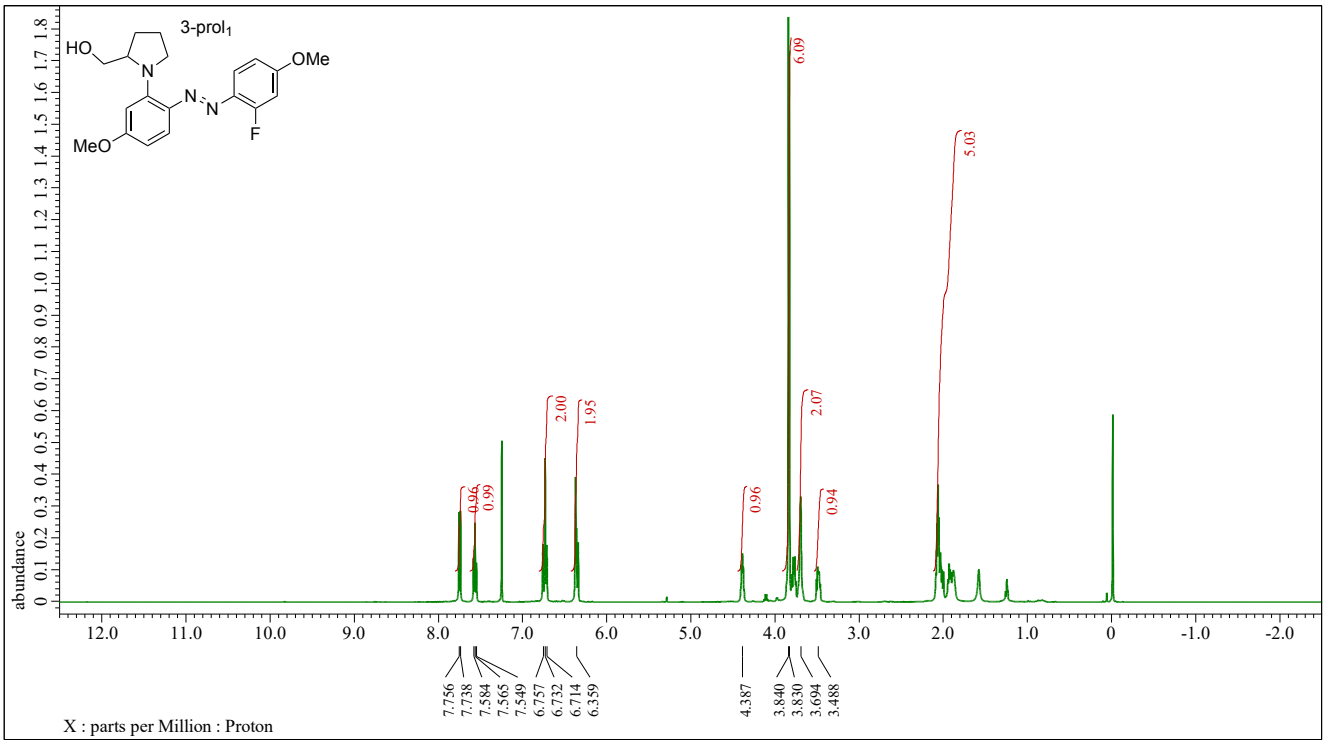

Figure S27. ^{1}H NMR spectrum of **3-prol$_1$**.

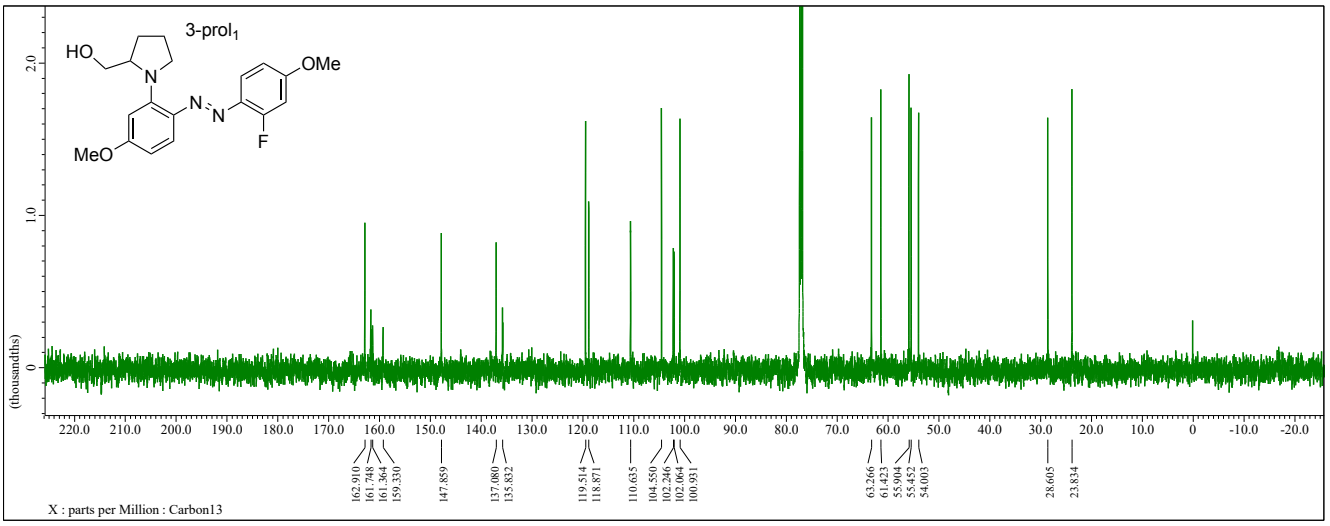

Figure S28. ^{13}C NMR spectrum of **3-prol$_1$**.

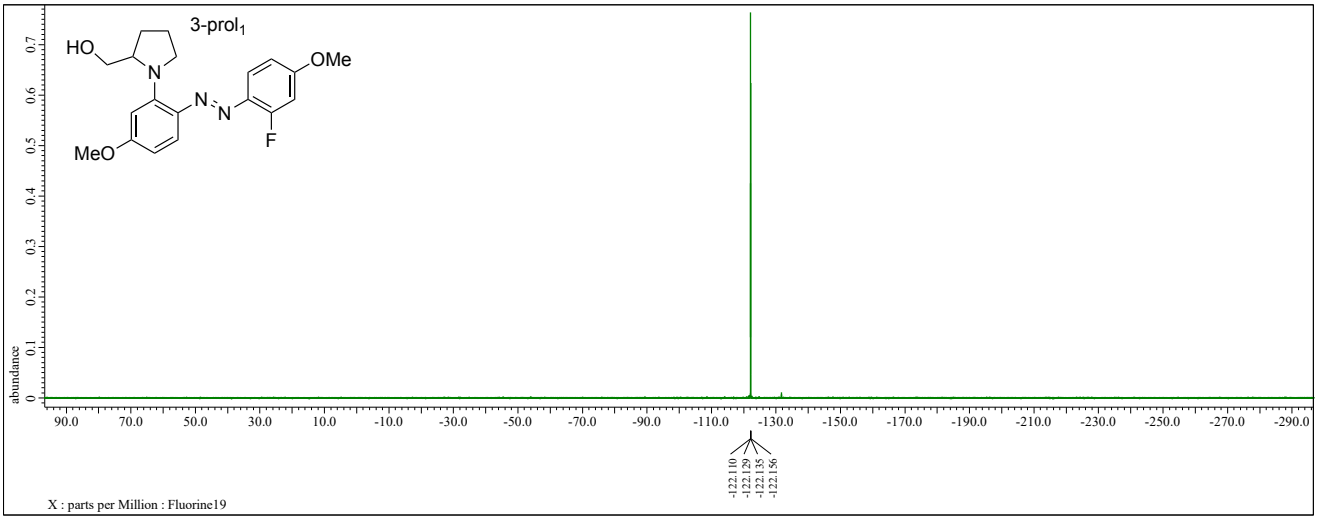

Figure S29. [19]F NMR spectrum of **3-prol$_1$**.

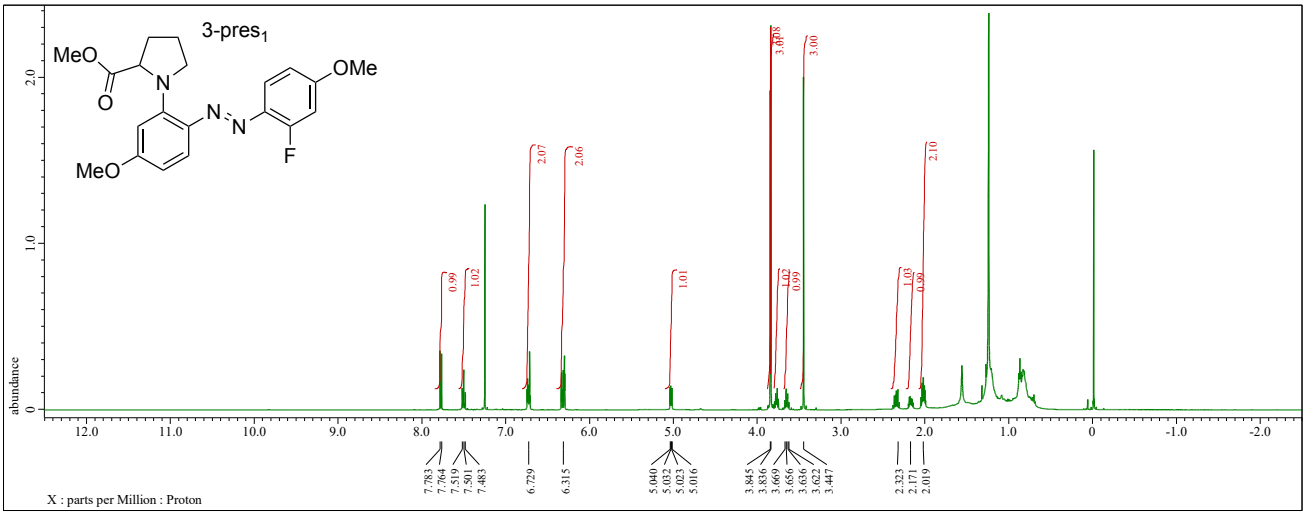

Figure S30. [1]H NMR spectrum of **3-pres$_1$**.

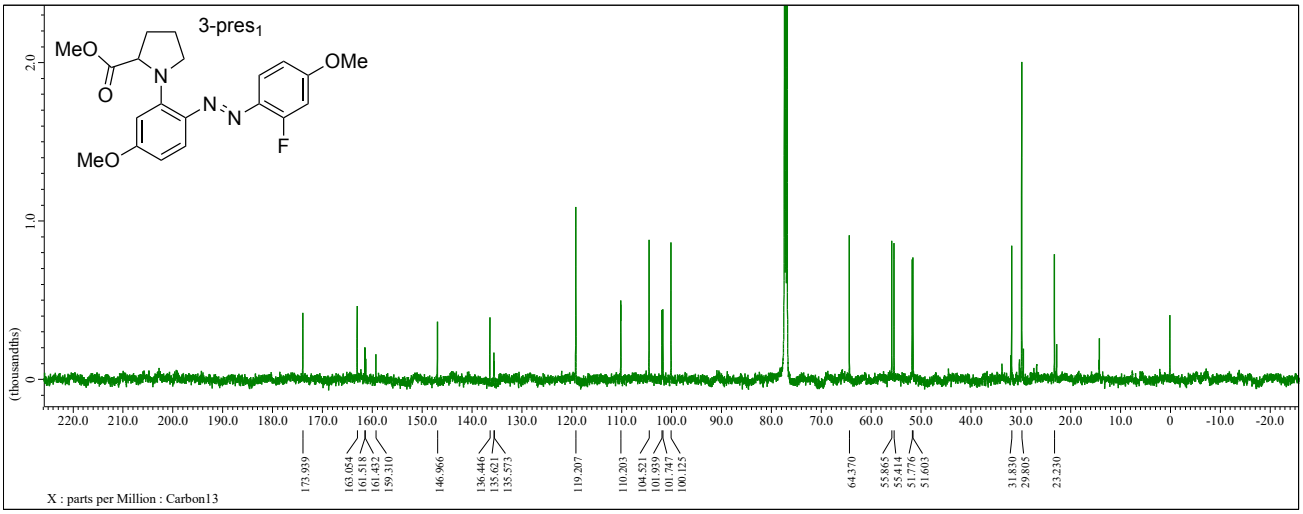

Figure S31. [13]C NMR spectrum of **3-pres$_1$**.

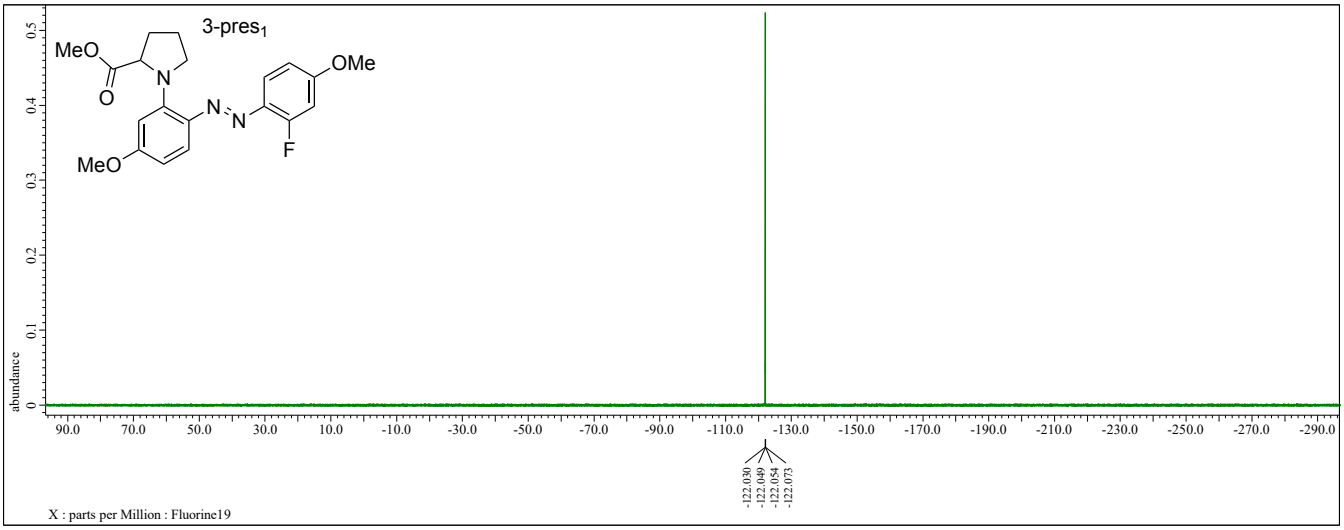

Figure S32. [19]F NMR spectrum of **3-pres$_1$**.

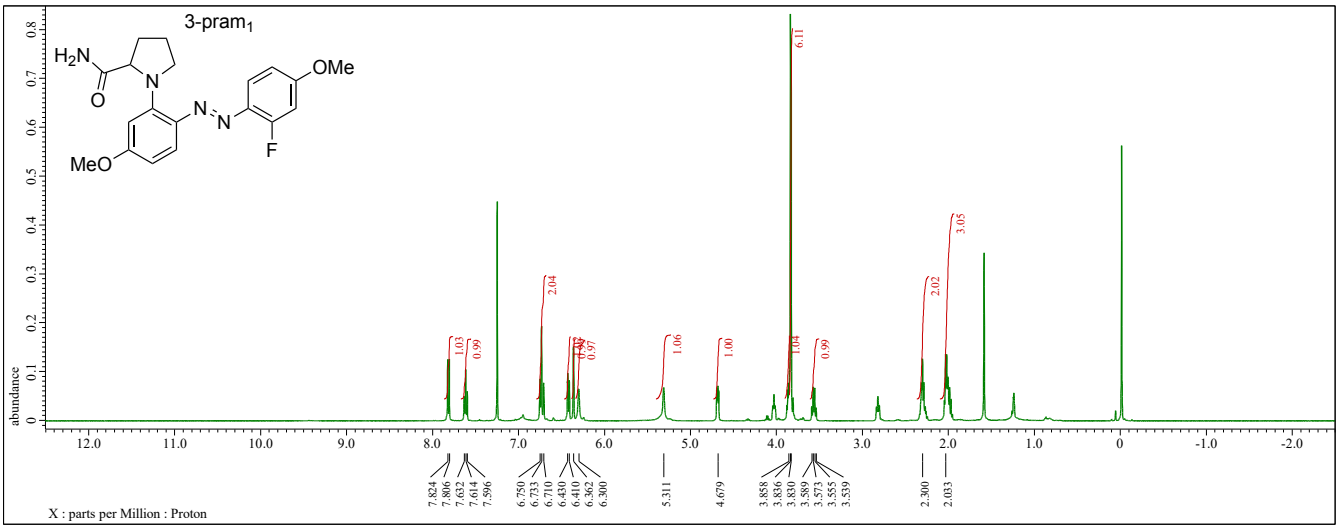

Figure S33. [1]H NMR spectrum of **3-pram$_1$**.

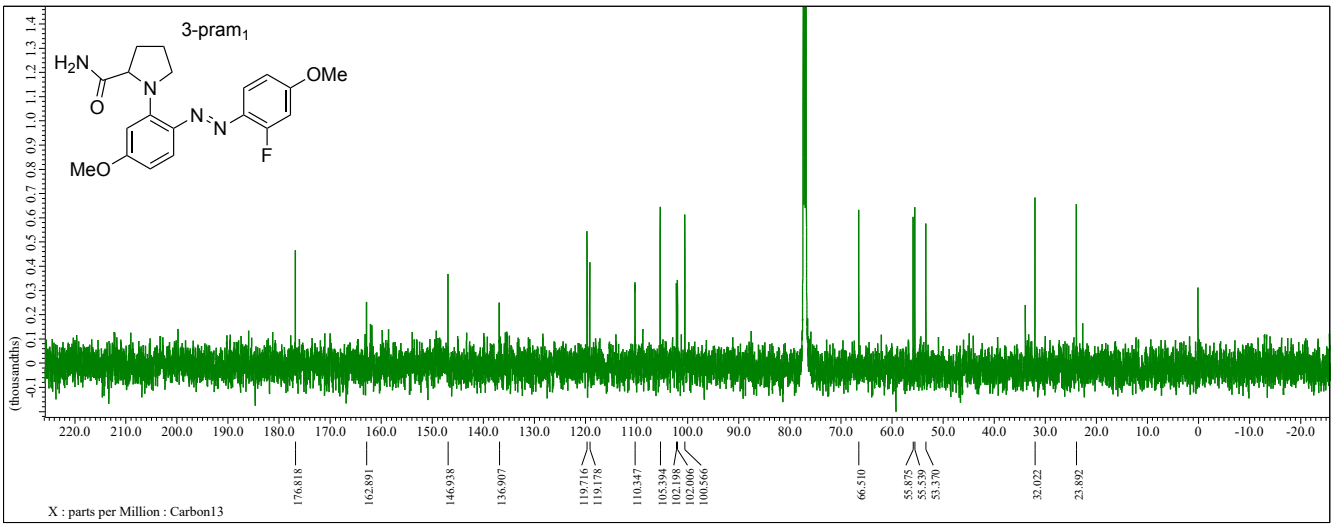

Figure S34. [13]C NMR spectrum of **3-pram$_1$**.

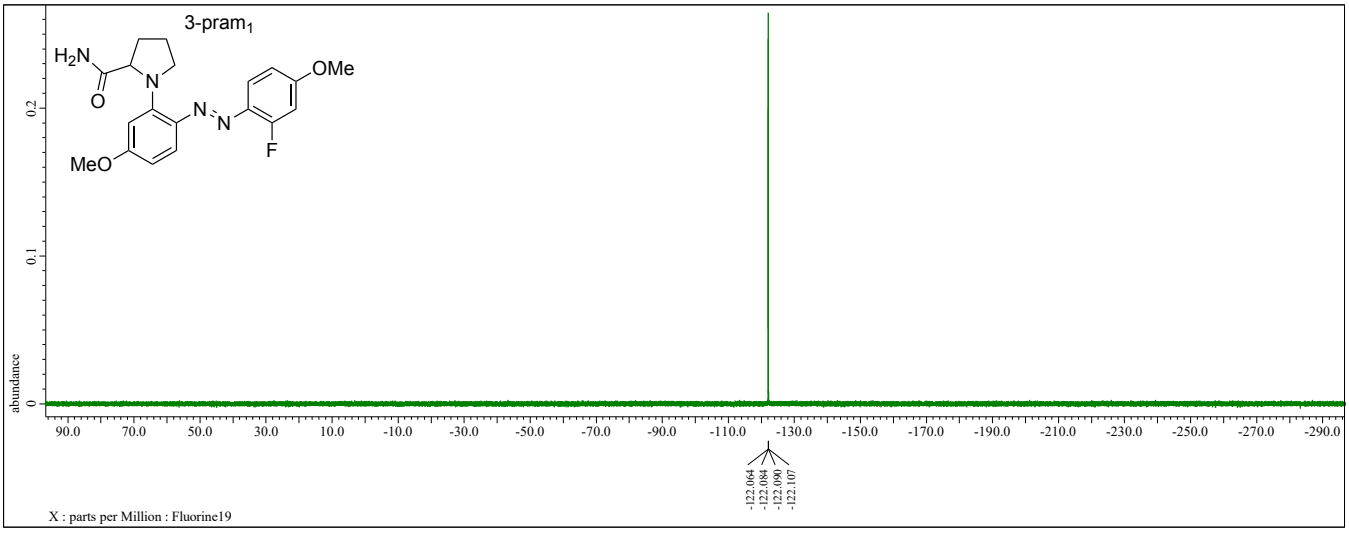

Figure S35. ^{19}F NMR spectrum of **3-pram$_1$**.

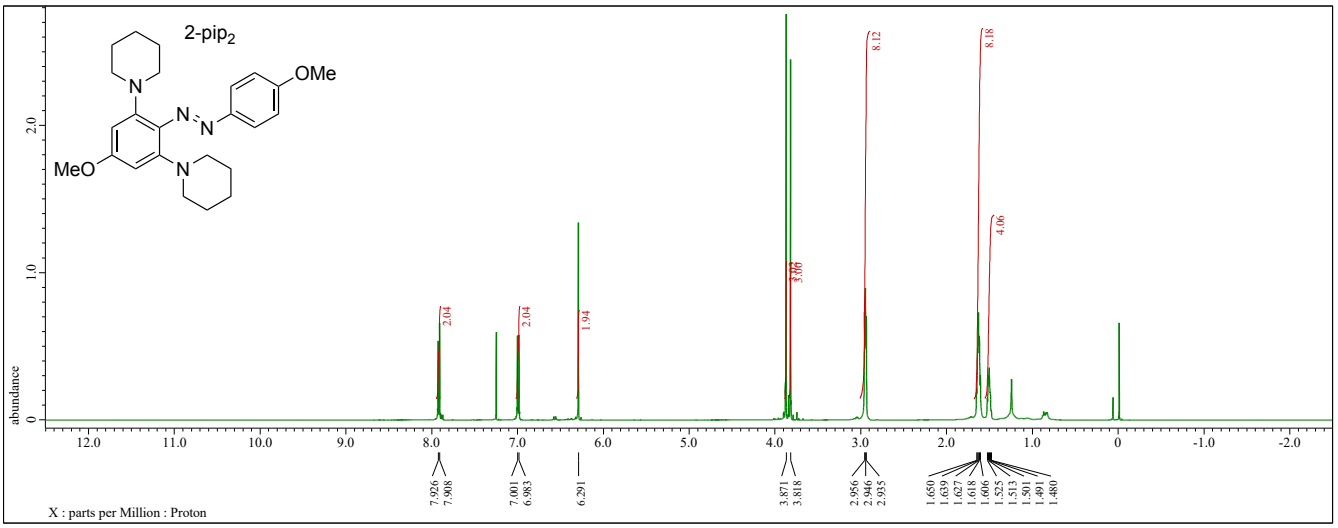

Figure S36. ^{1}H NMR spectrum of **2-pip$_2$**.

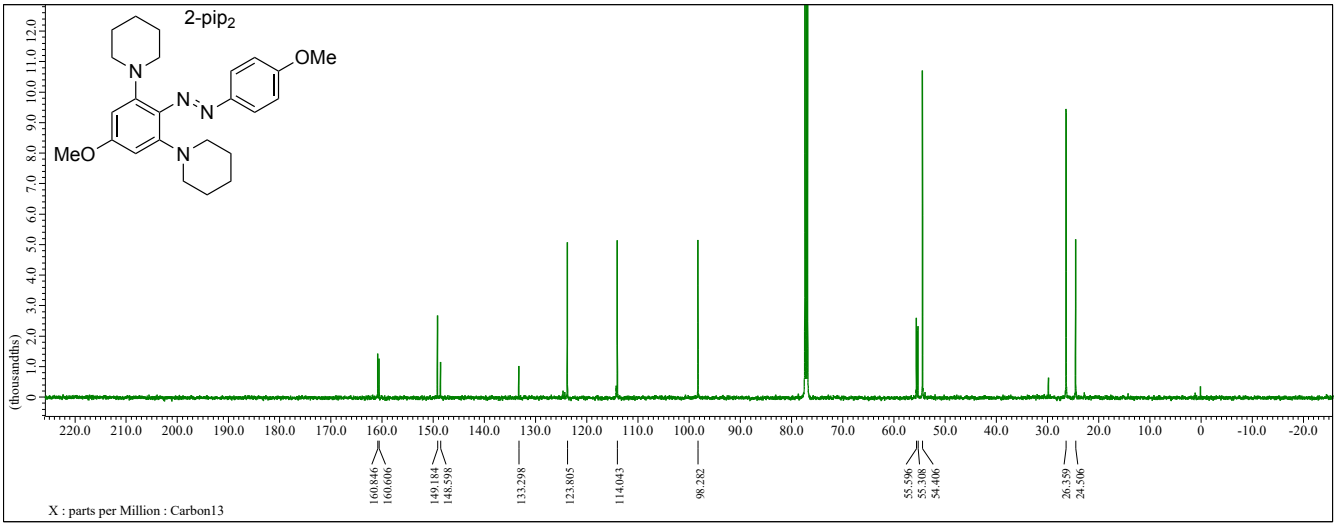

Figure S37. ^{13}C NMR spectrum of **2-pip$_2$**.

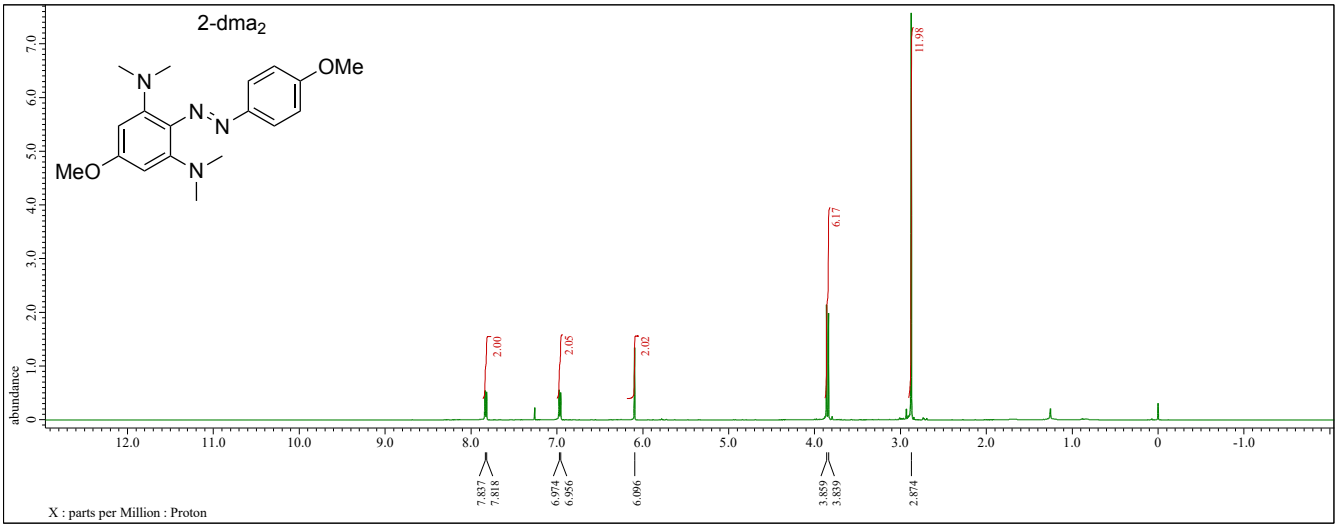

Figure S38. ^{1}H NMR spectrum of **2-dma$_2$**.

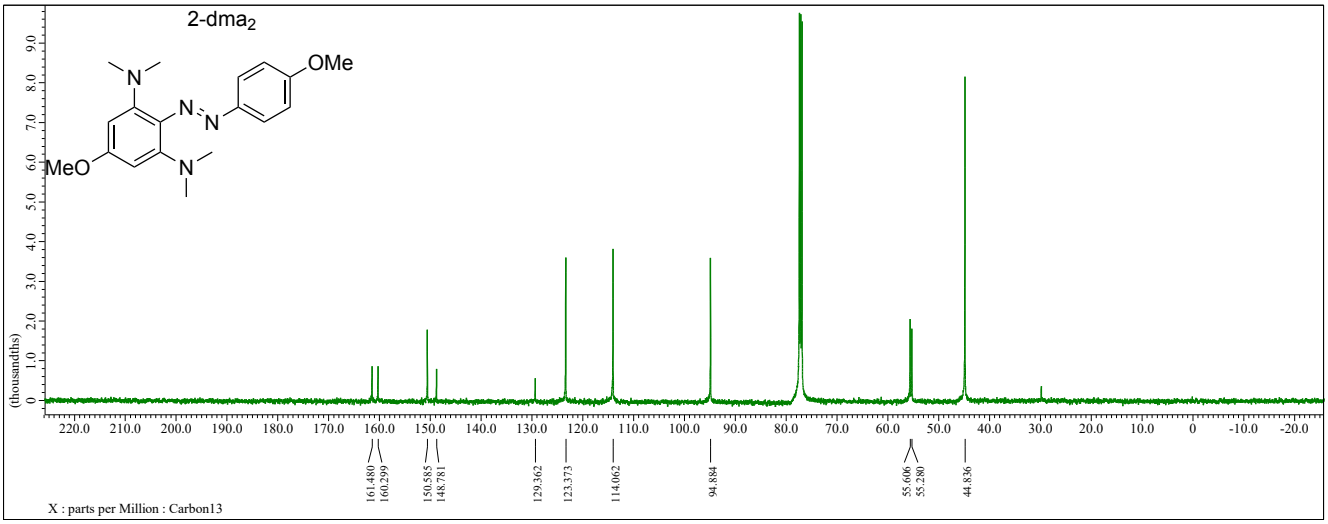

Figure S39. ^{13}C NMR spectrum of **2-dma$_2$**.

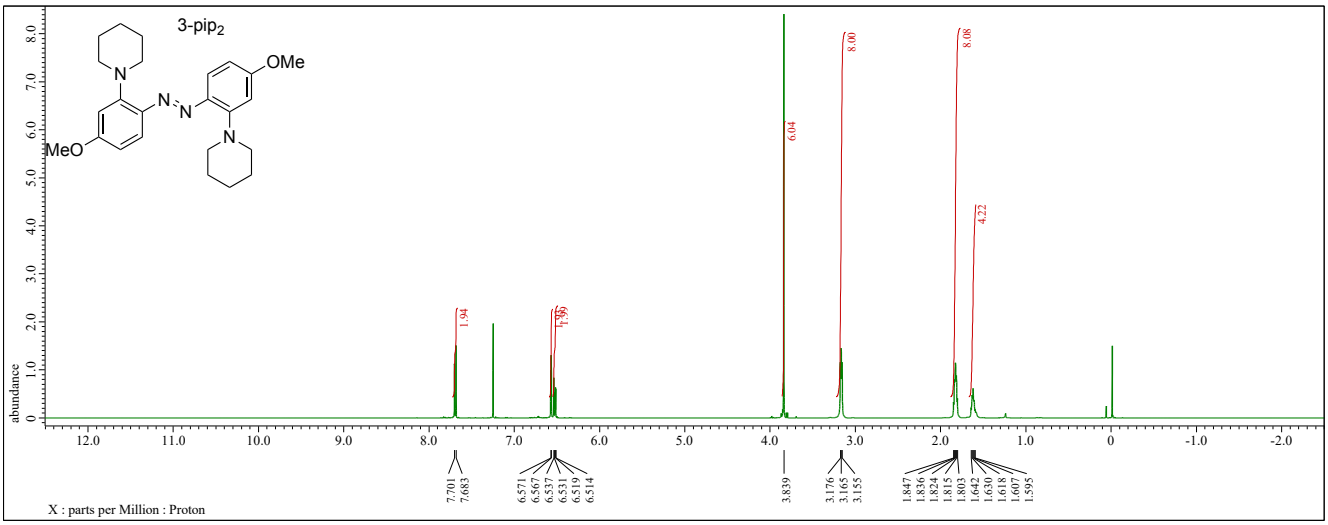

Figure S40. ^{1}H NMR spectrum of **3-pip$_2$**.

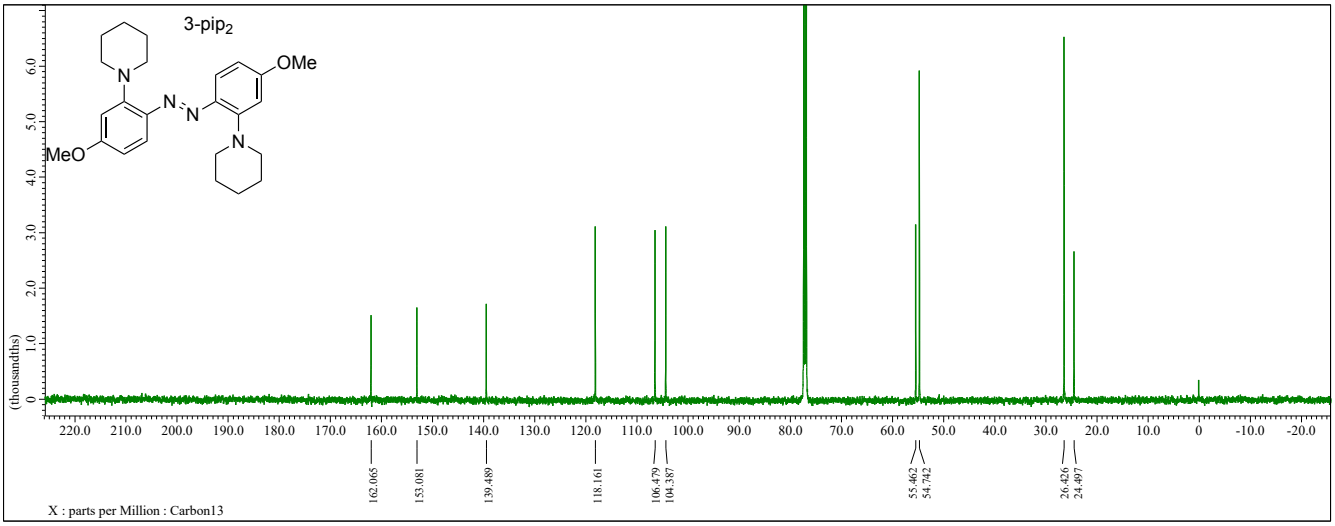

Figure S41. ^{13}C NMR spectrum of **3-pip$_2$**.

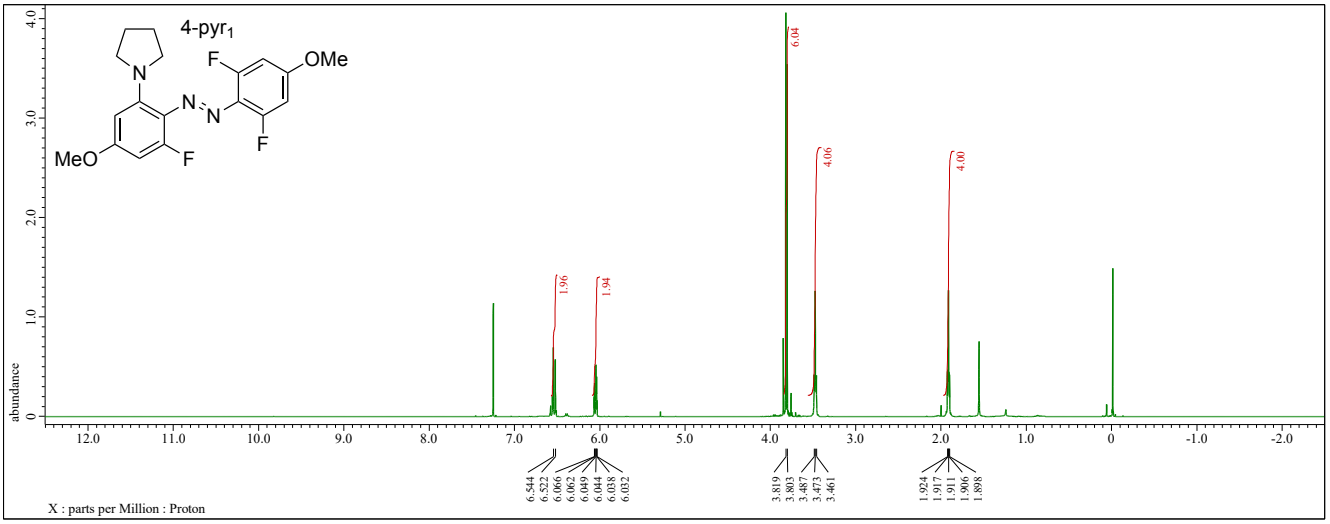

Figure S42. ^{1}H NMR spectrum of **4-pyr$_1$**.

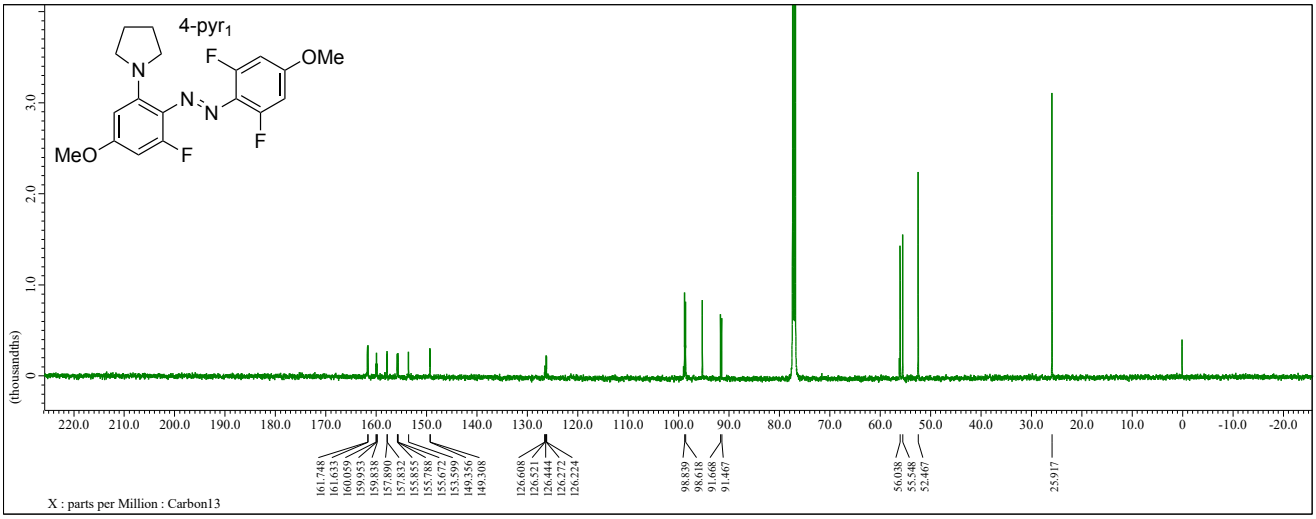

Figure S43. ^{13}C NMR spectrum of **4-pyr$_1$**.

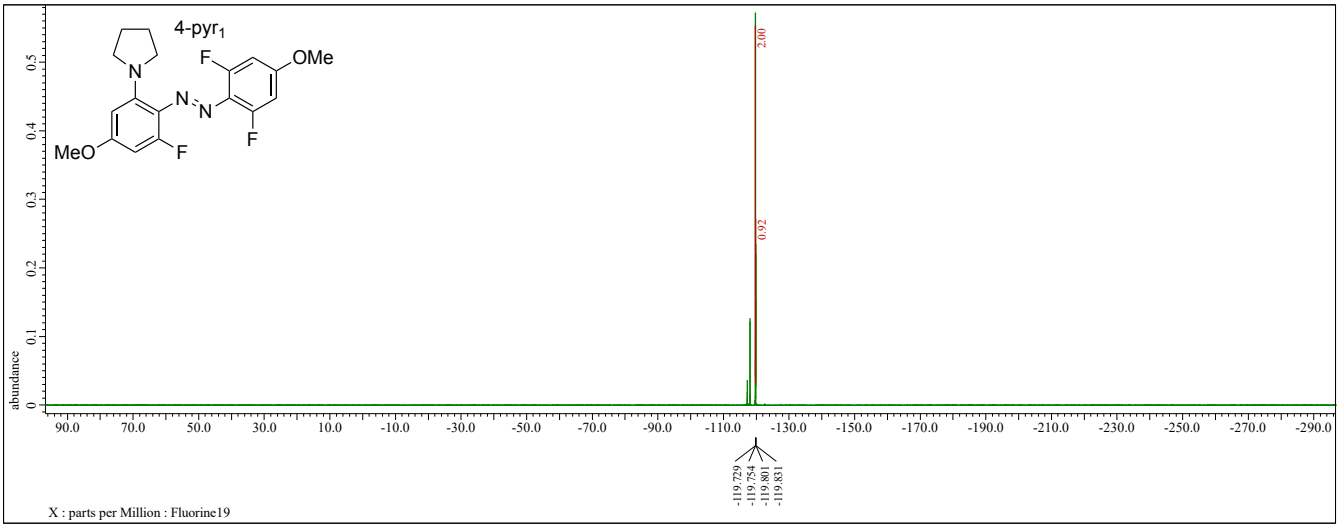

Figure S44. [19]F NMR spectrum of **4-pyr1**.

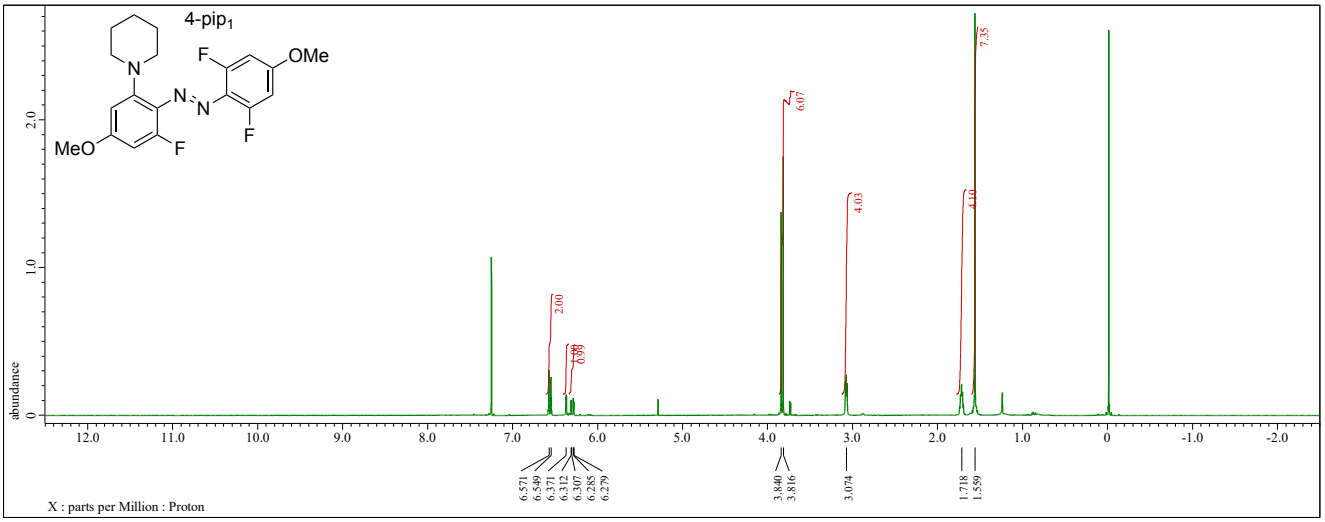

Figure S45. [1]H NMR spectrum of **4-pip1**.

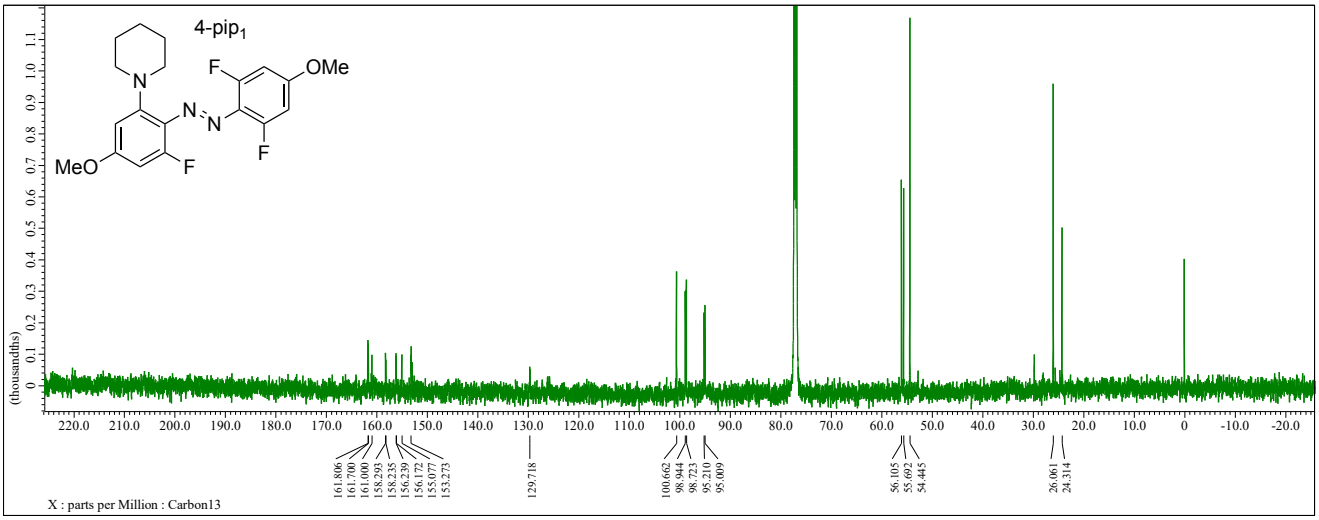

Figure S46. [13]C NMR spectrum of **4-pip1**.

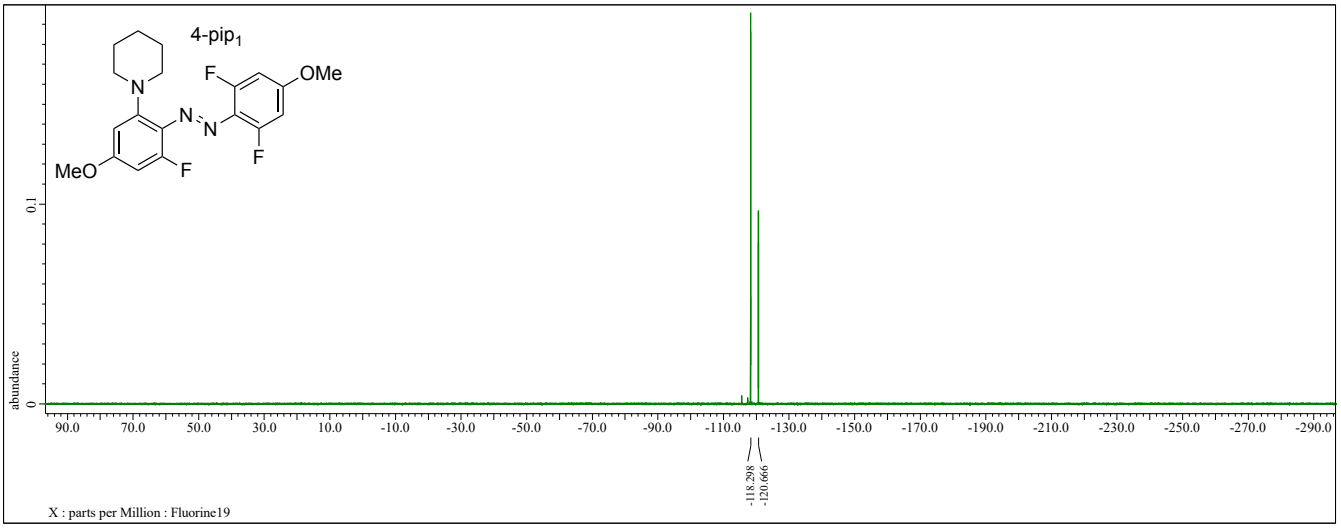

Figure S47. ^{19}F NMR spectrum of **4-pip$_1$**.

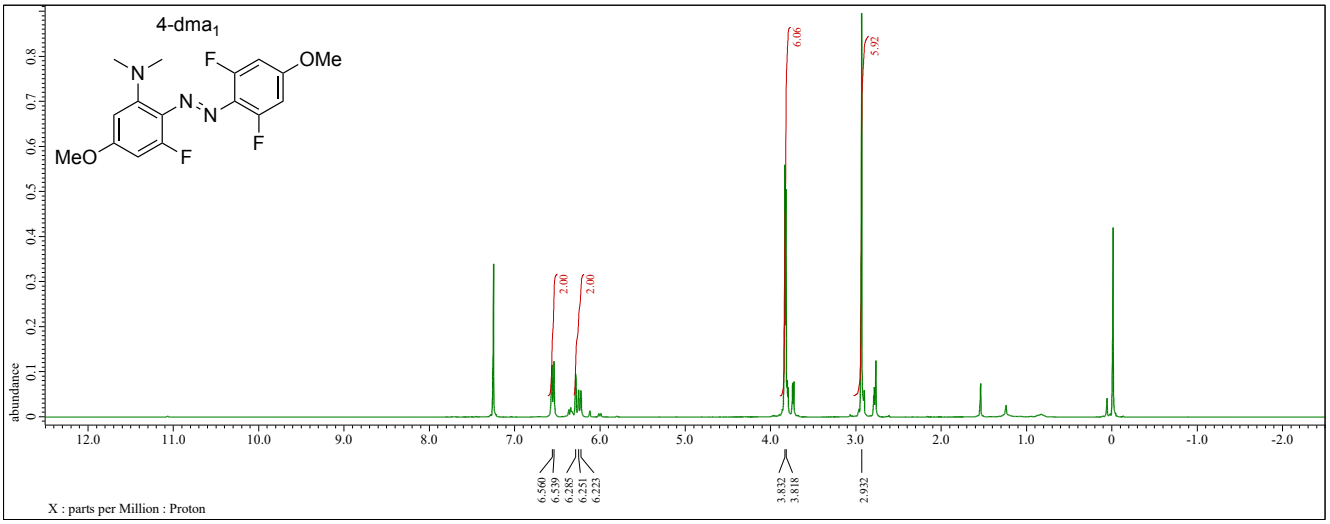

Figure S48. ^{1}H NMR spectrum of **4-dma$_1$**.

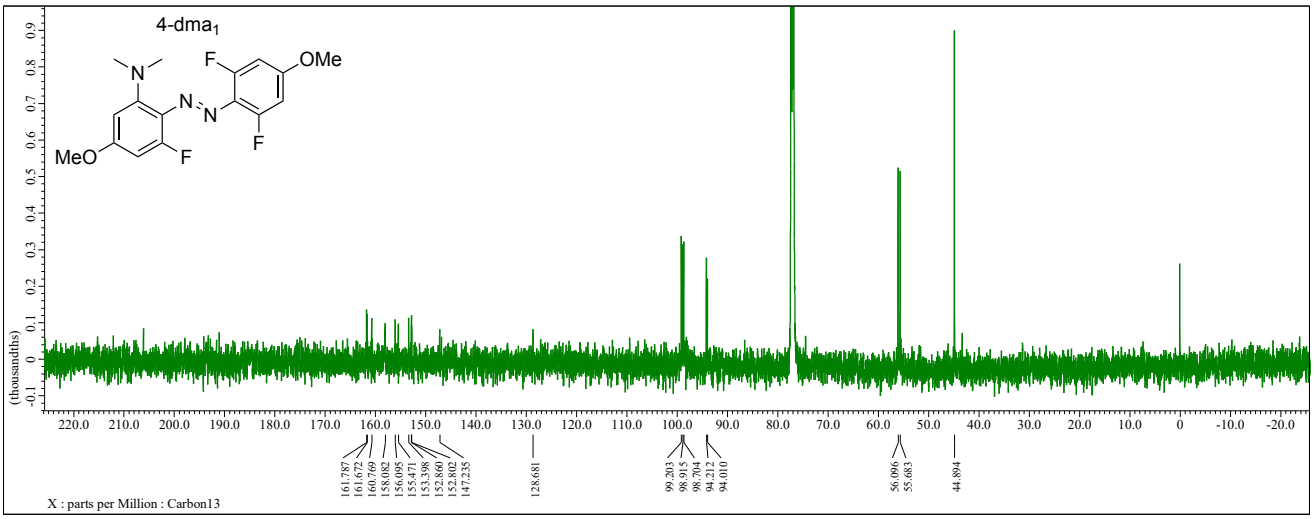

Figure S49. ^{13}C NMR spectrum of **4-dma$_1$**.

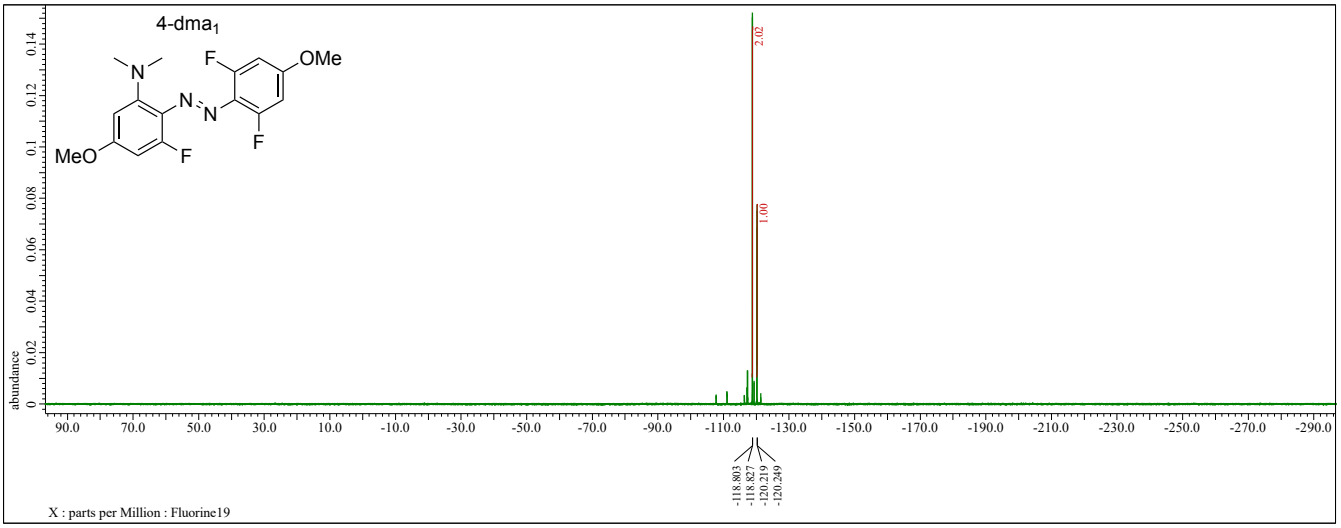

Figure S50. [19]F NMR spectrum of **4-dma$_1$**.

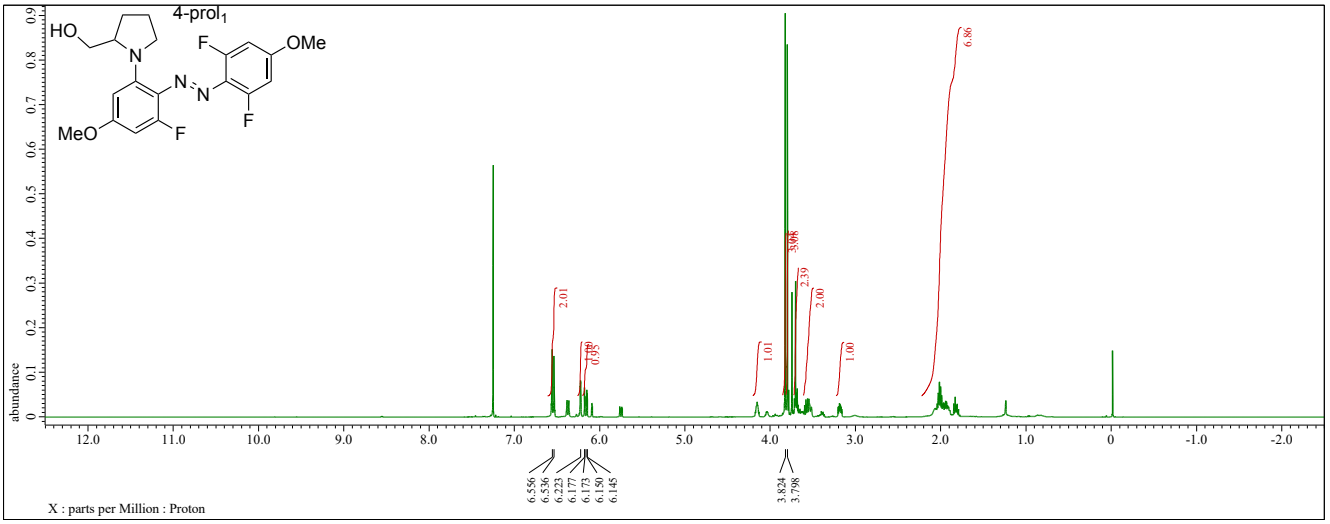

Figure S51. [1]H NMR spectrum of **4-prol$_1$**.

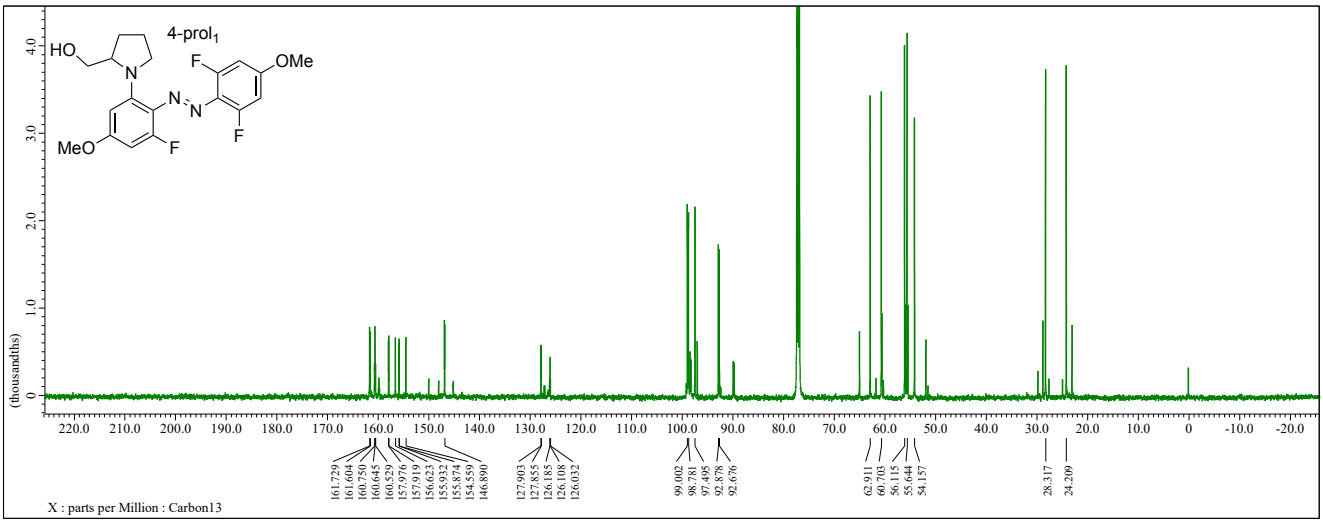

Figure S52. [13]C NMR spectrum of **4-prol$_1$**.

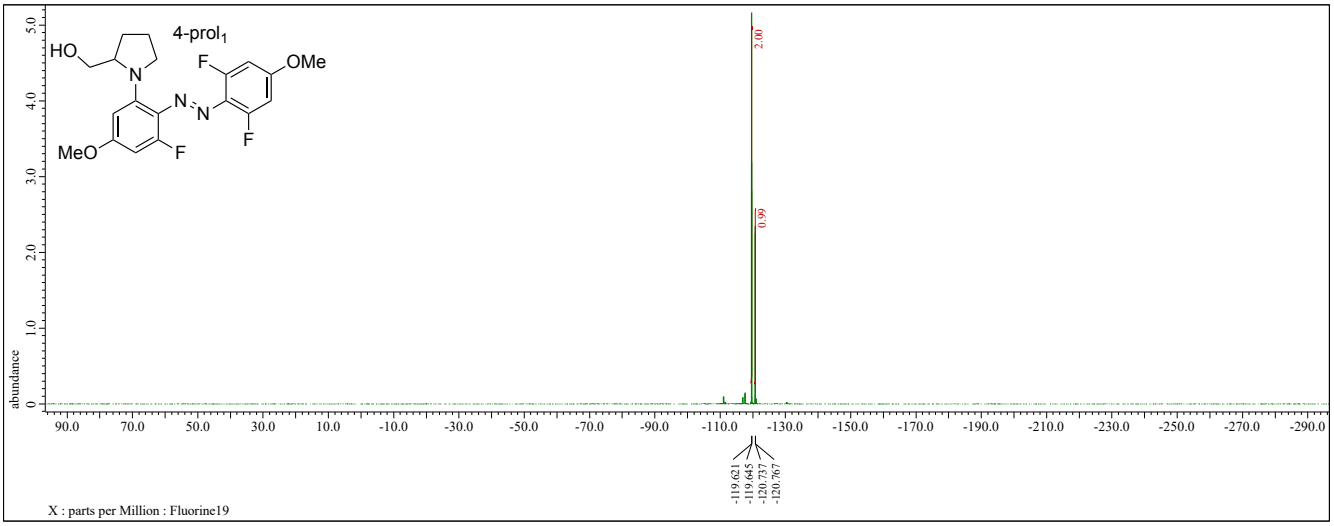

Figure S53. ^{19}F NMR spectrum of **4-prol$_1$**.

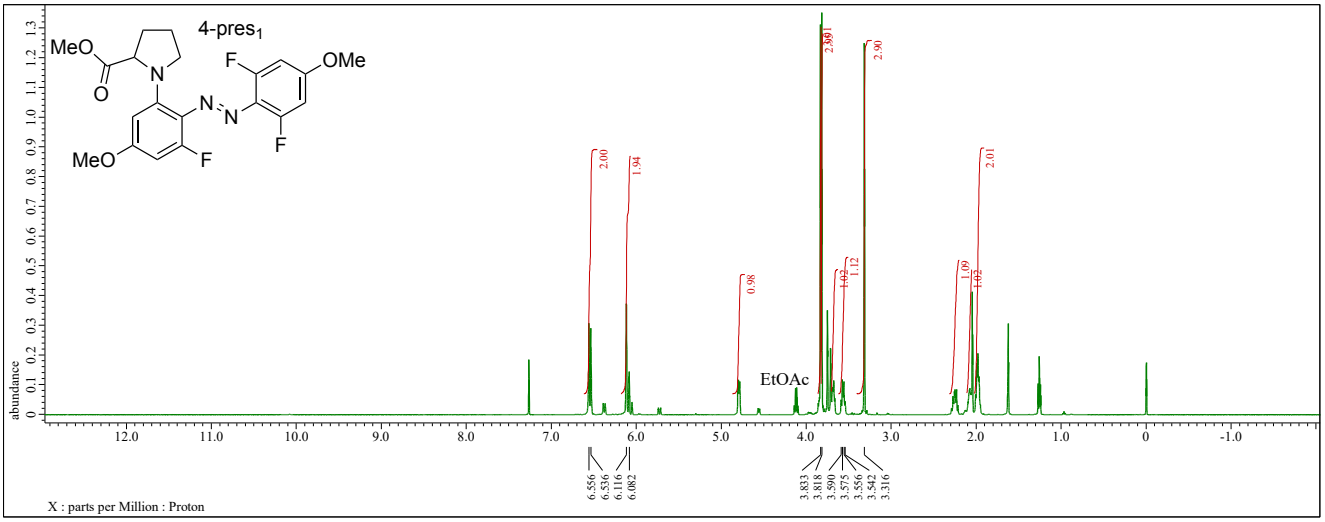

Figure S54. ^{1}H NMR spectrum of **4-pres$_1$**.

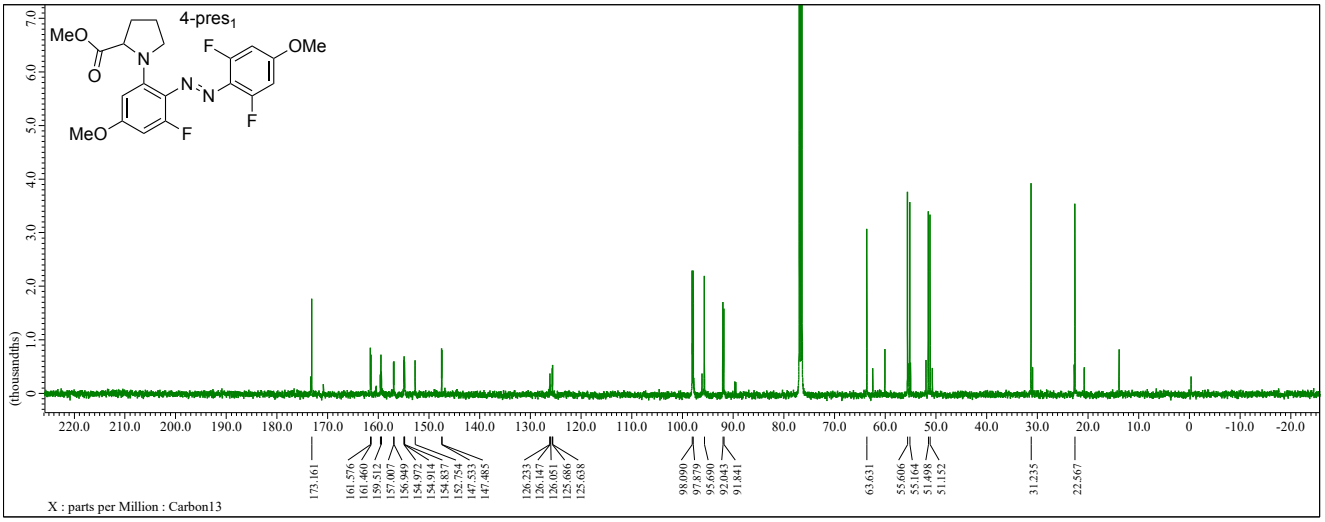

Figure S55. ^{13}C NMR spectrum of **4-pres$_1$**.

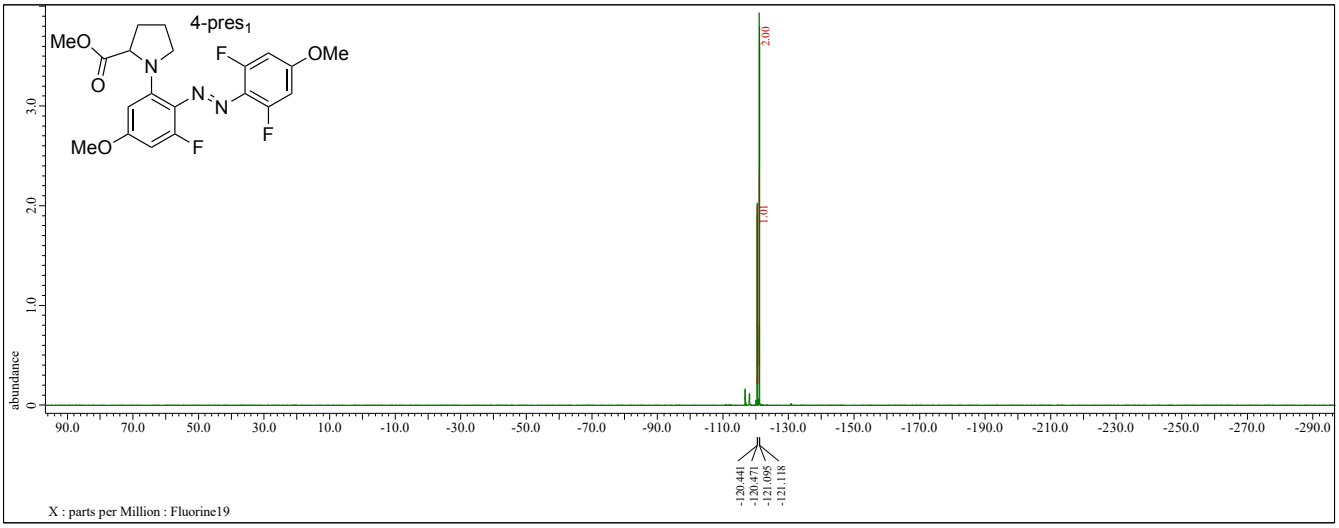

Figure S56. [19]F NMR spectrum of **4-pres1**.

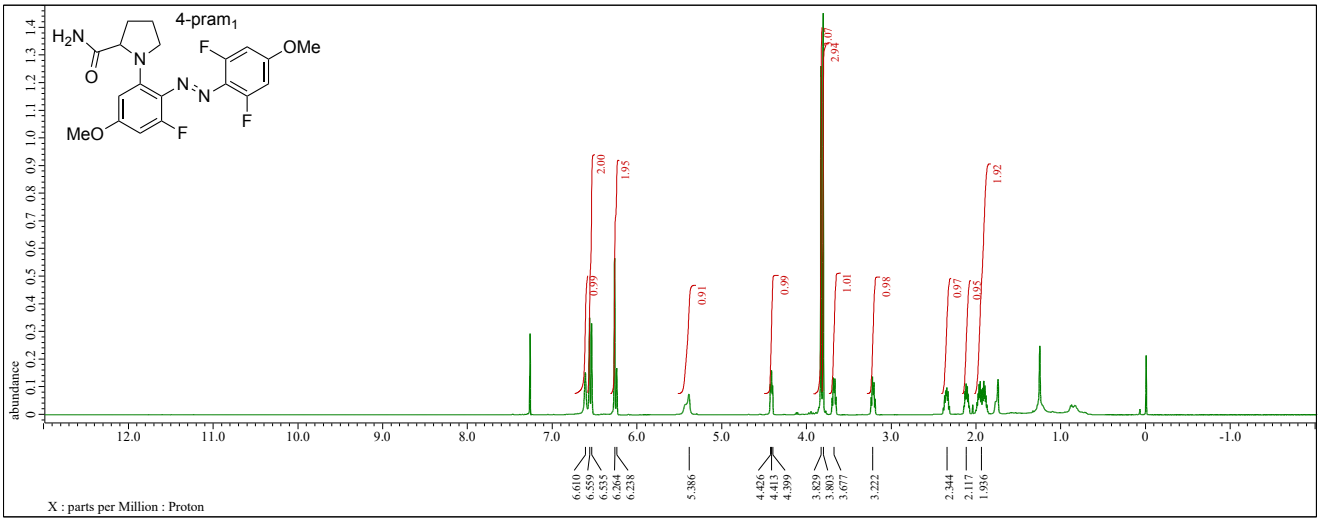

Figure S57. [1]H NMR spectrum of **4-pram1**.

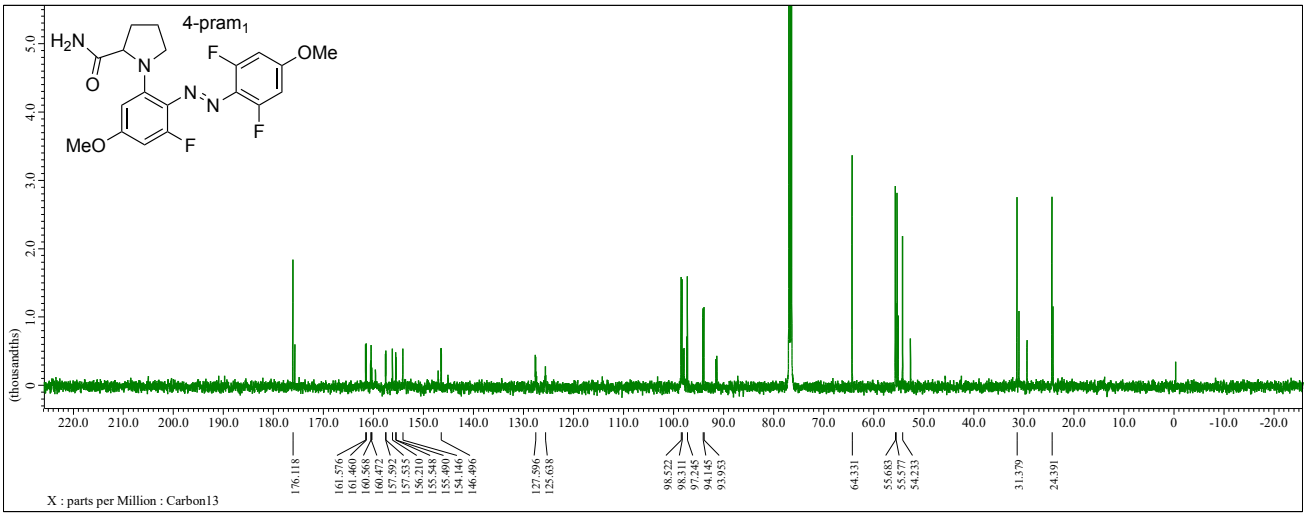

Figure S58. [13]C NMR spectrum of **4-pram1**.

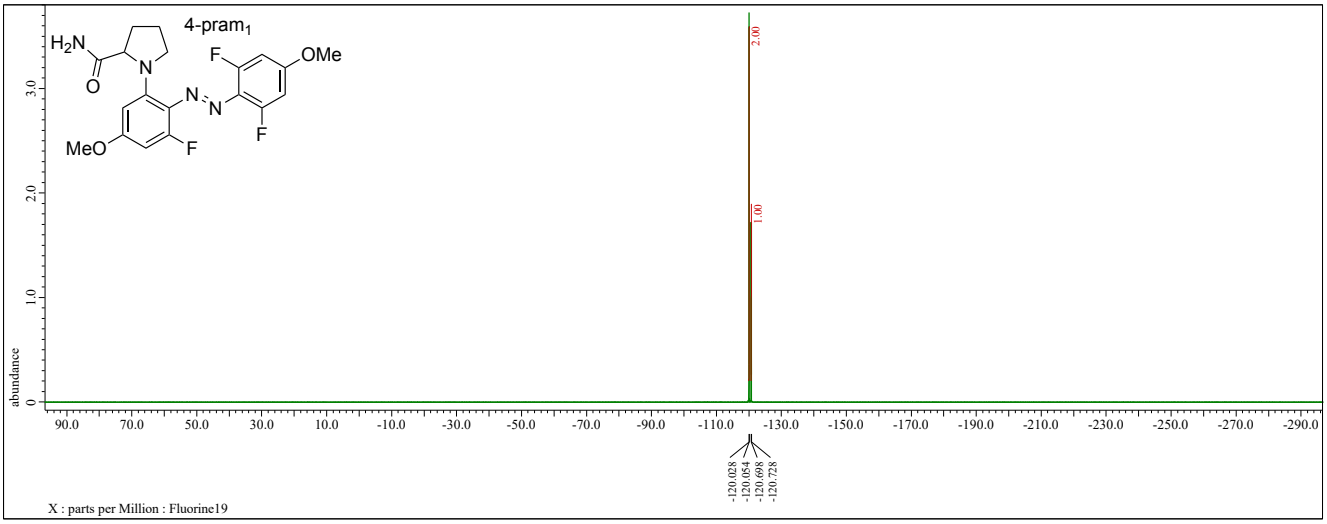

Figure S59. ^{19}F NMR spectrum of **4-pram$_1$**.

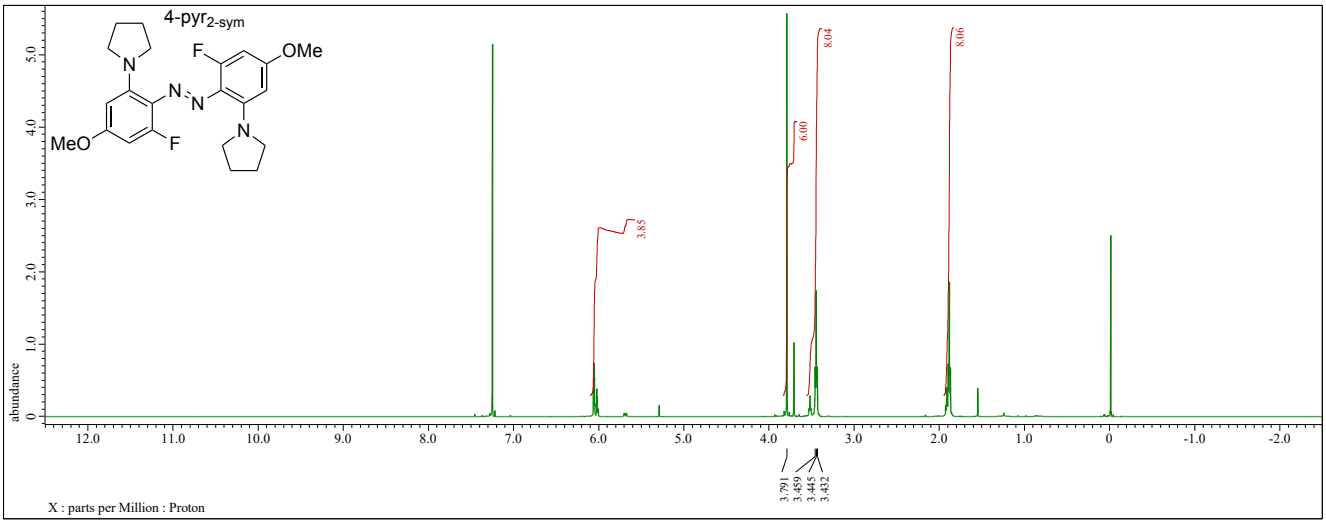

Figure S60. ^{1}H NMR spectrum of **4-pyr$_{2\text{-sym}}$**.

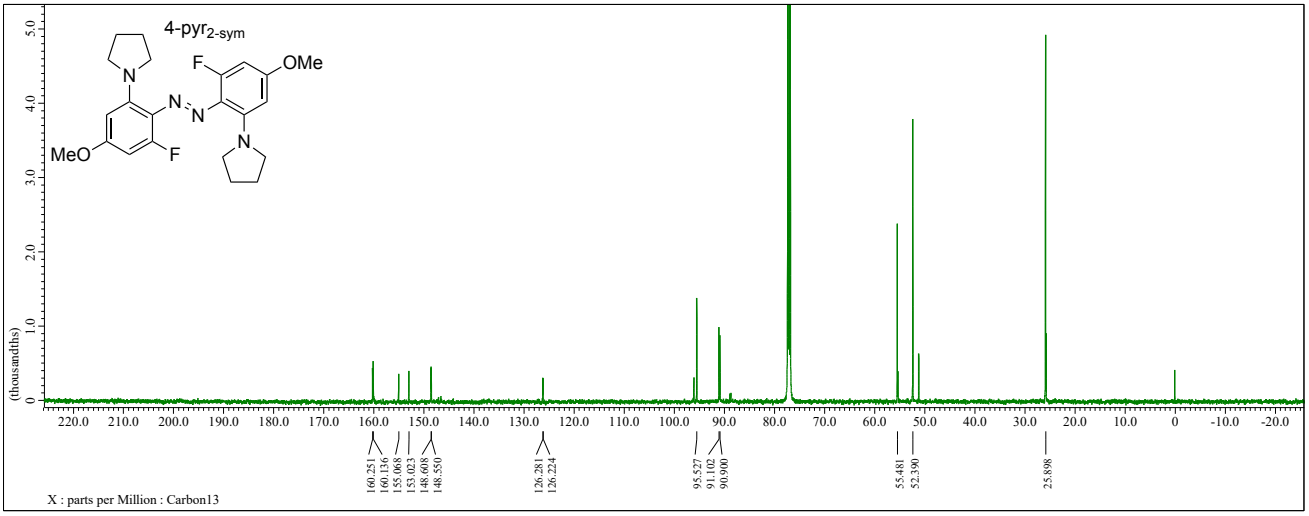

Figure S61. ^{13}C NMR spectrum of **4-pyr$_{2\text{-sym}}$**.

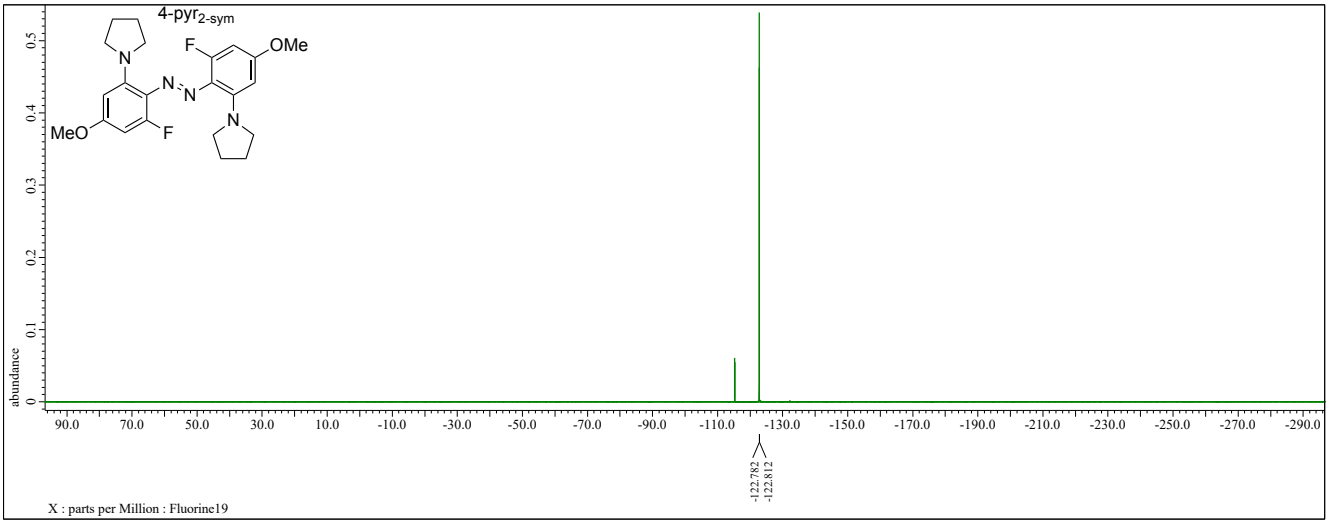

Figure S62. ^{19}F NMR spectrum of **4-pyr$_{2\text{-sym}}$**.

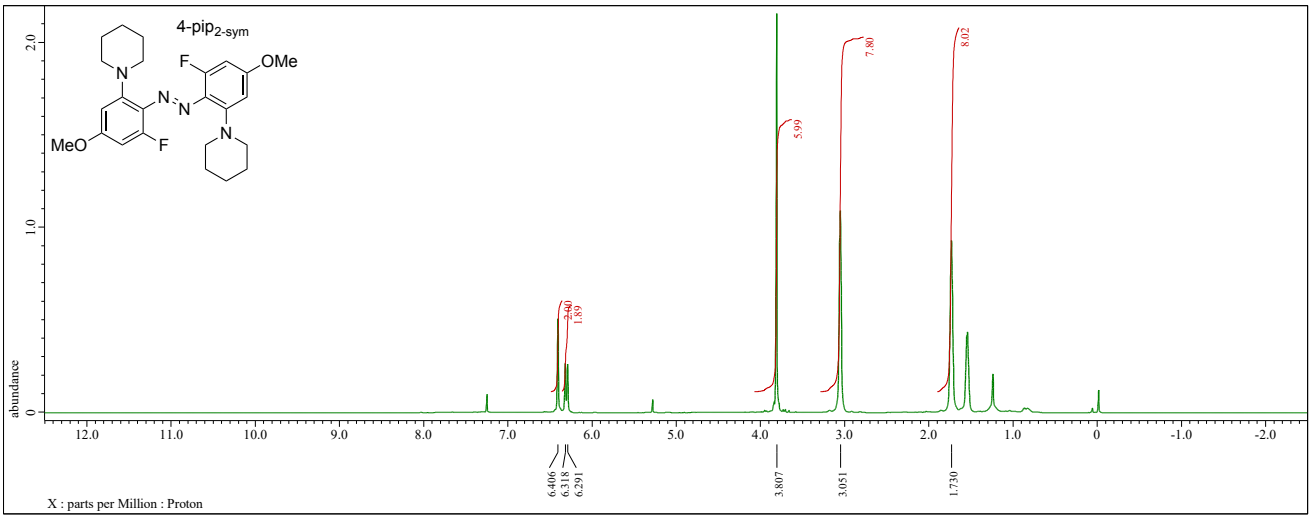

Figure S63. ^{1}H NMR spectrum of **4-pip$_{2\text{-sym}}$**.

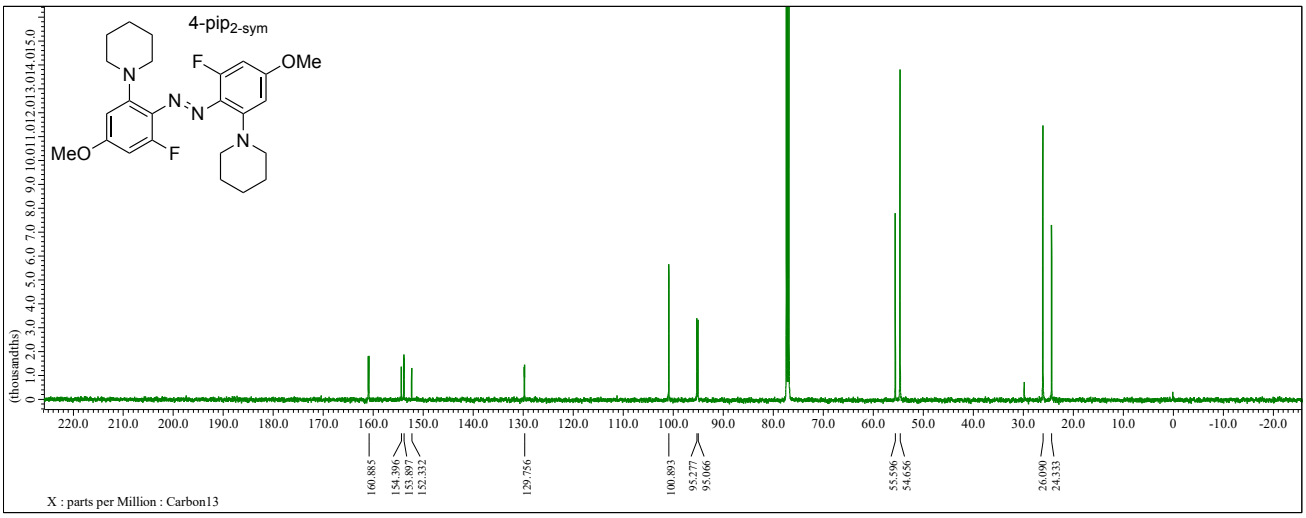

Figure S64. ^{13}C NMR spectrum of **4-pip$_{2\text{-sym}}$**.

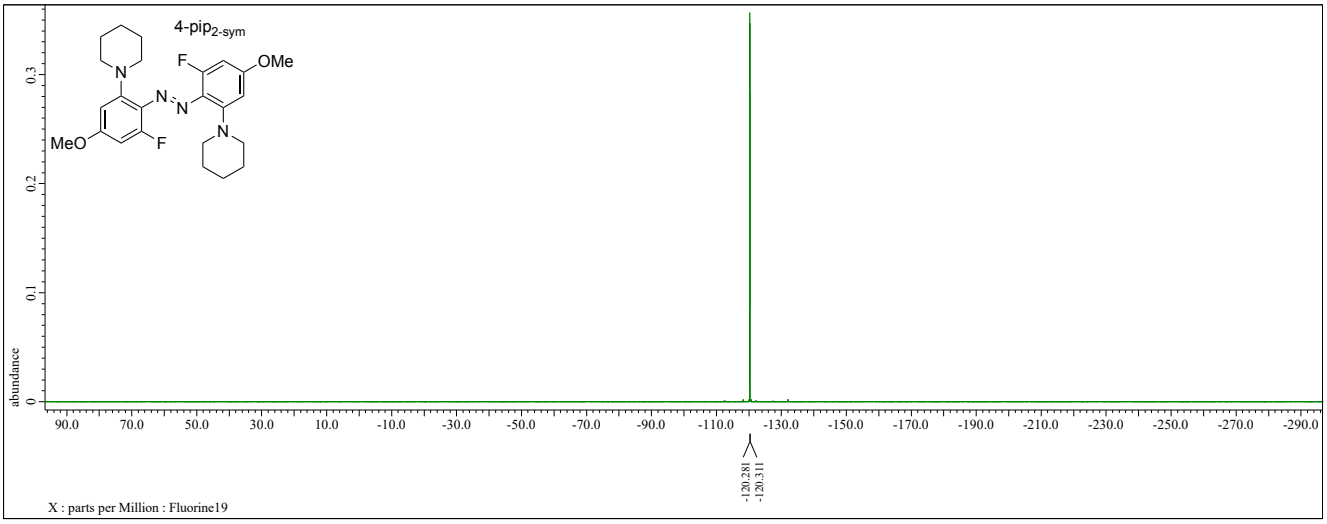

Figure S65. ^{19}F NMR spectrum of **4-pip$_{2\text{-sym}}$**.

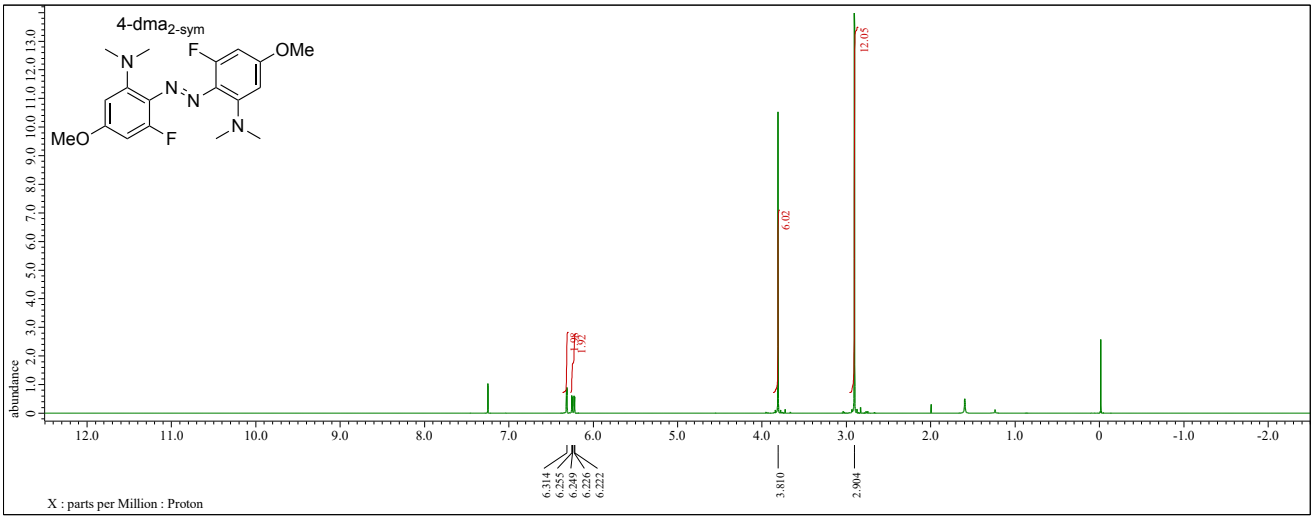

Figure S66. ^{1}H NMR spectrum of **4-dma$_{2\text{-sym}}$**.

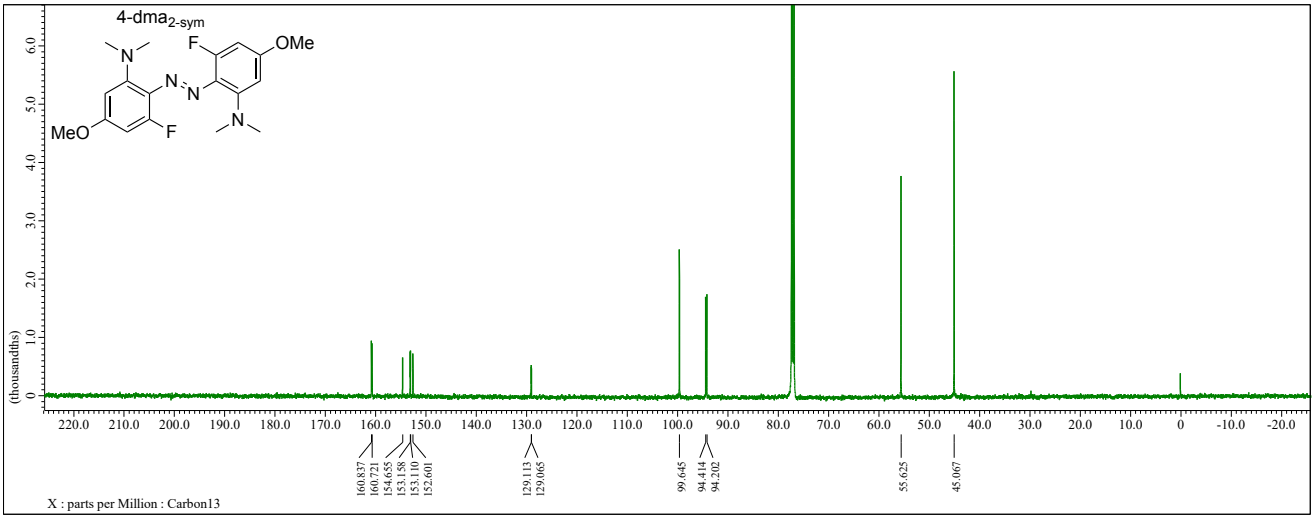

Figure S67. ^{13}C NMR spectrum of **4-dma$_{2\text{-sym}}$**.

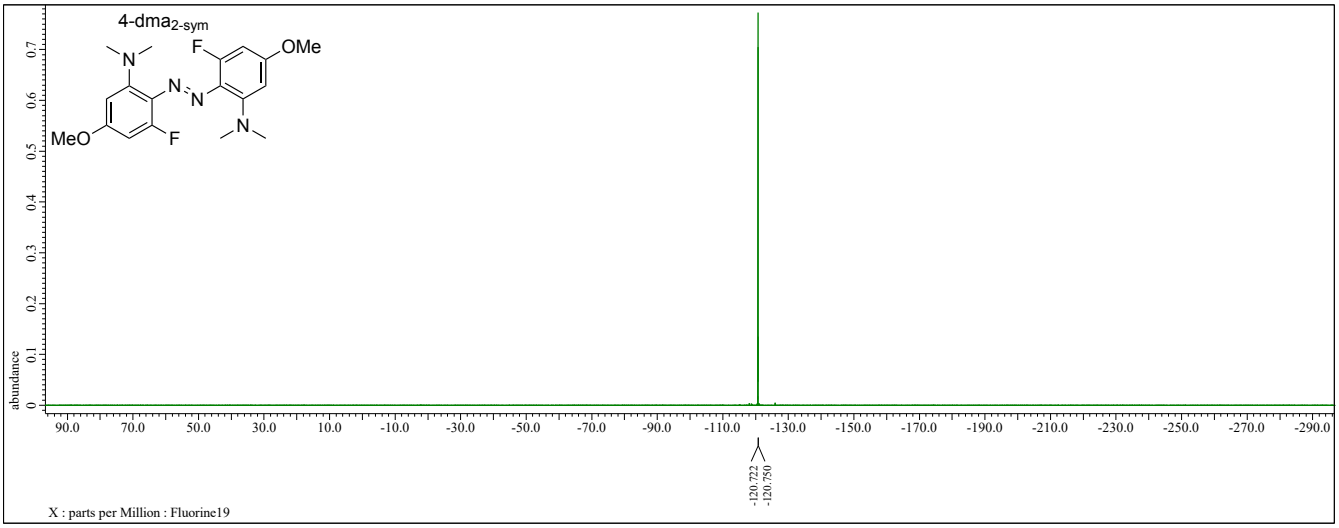

Figure S68. ^{19}F NMR spectrum of **4-dma$_{2\text{-sym}}$**.

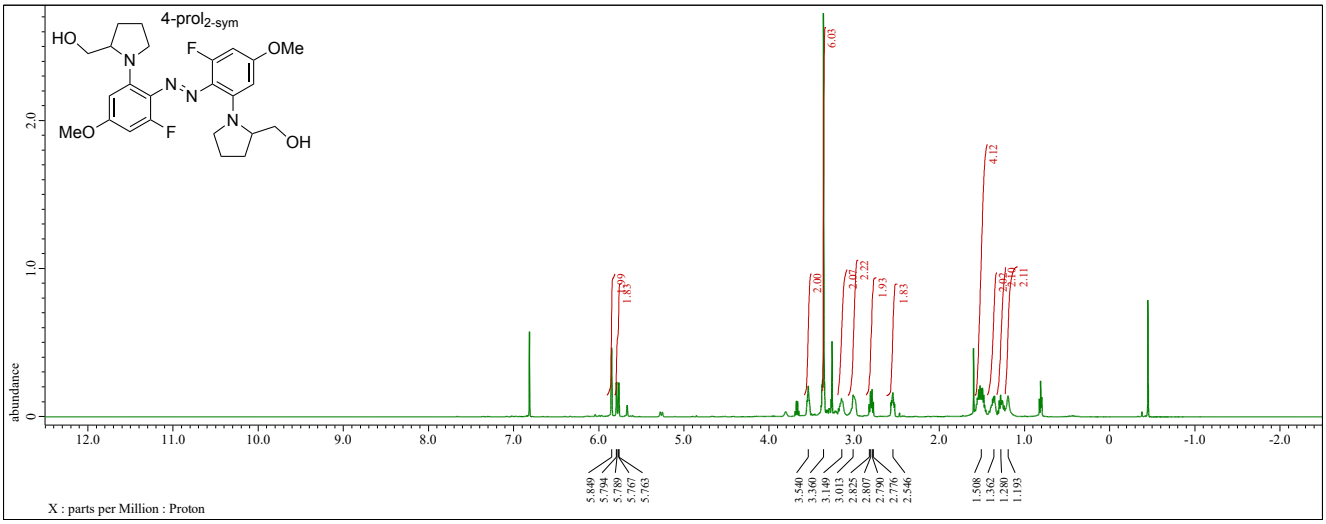

Figure S69. ^{1}H NMR spectrum of **4-prol$_{2\text{-sym}}$**.

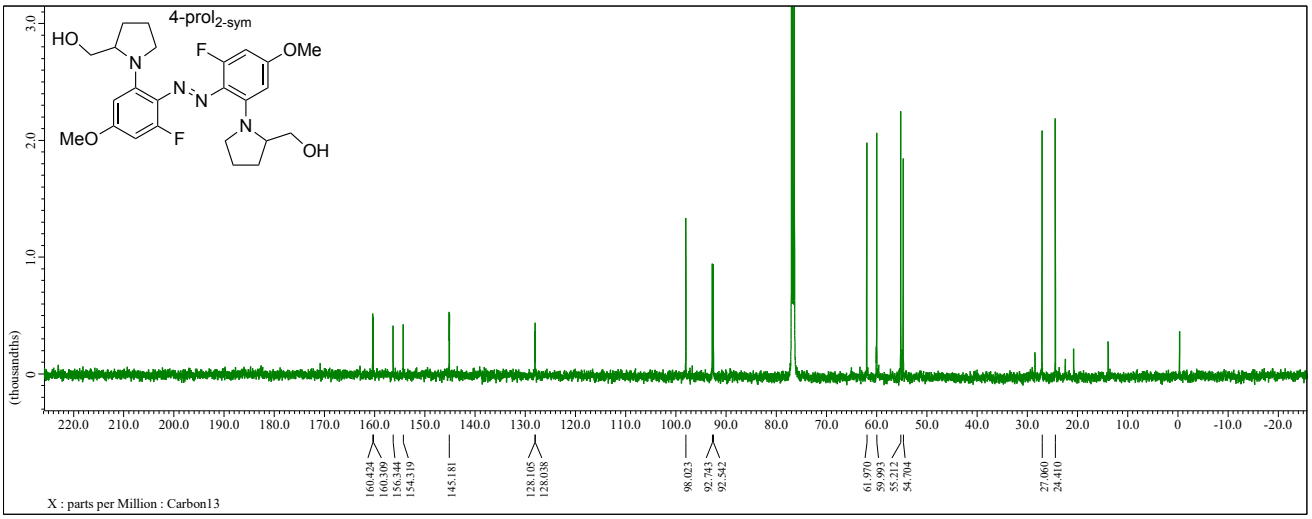

Figure S70. ^{13}C NMR spectrum of **4-prol$_{2\text{-sym}}$**.

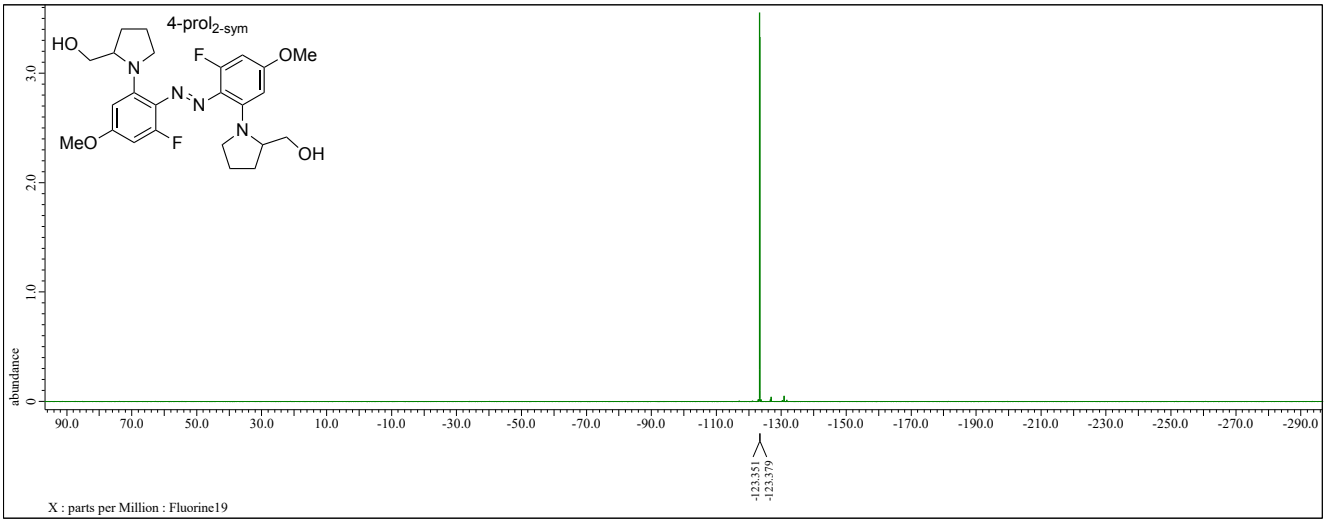

Figure S71. ^{19}F NMR spectrum of **4-prol$_{2\text{-sym}}$**.

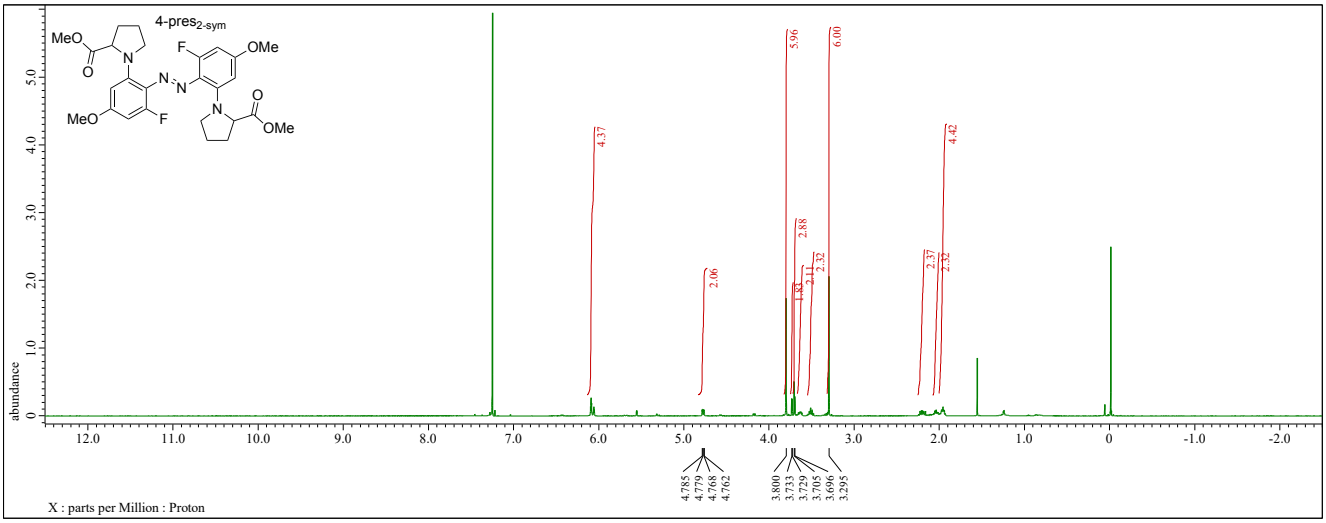

Figure S72. ^{1}H NMR spectrum of **4-pres$_{2\text{-sym}}$**.

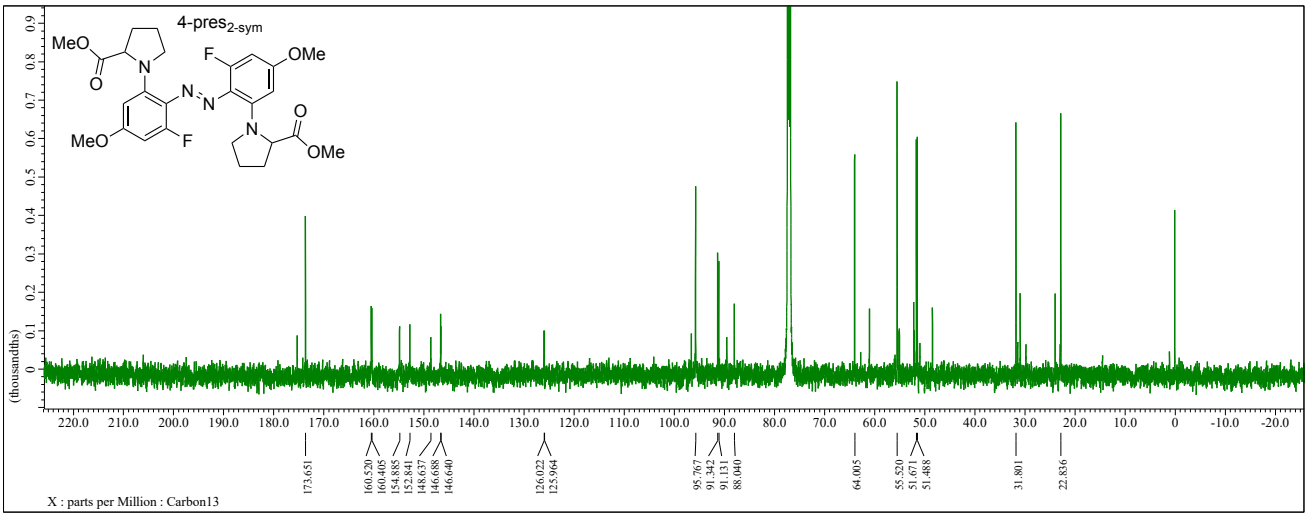

Figure S73. ^{13}C NMR spectrum of **4-pres$_{2\text{-sym}}$**.

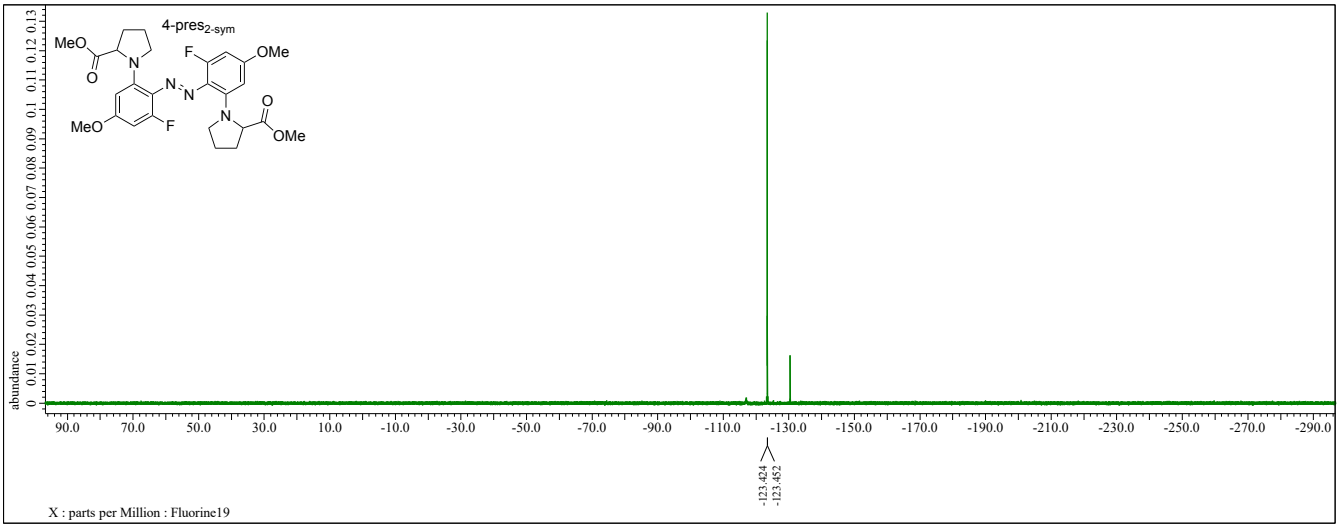

Figure S74. ^{19}F NMR spectrum of **4-pres$_{2\text{-sym}}$**.

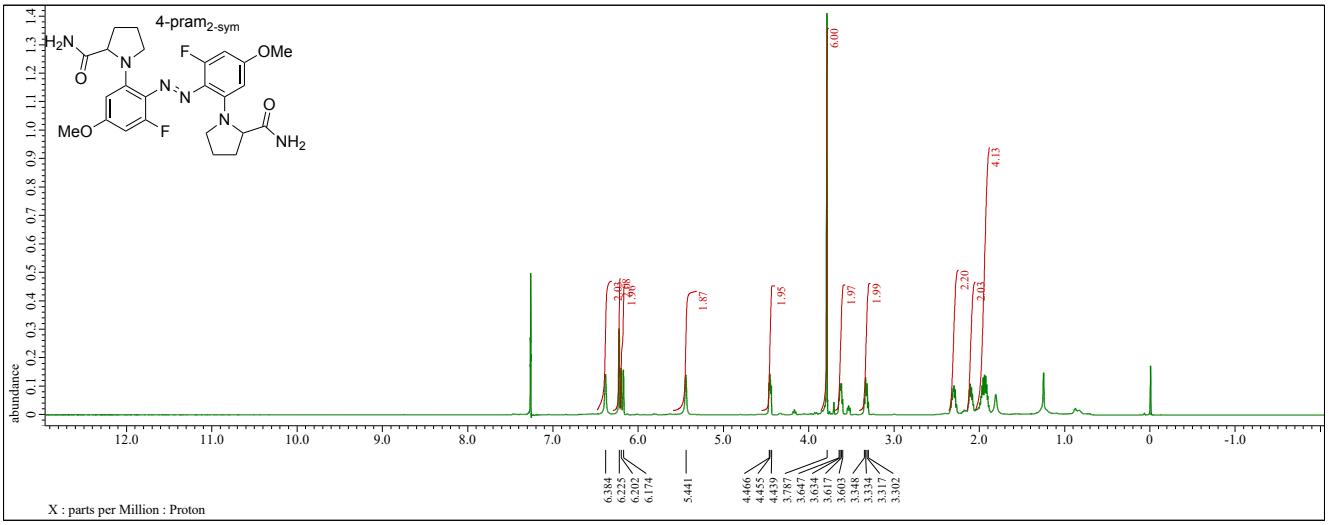

Figure S75. ^{1}H NMR spectrum of **4-pram$_{2\text{-sym}}$**.

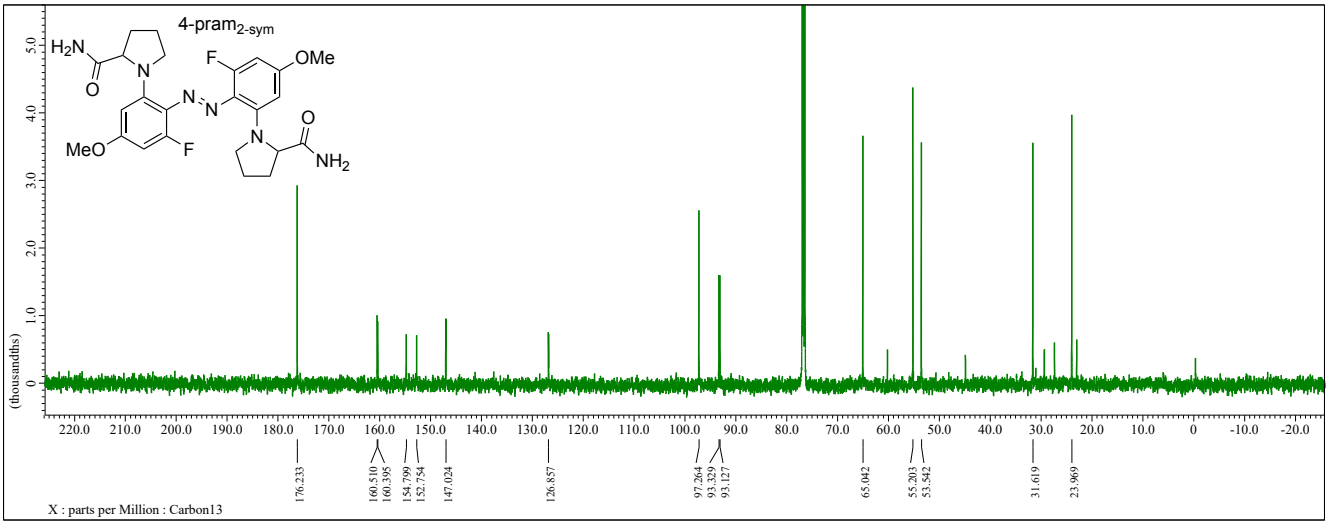

Figure S76. ^{13}C NMR spectrum of **4-pram$_{2\text{-sym}}$**.

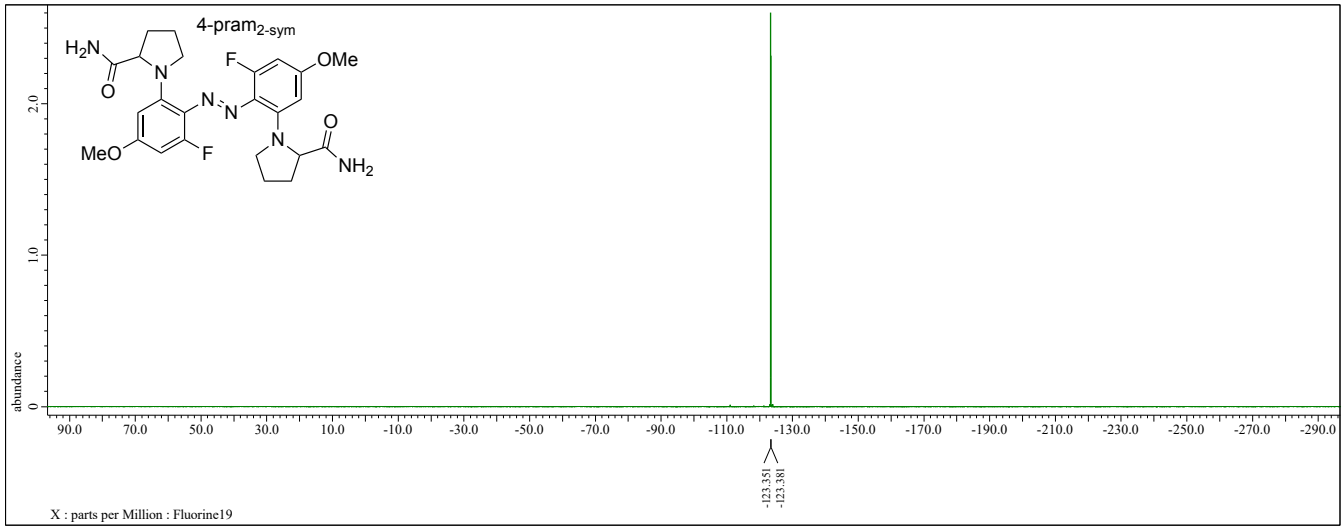

Figure S77. ^{19}F NMR spectrum of **4-pram$_{2\text{-sym}}$**.

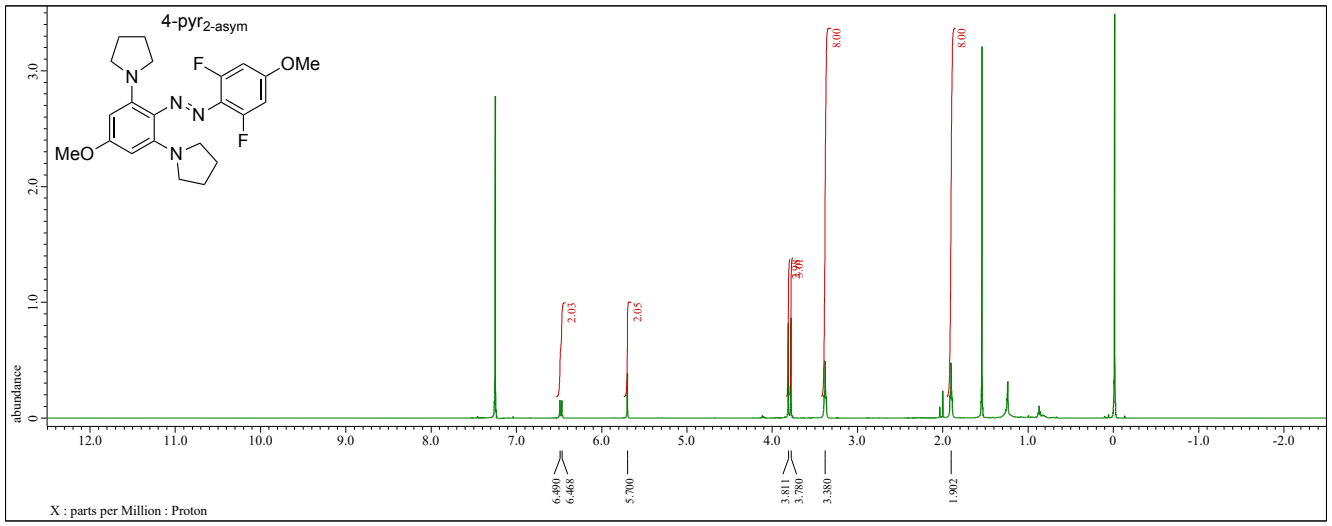

Figure S78. ^{1}H NMR spectrum of **4-pyr$_{2\text{-asym}}$**.

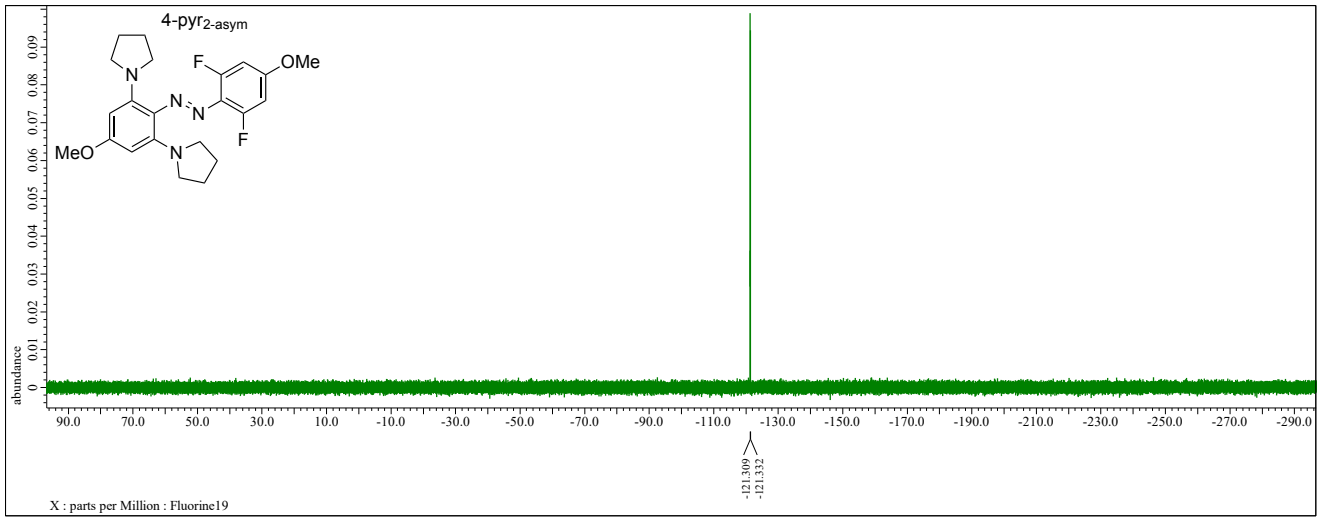

Figure S79. ^{19}F NMR spectrum of **4-pyr$_{2\text{-asym}}$**.

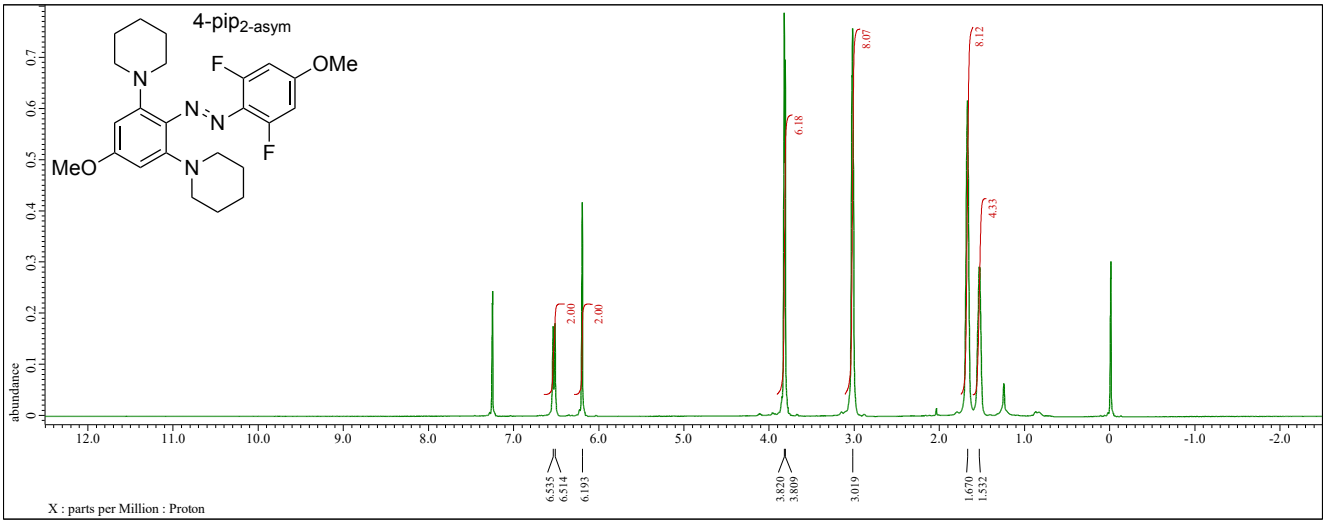

Figure S80. ^{1}H NMR spectrum of **4-pip$_{2\text{-asym}}$**.

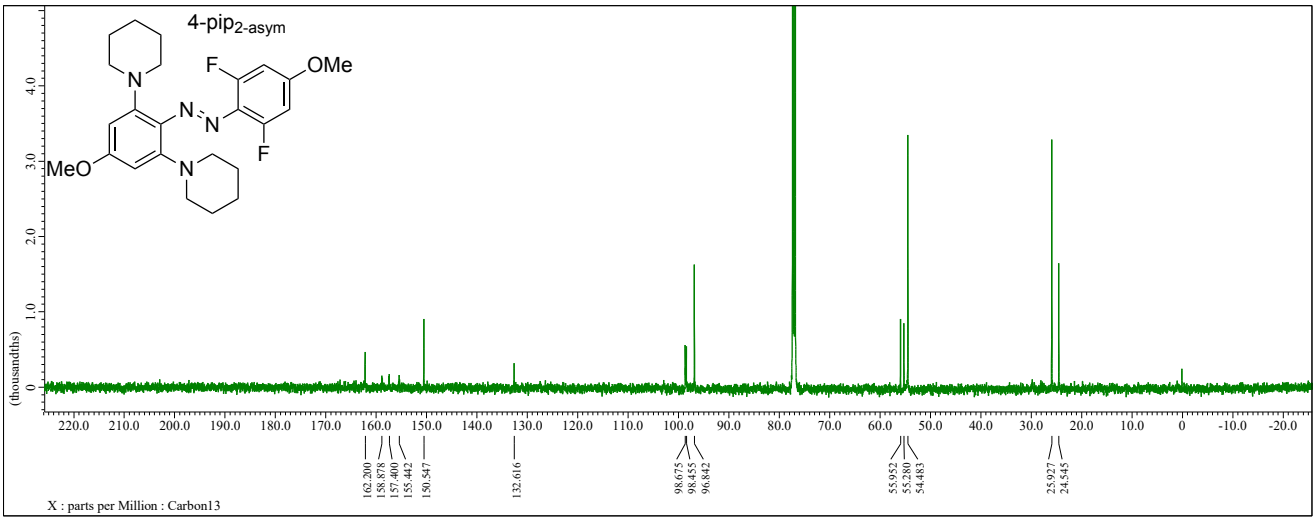

Figure S81. ^{13}C NMR spectrum of **4-pip$_{2\text{-asym}}$**.

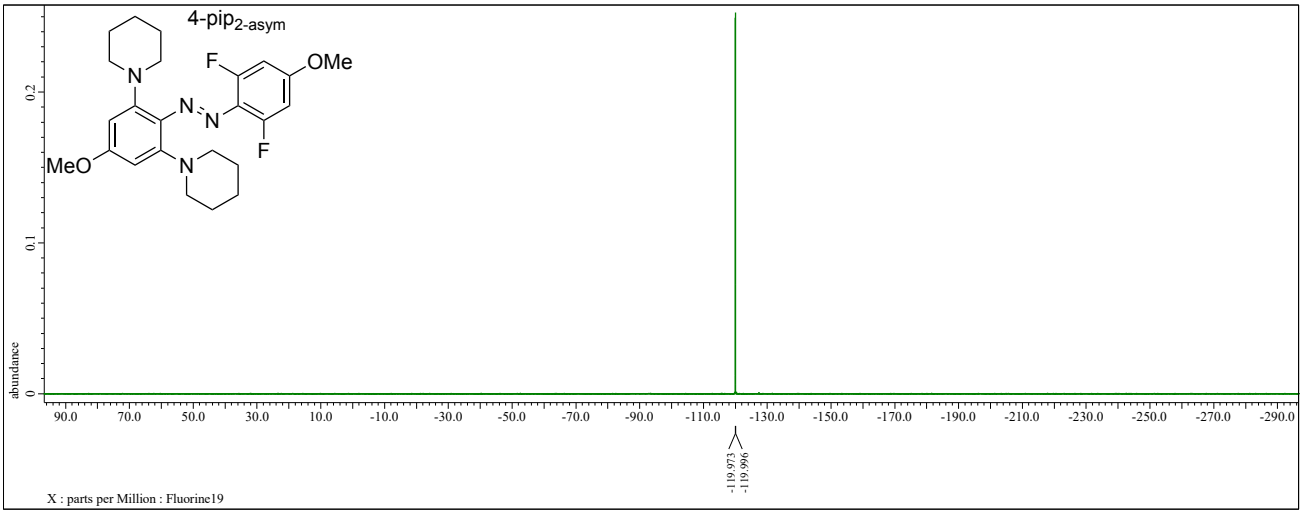

Figure S82. ^{19}F NMR spectrum of **4-pip$_{2\text{-asym}}$**.

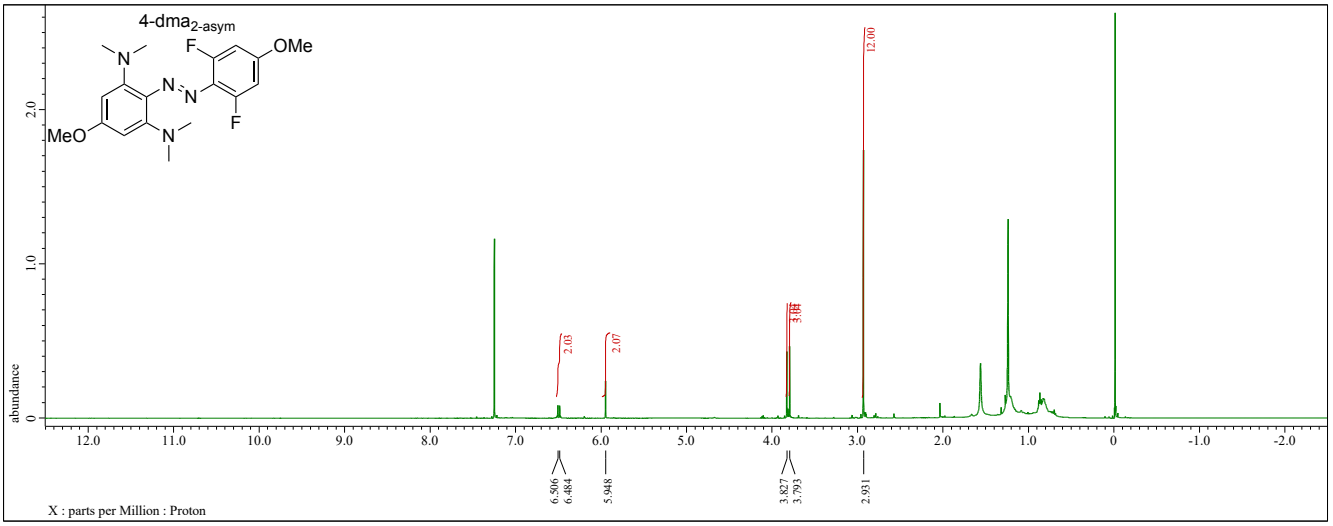

Figure S83. [1]H NMR spectrum of **4-dma$_{2\text{-asym}}$**.

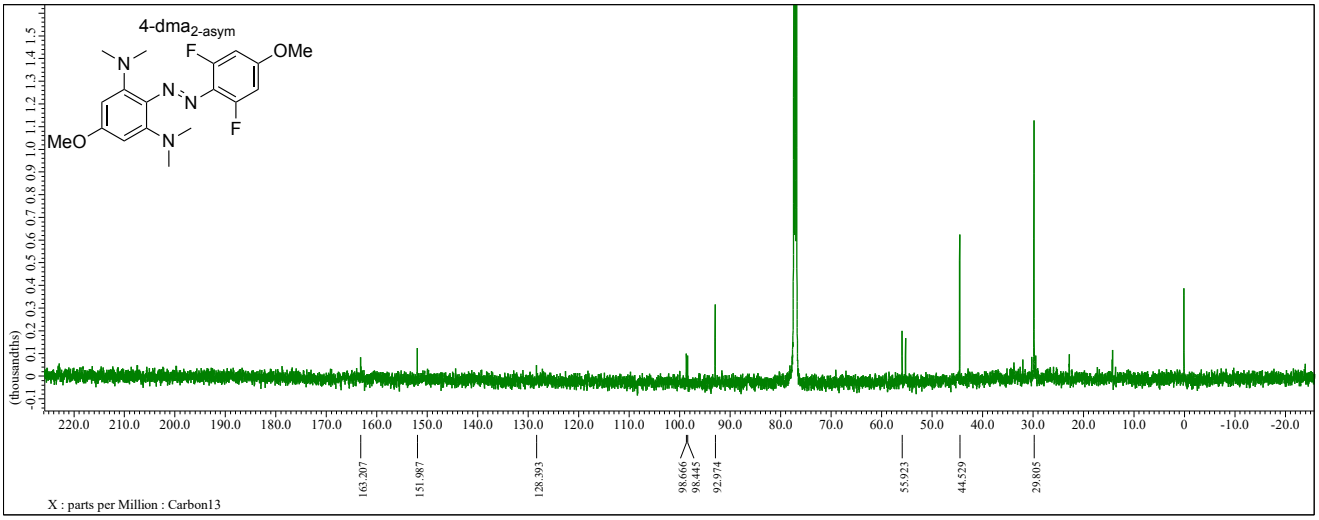

Figure S84. [13]C NMR spectrum of **4-dma$_{2\text{-asym}}$**.

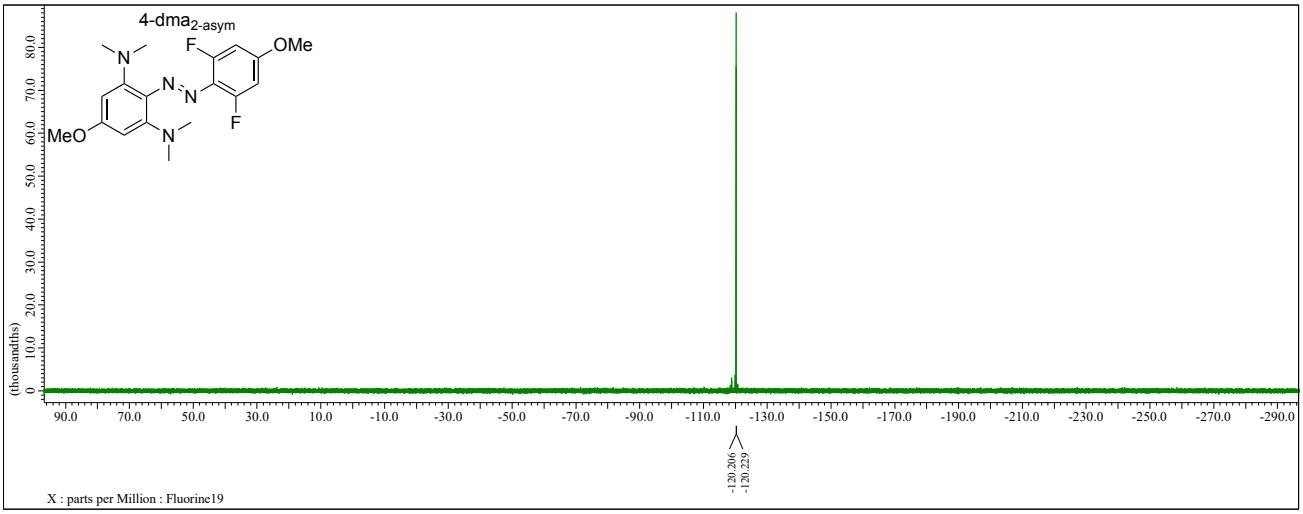

Figure S85. [19]F NMR spectrum of **4-dma$_{2\text{-asym}}$**.

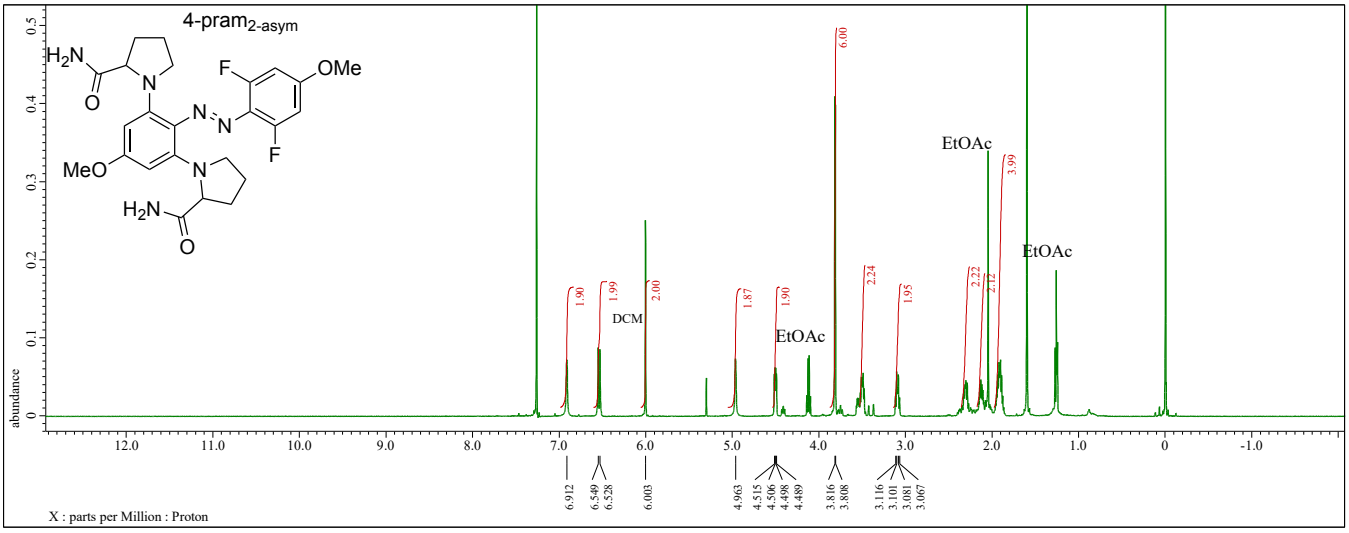

Figure S86. ^{1}H NMR spectrum of **4-pram$_{2\text{-asym}}$**.

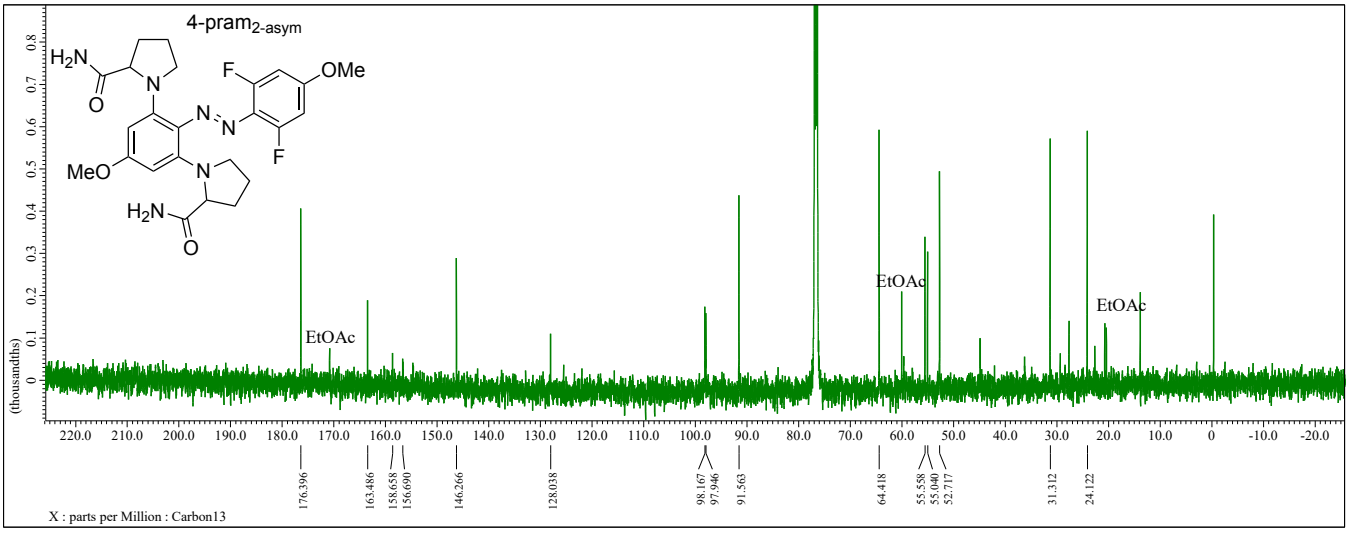

Figure S87. ^{13}C NMR spectrum of **4-pram$_{2\text{-asym}}$**.

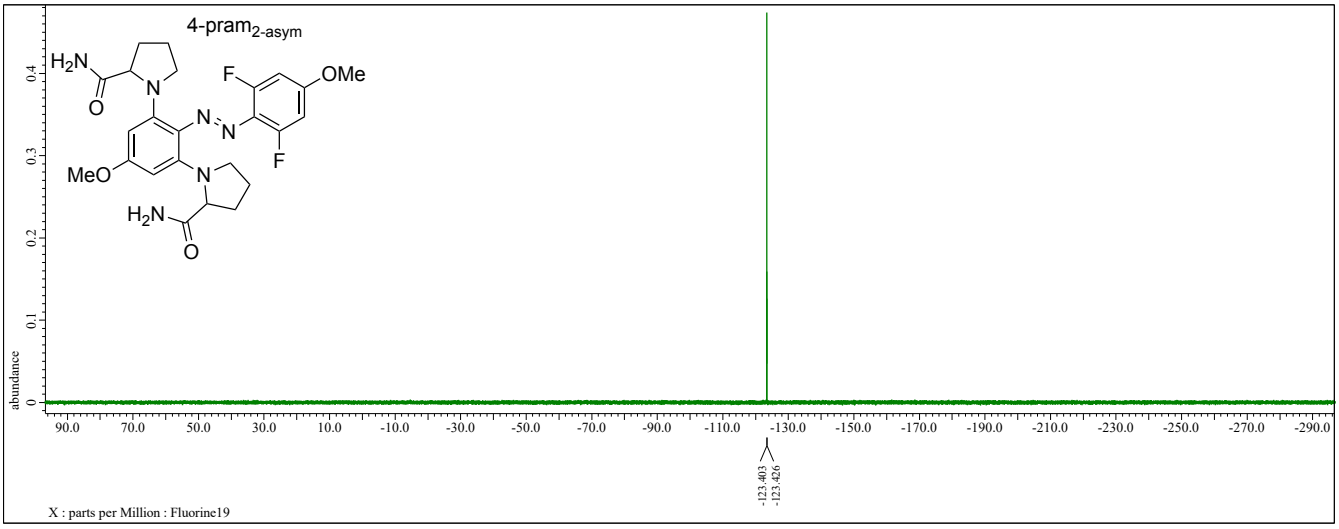

Figure S88. ^{19}F NMR spectrum of **4-pram$_{2\text{-asym}}$**.

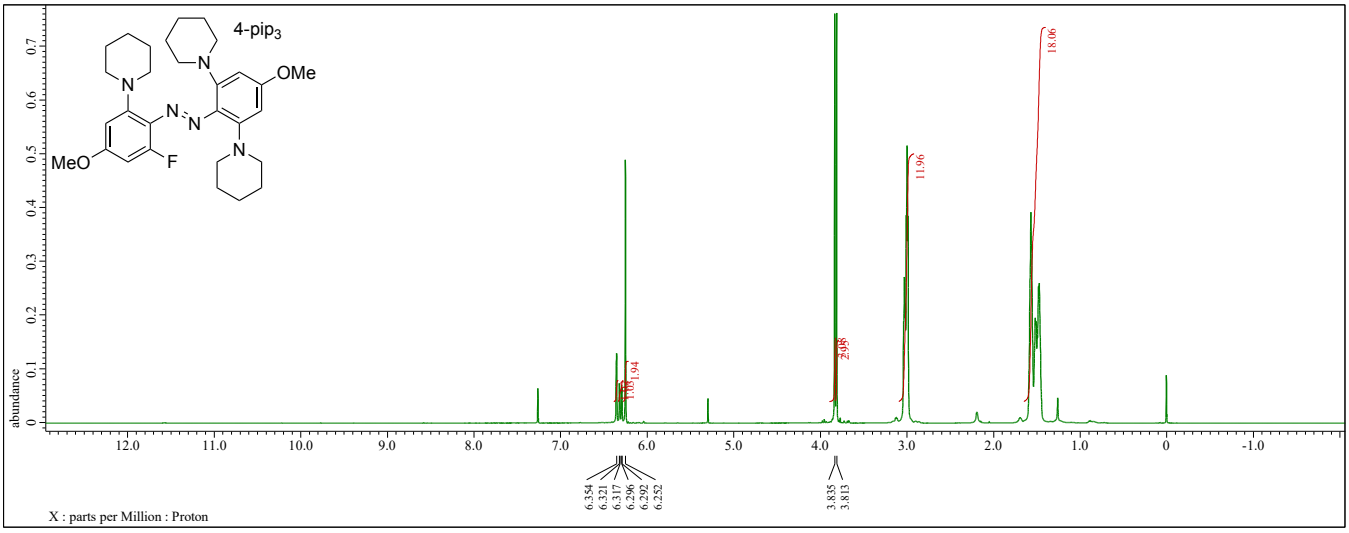

Figure S89. ^{1}H NMR spectrum of **4-pip$_3$**.

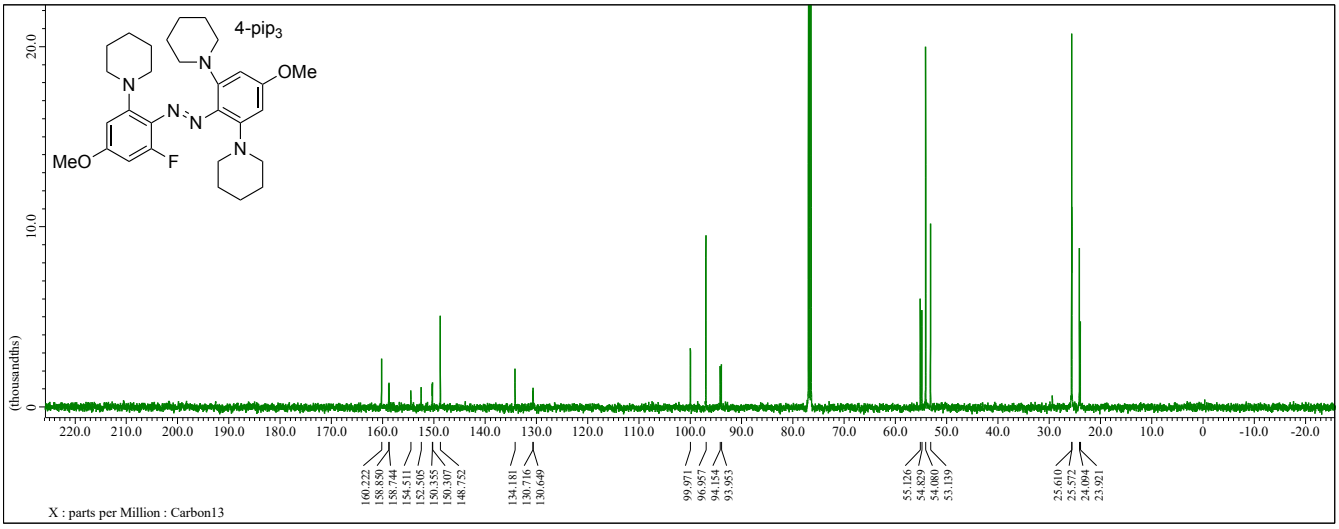

Figure S90. ^{13}C NMR spectrum of **4-pip$_3$**.

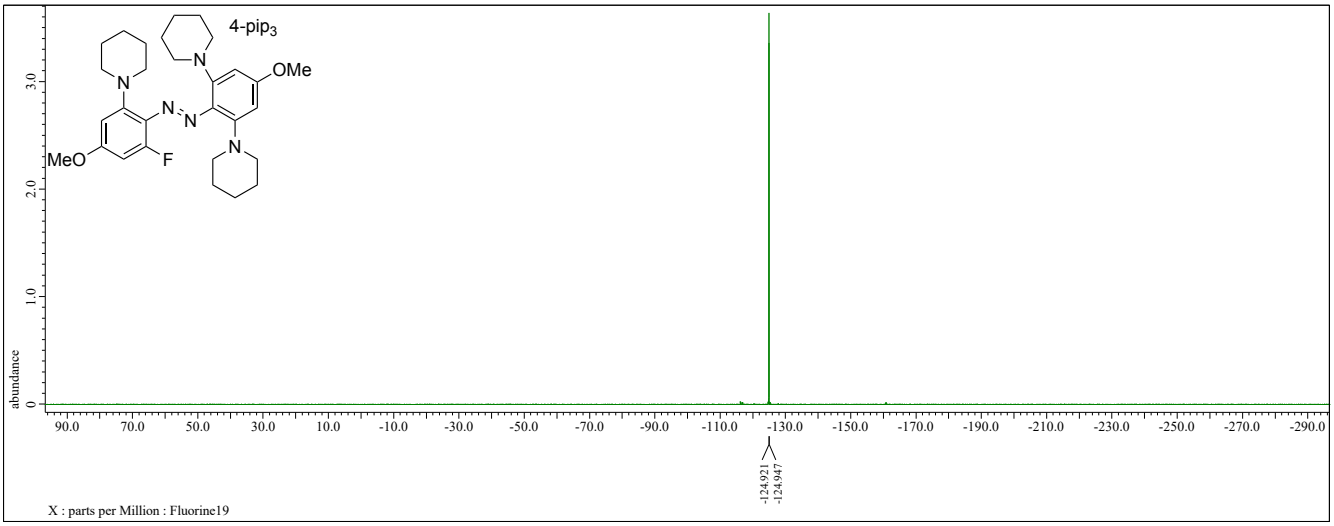

Figure S91. ^{19}F NMR spectrum of **4-pip$_3$**.

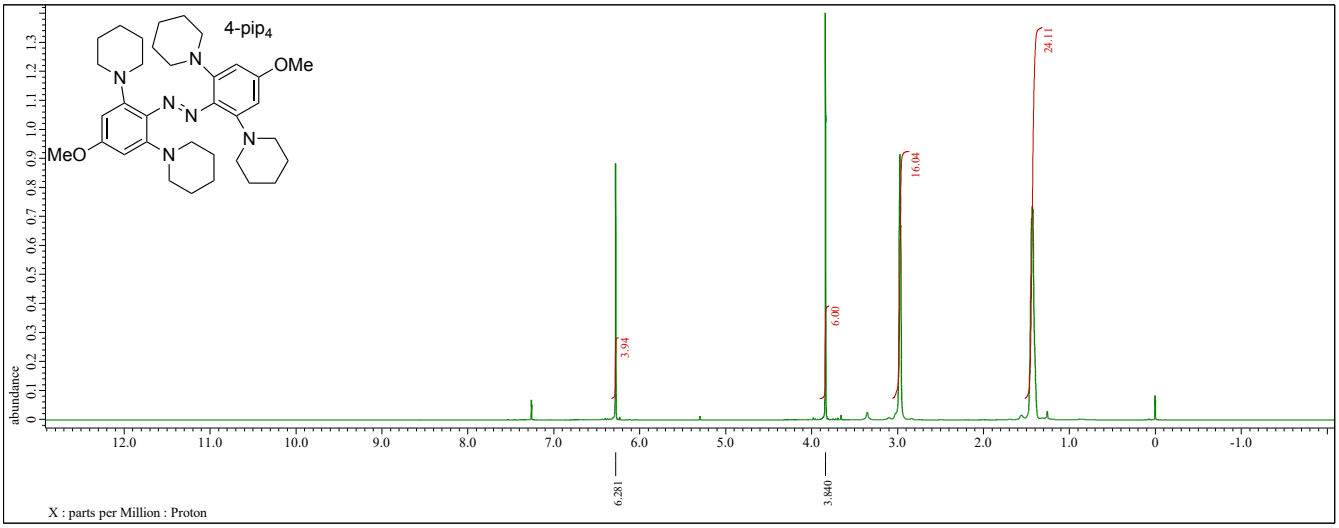

Figure S92. ^{1}H NMR spectrum of **4-pip$_4$**.

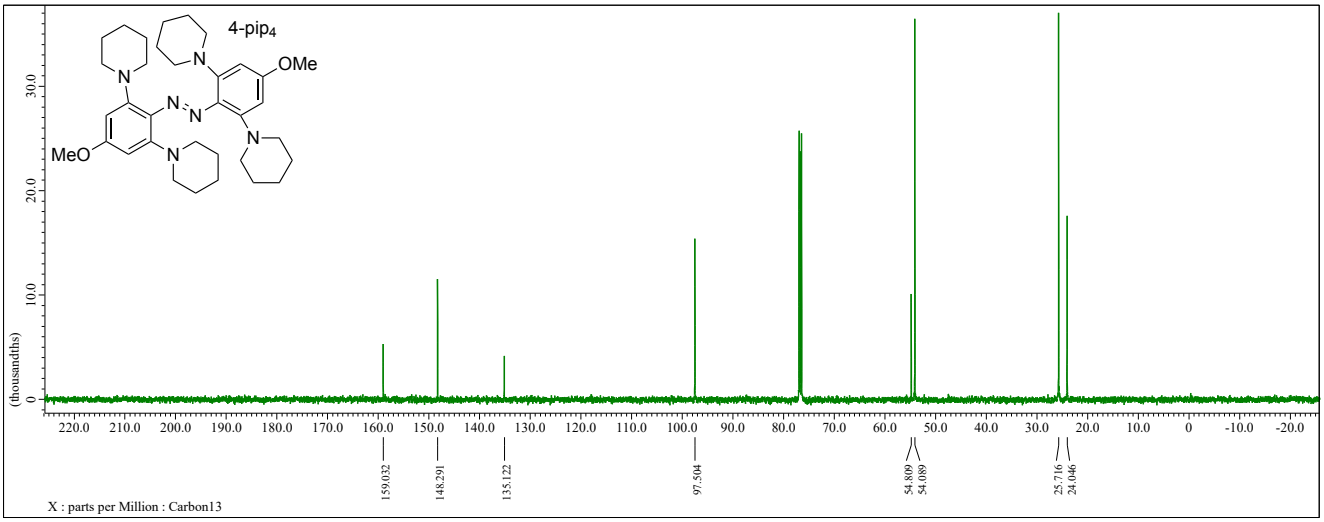

Figure S93. ^{13}C NMR spectrum of **4-pip$_4$**.

Photochemical studies

UV-Visible absorption spectra were recorded with an Agilent Cary 60 spectrophotometer equipped with an Ocean Optics Qpod 2e Peltier-thermostated cell holder whose temperature accuracy is 0.1 °C. Photoexcitation was conducted using a Prior Lumen 1600 light source containing multiple narrow-band LEDs at different wavelengths. The illumination intensities were acquired by measuring the illumination powers with a Coherent LabMax thermal power meter and dividing the number by the area of the cuvette being illuminated (0.78 cm^2). Quartz fluorescence cuvettes with an optical path of 1.0 cm were used for all measurements. The molar absorption coefficients were calculated with the Beer-Lambert law for each distinguishable absorption peak. For figures the absorption spectra were normalized to 1 with respect to the π–π* band.

Photostationary state (*PSS*) refers to the mixture of isomers upon constant illumination with a chosen excitation wavelength. *Dark*, in turn, refers to the mixture of isomers after an elongated period in a dark cavity at room temperature or in an elevated temperature. Based on the thermal relaxation lifetime of the molecules, the time and temperature were chosen so that the mixture would consist of azobenzenes only in the *trans* state.

The photostationary state compositions were determined by comparing the absorbance values of the photostationary state mixture with those in the dark spectrum. The *cis*-fraction was calculated from the wavelength that had the greatest difference in the absorbance values. If the *cis*-absorbance at this wavelength is assumed zero and the dark spectrum is assumed to equal to that of pure *trans* isomer, the *cis*-fraction is $1 - \frac{Abs_{pss}}{Abs_{dark}}$. This is a minimum value, as the *cis*-absorbance is typically non-zero. If the dark spectrum is not entirely *trans* (i.e., the mixture has not been in dark for long enough to isomerize completely to *trans*), this will also lower the calculated *cis*-fraction compared to the true value.

Thermal isomerization studies

The thermal isomerization rates were determined with the same methodology as in our earlier study[1]. The 50–150 µM acetonitrile solutions were illuminated with 365, 385 or 405 nm light until a photostationary state was reached. The illumination was then stopped and the absorbance near the absorption maximum of the *trans* isomer was monitored as a function of time. The measured absorbance values were fitted with a monoexponential function. If the thermal *cis*-to-*trans* isomerization was fast, one measurement at 25°C was carried out. Otherwise, the rates were determined at 50, 60 and 70°C and extrapolated to 25°C using the Arrhenius equation. The analyses are presented for all new compounds in Fig. S94–S125.

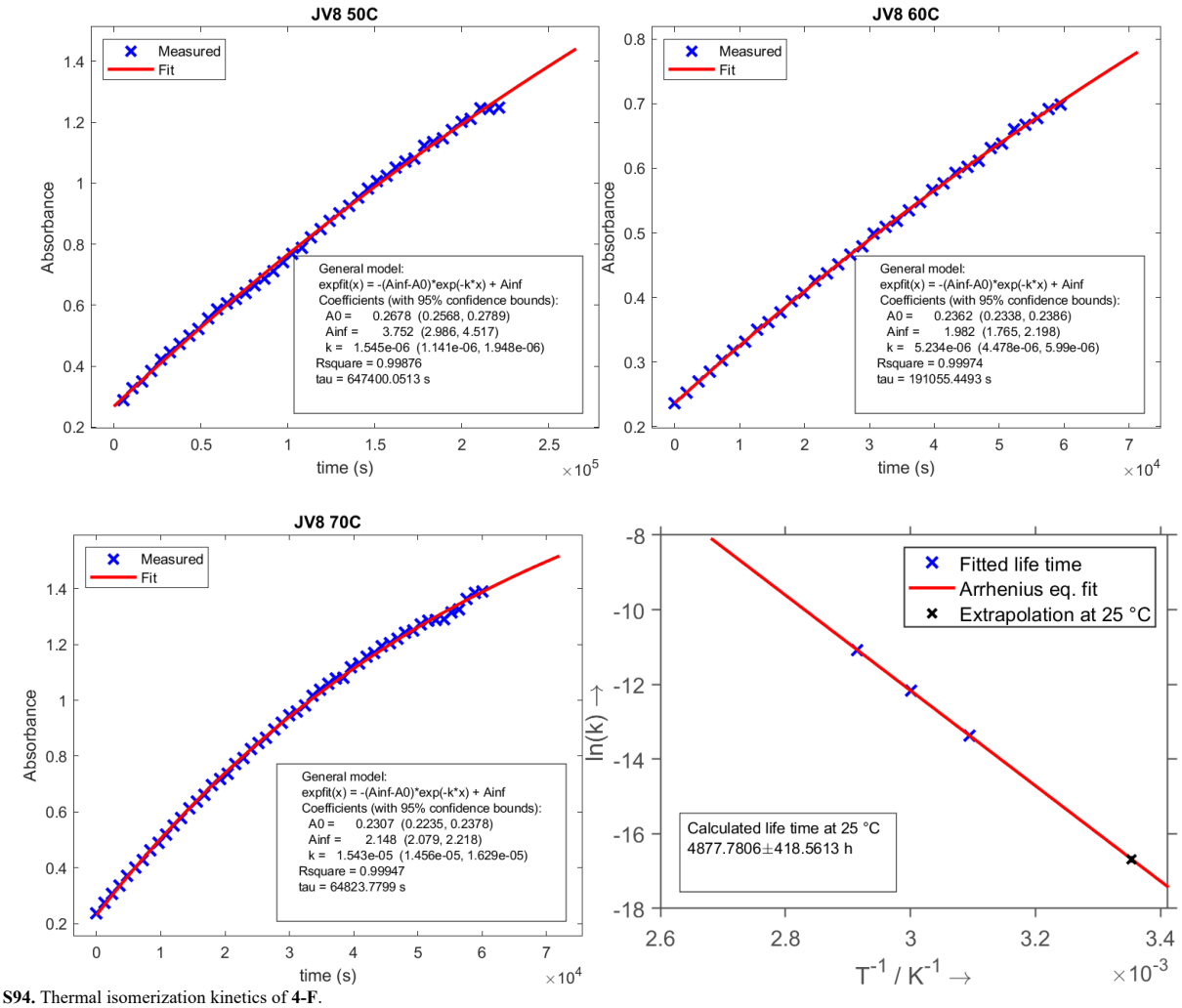

Figure S94. Thermal isomerization kinetics of **4-F**.

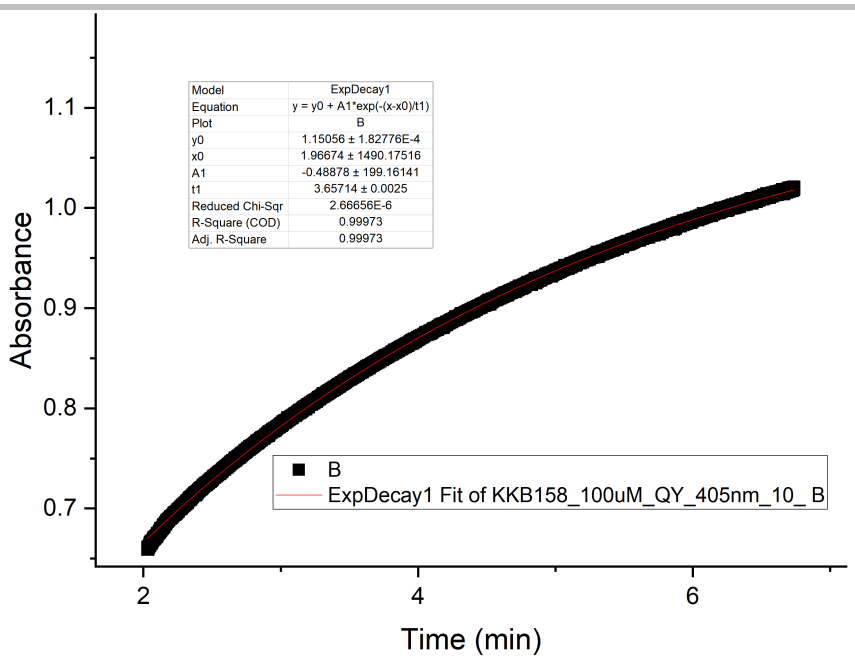

Figure S95. Thermal isomerization kinetics of **1-dma**.

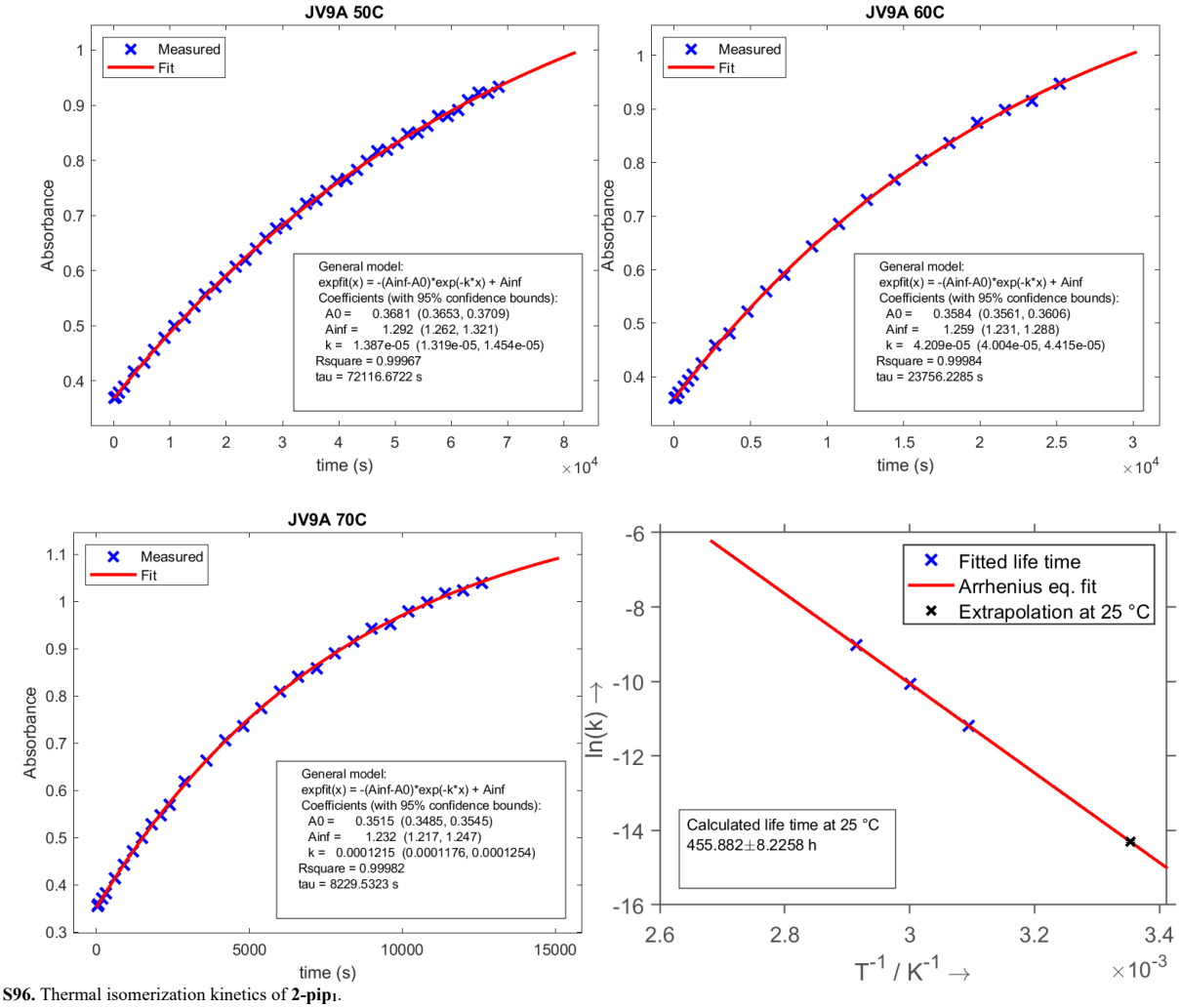

Figure S96. Thermal isomerization kinetics of **2-pip**$_1$.

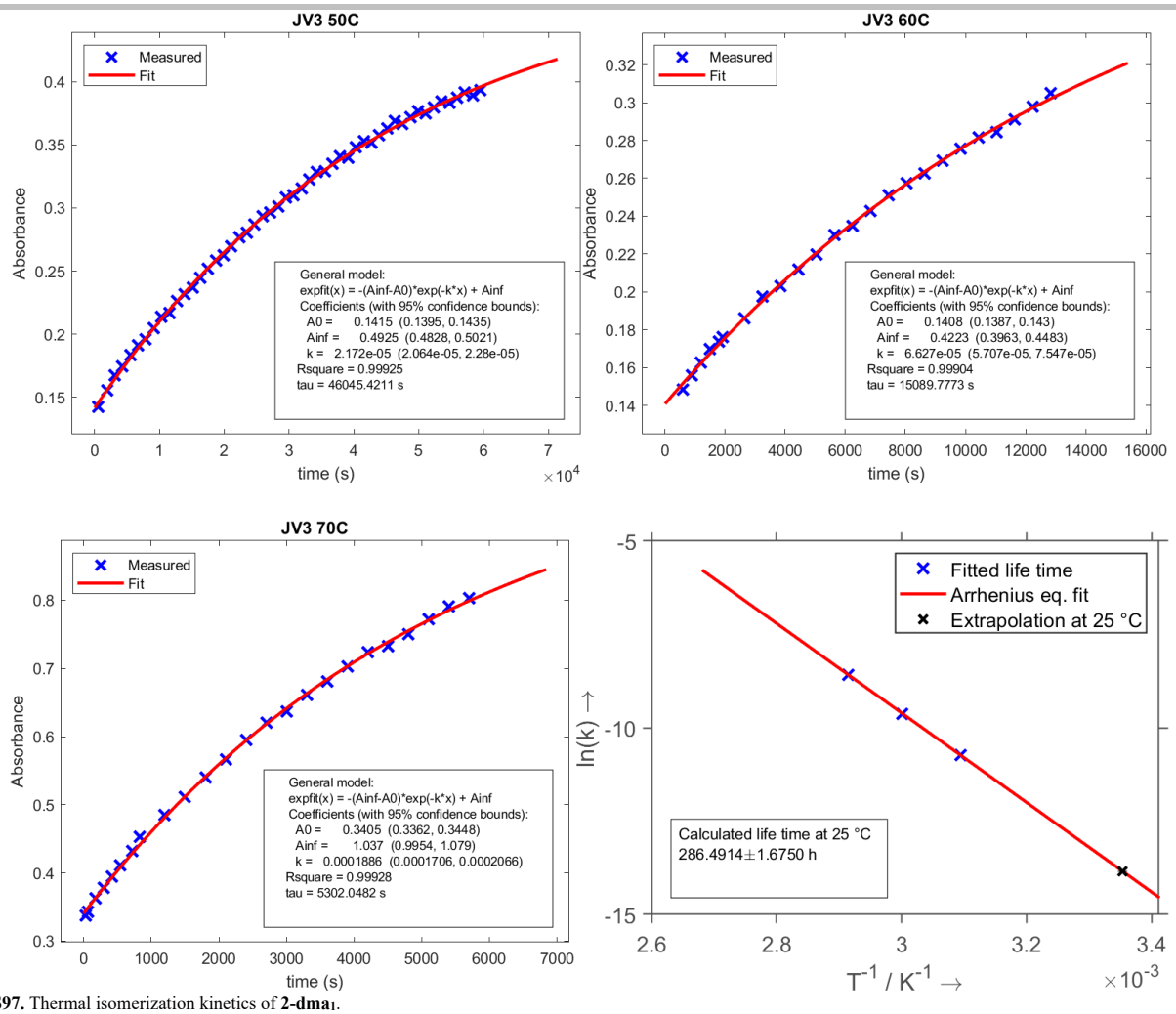

Figure S97. Thermal isomerization kinetics of **2-dma$_1$**.

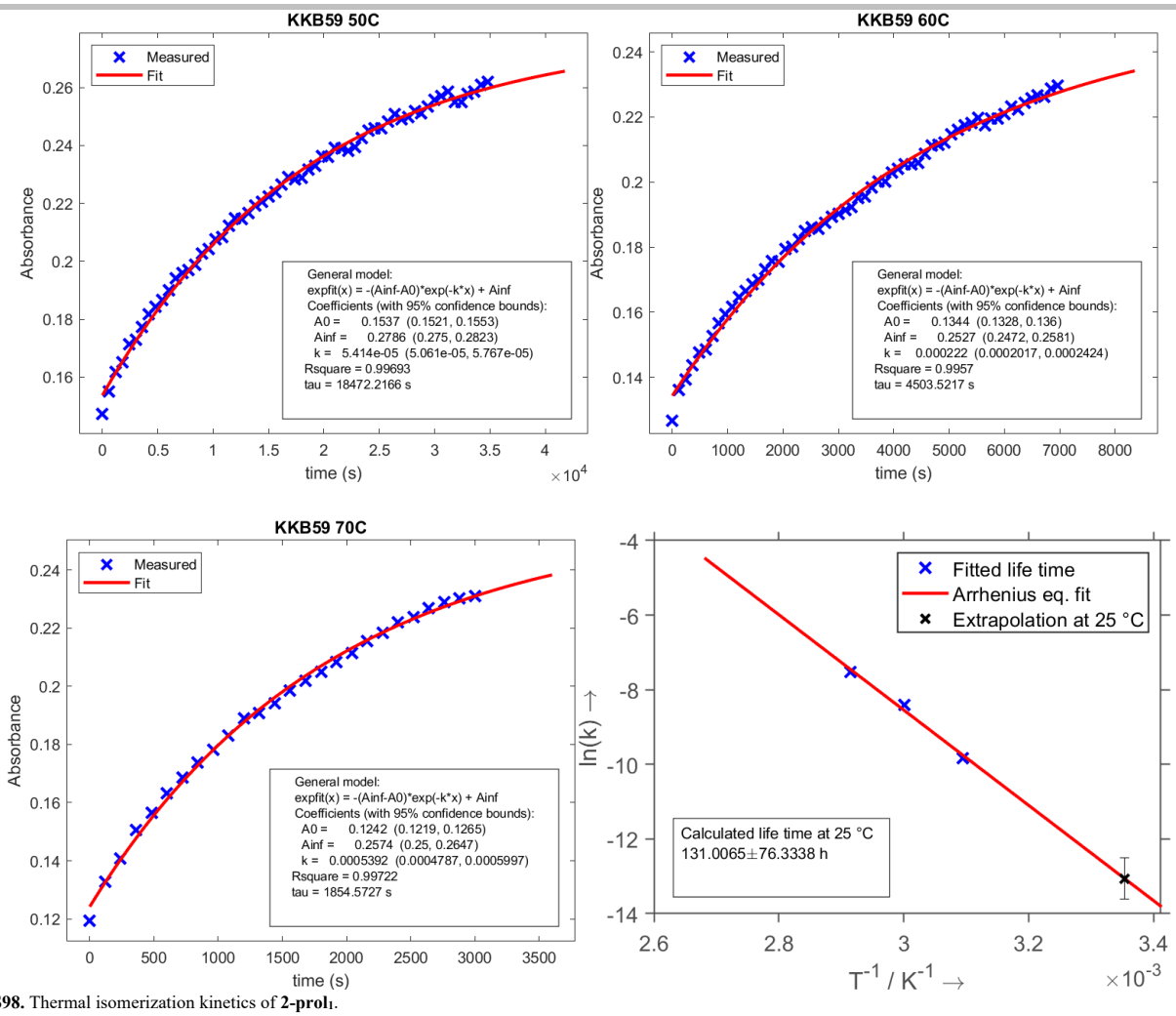

Figure S98. Thermal isomerization kinetics of **2-prol$_1$**.

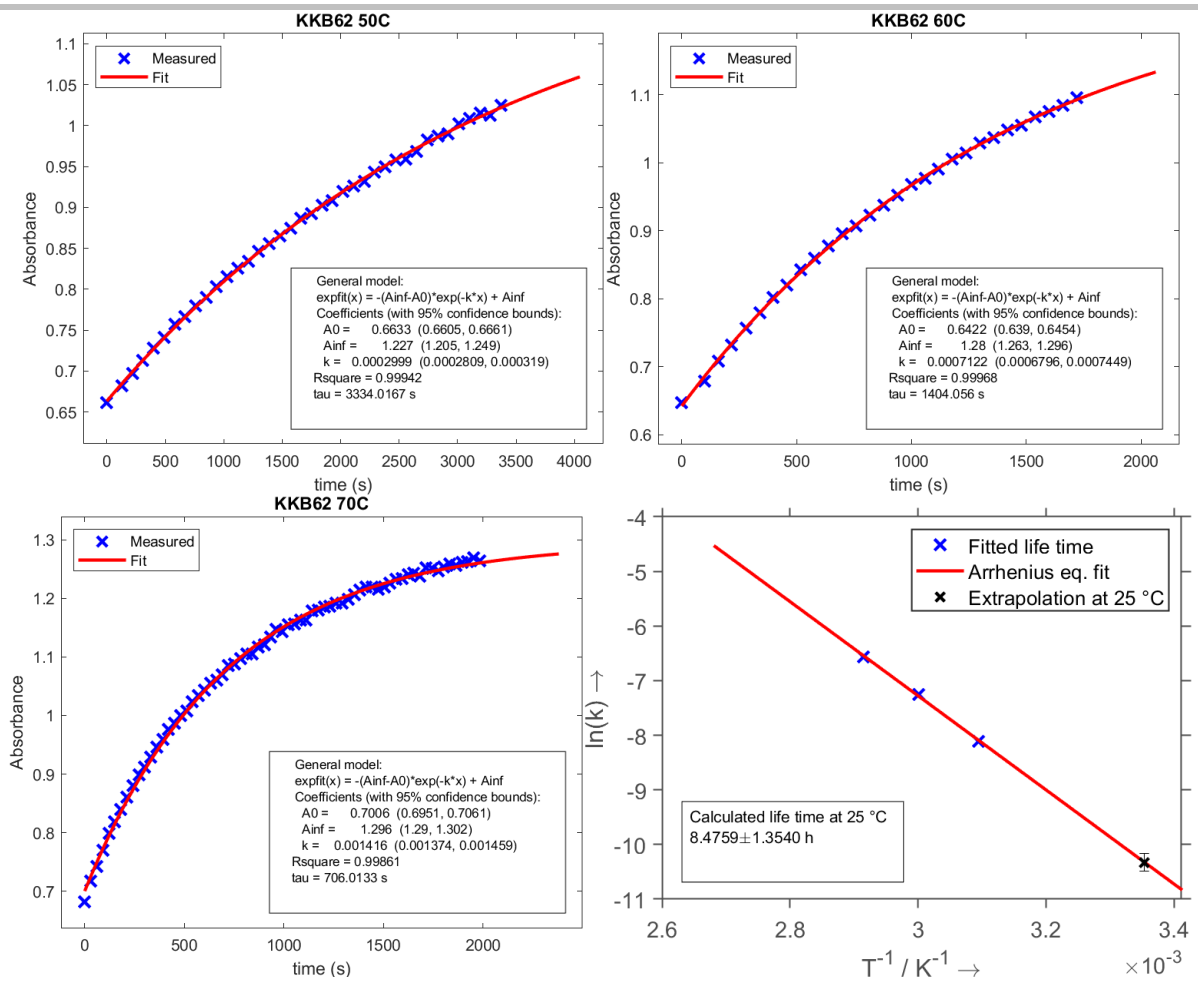

Figure S99. Thermal isomerization kinetics of **2-pres**$_1$.

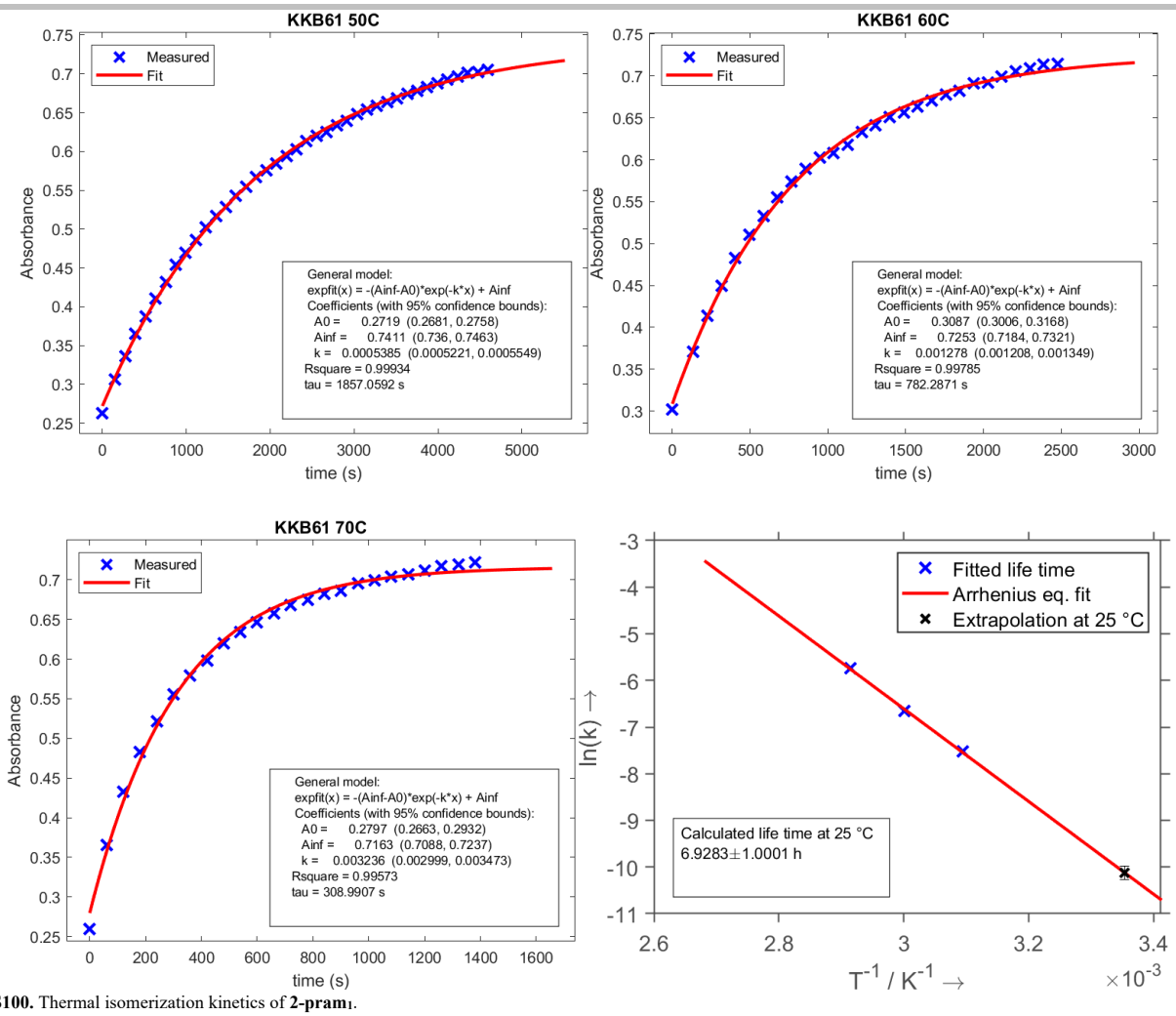

Figure S100. Thermal isomerization kinetics of **2-pram**$_1$.

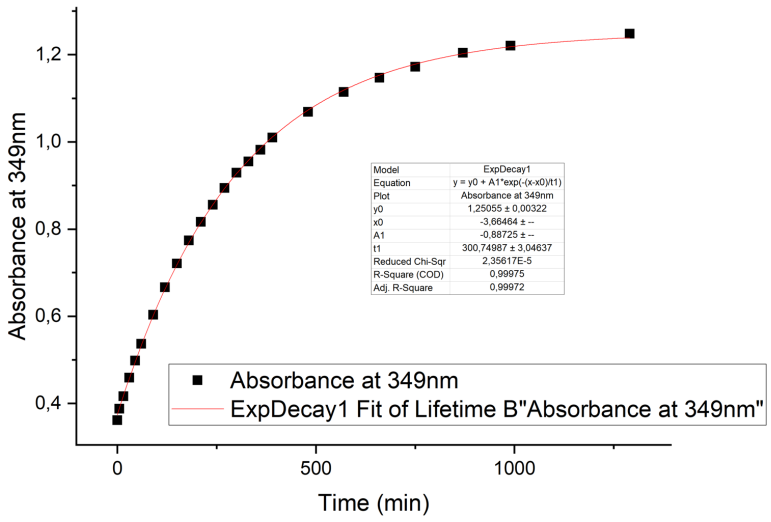

Figure S101. Thermal isomerization kinetics of **3-pip**$_1$.

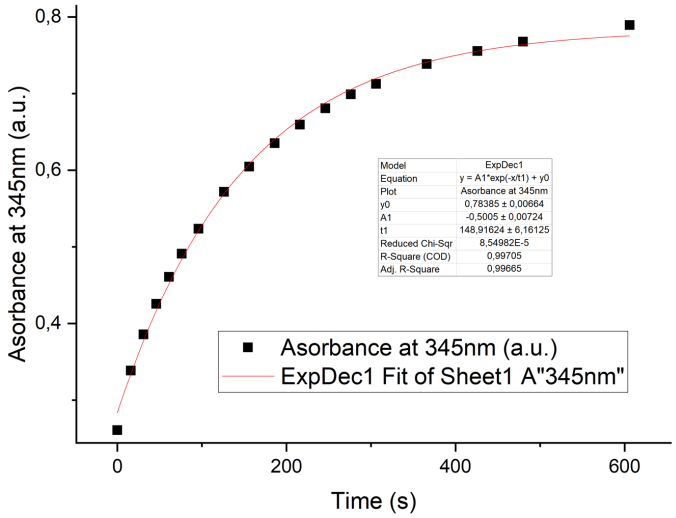

Figure S102. Thermal isomerization kinetics of **3-dma**$_1$.

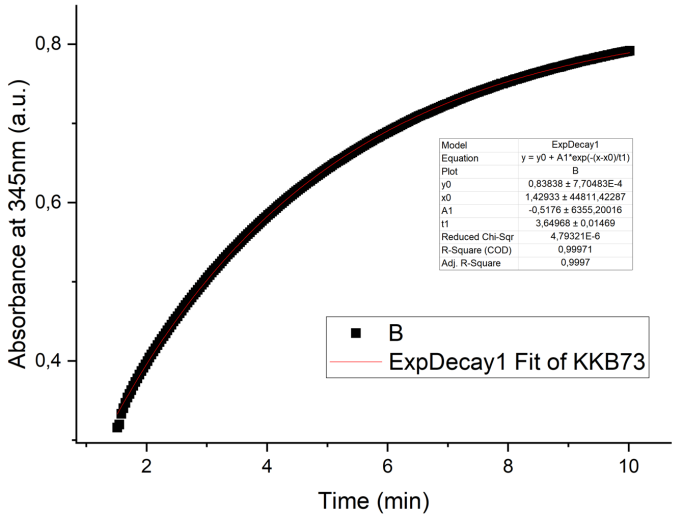

Figure S102. Thermal isomerization kinetics of **3-prol**$_1$.

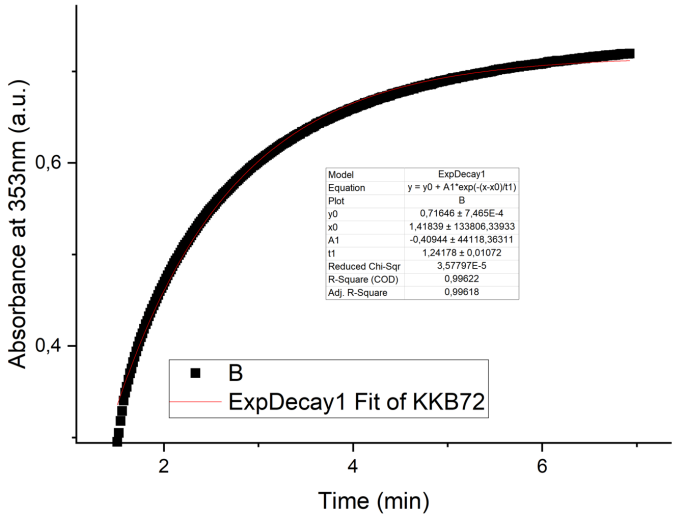

Figure S103. Thermal isomerization kinetics of **3-pres**$_1$.

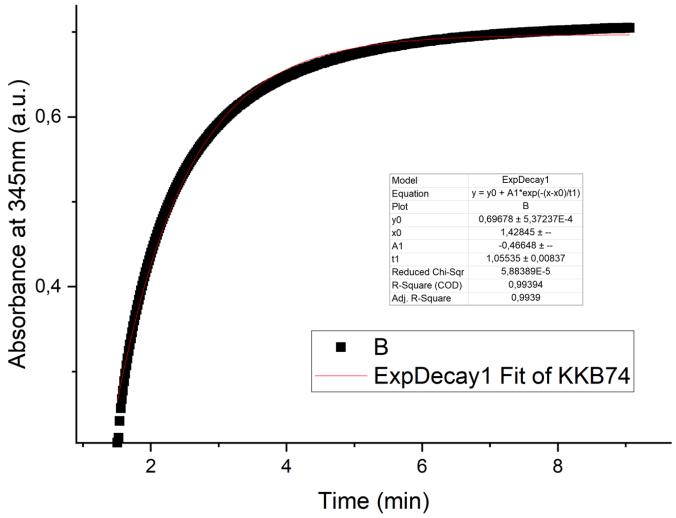

Figure S104. Thermal isomerization kinetics of **2-pram**$_1$.

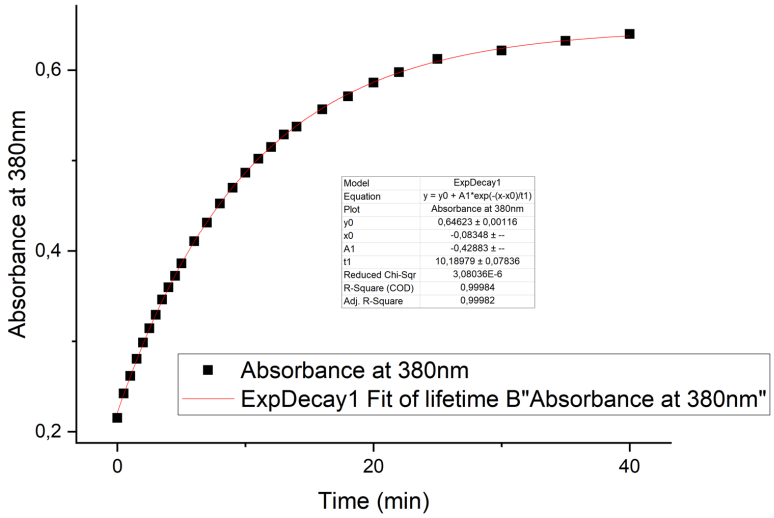

Figure S105. Thermal isomerization kinetics of **2-pip**$_2$.

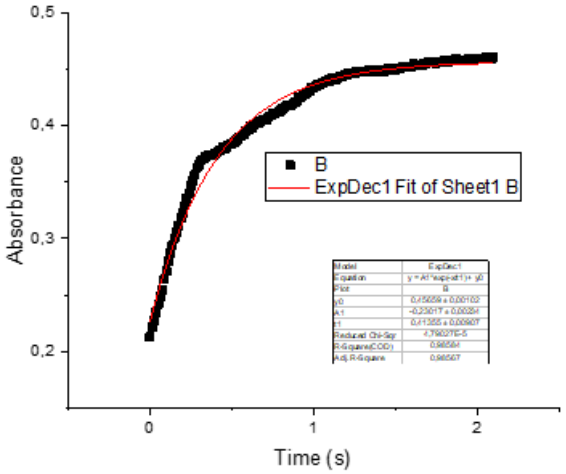

Figure S106. Thermal isomerization kinetics of **2-dma**$_2$.

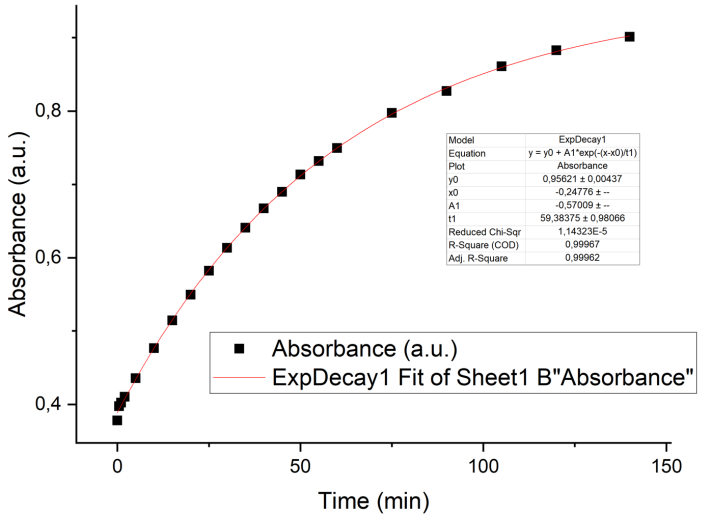

Figure S107. Thermal isomerization kinetics of **3-pip**$_2$.

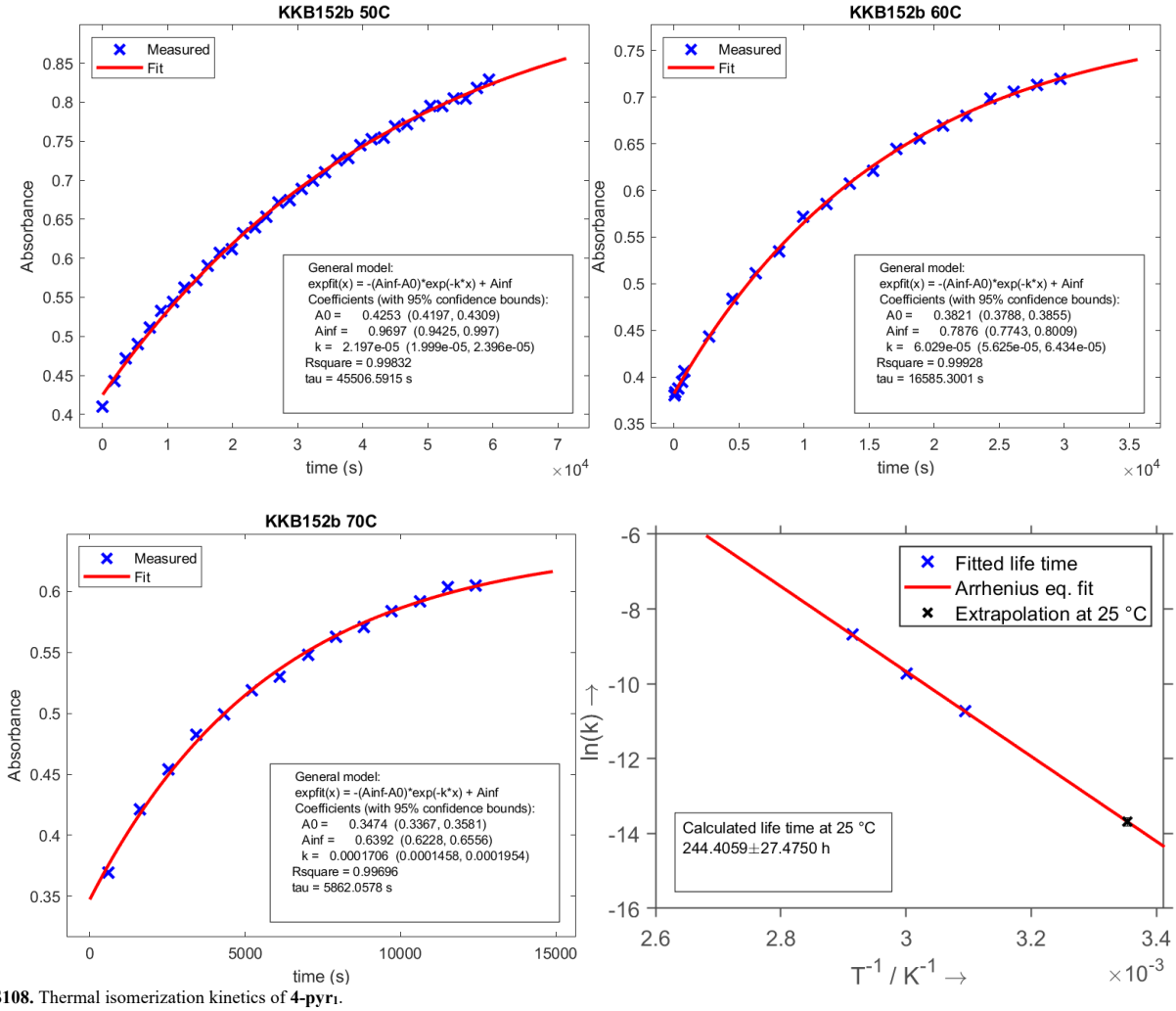

Figure S108. Thermal isomerization kinetics of **4-pyr**$_1$.

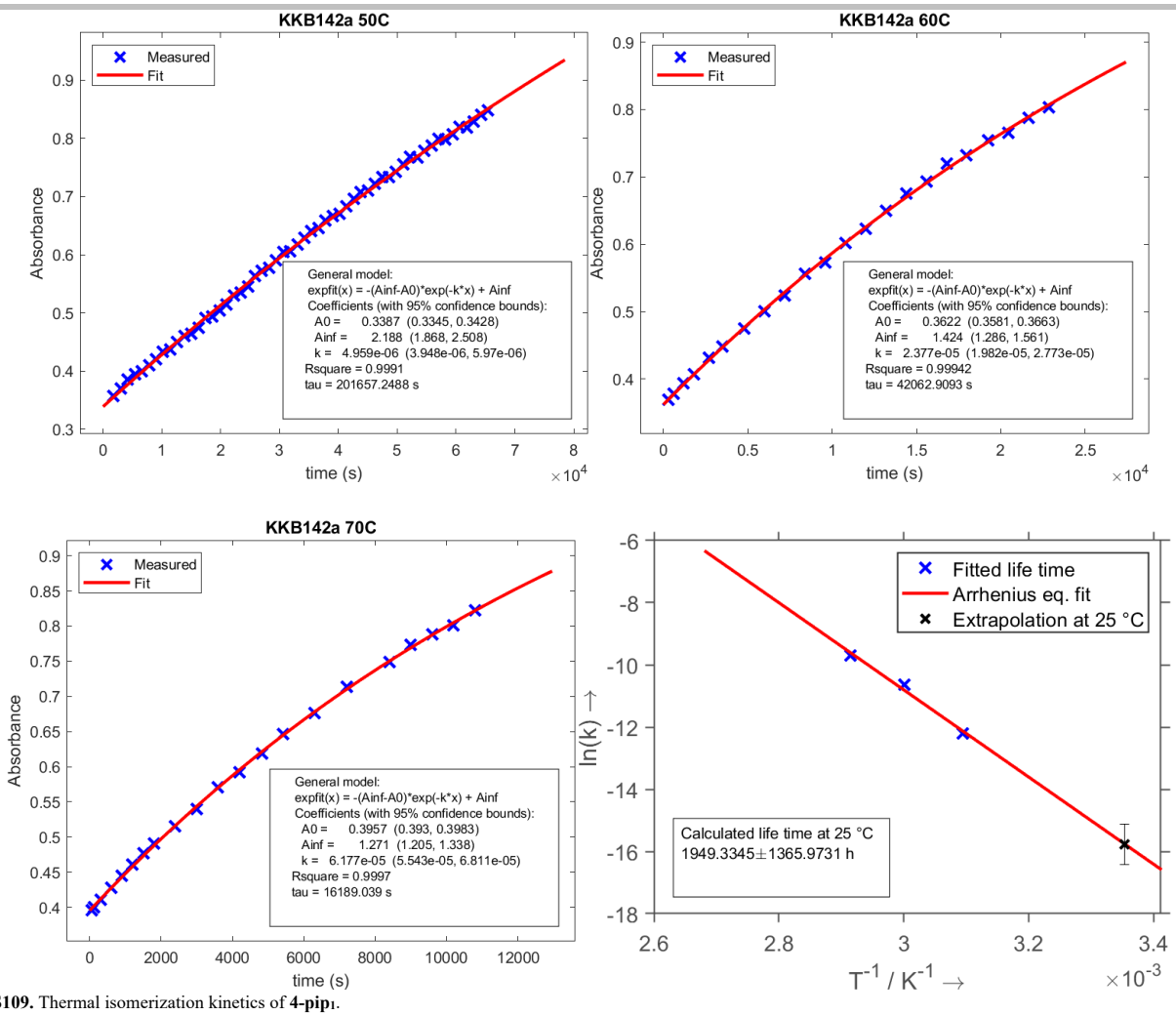

Figure S109. Thermal isomerization kinetics of **4-pip**$_1$.

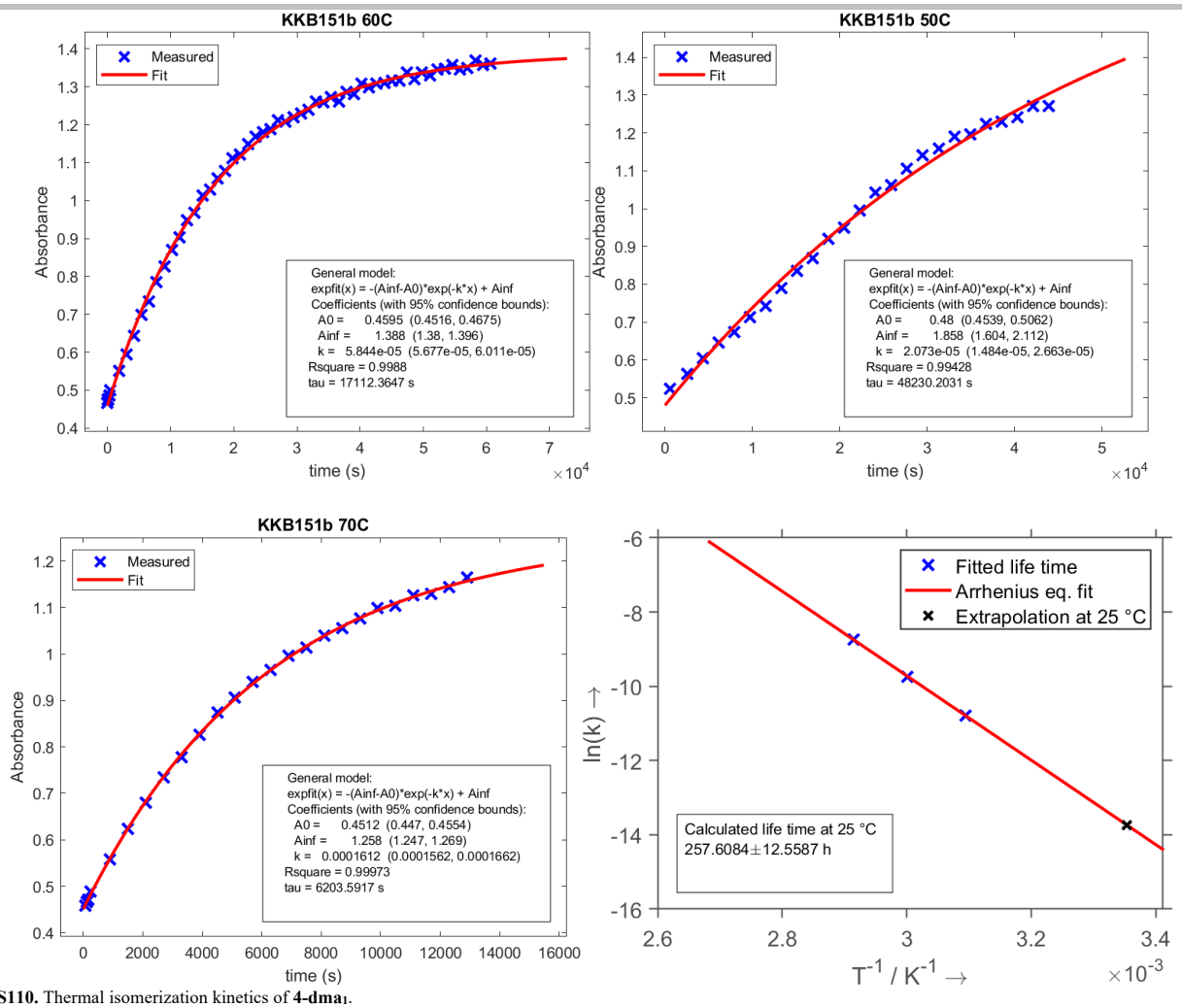

Figure S110. Thermal isomerization kinetics of **4-dma**$_1$.

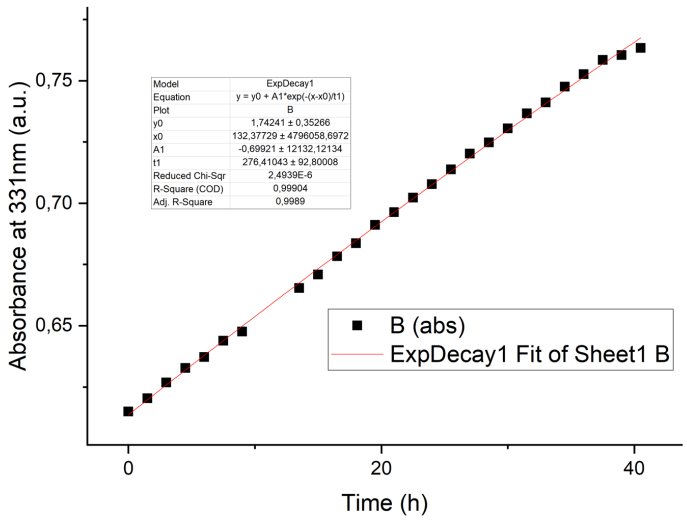

Figure S111. Thermal isomerization kinetics of **4-prol**$_1$.

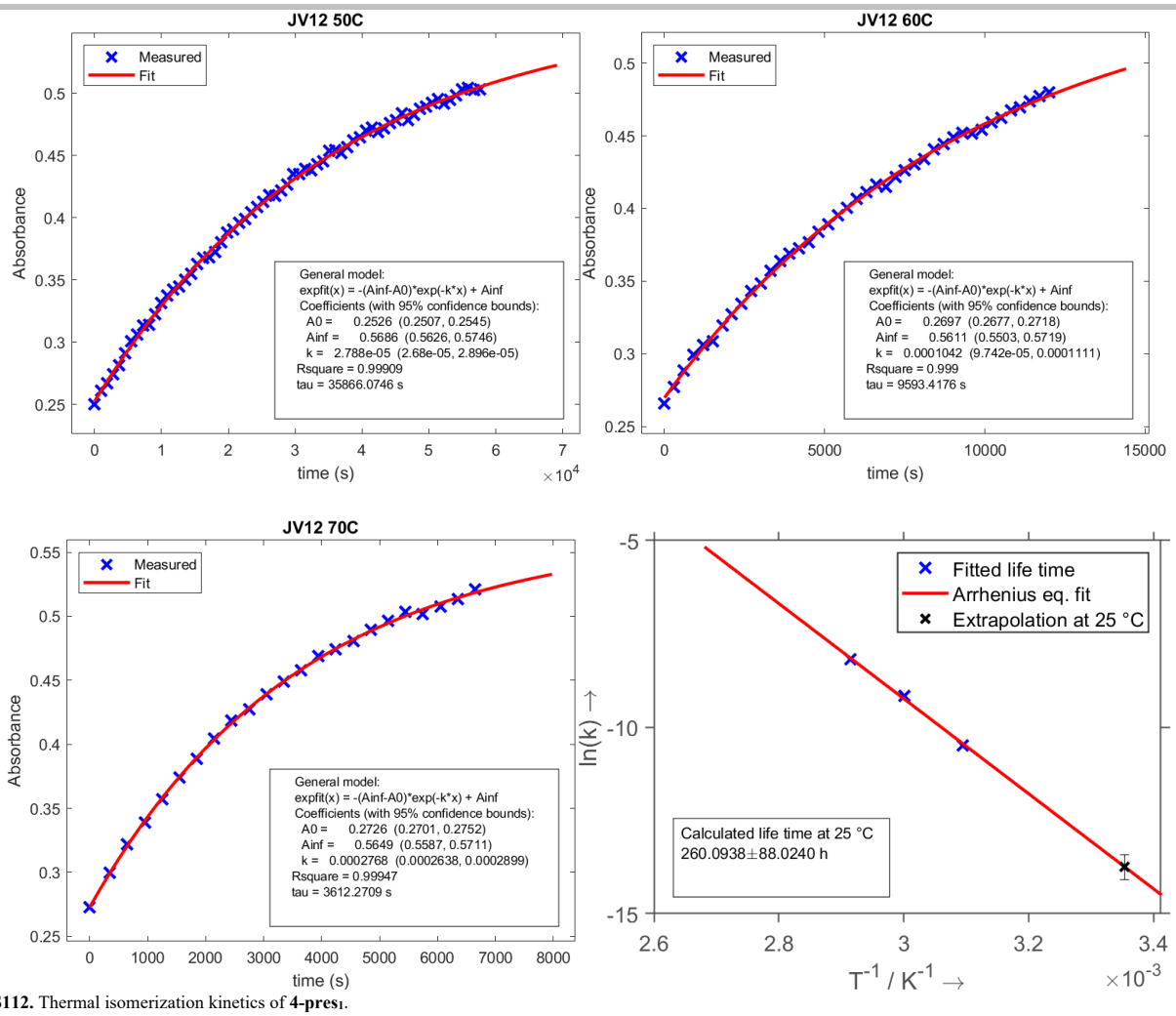

Figure S112. Thermal isomerization kinetics of **4-pres**$_1$.

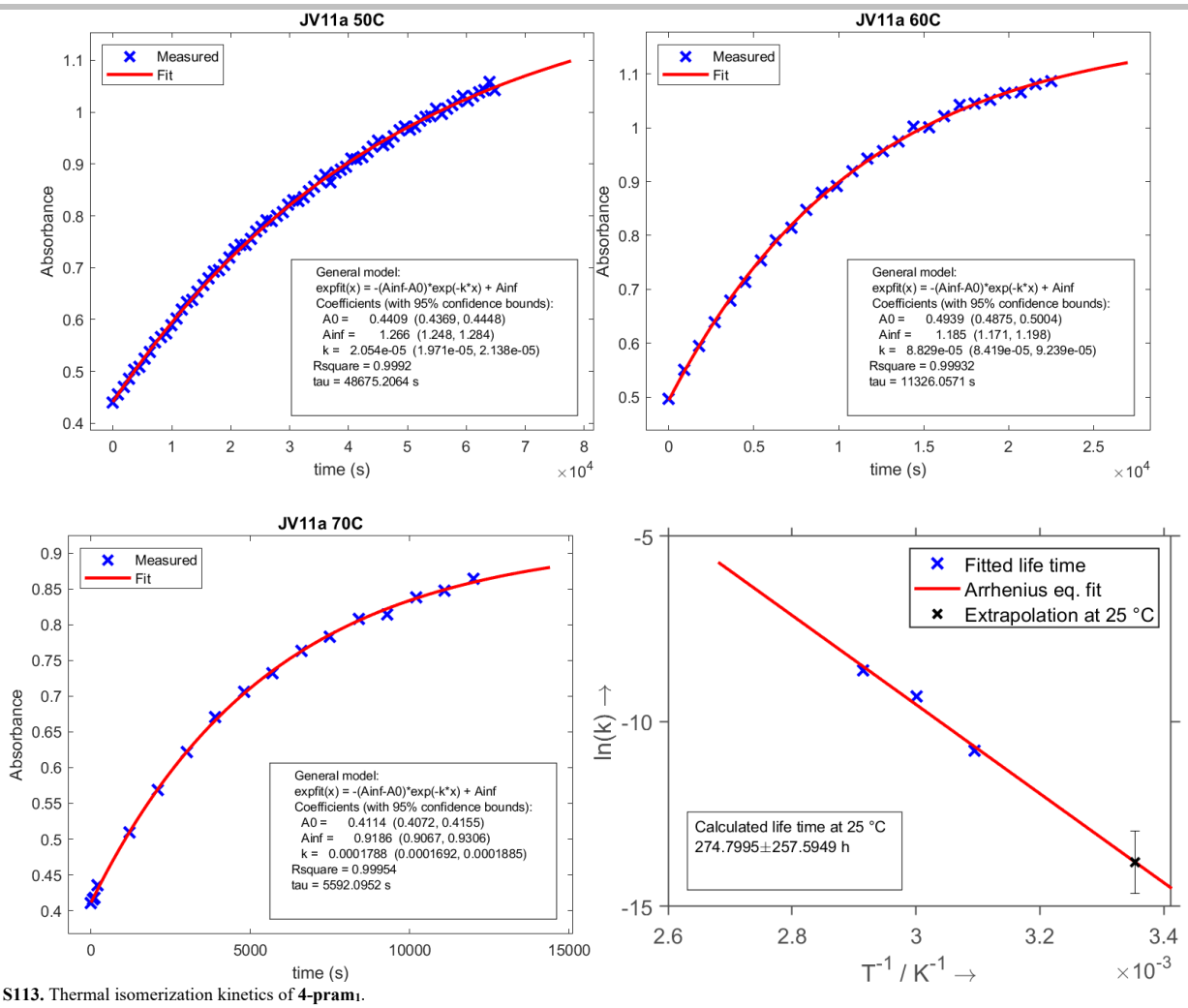

Figure S113. Thermal isomerization kinetics of **4-pram**$_1$.

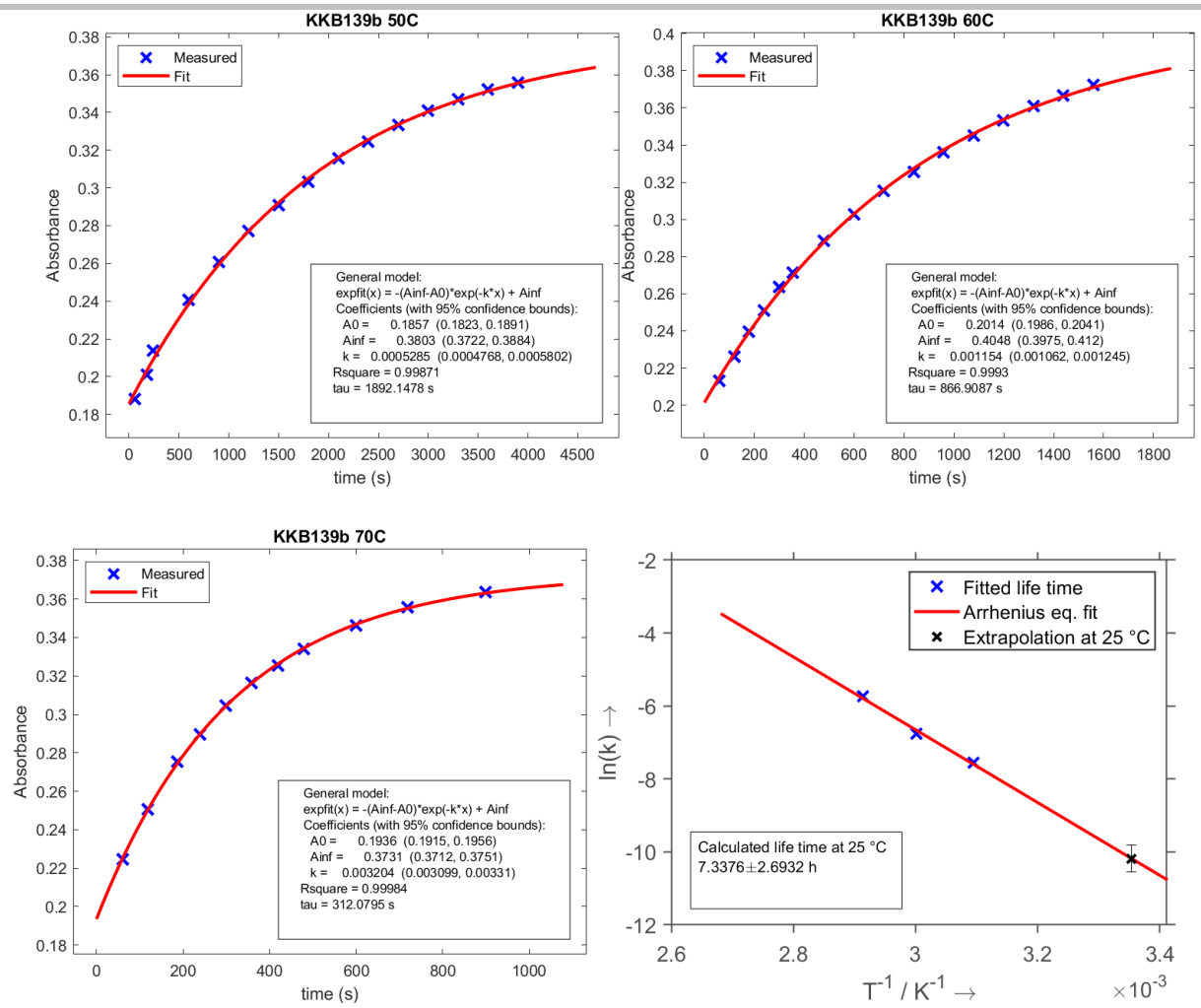

Figure S114. Thermal isomerization kinetics of **4-pyr$_{2\text{-sym}}$**.

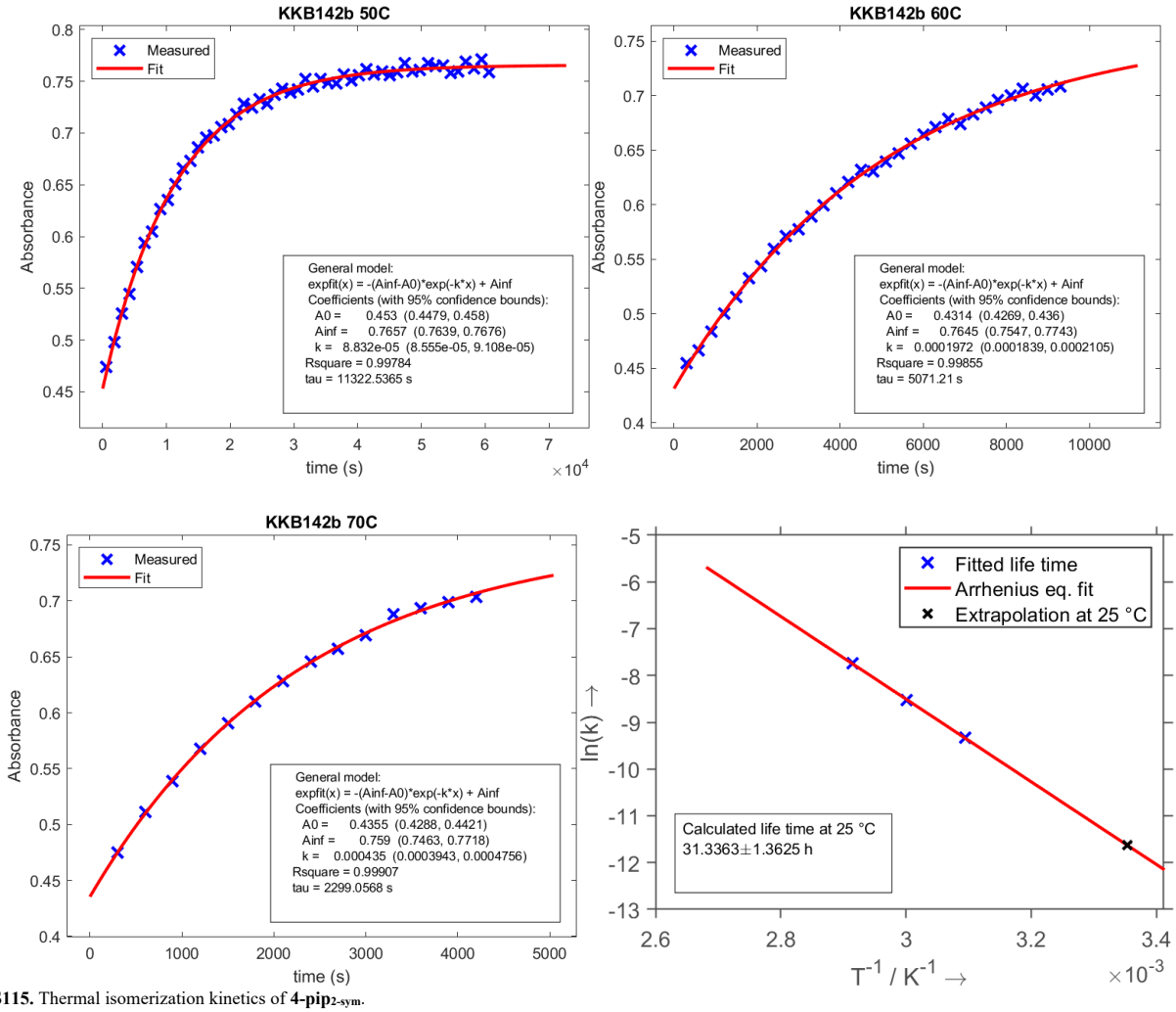

Figure S115. Thermal isomerization kinetics of **4-pip$_{2\text{-sym}}$**.

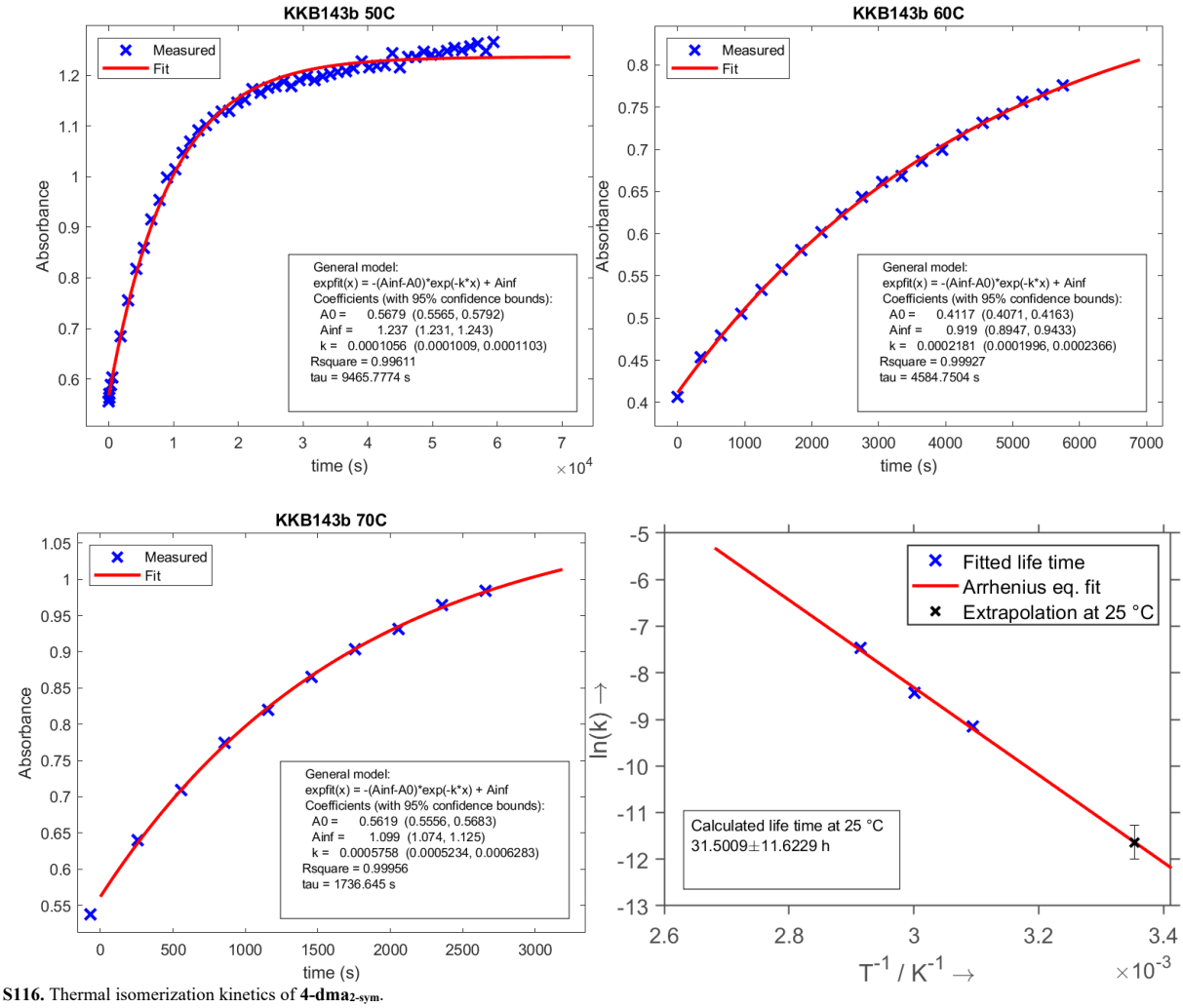

Figure S116. Thermal isomerization kinetics of **4-dma**$_{2\text{-sym}}$.

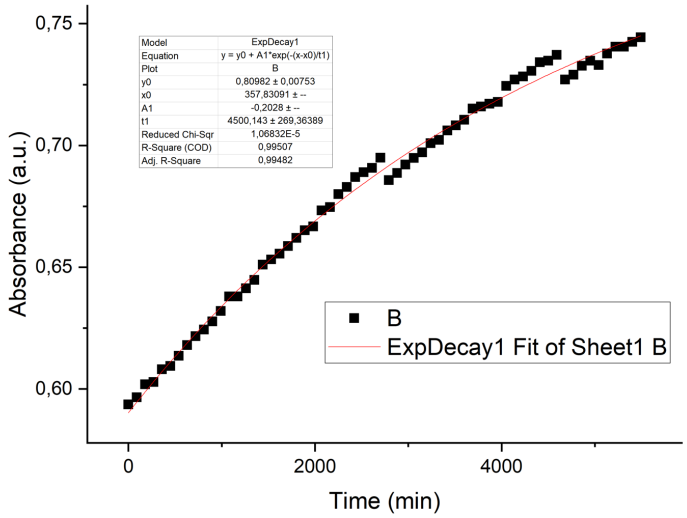

Figure S117. Thermal isomerization kinetics of **4-prol**$_{2\text{-sym}}$.

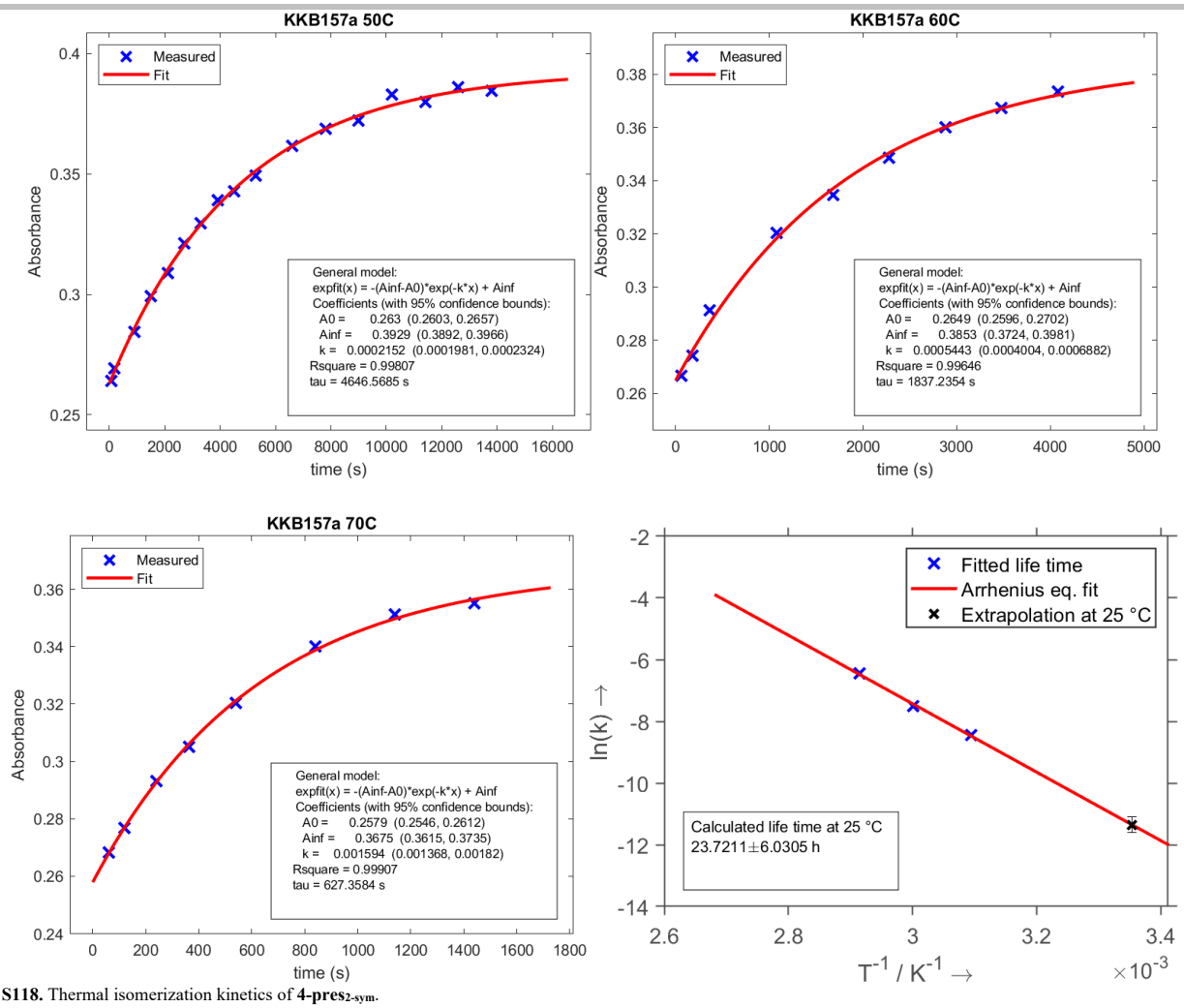

Figure S118. Thermal isomerization kinetics of **4-pres**$_{2\text{-sym}}$.

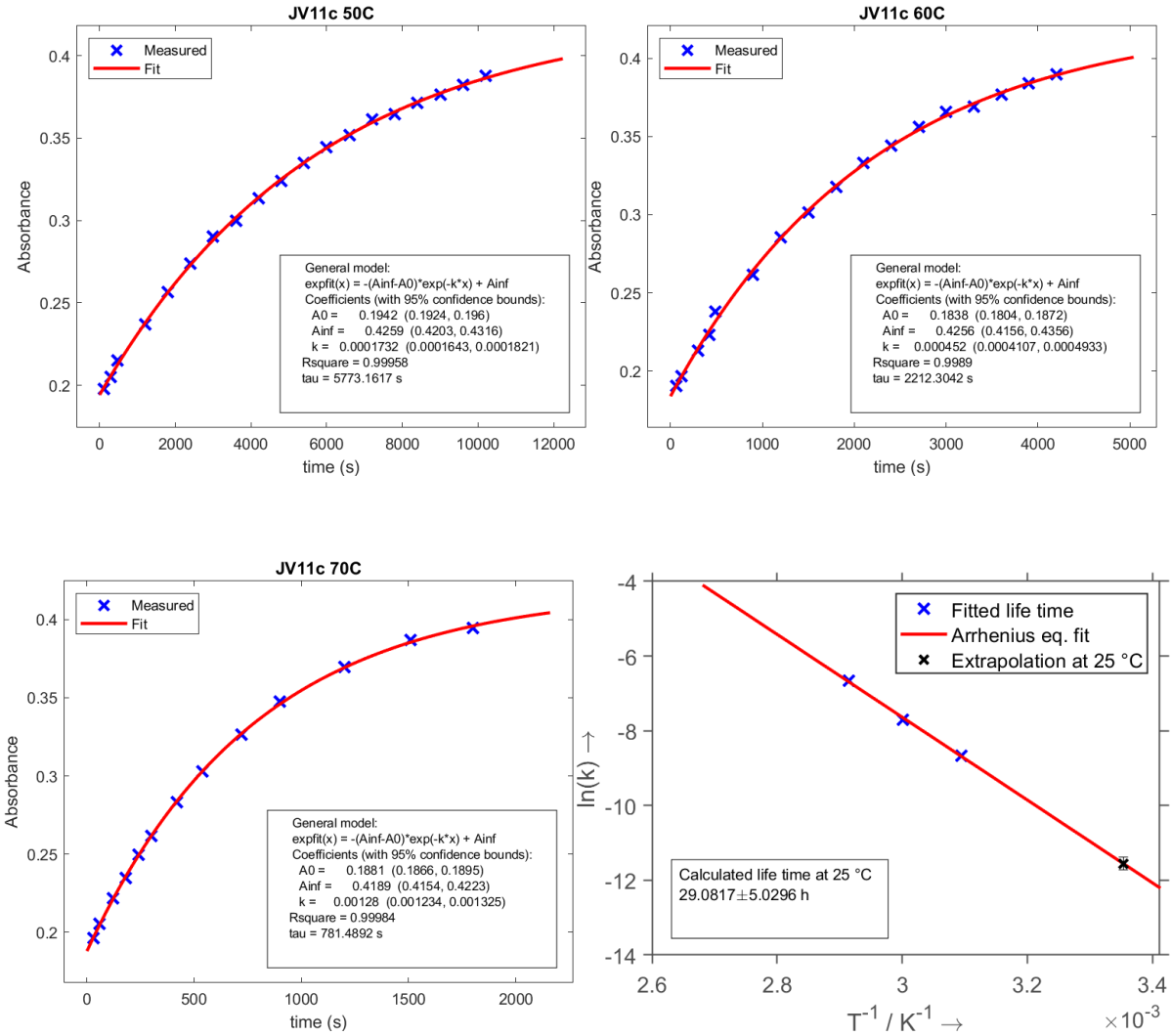

Figure S119. Thermal isomerization kinetics of **4-pram$_{2\text{-sym}}$**.

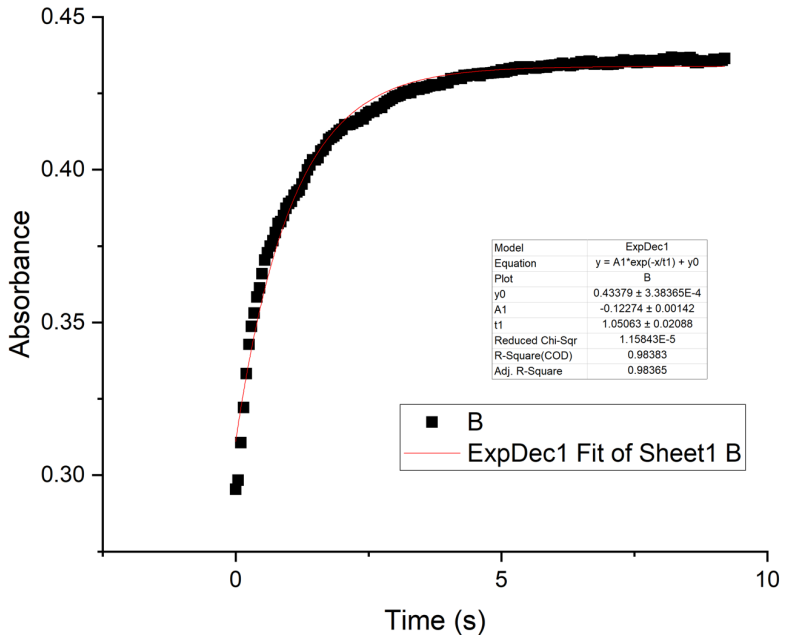

Figure S120. Thermal isomerization kinetics of **4-pyr$_{2\text{-asym}}$**.

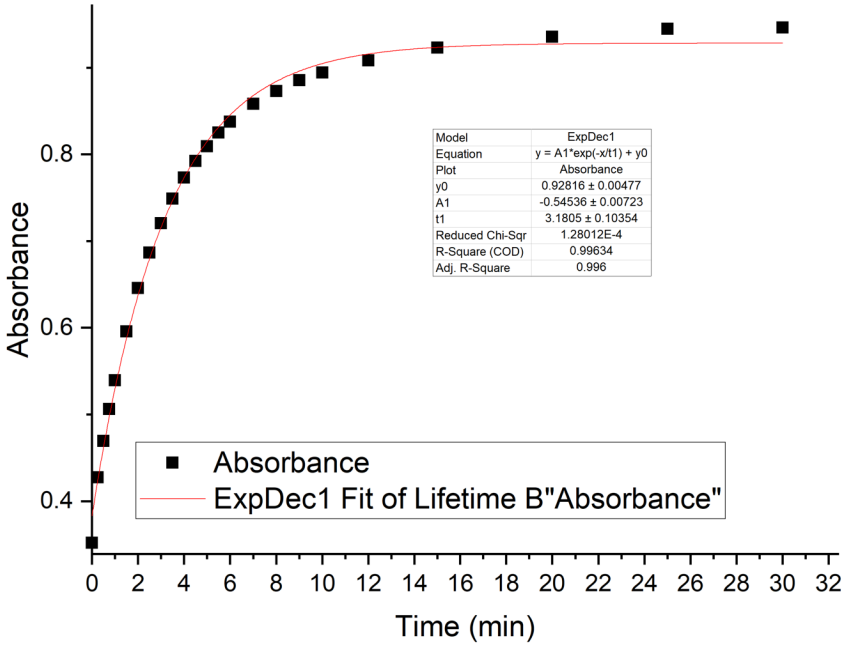

Figure S121. Thermal isomerization kinetics of **4-pip$_{2\text{-asym}}$**.

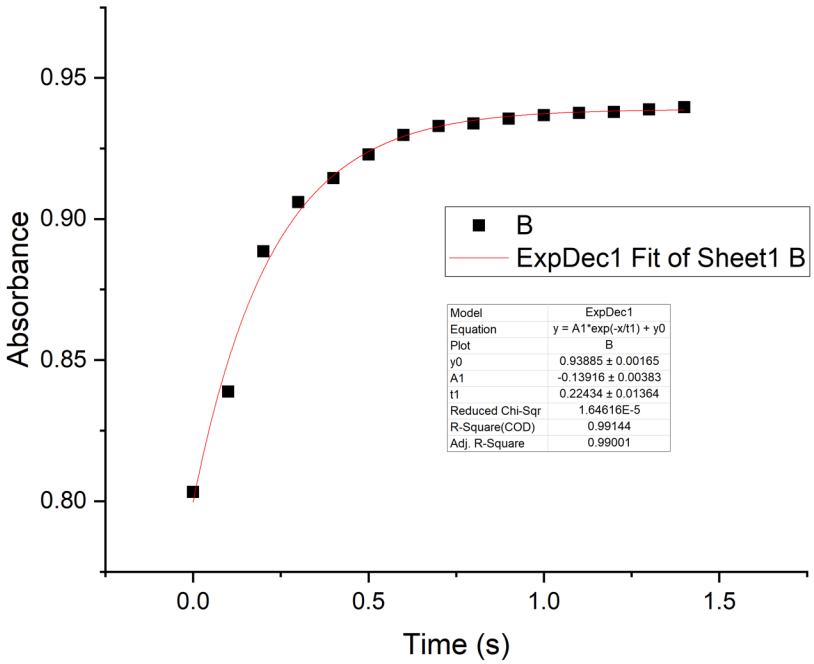

Figure S122. Thermal isomerization kinetics of **4-dma$_{2\text{-asym}}$**.

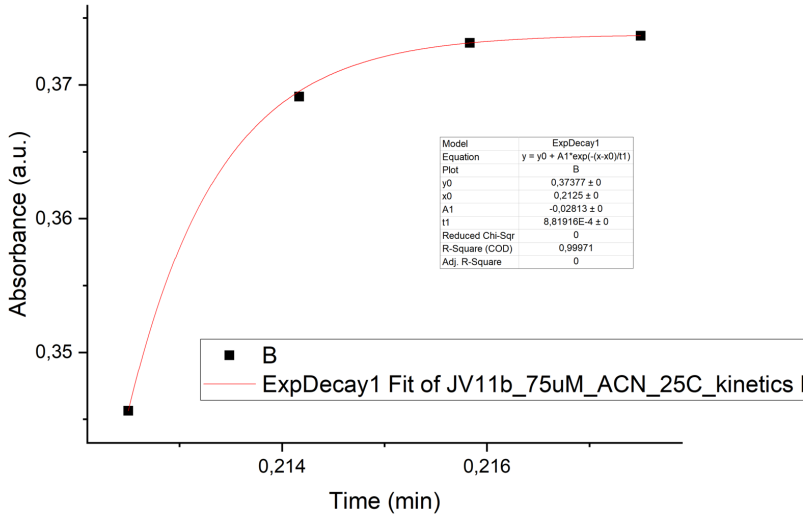

Figure S123. Thermal isomerization kinetics of **4-pram$_{2\text{-asym}}$**.

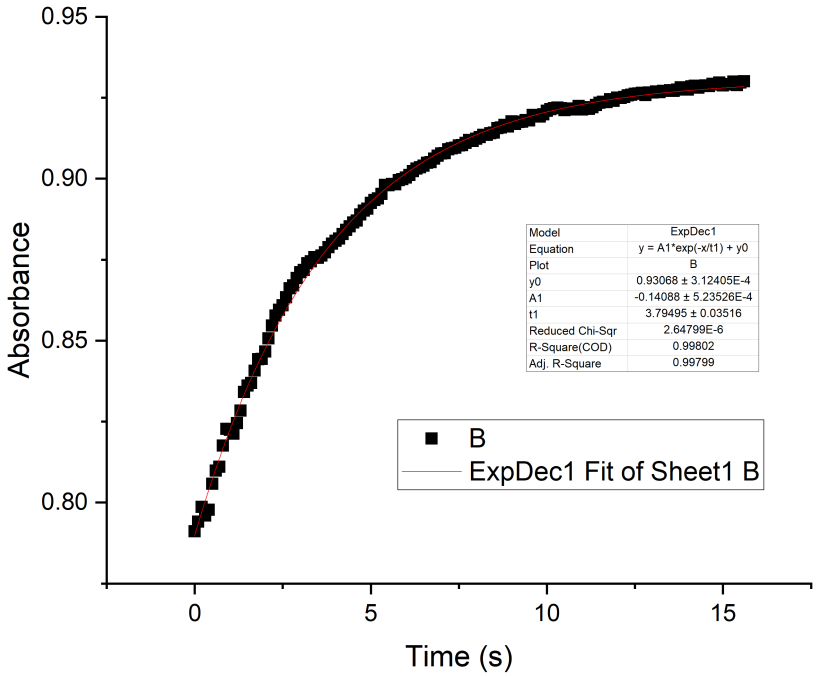

Figure S124. Thermal isomerization kinetics of **4-pip$_3$**.

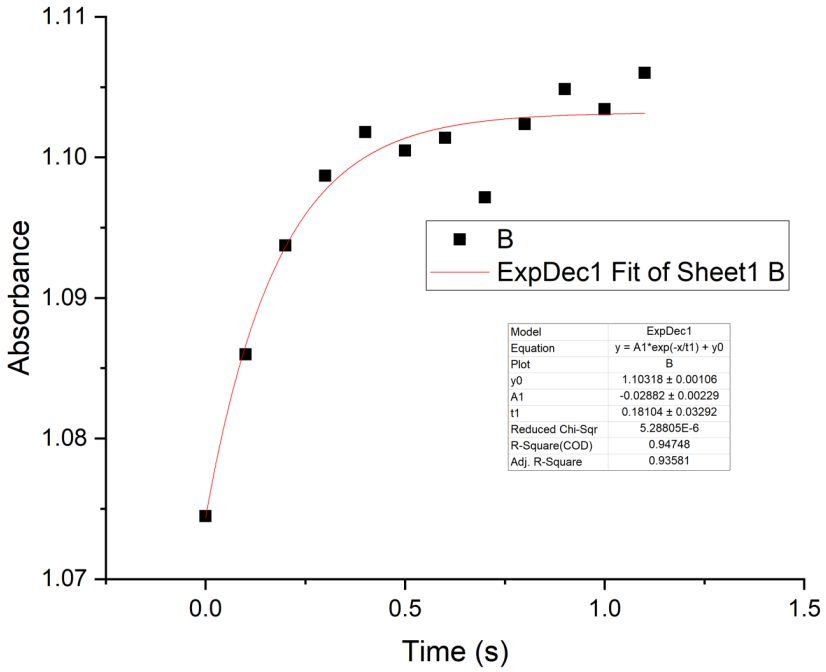

Figure S125. Thermal isomerization kinetics of **4-pip**$_4$.

Computational details

All calculations have been done with Gaussian 16, revision C.01[2]. The B3LYP functional[3,4] with D3(BJ)[5] dispersion correction and PCM(ACN)[6,7] has been used for geometry optimizations to produce structures for spectra calculations. Low-lying electronically excited states have been calculated with TD-DFT[8] using B3LYP and ωB97X-D[9] functionals, with PCM(ACN). Natural transition orbitals (NTOs)[10] have been computed (using Gaussian) to visualize the nature of the excited states.

NTO analysis allows one to simplify an orbital description of electronic transitions. Often, a single NTO hole-particle pair may describe the transition in question whereas several conventional occupied-virtual orbital pairs are needed to characterize the same transition. Upon the electronic transition the excited electron goes from the hole NTO to the particle NTO.

The geometries of the transition states (TSs) and the *cis* (Z) isomers have been optimized using spin-restricted (R) und spin-unrestricted (U) B3LYP+D3(BJ)/6-31G*/PCM(ACN) calculations. In the case of spin-restricted calculations, we have also performed calculations without dispersion correction and without PCM to determine the influence of these corrections on thermal lifetimes. Reaction rate constants for the thermal *cis*→*trans* isomerization have been calculated using Eyring's transition state theory[11]:

$$k = \frac{k_B T}{h} exp\left(-\frac{\Delta G^{\ddagger}}{k_B T}\right)$$

and the corresponding thermal lifetime as:

$$\tau = \frac{1}{k}$$

Here, k_B and h are the Boltzmann and Planck constants, respectively, and T is the temperature. We used $T = 298.15$ K (25 °C). $\Delta G^{\ddagger} = G(\mathrm{TS}) - G(\mathrm{Z})$ is the activation Gibbs free energy.

We have located transition states using the Berny algorithm as implemented in Gaussian (TS keyword). The intrinsic reaction coordinate[12,13] calculations (IRC keyword) have been done to locate the corresponding *cis* isomers, which have been further reoptimized. We have located two transition states and two *cis* isomers for each molecule. Energy differences between different *cis* isomers of the same molecule were calculated with respect to the lowest energy *cis* isomer (of two isomers) of this molecule:

$$\Delta B_{ZZ}^{rel} = B(\mathrm{Z}_i) - B\left(\mathrm{Z}_{\text{lowest energy}}\right); B = G, E;$$

G is Gibbs free energy; *E* is energy, i.e. a point on the potential energy surface (PES). Thus, $\Delta B_{ZZ}^{rel} = 0$ for the lowest energy *cis* isomer, and positive for the second isomer.

Normal mode analysis has been performed to confirm the nature of minima (no imaginary frequency) and transition states (one imaginary frequency).

In the case of spin-unrestricted calculations (performed at the UB3LYP+D3(BJ)/6-31G*/PCM(ACN) level), the Guess(Mix) keyword was used to generate an initial orbital guess, and the broken-symmetry solution was found for all considered molecules. The $\langle S^2 \rangle$ values (at the rotational TS geometries) were slightly above 1 for all the molecules.

To estimate the energy of a pure-singlet state $\Delta E_{UDFT}^{(S,\ddagger)}$ (at the rotational TS geometry), we used an approach proposed by Yamaguchi et al.[14]

$$\Delta E_{UDFT}^{(S,\ddagger)} = \Delta E_{UDFT}^{\ddagger} + \frac{\langle S^2 \rangle}{2 - \langle S^2 \rangle}\left(\Delta E_{UDFT}^{\ddagger} - \Delta E_{UDFT}^{(T,\ddagger)}\right)$$

Here, the $\langle S^2 \rangle$ values are for rotational TSs, i.e., about 1; $\Delta E_{UDFT}^{\ddagger}$ is the energy of the mixed-spin state, and $\Delta E_{UDFT}^{(T,\ddagger)}$ is the energy of the triplet state at the rotational TS geometry. The second term on the r.h.s. was added to the UDFT activation Gibbs free energies $\Delta G_{UDFT}^{\ddagger}$ to obtain the corrected activation Gibbs free energies $\Delta G_{UDFT}^{(S,\ddagger)}$ corresponding to the pure-singlet state.

The lowest triplet state was optimized starting from the rotational TS structures using the same level of theory, i.e., UB3LYP+D3(BJ)/6-31G*/PCM(ACN). The $\langle S^2 \rangle$ values were slightly above 2, for the optimized triplets. The optimized triplet geometries are similar to the rotational TS structures.

In all the calculations the 6-31G* basis set[15] has been used.

The molecular structures and NTOs have been visualized using Jmol, an open-source Java viewer for chemical structures in 3D (http://www.jmol.org/).

Supplementary Results and Discussion

UV-Vis spectra of synthesized compounds

The UV-Vis spectra of all new compounds in dark and in the most *cis*-rich photostationary state are given in **Fig. S126**–**S136**.

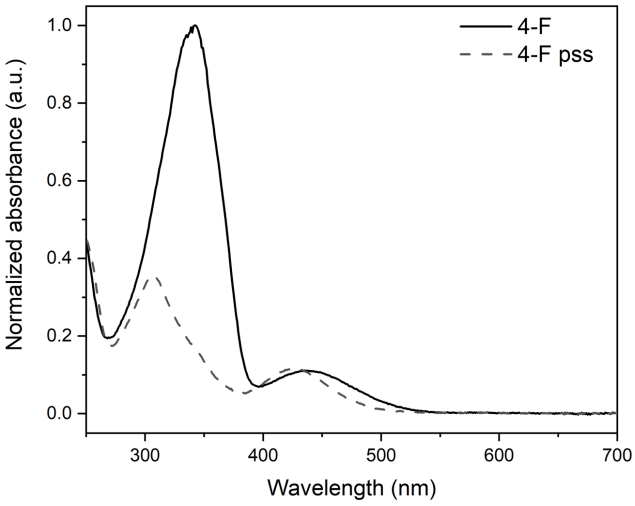

Figure S126. Absorption spectra of **4-F**.

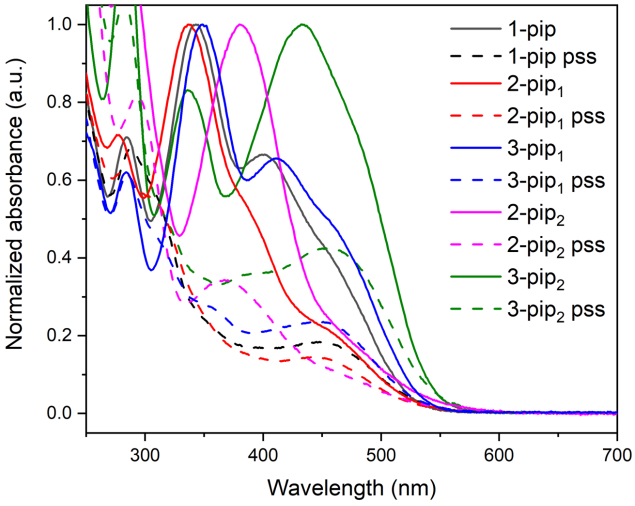

Figure S127. Absorption spectra of **1-pip**, **2-pip$_1$**, **3-pip$_1$**, **2-pip$_2$** and **3-pip$_2$**.

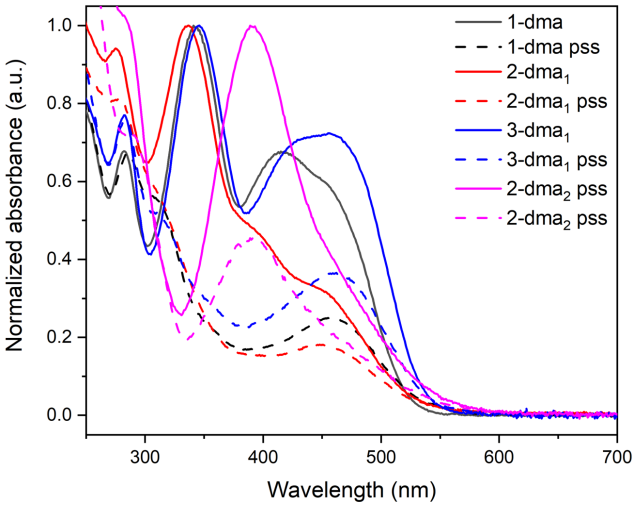

Figure S128. Absorption spectra of **1-dma**, **2-dma$_1$**, **3-dma$_1$** and **2-dma$_2$**.

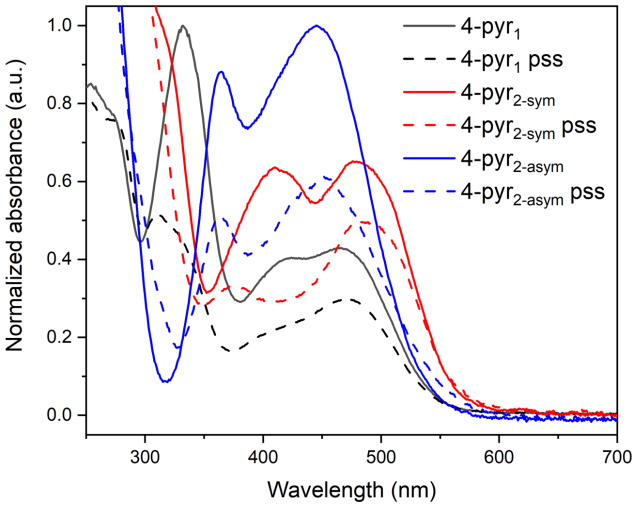

Figure S129. Absorption spectra of **4-pyr$_1$**, **4-pyr$_{2\text{-sym}}$** and **4-pyr$_{2\text{-asym}}$**.

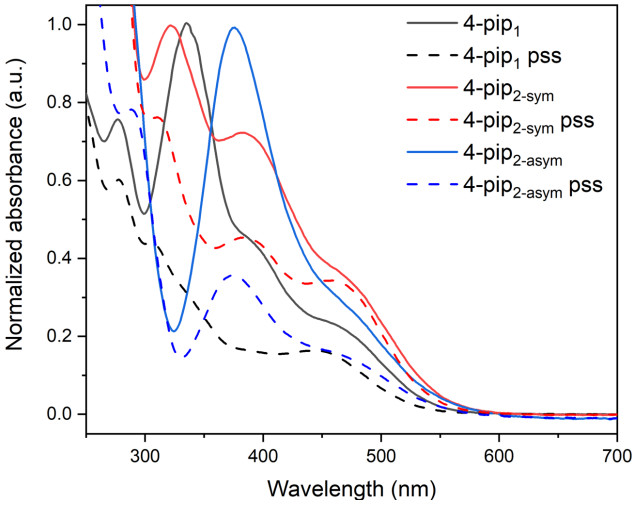

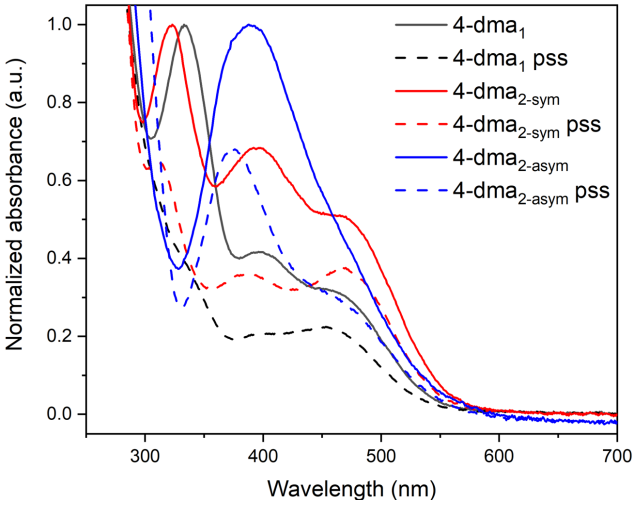

Figure S130. Absorption spectra of **4-pip$_1$**, **4-pip$_{2\text{-sym}}$** and **4-pip$_{2\text{-asym}}$**.

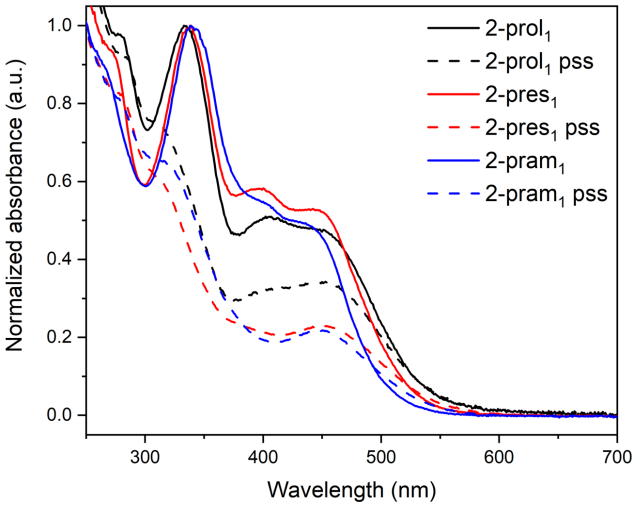

Figure S131. Absorption spectra of **4-dma$_1$**, **4-dma$_{2\text{-sym}}$** and **4-dma$_{2\text{-asym}}$**.

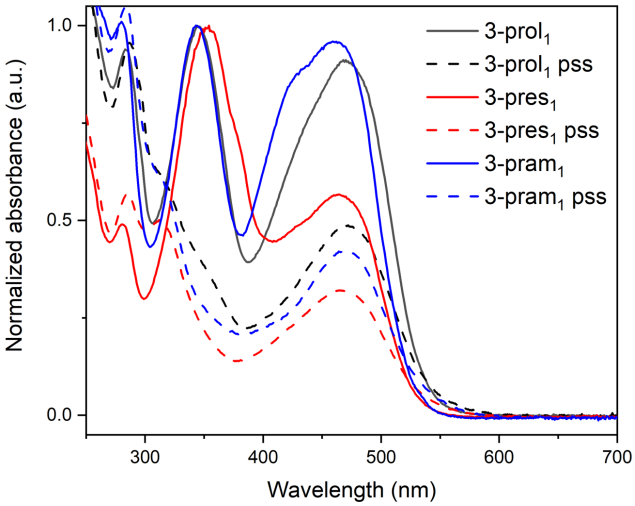

Figure S132. Absorption spectra of **2-prol$_1$**, **2-pres$_1$** and **2-pram$_1$**.

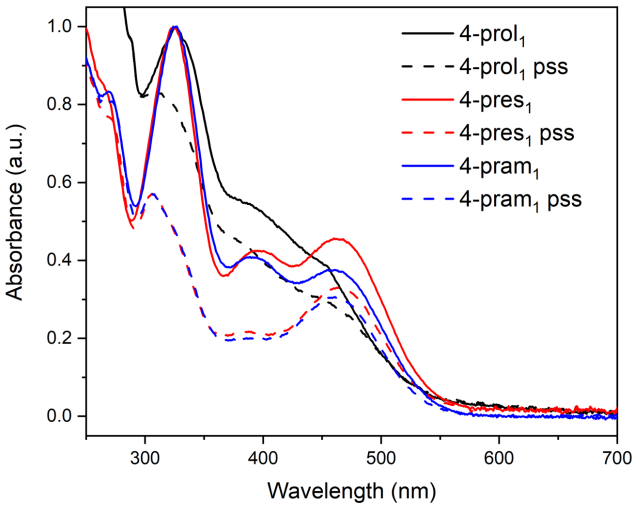

Figure S133. Absorption spectra of **3-prol$_1$**, **3-pres$_1$** and **3-pram$_1$**.

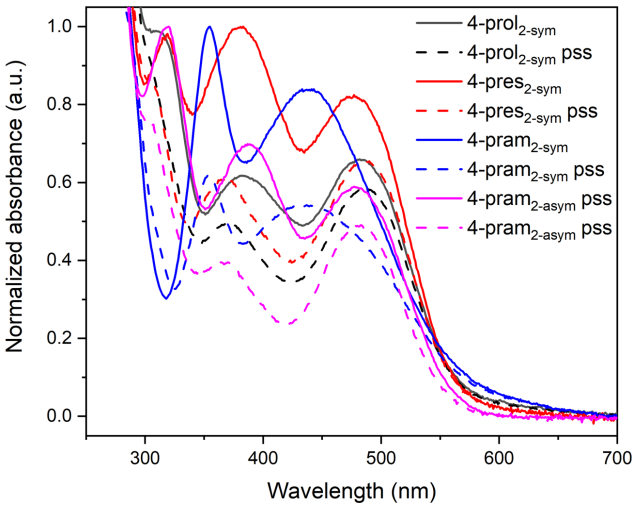

Figure S134. Absorption spectra of **4-prol$_1$**, **4-pres$_1$** and **4-pram$_1$**.

Figure S135. Absorption spectra of **4-prol$_{2\text{-sym}}$**, **4-pres$_{2\text{-sym}}$**, **4-pram$_{2\text{-sym}}$** and **4-pram$_{2\text{-asym}}$**.

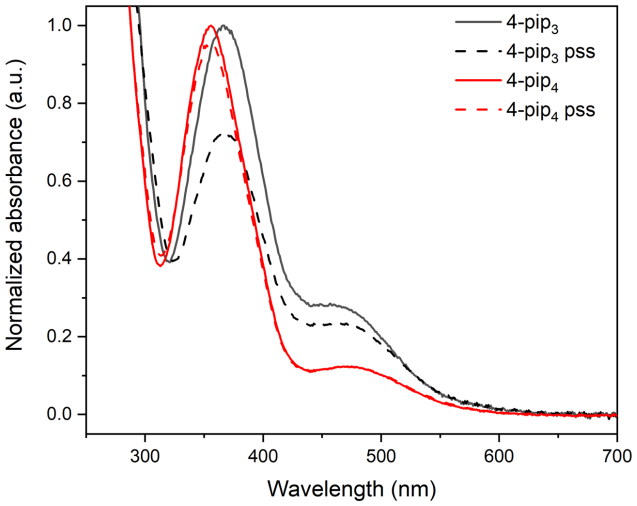

Figure S136. Absorption spectra of **4-pip$_3$** and **4-pip$_4$**.

Vertical excitation wavelengths, oscillator strengths and NTOs

The calculated vertical excitation wavelengths and oscillator strengths of the *trans* and *cis* isomers of selected products and the NTOs related to each transition are presented in **Table S1** and **Table S2**–**S3**, respectively.

Table S1. Vertical excitation wavelengths in nm and oscillator strengths (in parentheses) of the *trans* and *cis* isomers of selected products, calculated at the TD-B3LYP+D3(BJ)/6-31G*/PCM(ACN) and TD-ωB97X-D/6-31G*/PCM(ACN) level of theory at the B3LYP+D3(BJ)/6-31G*/PCM(ACN) geometries.

		trans		*cis*				*trans*		*cis*	
		B3LYP	ωB97X-D	B3LYP	ωB97X-D			B3LYP	ωB97X-D	B3LYP	ωB97X-D
1-F	S_1	462 (0.00)	441 (0.00)	487 (0.12)	459 (0.08)	**2-dma$_1$**	S_1	477 (0.09)	456 (0.06)	490 (0.07)	445 (0.05)
	S_2	392 (1.11)	353 (1.15)	336 (0.17)	298 (0.29)		S_2	426 (0.31)	364 (0.66)	392 (0.01)	323 (0.04)
	S_3	302 (0.01)	262 (0.01)	323 (0.07)	279 (0.09)		S_3	362 (0.61)	305 (0.37)	341 (0.03)	288 (0.22)
	S_4	299 (0.02)	260 (0.00)	299 (0.01)	262 (0.00)		S_4	297 (0.00)	257 (0.00)	328 (0.17)	283 (0.04)
1-pyr	S_1	465 (0.00)	443 (0.00)	525 (0.13)	486 (0.10)	**3-pip$_1$**	S_1	473 (0.01)	451 (0.02)	493 (0.04)	438 (0.03)
	S_2	447 (0.60)	401 (0.77)	404 (0.03)	344 (0.11)		S_2	458 (0.40)	394 (0.65)	391 (0.02)	328 (0.01)
	S_3	366 (0.42)	307 (0.29)	333 (0.15)	290 (0.17)		S_3	375 (0.58)	314 (0.37)	344 (0.02)	282 (0.21)
	S_4	296 (0.00)	258 (0.01)	321 (0.05)	275 (0.04)		S_4	300 (0.01)	261 (0.00)	320 (0.17)	275 (0.04)
1-pip	S_1	470 (0.03)	449 (0.02)	491 (0.03)	440 (0.03)	**4-pip$_1$**	S_1	493 (0.06)	468 (0.05)	496 (0.08)	449 (0.06)
	S_2	449 (0.41)	386 (0.66)	386 (0.02)	323 (0.01)		S_2	440 (0.26)	371 (0.56)	411 (0.02)	338 (0.04)
	S_3	371 (0.55)	310 (0.35)	340 (0.02)	282 (0.25)		S_3	359 (0.70)	307 (0.51)	340 (0.06)	290 (0.08)
	S_4	301 (0.00)	258 (0.00)	322 (0.18)	272 (0.02)		S_4	299 (0.01)	260 (0.01)	326 (0.14)	286 (0.20)
2-pyr$_1$	S_1	486 (0.16)	459 (0.10)	515 (0.10)	470 (0.07)	**4-pip$_{2\text{-sym}}$**	S_1	506 (0.04)	480 (0.04)	512 (0.07)	460 (0.05)
	S_2	426 (0.24)	373 (0.58)	406 (0.02)	338 (0.08)		S_2	450 (0.43)	386 (0.62)	424 (0.00)	339 (0.00)
	S_3	359 (0.60)	304 (0.40)	334 (0.06)	287 (0.18)		S_3	406 (0.01)	327 (0.01)	391 (0.02)	323 (0.12)
	S_4	293 (0.00)	257 (0.01)	326 (0.17)	284 (0.09)		S_4	349 (0.49)	295 (0.37)	338 (0.05)	286 (0.10)
2-pip$_1$	S_1	477 (0.07)	455 (0.05)	488 (0.05)	440 (0.04)		S_5			334 (0.12)	283 (0.06)
	S_2	429 (0.32)	365 (0.63)	391 (0.01)	322 (0.02)						
	S_3	362 (0.59)	306 (0.38)	344 (0.03)	288 (0.22)						
	S_4	298 (0.00)	257 (0.00)	329 (0.16)	281 (0.04)						

Table S2. Dominant natural transition orbitals (NTOs) for the lowest electronic transitions of the *trans* isomers.

		B3LYP		ωB97X-D	
		Hole	**Particle**	**Hole**	**Particle**
1-F	S_1	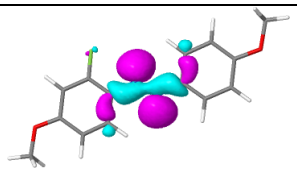	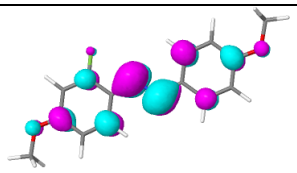	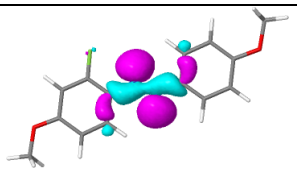	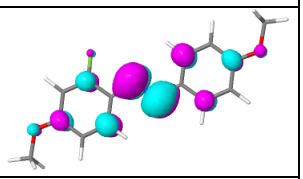
	S_2	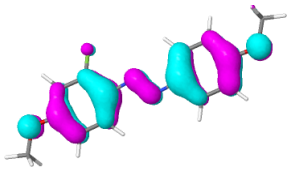	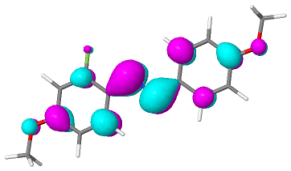	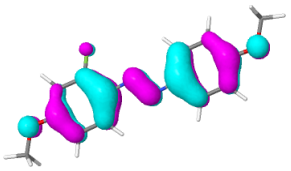	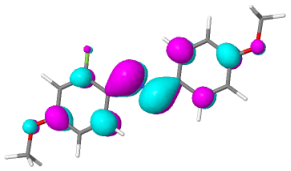
	S_3	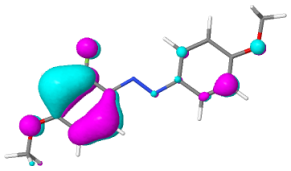	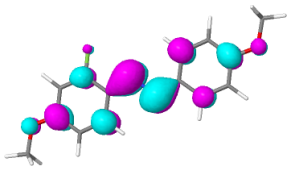	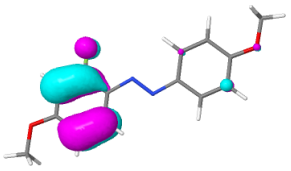	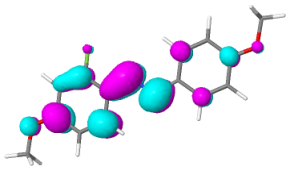
	S_4	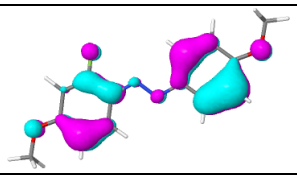	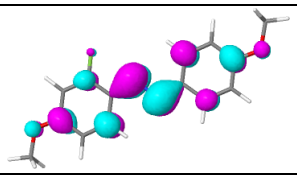	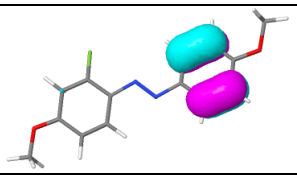	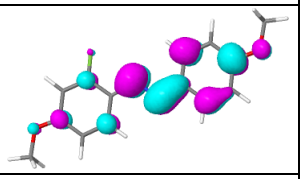
1-pyr	S_1	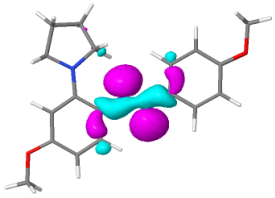	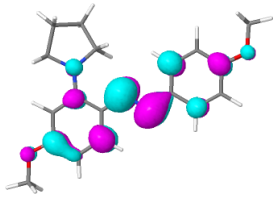	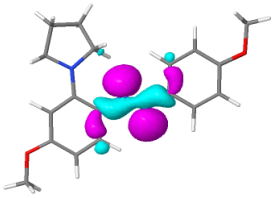	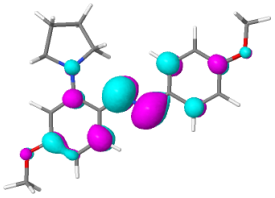
	S_2	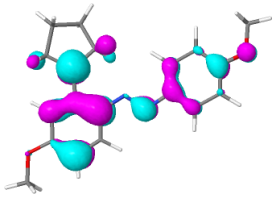	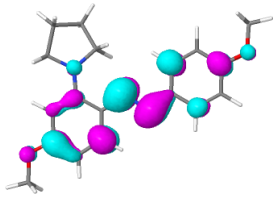	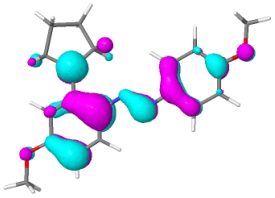	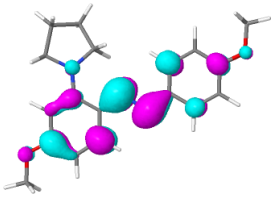
	S_3	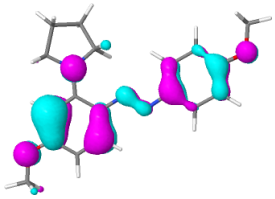	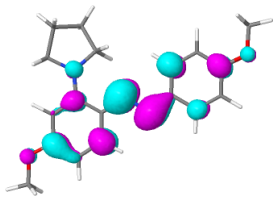	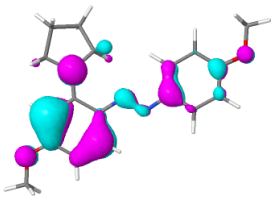	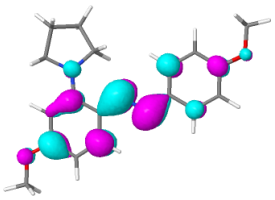
	S_4	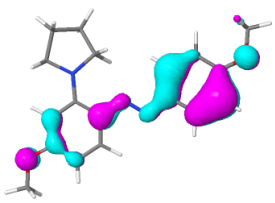	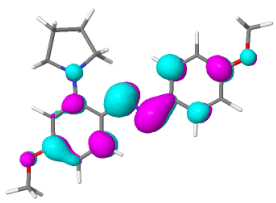	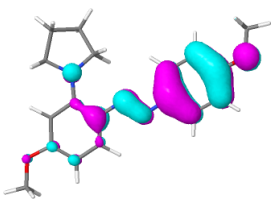	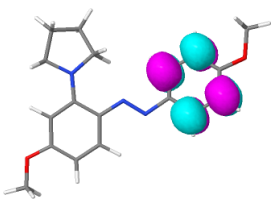

1-pip	S_1	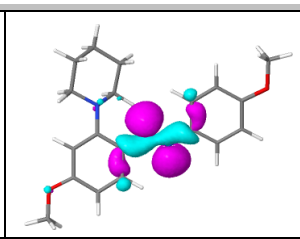	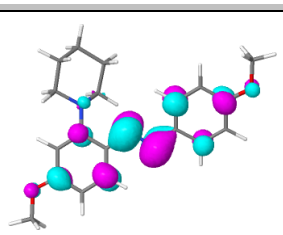	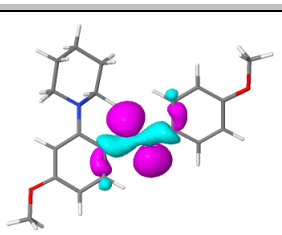	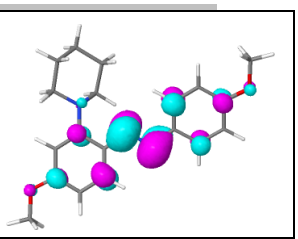
	S_2	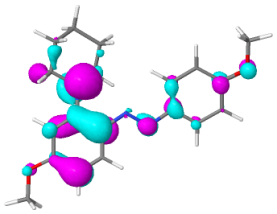	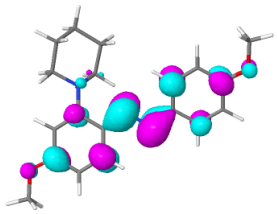	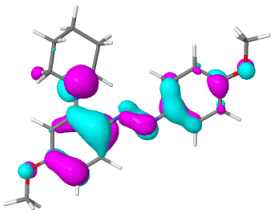	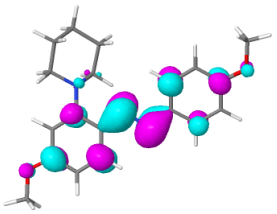
	S_3	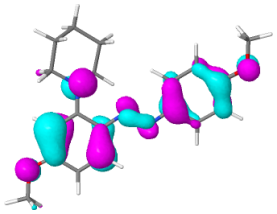	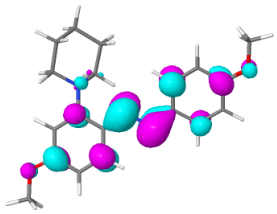	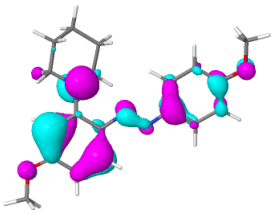	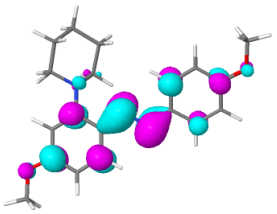
	S_4	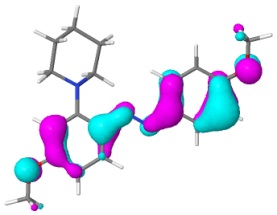	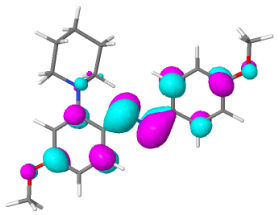	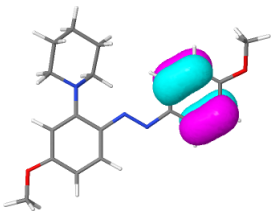	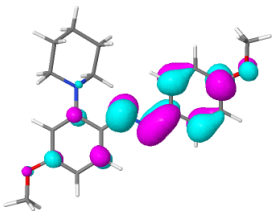
2-pyr$_1$	S_1	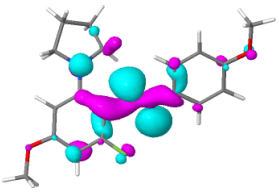	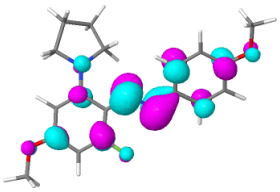	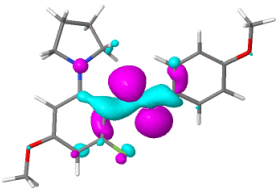	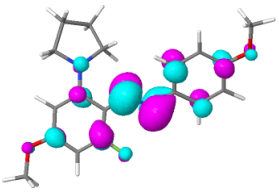
	S_2	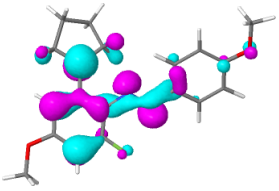	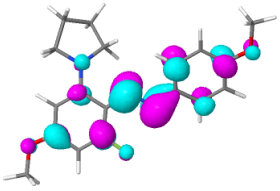	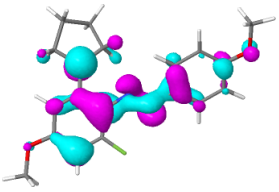	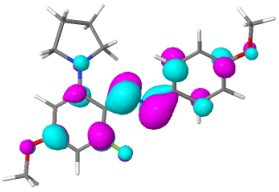
	S_3	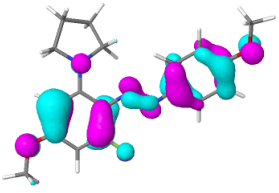	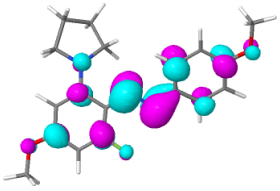	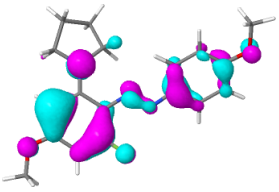	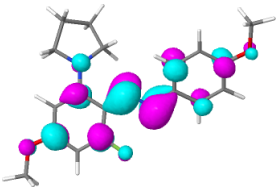
	S_4	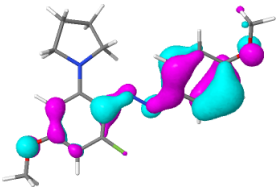	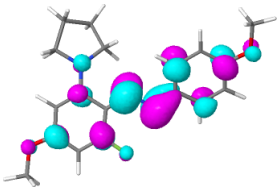	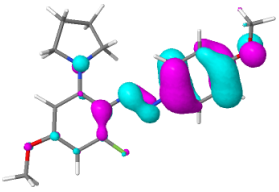	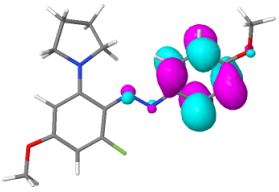

2-pip$_1$	**S_1**	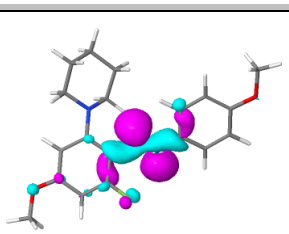	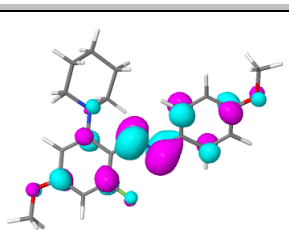	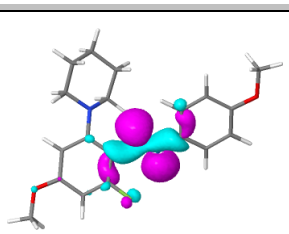	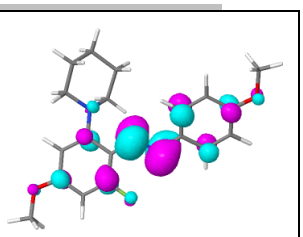
	S_2	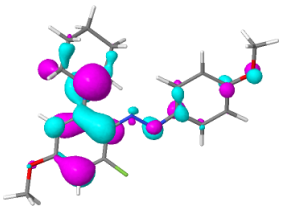	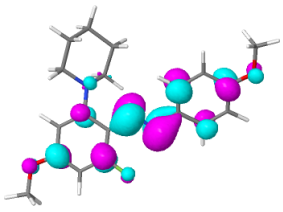	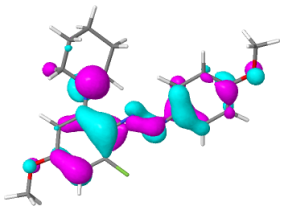	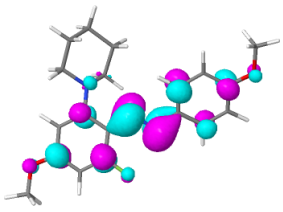
	S_3	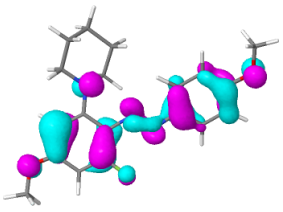	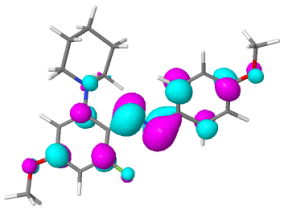	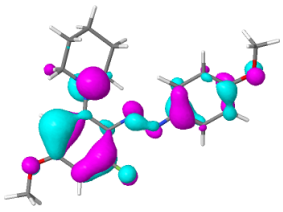	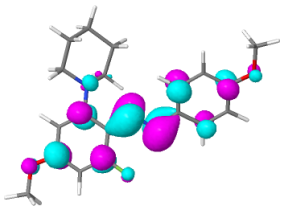
	S_4	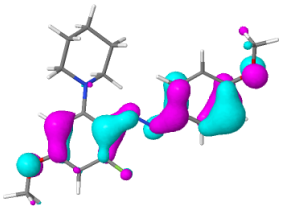	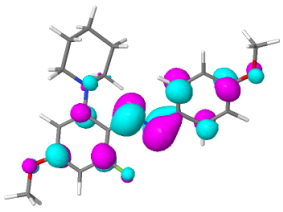	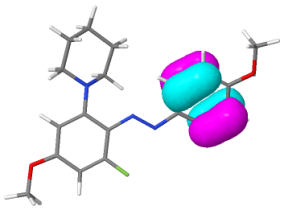	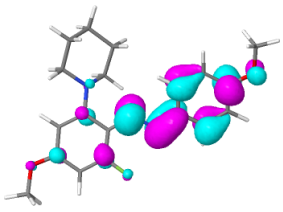
2-dma$_1$	**S_1**	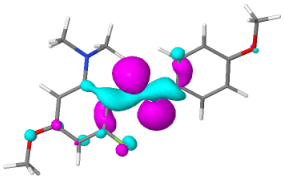	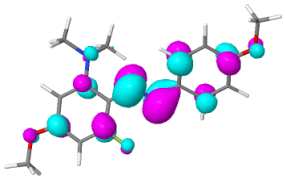	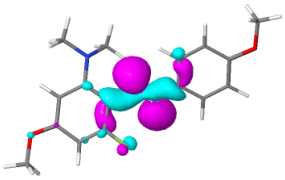	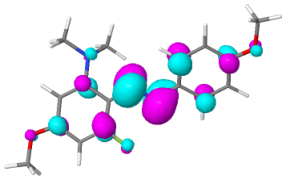
	S_2	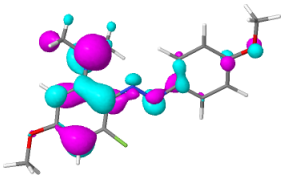	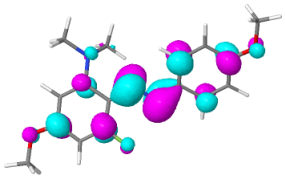	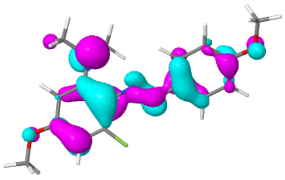	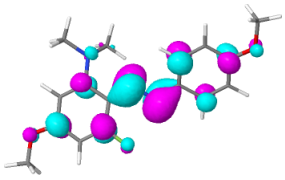
	S_3	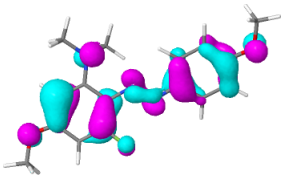	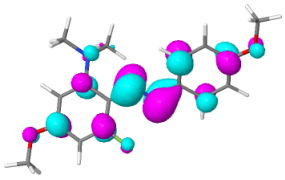	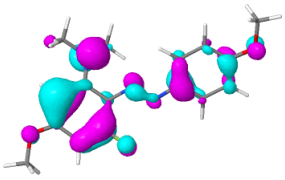	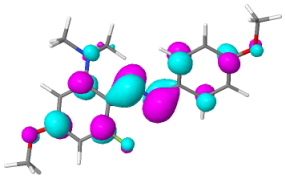
	S_4	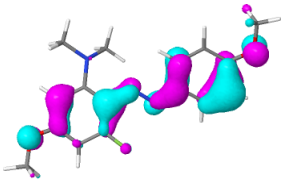	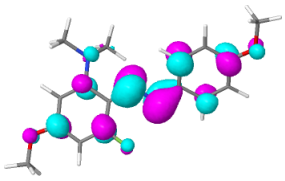	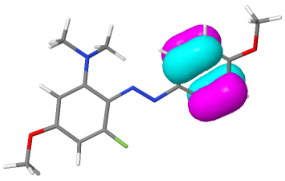	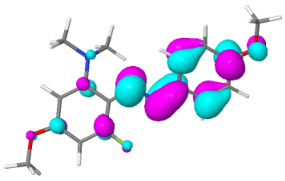

3-pip$_1$	S_1	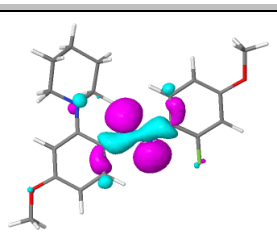	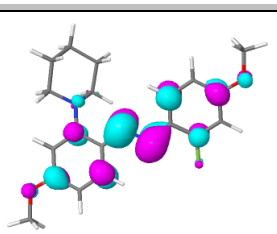	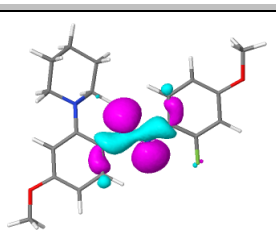	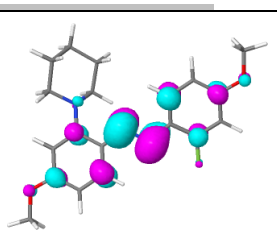
	S_2	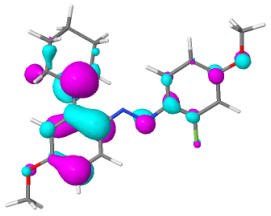	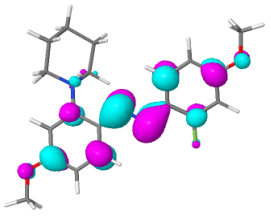	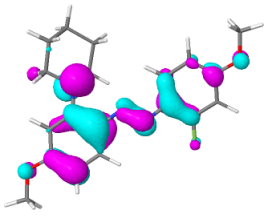	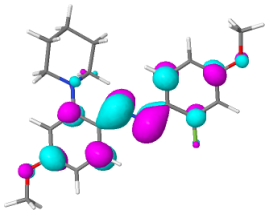
	S_3	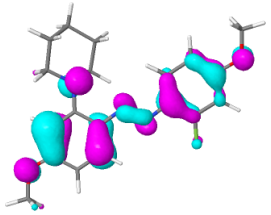	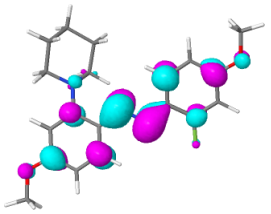	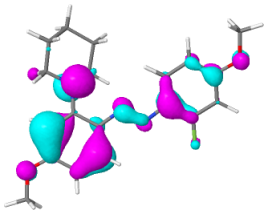	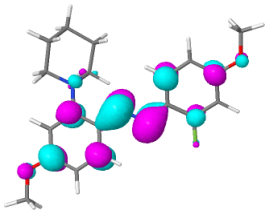
	S_4	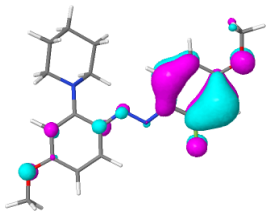	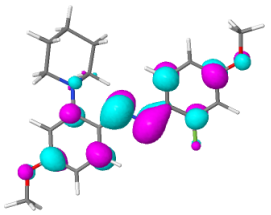	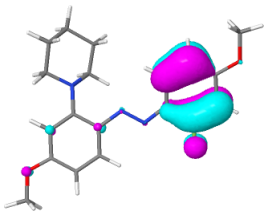	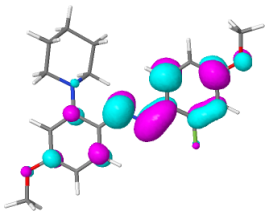
4-pip$_1$	S_1	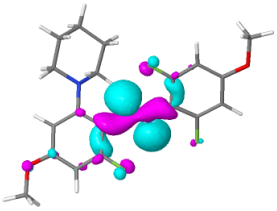	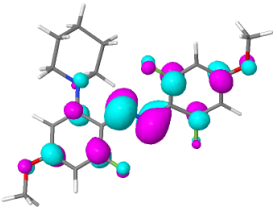	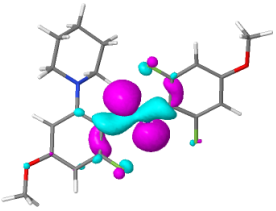	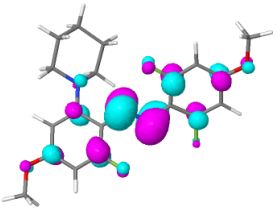
	S_2	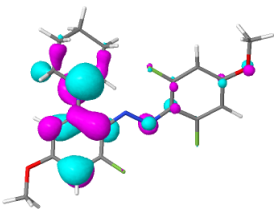	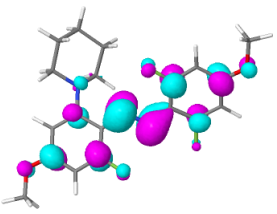	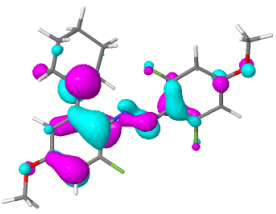	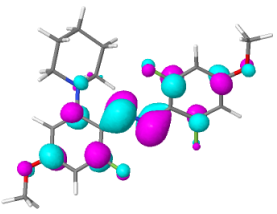
	S_3	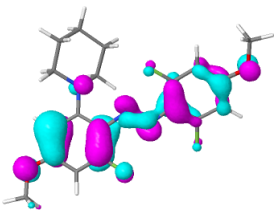	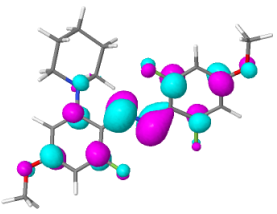	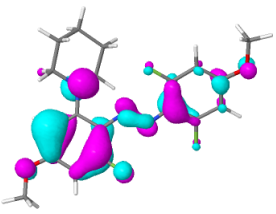	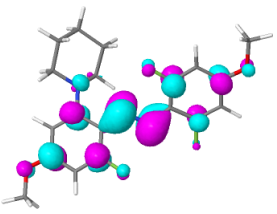
	S_4	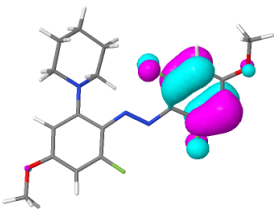	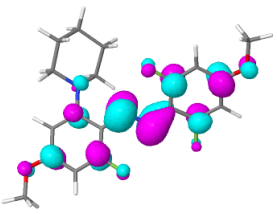	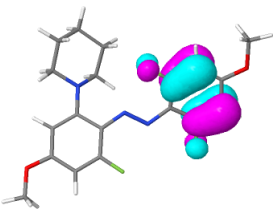	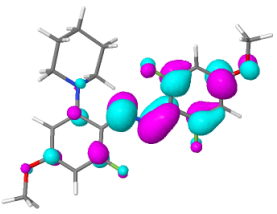

4-pip$_{2\text{-sym}}$	**S_1**	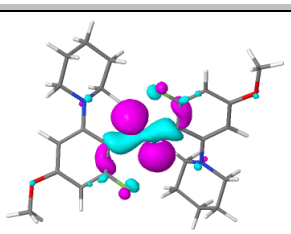	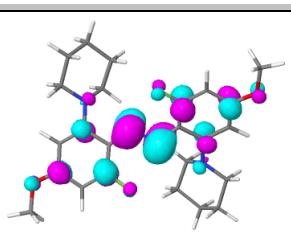	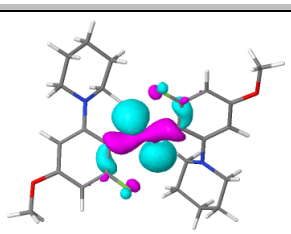	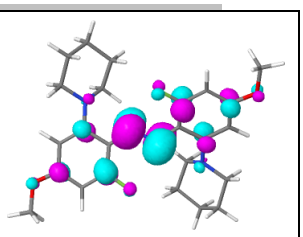
	S_2	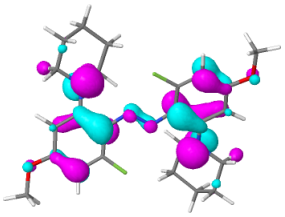	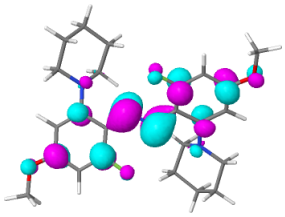	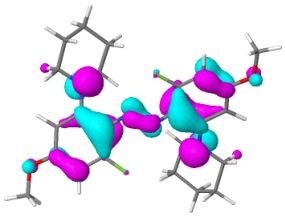	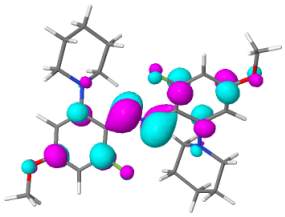
	S_3	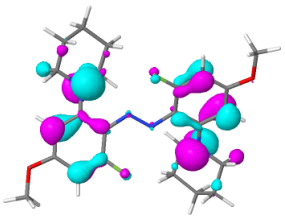	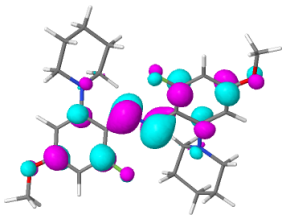	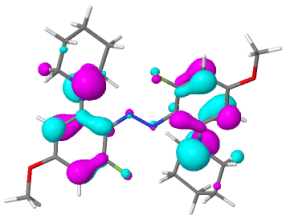	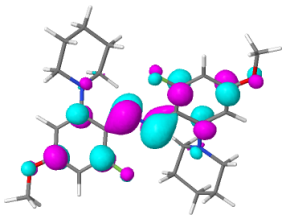
	S_4	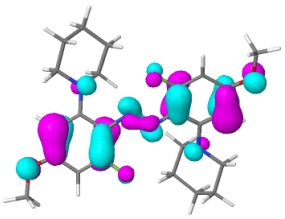	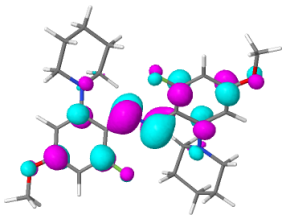	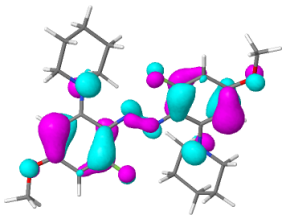	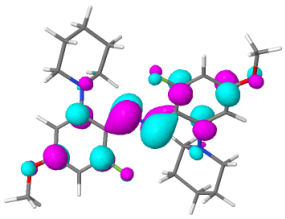

Table S3. Dominant natural transition orbitals (NTOs) for the lowest electronic transitions of the *cis* isomers.

		B3LYP		ωB97X-D	
		Hole	**Particle**	**Hole**	**Particle**
1-F	S_1	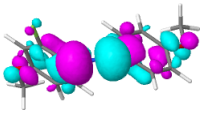	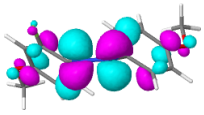	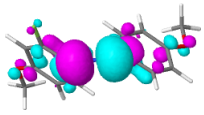	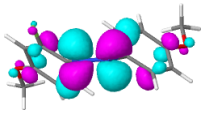
	S_2	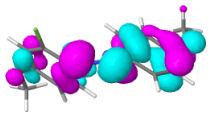	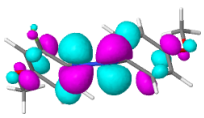	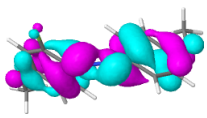	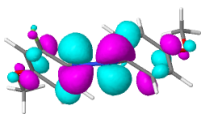
	S_3	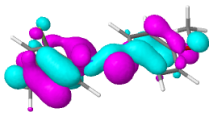	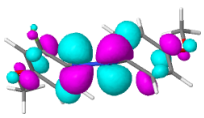	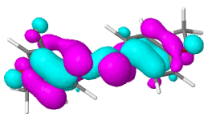	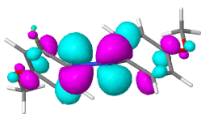
	S_4	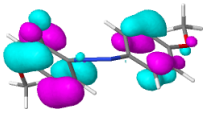	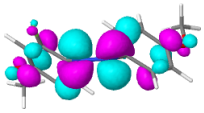	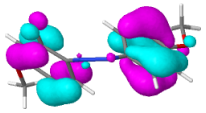	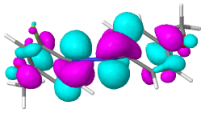
1-pyr	S_1	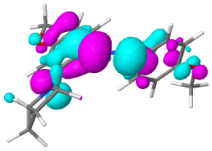	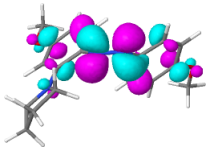	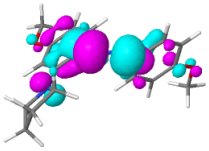	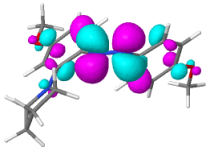
	S_2	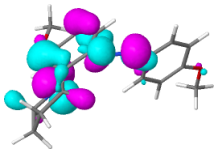	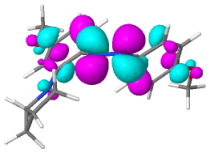	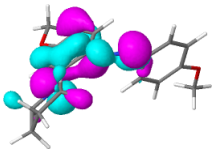	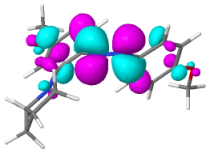
	S_3	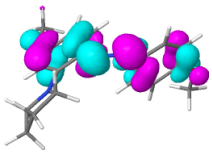	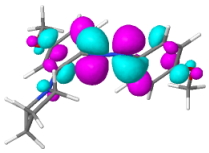	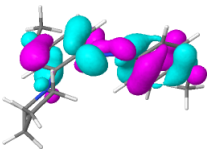	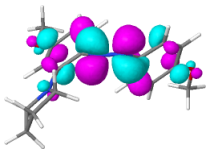
	S_4	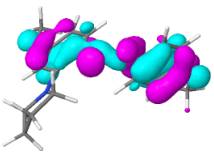	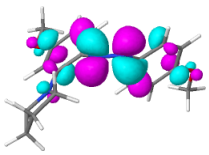	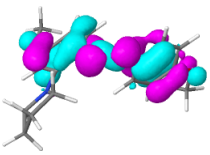	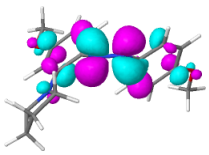

1-pip	S_1	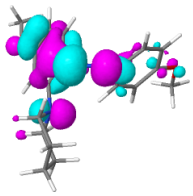	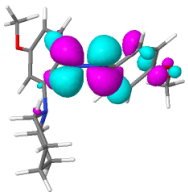	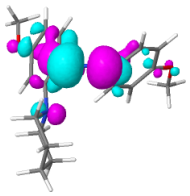	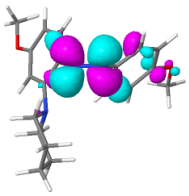
	S_2	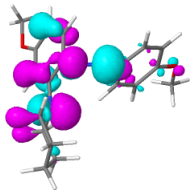	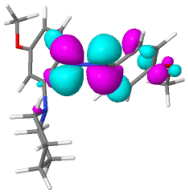	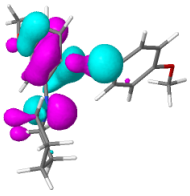	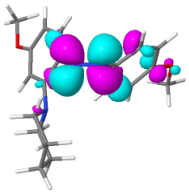
	S_3	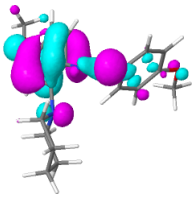	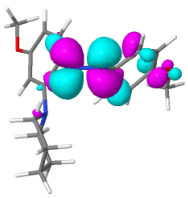	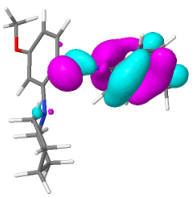	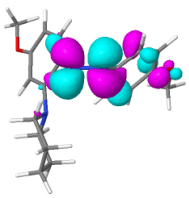
	S_4	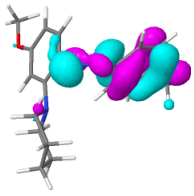	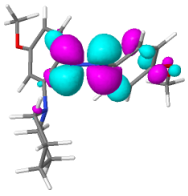	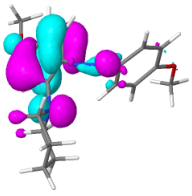	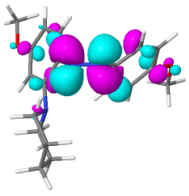
2-pyr$_1$	S_1	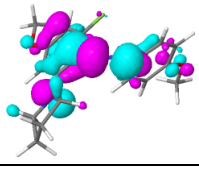	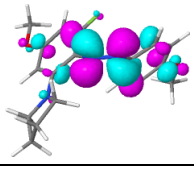	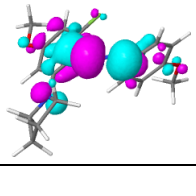	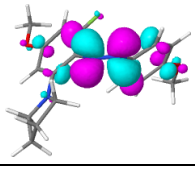
	S_2	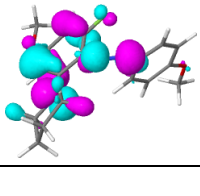	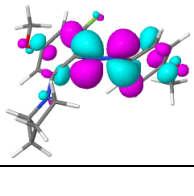	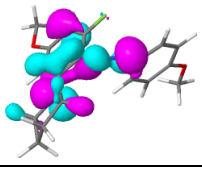	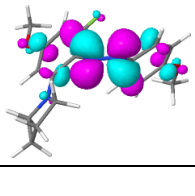
	S_3	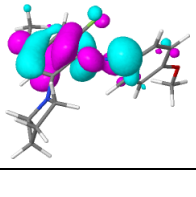	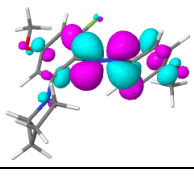	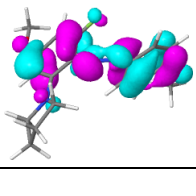	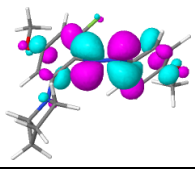
	S_4	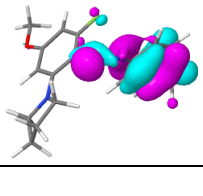	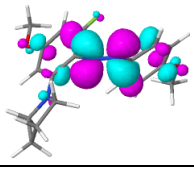	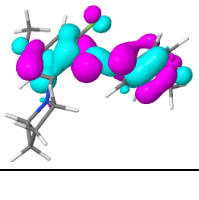	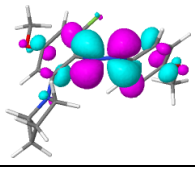

2-pip$_1$	S_1	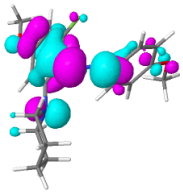	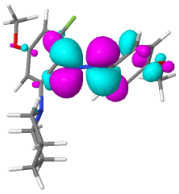	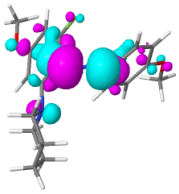	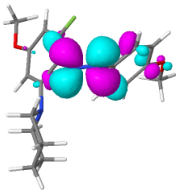
	S_2	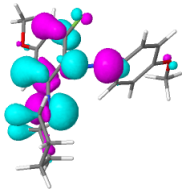	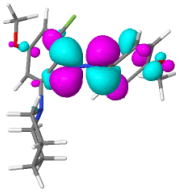	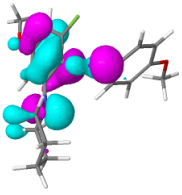	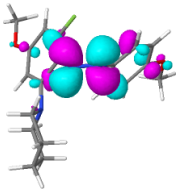
	S_3	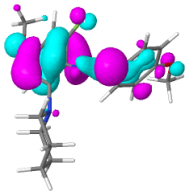	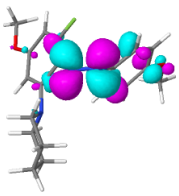	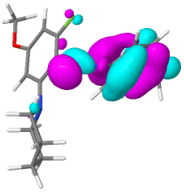	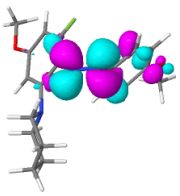
	S_4	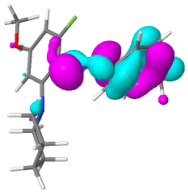	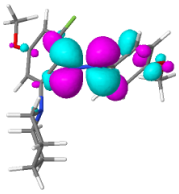	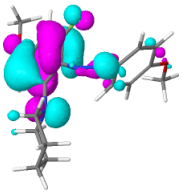	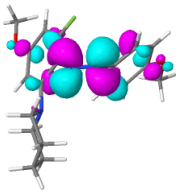
2-dma$_1$	S_1	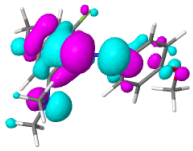	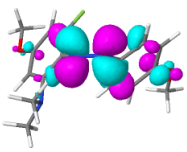	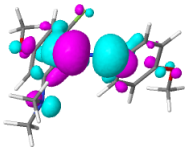	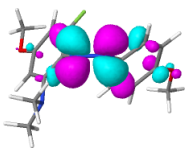
	S_2	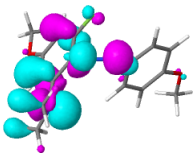	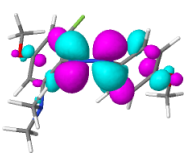	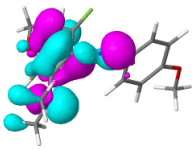	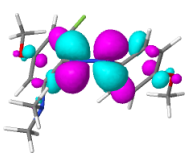
	S_3	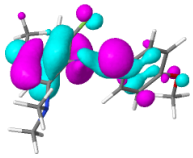	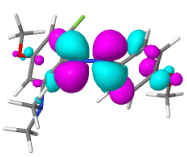	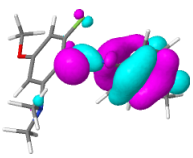	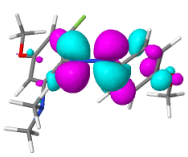
	S_4	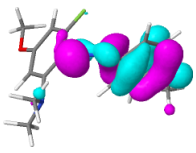	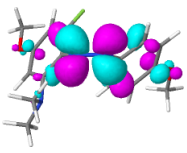	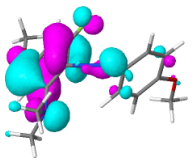	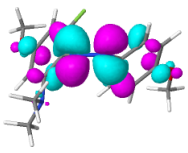

3-pip$_1$	S_1	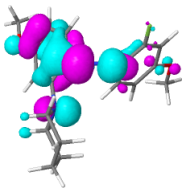	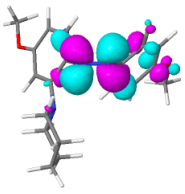	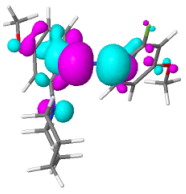	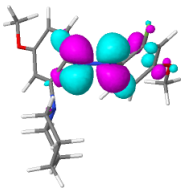
	S_2	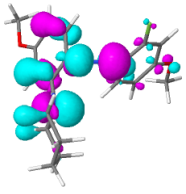	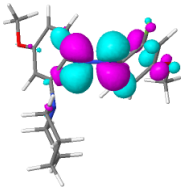	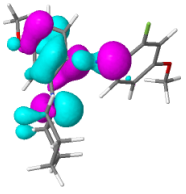	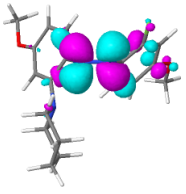
	S_3	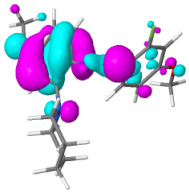	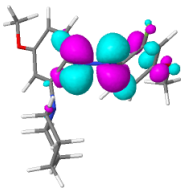	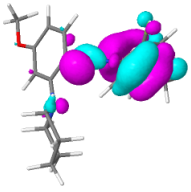	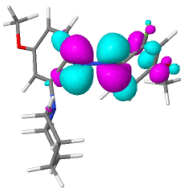
	S_4	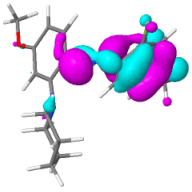	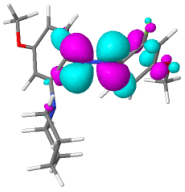	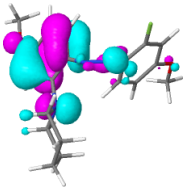	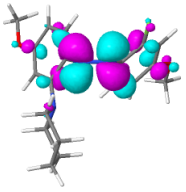
4-pip$_1$	S_1	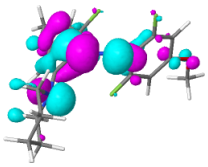	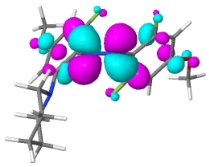	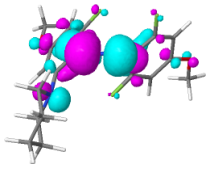	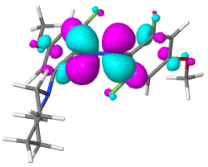
	S_2	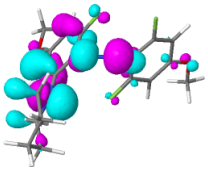	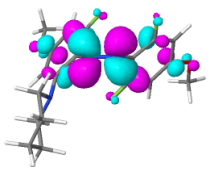	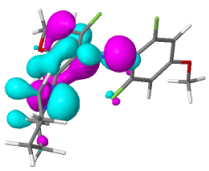	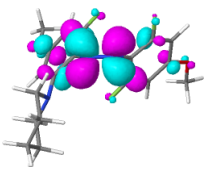
	S_3	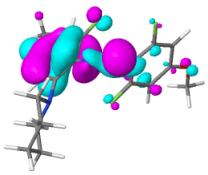	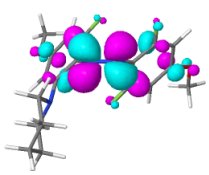	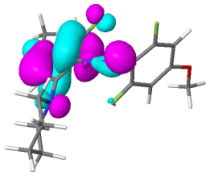	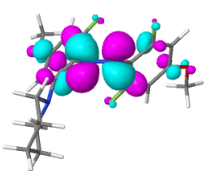
	S_4	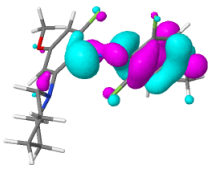	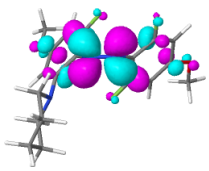	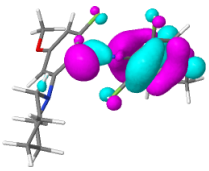	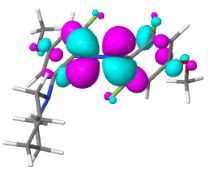

4-pip$_{2\text{-sym}}$	**S_1**	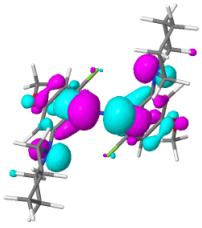	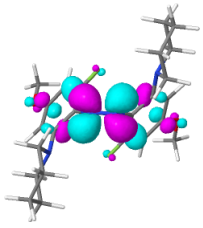	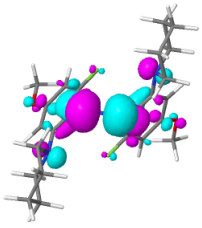	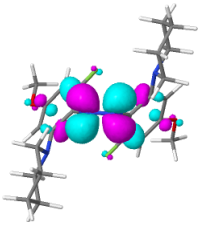
	S_2	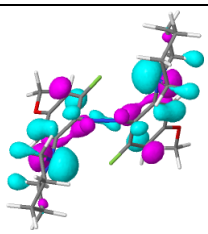	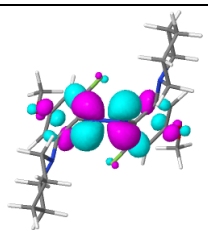	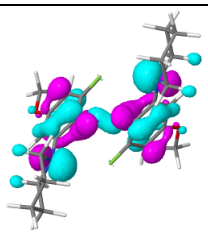	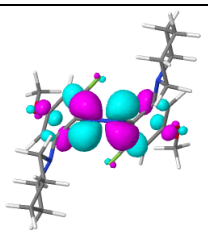
	S_3	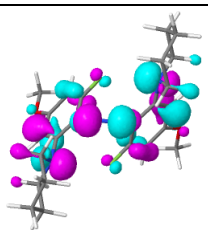	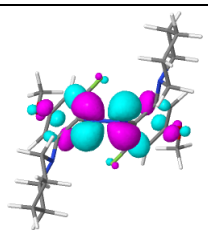	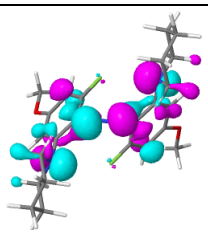	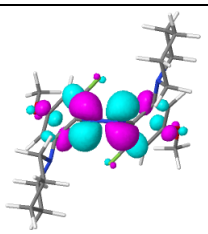
	S_4	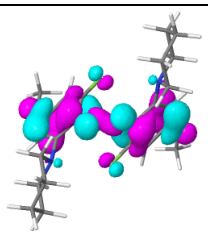	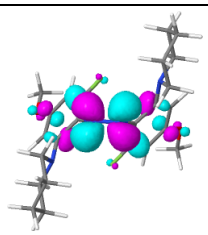	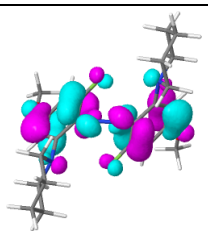	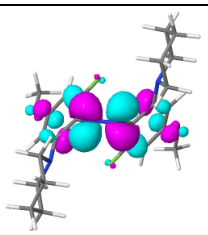
	S_5	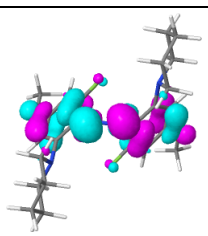	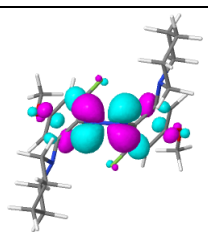	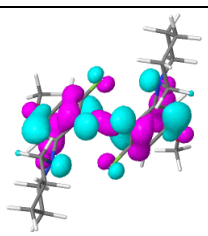	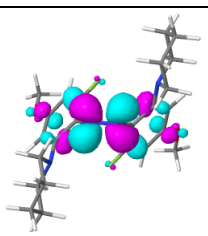

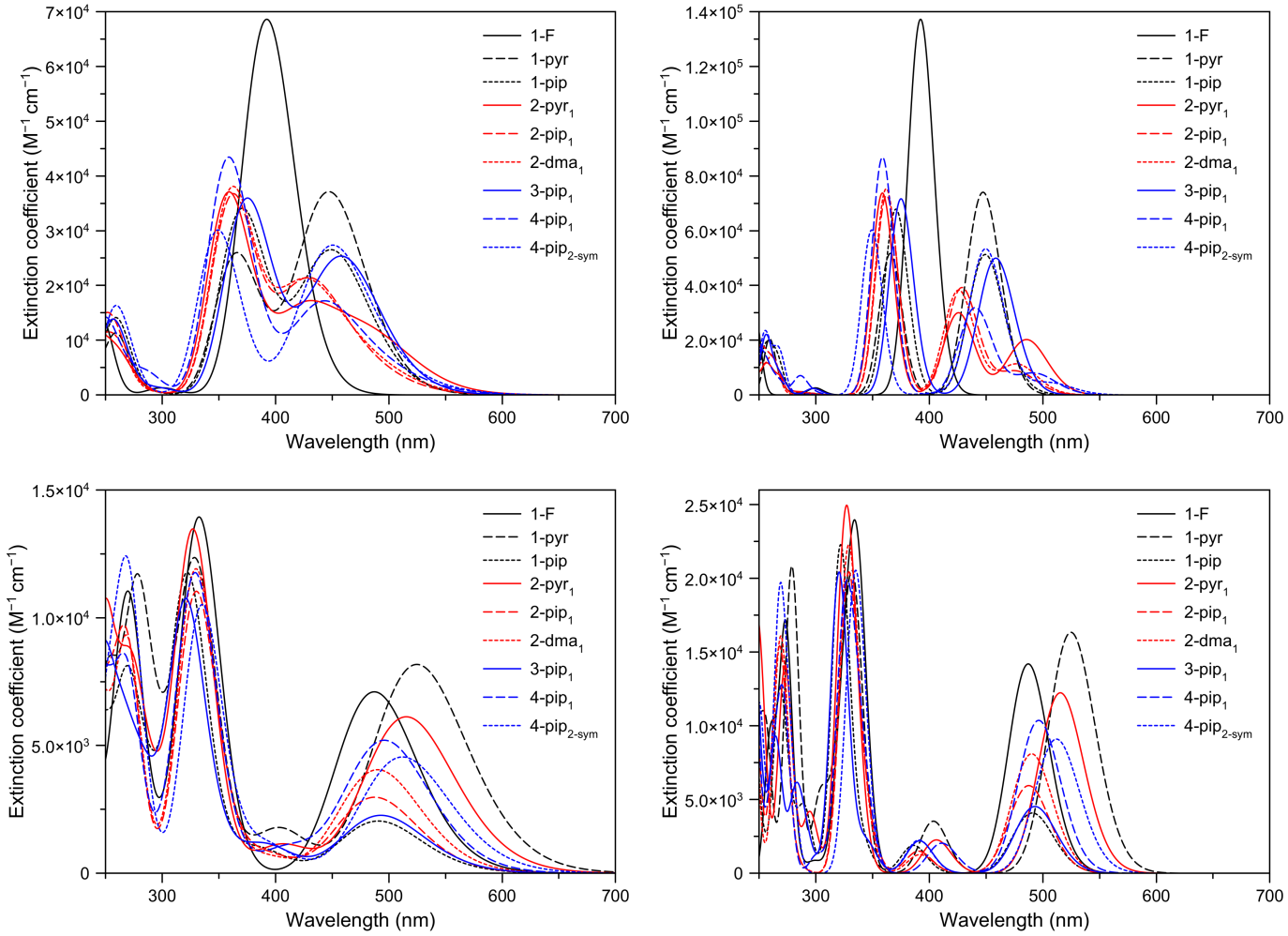

Figure S137. Calculated broadened absorption spectra of the trans (top row) and the cis (bottom row) isomers with broadening parameter σ = 1500 cm^{-1} (left column) and σ = 750 cm^{-1} (right column). *The spectra were calculated as*[16] $\varepsilon(\lambda) = \frac{1}{\kappa\sigma\sqrt{2\pi}}\sum_i f_i \, exp\left(-\frac{1}{2\sigma^2}\left(\frac{1}{\lambda}-\frac{1}{\lambda_i}\right)^2\right)$. *Here, ε is extinction coefficient, λ is wavelength, f_i and λ_i are computed oscillator strengths and wavelengths, respectively, for the i^{th} electronic transition, κ = 4.319 × 10^{-10} mol m^{-1}, and σ is the broadening parameter. Calculations are performed at the (TD-)B3LYP+D3(BJ)/6-31G*/PCM(ACN) level of theory.*

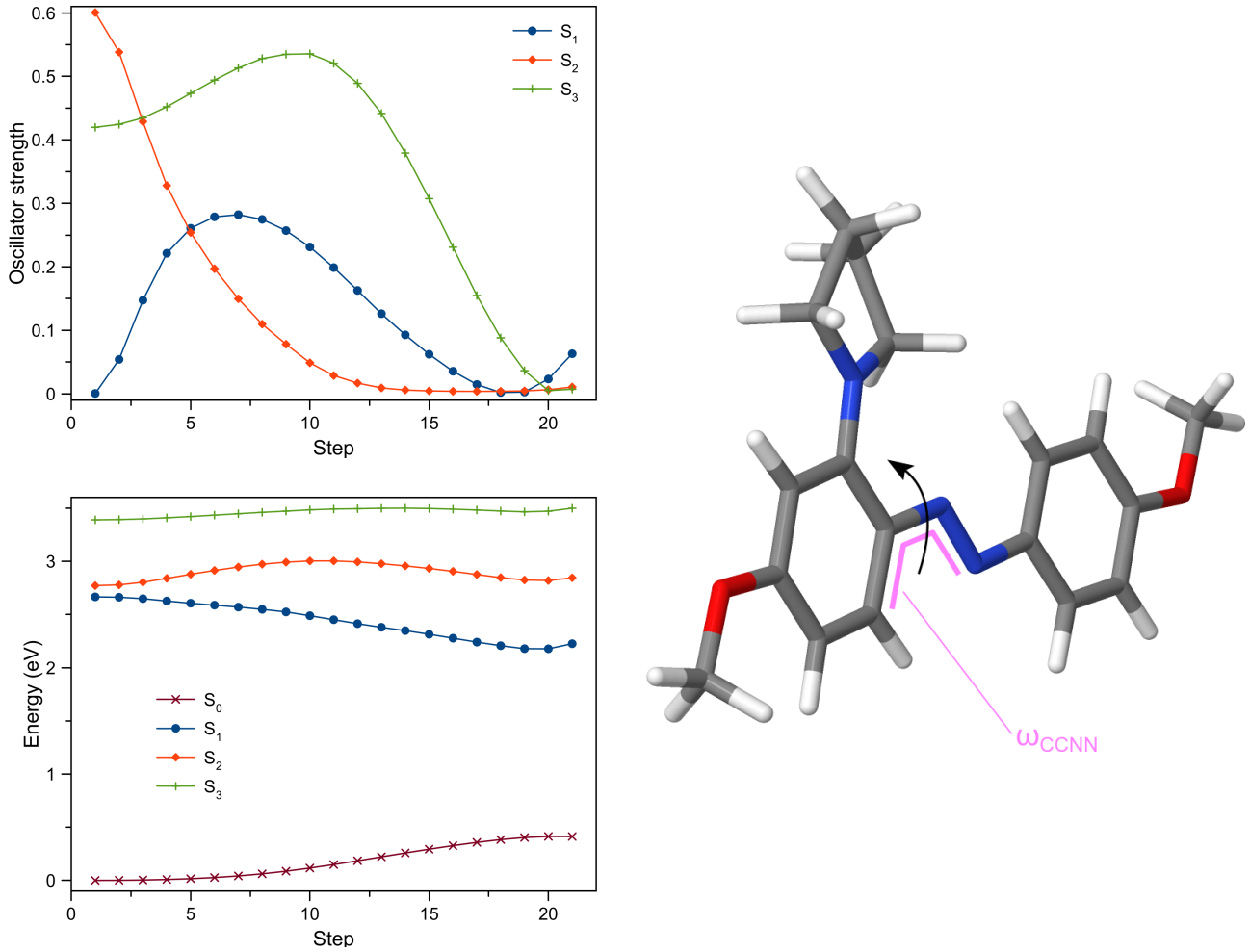

Figure S138. Variation in the oscillator strengths (top left) and energies (bottom left) of the lowest states of **1-pyr** upon a relaxed scan about the C–N bond corresponding to the change in the marked ω_{CCNN} dihedral angle (right). The equilibrium S_0 value of ω_{CCNN} is 1.9°. Step size is 5°. Calculations are performed at the (TD-)B3LYP+D3(BJ)/6-31G*/PCM(ACN) level of theory.

Photostationary state mixture compositions

Table S4. Molar *cis*-fractions (%) in the photostationary state with different illumination wavelengths (nm).

Peak wavelength (nm)	**365**	**385**	**405**	**435**	**470**	**500**	**550**	**595**
FWHM (nm)	9	11	17	17	24	28	77	17
Power (mW cm^{-2})	16.3	36.7	54.0	40.8	53.0	20.4	77.5	11.2
1-pyr	57	57	58	58	72	63	54	21
1-pip	76	76	77	70	54	53	32	30
1-dma	72	74	75	70	61	55	26	21
2-pyr$_1$	63	65	68	60	47	39	19	18
2-pip$_1$	76	76	71	54	43	42	38	37
2-dma$_1$	73	73	69	53	43	39	30	28
2-prol$_1$	63	75	64	44	17	11	10	10
2-pres$_1$	60	62	62	53	40	31	16	15
2-pram$_1$	68	69	67	60	42	30	18	18
3-pyr$_1$	61	57	68	68	68	65	46	36
3-pip$_1$	69	67	67	61	54	53	37	34
3-dma$_1$	66	65	69	67	63	62	42	32
3-prol$_1$	61	56	61	60	56	52	34	22
3-pres$_1$	57	54	64	54	50	22	11	2
3-pram$_1$	48	55	67	66	57	44	21	4
4-pyr$_1$	60	54	53	50	45	44	41	40
4-pip$_1$	71	68	59	68	49	55	64	64
4-dma$_1$	64	61	57	49	45	48	52	52
4-prol$_1$	36	36	39	36	28	26	28	26
4-pres$_1$	53	55	58	48	39	40	44	43
4-pram$_1$	54	54	55	45	38	39	44	44
4-pyr$_{2\text{-sym}}$	34	43	54	48	32	30	26	25
4-pip$_{2\text{-sym}}$	42	42	43	36	26	28	39	40
4-dma$_{2\text{-sym}}$	49	56	51	58	36	39	42	42
4-prol$_{2\text{-sym}}$	28	35	44	42	30	27	23	24
4-pres$_{2\text{-sym}}$	33	41	47	47	29	26	25	24
4-pram$_{2\text{-sym}}$	40	50	60	52	36	35	38	38

Computational results for thermal *cis*-to-*trans* isomerization

Table S5. Calculated activation Gibbs free energies, *Z* isomer energy differences, rate constants, and calculated and experimental lifetimes at 25 °C (298.15 K).

molecule	path	$\Delta G^{\ddagger}$ (eV)	ΔG_{ZZ}^{rel} (ΔE_{ZZ}^{rel}) (eV) [a]	k (s^{-1})	τ (hour)	τ_{exp} (hour)
RB3LYP/6-31G*/gas						
1-F	1	1.08	0	2.9×10^{-6}	94	42
	2	1.15	0.03 (0.04)	2.7×10^{-7}	1014	
1-pyr	1	1.04	0.12 (0.11)	1.3×10^{-5}	20	0.0042
	2	1.07	0	5.8×10^{-6}	48	
1-pip	1	1.03	0.05 (0.04)	2.4×10^{-5}	12	9.1
	2	1.12	0	7.4×10^{-7}	377	
2-pyr$_1$	1	0.97	0.01 (0.01)	2.4×10^{-4}	1	72
	2	1.17	0	9.4×10^{-8}	2945	
2-pip$_1$	1	1.05	0.05 (0.05)	1.0×10^{-5}	27	445
	2	1.20	0	3.1×10^{-8}	9021	
2-dma$_1$	1	1.03	0	2.9×10^{-5}	10	286
	2	1.19	0.02 (0.03)	4.4×10^{-8}	6247	
3-pip$_1$	1	1.08	0.08 (0.07)	3.3×10^{-6}	85	5
	2	1.17	0	1.2×10^{-7}	2224	
4-pip$_1$	1	1.16	0.05 (0.01)	1.4×10^{-7}	1950	1944
	2	1.18	0	5.3×10^{-8}	5239	
4-pip$_{2\text{-sym}}$	1	1.19	0	4.0×10^{-8}	6996	31
	2	0.91	0.34 (0.37)	2.8×10^{-3}	0.10	
RB3LYP/6-31G*/PCM(ACN)						
1-F	1	1.14	0	3.3×10^{-7}	848	42
	2	1.19	0.01 (0.02)	5.1×10^{-8}	5495	
1-pyr	1	1.06	0	7.3×10^{-6} [b]	38 [c]	0.0042
	2	1.06	0	6.3×10^{-6} [b]	44 [c]	
1-pip	1	1.06	0.09 (0.08)	7.4×10^{-6}	37	9.1
	2	1.17	0	9.6×10^{-8}	2895	
2-pyr$_1$	1	1.00	0.02 (0.03)	6.8×10^{-5}	4	72
	2	1.19	0	4.8×10^{-8}	5745	
2-pip$_1$	1	1.07	0.08 (0.09)	4.6×10^{-6}	60	445
	2	1.25	0	5.4×10^{-9}	51130	
2-dma$_1$	1	1.07	0.01 (0.03)	6.0×10^{-6}	46	286
	2	1.23	0	1.2×10^{-8}	24079	
3-pip$_1$	1	1.10	0.11 (0.09)	1.6×10^{-6}	178	5
	2	1.23	0	9.6×10^{-9}	29044	
4-pip$_1$	1	1.15	0.05 (0.02)	2.2×10^{-7}	1277	1944
	2	1.22	0	1.6×10^{-8}	16941	
4-pip$_{2\text{-sym}}$	1	1.22	0	1.5×10^{-8}	18244	31
	2	0.93	0.36 (0.36)	1.1×10^{-3}	0.25	
RB3LYP+D3(BJ)/6-31G*/PCM(ACN)						
1-F	1	1.24	0	6.1×10^{-9}	45267	42
	2	1.29	0.02 (0.03)	9.8×10^{-10}	282829	
1-pyr	1	1.16	0	1.5×10^{-7} [d]	1889 [e]	0.0042
	2	1.16	0	1.5×10^{-7} [d]	1872 [e]	
1-pip	1	1.19	0	4.9×10^{-8}	5619	9.1
	2	1.30	0.04 (0.06)	6.1×10^{-10}	455040	
2-pyr$_1$	1	1.11	0.01 (0.03)	1.2×10^{-6}	226	72
	2	1.33	0	2.1×10^{-10}	1294306	
2-pip$_1$	1	1.18	0	8.3×10^{-8}	3330	445
	2	1.38	0.04 (0.03)	3.1×10^{-11}	8867443	
2-dma$_1$	1	1.17	0.01 (0.03)	9.8×10^{-8}	2844	286
	2	1.36	0	7.5×10^{-11}	3712823	
3-pip$_1$	1	1.25	0	5.6×10^{-9}	49900	5
	2	1.35	0.04 (0.06)	9.2×10^{-11}	3026429	
4-pip$_1$	1	1.27	0	1.9×10^{-9}	143597	1944
	2	1.36	0.08 (0.12)	7.5×10^{-11}	3720707	
4-pip$_{2\text{-sym}}$	1	1.32	0	2.8×10^{-10}	1008055	31
	2	1.09	0.18 (0.14)	2.0×10^{-6}	140	

[a] $\Delta B_{ZZ}^{rel} = B(\mathrm{Z}_i) - B(\mathrm{Z}_{\text{lowest energy}})$; $B = G, E$; G is Gibbs free energy; E is energy, i.e. a point on the potential energy surface (PES)
[b] $k_{tot} = k_1 + k_2 = 1.4 \times 10^{-5}\ s^{-1}$
[c] $\tau_{tot} = 1/k_{tot} = 20$ h
[d] $k_{tot} = k_1 + k_2 = 3.0 \times 10^{-7}\ s^{-1}$
[e] $\tau_{tot} = 1/k_{tot} = 940$ h

Table S6. Notations for the UDFT calculations.

All energies are calculated w.r.t. the *cis* isomer energy	
$\Delta E_{UDFT}^{\ddagger}$	Electronic energy of the rotational TS calculated with the unrestricted DFT (UDFT) method. It corresponds to the broken-symmetry (mixed-spin) state with $\langle S^2 \rangle \approx 1$.
$\Delta E_{UDFT}^{(S,\ddagger)}$	Energy of a pure-singlet (i.e. $\langle S^2 \rangle = 0$) state at the rotational TS geometry. This energy is estimated using Yamaguchi's formula (see Computational Details).
$\Delta E_{RDFT}^{(S,\ddagger)}$	Energy of the singlet state at the rotational TS geometry, calculated with the restricted DFT (RDFT) method.
$\Delta E_{UDFT}^{(T,\ddagger)}$	Energy of the triplet state at the rotational TS geometry, calculated with UDFT. $\langle S^2 \rangle \approx 2$ for this state.
$\Delta E_{UDFT}^{(T,opt)}$	Energy of the triplet state at the minimum of the triplet PES.
$\Delta G_{UDFT}^{\ddagger}$	Activation Gibbs free energy calculated using broken-symmetry UDFT.
$\Delta G_{UDFT}^{(S,\ddagger)}$	Activation Gibbs free energy calculated using broken-symmetry UDFT and applying Yamaguchi's formula to correct electronic energy.
$\Delta G_{corr}^{(S,\ddagger)}$	$\Delta G_{UDFT}^{\ddagger} + 0.26\ eV$, where 0.26 eV comes from the difference in UDFT and CASPT2 energies for rotational TS of parent azobenzene (taken from ref. [17].
k_{UDFT} , τ_{UDFT}	Rate constant and lifetime calculated from $\Delta G_{UDFT}^{\ddagger}$.
$k_{UDFT}^{(S)}$, $\tau_{UDFT}^{(S)}$	Rate constant and lifetime calculated from $\Delta G_{UDFT}^{(S,\ddagger)}$.
$k_{corr}^{(S)}$, $\tau_{corr}^{(S)}$	Rate constant and lifetime calculated from $\Delta G_{corr}^{(S,\ddagger)}$.
τ_{exp}	Experimental lifetime.

Table S7. Electronic energies (differences between PES points, w.r.t. the *cis* isomer), calculated at B3LYP+D3(BJ)/6-31G*/PCM(ACN).

	$\Delta E_{UDFT}^{\ddagger}$	$\Delta E_{UDFT}^{(S,\ddagger)}$	$\Delta E_{RDFT}^{(S,\ddagger)}$	$\Delta E_{UDFT}^{(T,\ddagger)}$	$\Delta E_{UDFT}^{(T,opt)}$
1-F	0.85	0.96	1.49	0.74	0.72
1-pyr	0.68	0.78	1.20	0.60	0.57
1-pip	0.77	0.88	1.38	0.68	0.66
2-pyr$_1$	0.81	0.92	1.41	0.71	0.70
2-pip$_1$	0.86	0.97	1.48	0.75	0.74
2-dma$_1$	0.85	0.96	1.47	0.74	0.73
3-pip$_1$	0.85	0.96	1.43	0.75	0.73
4-pip$_1$	0.87	0.99	1.46	0.75	0.74
4-pip$_{2\text{-sym}}$	0.88	1.00	1.46	0.78	0.76

Table S8. Calculated activation Gibbs free energies, rate constants, and calculated and experimental lifetimes at 25 °C (298.15 K). The calculations are done at the UB3LYP+D3(BJ)/6-31G*/PCM(ACN) level.

	$\Delta G_{UDFT}^{\ddagger}$ (eV)	$\Delta G_{UDFT}^{(S,\ddagger)}$ (eV)	$\Delta G_{corr}^{(S,\ddagger)}$ (eV)	k_{UDFT} (s^{-1})	$k_{UDFT}^{(S)}$ (s^{-1})	$k_{corr}^{(S)}$ (s^{-1})	τ_{UDFT} (h)	$\tau_{UDFT}^{(S)}$ (h)	$\tau_{corr}^{(S)}$ (h)	τ_{exp} (h)
1-F	0.78	0.90	1.04	4.2×10^{-1}	4.0×10^{-3}	1.7×10^{-5}	6.6×10^{-4}	6.9×10^{-2}	16	42
1-pyr	0.64	0.74	0.90	$8.1 \times 10^{+1}$	2.1×10^{0}	3.2×10^{-3}	3.5×10^{-6}	1.3×10^{-4}	0.09	0.0042
1-pip	0.71	0.81	0.97	6.9×10^{0}	1.2×10^{-1}	2.8×10^{-4}	4.0×10^{-5}	2.2×10^{-3}	1	9.1
2-pyr$_1$	0.74	0.85	1.00	1.6×10^{0}	2.4×10^{-2}	6.4×10^{-5}	1.7×10^{-4}	1.2×10^{-2}	4	72
2-pip$_1$	0.78	0.89	1.04	4.5×10^{-1}	5.2×10^{-3}	1.8×10^{-5}	6.1×10^{-4}	5.3×10^{-2}	15	445
2-dma$_1$	0.77	0.89	1.03	5.1×10^{-1}	6.2×10^{-3}	2.1×10^{-5}	5.4×10^{-4}	4.5×10^{-2}	13	286
3-pip$_1$	0.78	0.89	1.04	4.7×10^{-1}	6.2×10^{-3}	1.9×10^{-5}	5.9×10^{-4}	4.5×10^{-2}	15	5
4-pip$_1$	0.79	0.91	1.05	2.6×10^{-1}	2.2×10^{-3}	1.0×10^{-5}	1.1×10^{-3}	1.3×10^{-1}	27	1944
4-pip$_{2\text{-sym}}$	0.80	0.92	1.06	1.7×10^{-1}	2.0×10^{-3}	6.9×10^{-6}	1.6×10^{-3}	1.4×10^{-1}	40	31

Table S9. Geometries of the *cis* isomers and the transition states optimized at the RB3LYP/6-31G*/gas level of theory.

RB3LYP/6-31G*/gas			
	path	***cis***	**TS**
1-F	**1**	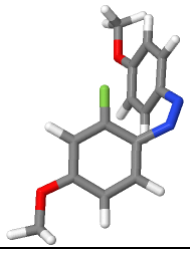	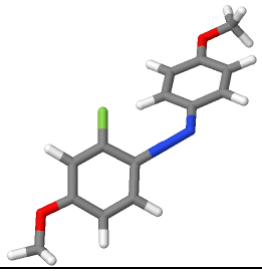
	2	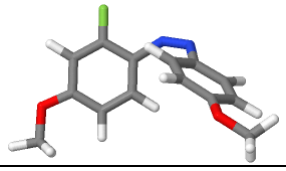	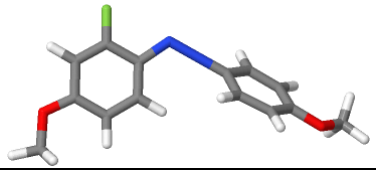
1-pyr	**1**	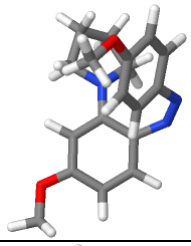	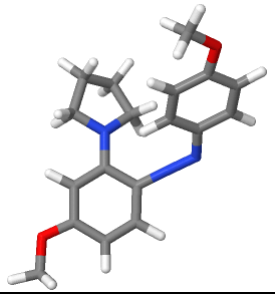
	2	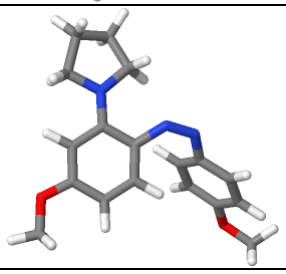	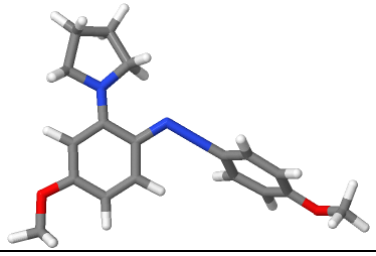
1-pip	**1**	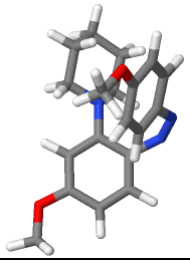	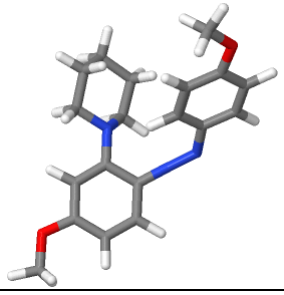
	2	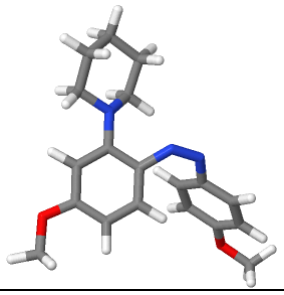	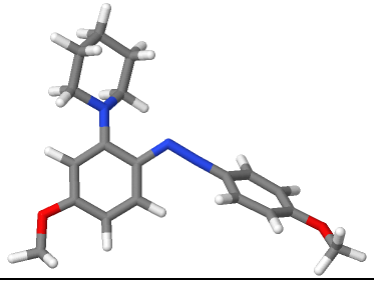

2-pyr$_1$	**1**	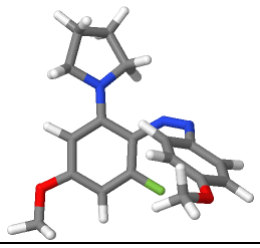	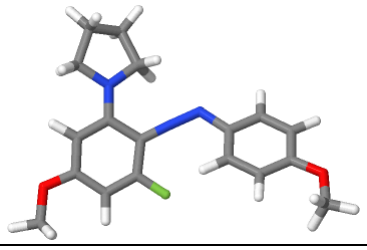
	2	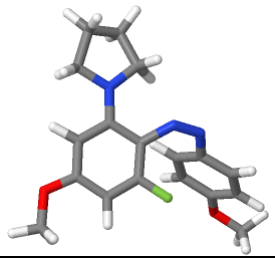	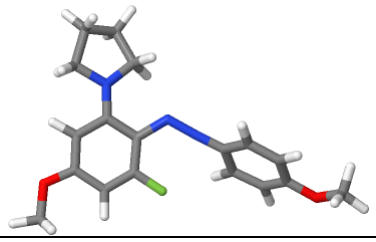
2-pip$_1$	**1**	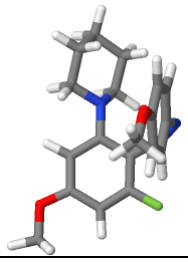	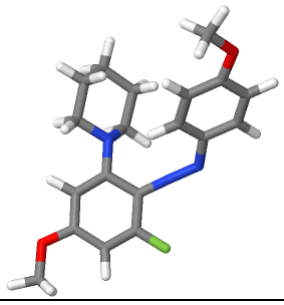
	2	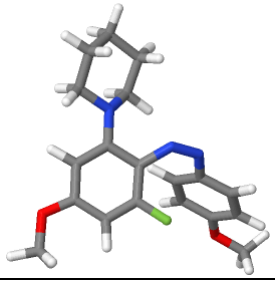	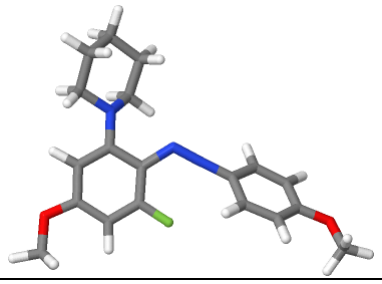
2-dma$_1$	**1**	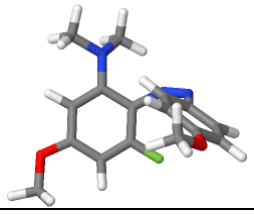	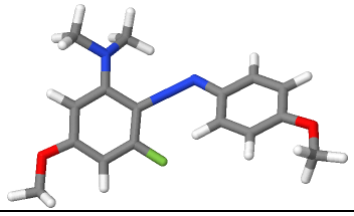
	2	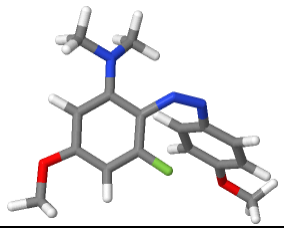	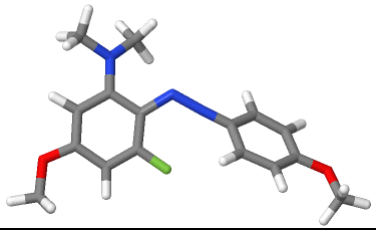

3-pip$_1$	**1**	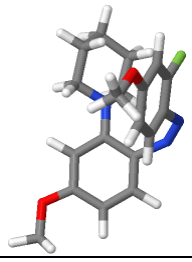	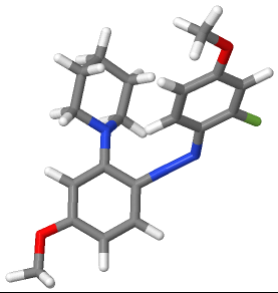
	2	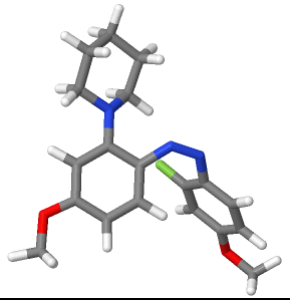	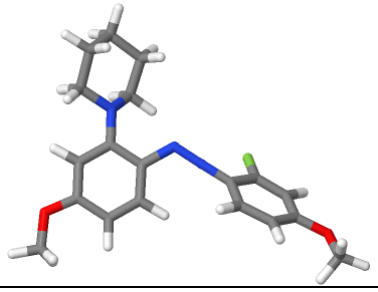
4-pip$_1$	**1**	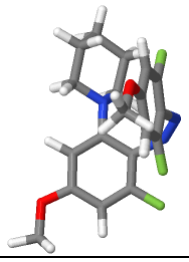	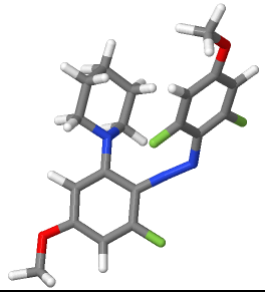
	2	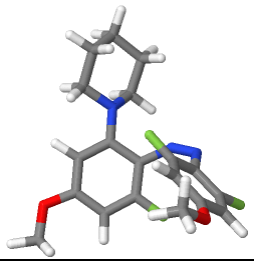	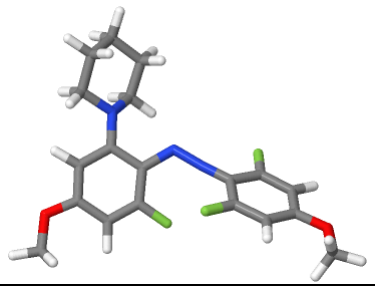
4-pip$_{2\text{-sym}}$	**1**	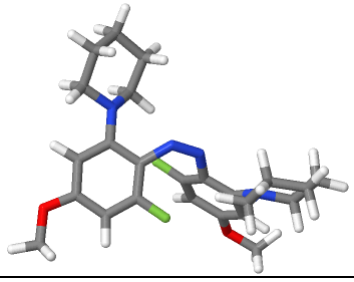	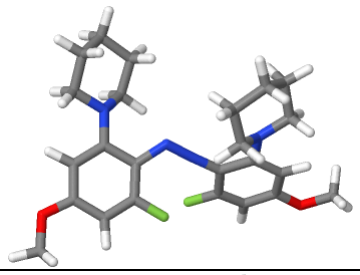
	2	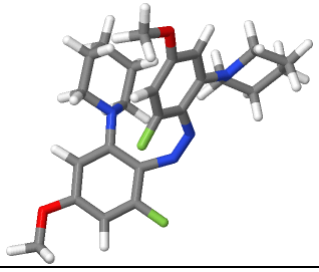	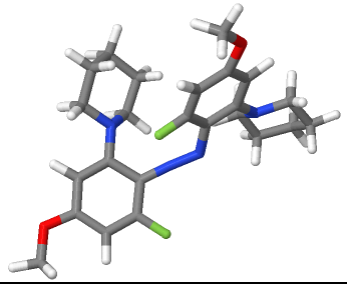

Table S10. Geometries of the *cis* isomers and the transition states optimized at the RB3LYP/6-31G*/PCM(ACN) level of theory.

RB3LYP/6-31G*/PCM(ACN)			
	path	***cis***	**TS**
1-F	1	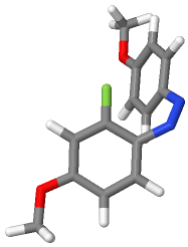	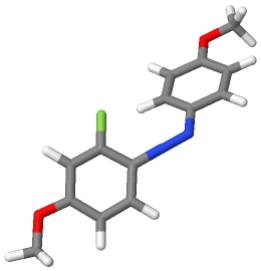
	2	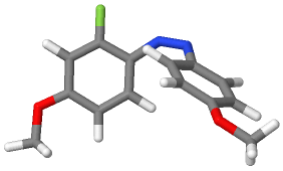	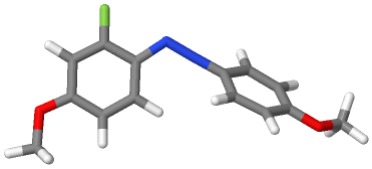
1-pyr	1 (rotation)	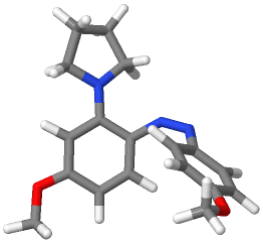	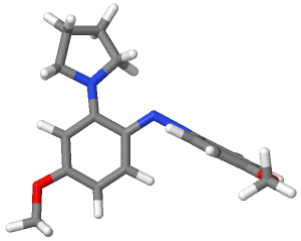
	2	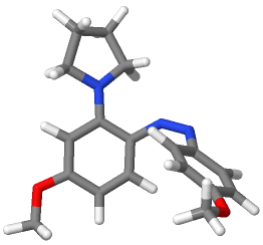	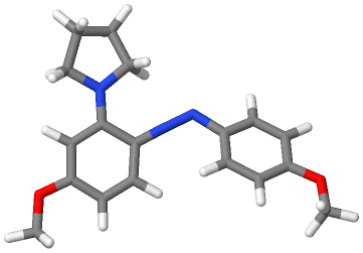
1-pip	1	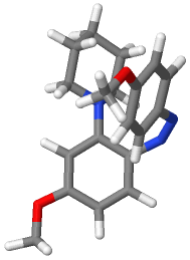	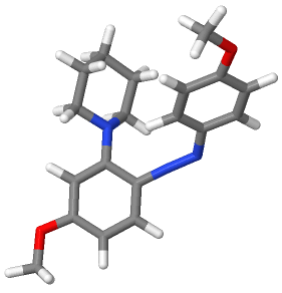
	2	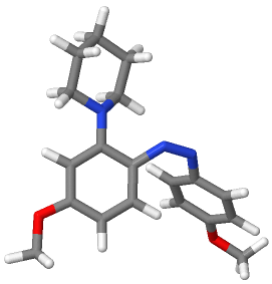	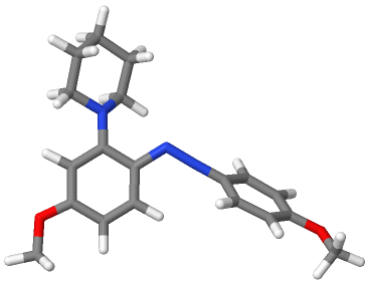

2-pyr$_1$	1	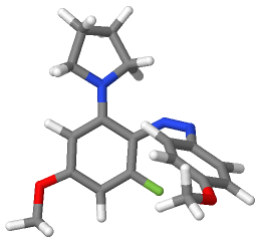	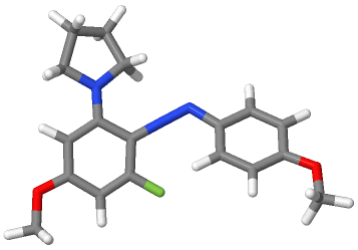
	2	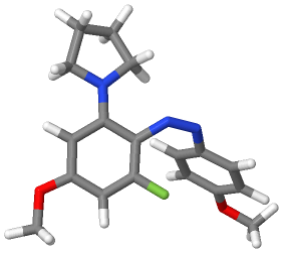	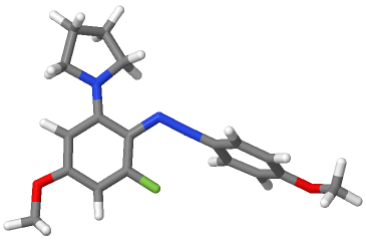
2-pip$_1$	1	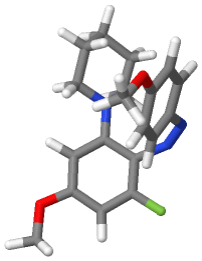	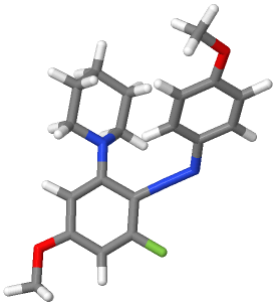
	2	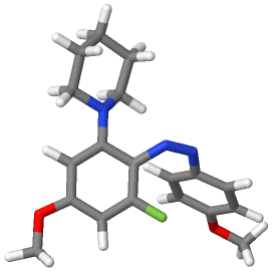	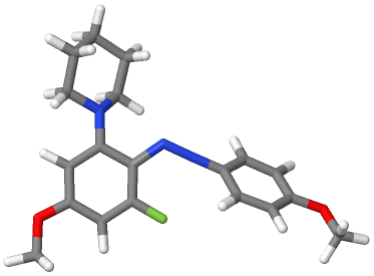
2-dma$_1$	1	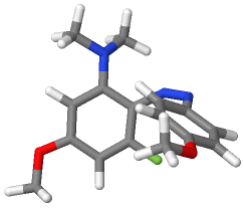	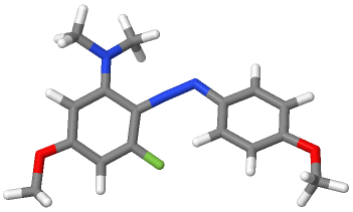
	2	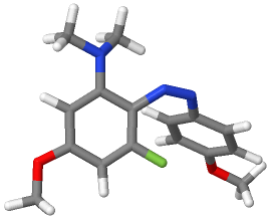	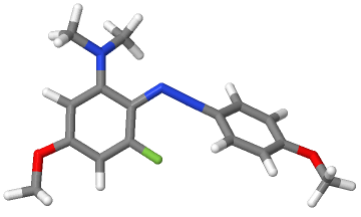

3-pip$_1$	1	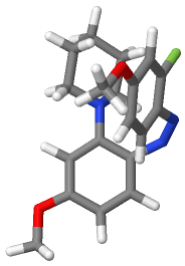	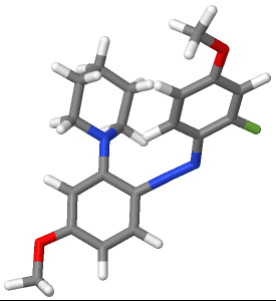
	2	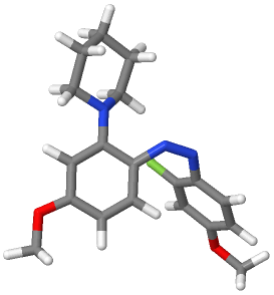	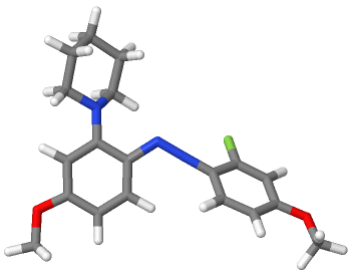
4-pip$_1$	1	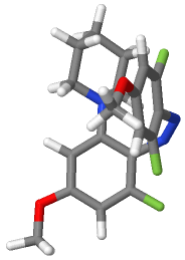	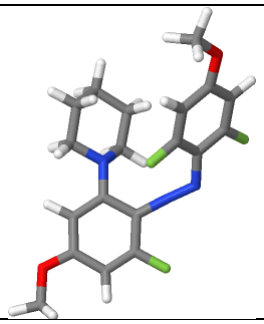
	2	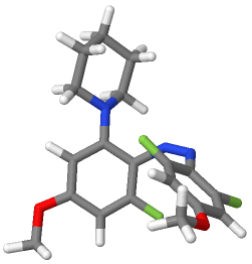	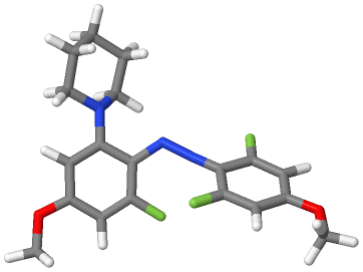
4-pip$_{2\text{-sym}}$	1	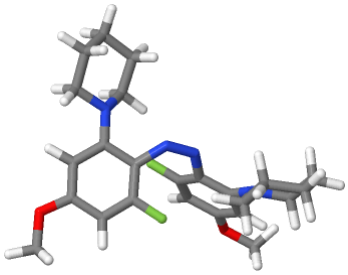	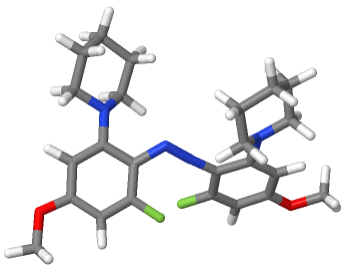
	2	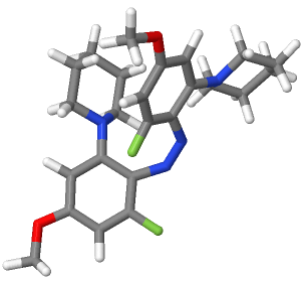	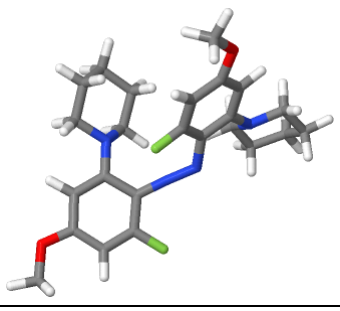

Table S11. Geometries of the *cis* isomers and the transition states optimized at the RB3LYP+D3(BJ)/6-31G*/PCM(ACN) level of theory.

RB3LYP+D3(BJ)/6-31G*/PCM(ACN)			
	path	***cis***	**TS**
1-F	1	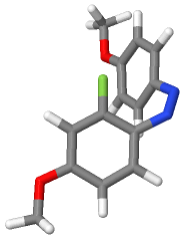	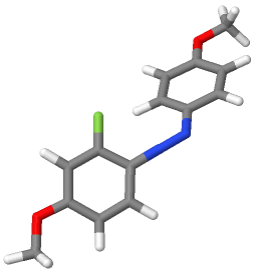
	2	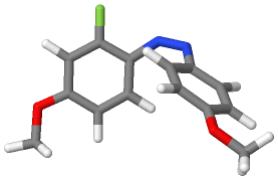	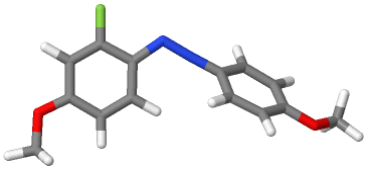
1-pyr	1 (rotation)	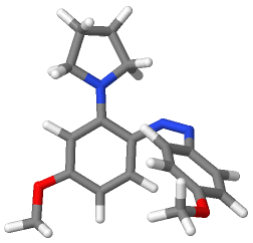	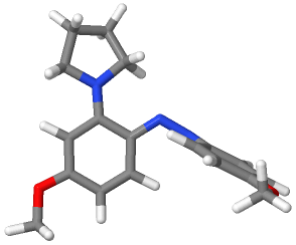
	2	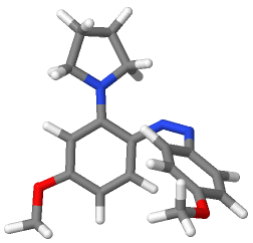	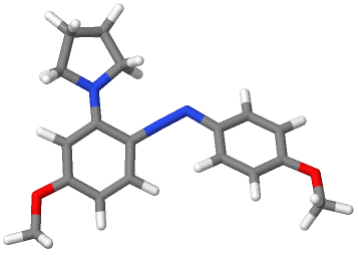
1-pip	1	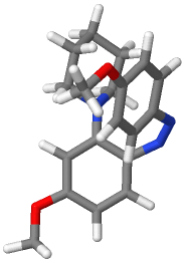	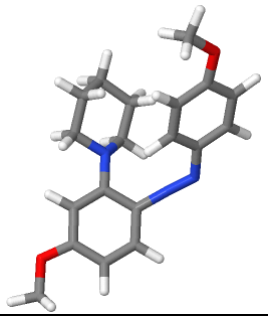
	2	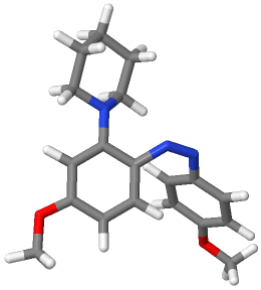	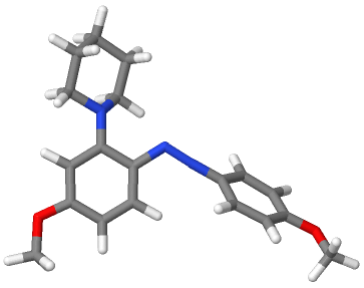

2-pyr$_1$	1	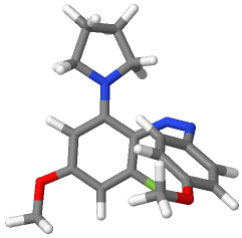	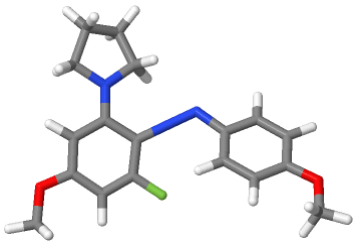
	2	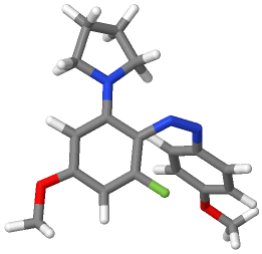	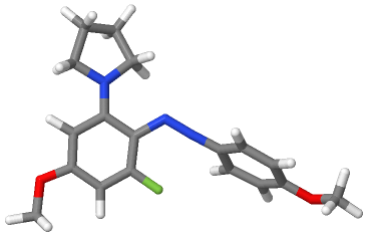
2-pip$_1$	1	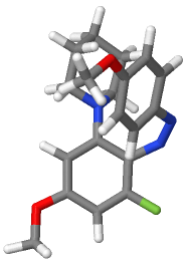	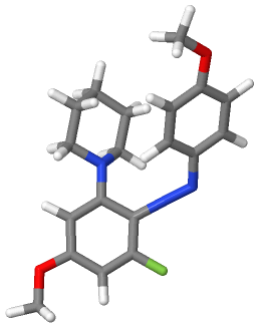
	2	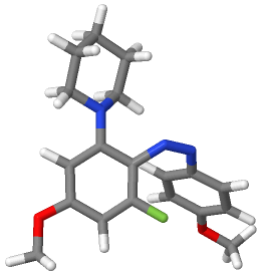	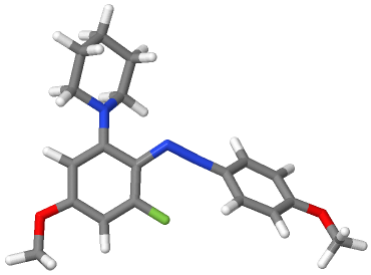
2-dma$_1$	1	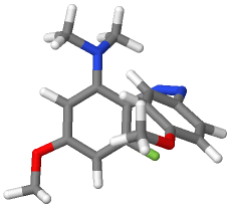	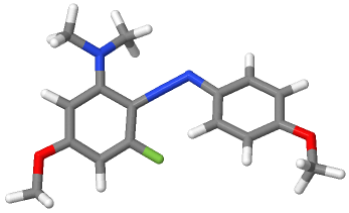
	2	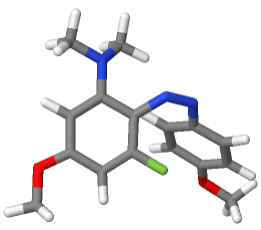	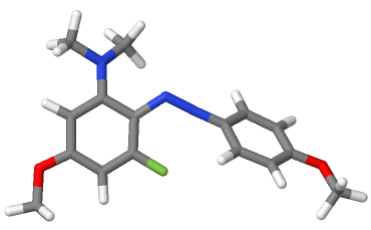

3-pip$_1$	1	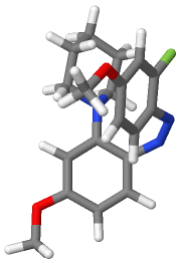	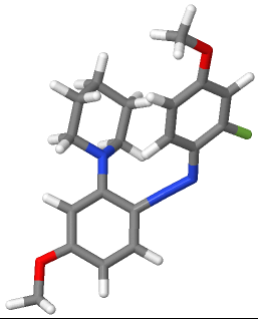
	2	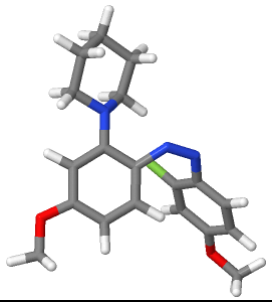	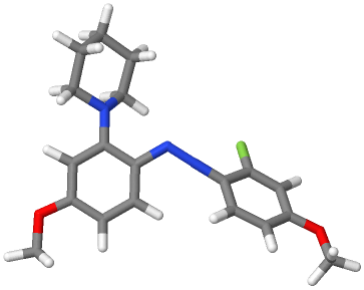
4-pip$_1$	1	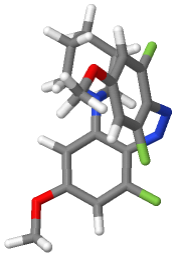	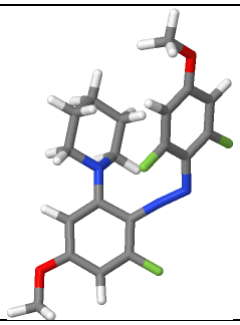
	2	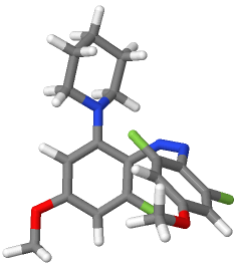	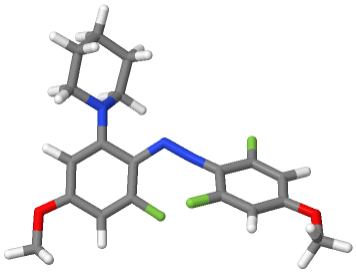
4-pip$_{2\text{-sym}}$	1	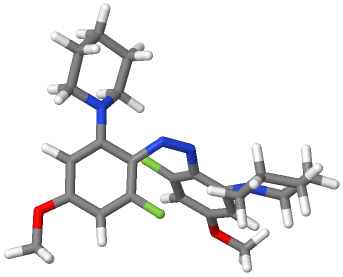	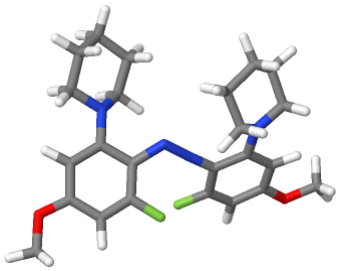
	2	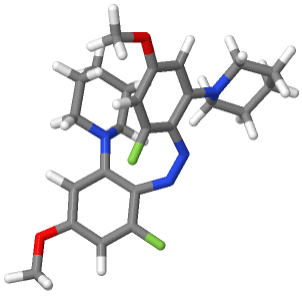	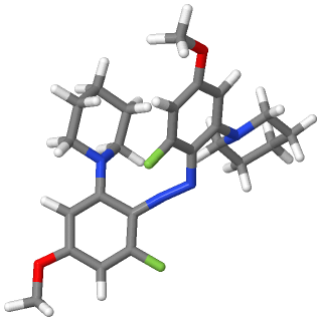

Table 12. Geometries of the *cis* isomers and the transition states optimized at the UB3LYP+D3(BJ)/6-31G*/PCM(ACN) level of theory.

UB3LYP+D3(BJ)/6-31G*/PCM(ACN)		
	cis	**TS**
1-F	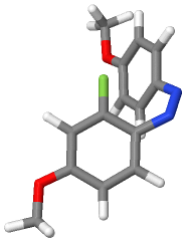	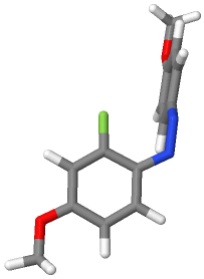
1-pyr	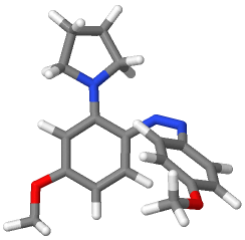	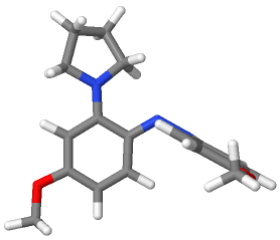
1-pip	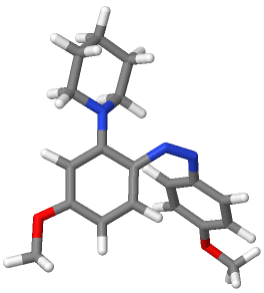	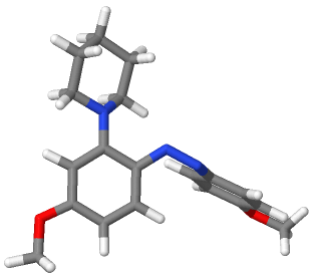
2-pyr$_1$	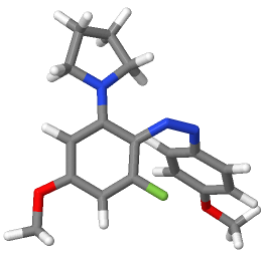	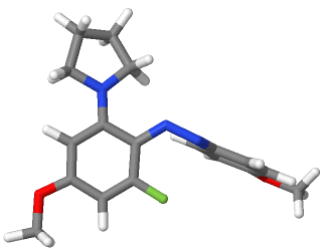
2-pip$_1$	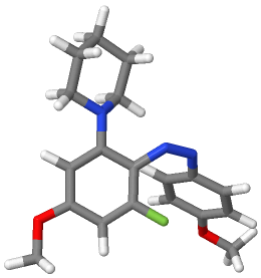	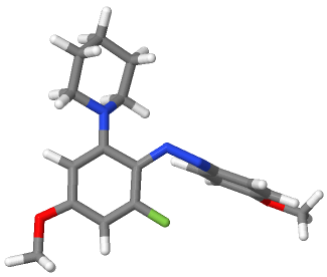

2-dma$_1$	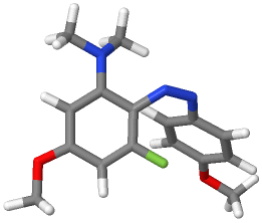	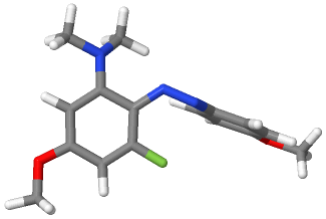
3-pip$_1$	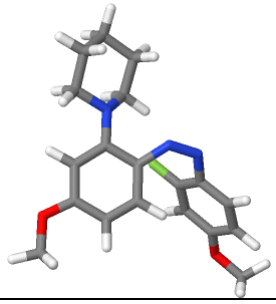	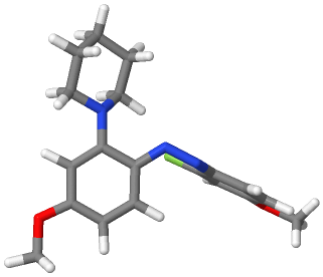
4-pip$_1$	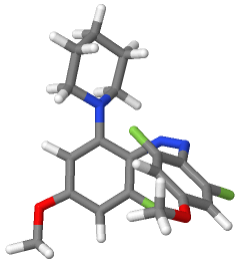	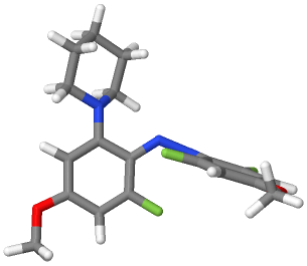
4-pip$_{2\text{-sym}}$	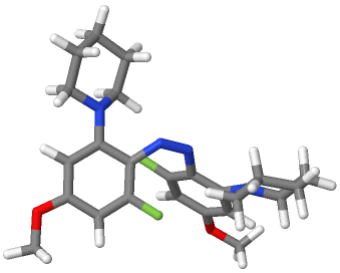	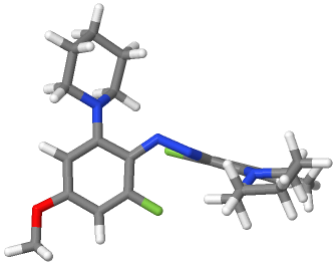

Other results

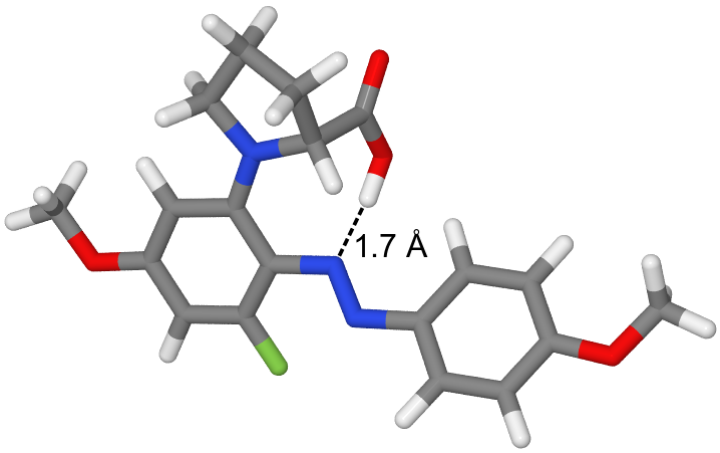

Figure S139. Geometry of **2-proline$_1$** optimized at the B3LYP+D3(BJ)/6-31G*/PCM(ACN) level of theory.

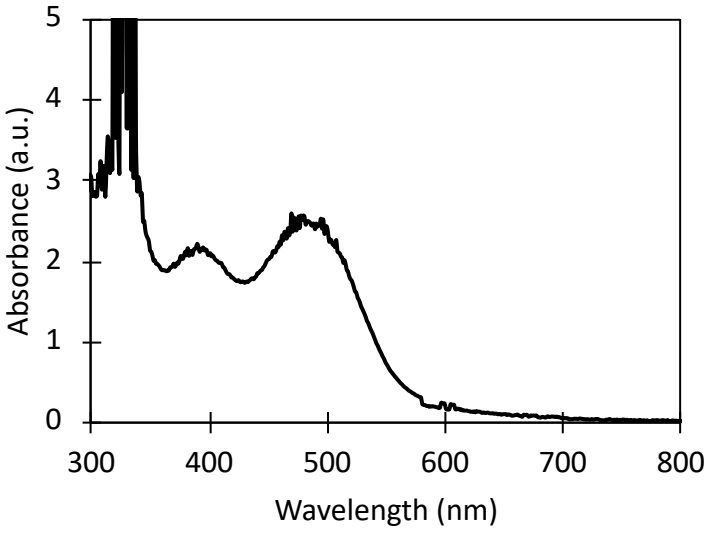

Figure S140. Absorption spectrum of a saturated aqueous solution of **4-pram$_{2\text{-sym}}$** at 25°C. The concentration was calculated with the Beer-Lambert law using the molar extinction coefficients of the peaks at 392 and 482 nm (4039 and 3406 M^{-1} cm^{-1}) to be 534 or 733 µM depending on which peak is chosen. The values should be viewed as qualitative, as the shape of the spectrum (and, thus, the molar extinction values) is clearly solvent-dependent. However, this is enough to demonstrate that the water solubility is greatly enhanced.

References

1. Ahmed, Z., Siiskonen, A., Virkki, M. & Priimagi, A. Controlling azobenzene photoswitching through combined: Ortho -fluorination and -amination. *Chem. Commun.* **53**, 12520–12523 (2017).
2. Frisch, M. J. *et al.* Gaussian 16, Revision C.01. (2016).
3. Becke, A. D. Density-functional thermochemistry. III. The role of exact exchange. *J. Chem. Phys.* **98**, 5648–5652 (1993).
4. Stephens, P. J., Devlin, F. J., Chabalowski, C. F. & Frisch, M. J. Ab Initio Calculation of Vibrational Absorption and Circular Dichroism Spectra Using Density Functional Force Fields. *J. Phys. Chem.* **98**, 11623–11627 (1994).
5. Grimme, S., Ehrlich, S. & Goerigk, L. Effect of the damping function in dispersion corrected density functional theory. *J. Comput. Chem.* **32**, 1456–1465 (2011).
6. Miertuš, S., Scrocco, E. & Tomasi, J. Electrostatic interaction of a solute with a continuum. A direct utilizaion of AB initio molecular potentials for the prevision of solvent effects. *Chem. Phys.* **55**, 117–129 (1981).
7. Scalmani, G. & Frisch, M. J. Continuous surface charge polarizable continuum models of solvation. I. General formalism. *J. Chem. Phys.* **132**, 114110 (2010).
8. CASIDA, M. E. Time-Dependent Density Functional Response Theory for Molecules. in *Recent Advances in Density Functional Methods* vol. Volume 1 155–192 (WORLD SCIENTIFIC, 1995).
9. Chai, J.-D. & Head-Gordon, M. Long-range corrected hybrid density functionals with damped atom–atom dispersion corrections. *Phys. Chem. Chem. Phys.* **10**, 6615–6620 (2008).
10. Martin, R. L. Natural transition orbitals. *J. Chem. Phys.* **118**, 4775–4777 (2003).
11. Eyring, H. The Activated Complex and the Absolute Rate of Chemical Reactions. *Chem. Rev.* **17**, 65–77 (1935).
12. Fukui, K. The path of chemical reactions - the IRC approach. *Acc. Chem. Res.* **14**, 363–368 (1981).
13. Hratchian, H. P. & Schlegel, H. B. Chapter 10 - Finding minima, transition states, and following reaction pathways on ab initio potential energy surfaces. in (eds. Dykstra, C. E., Frenking, G., Kim, K. S. & Scuseria, G. E. B. T.-T. and A. of C. C.) 195–249 (Elsevier, 2005). doi:https://doi.org/10.1016/B978-044451719-7/50053-6.
14. Yamaguchi, K., Jensen, F., Dorigo, A. & Houk, K. N. A spin correction procedure for unrestricted Hartree-Fock and Møller-Plesset wavefunctions for singlet diradicals and polyradicals. *Chem. Phys. Lett.* **149**, 537–542 (1988).
15. Hariharan, P. C. & Pople, J. A. The influence of polarization functions on molecular orbital hydrogenation energies. *Theor. Chim. Acta* **28**, 213–222 (1973).
16. Bléger, D. *et al.* Electronic Decoupling Approach to Quantitative Photoswitching in Linear Multiazobenzene Architectures. *J. Phys. Chem. B* **115**, 9930–9940 (2011).
17. Gagliardi, L., Orlandi, G., Bernardi, F., Cembran, A. & Garavelli, M. A theoretical study of the lowest electronic states of azobenzene: the role of torsion coordinate in the cis–trans photoisomerization. *Theor. Chem. Acc.* **111**, 363–372 (2004).